Order Number 9417445

Electron spin polarization and relaxation in GaAs and GaAs/Al_x $Ga_{1-x}As$ quantum wells

Chao, Hsieh Shin, Ph.D.

City University of New York, 1994

U·M·I
300 N. Zeeb Rd.
Ann Arbor, MI 48106

Electron Spin Polarization and Relaxation in GaAs and GaAs/$Al_xGa_{1-x}As$ Quantum Wells

By

Hsieh Shin Chao

A dissertation submitted to the Graduate Faculty in Physics in partial fulfillment of the requirements for the degree of Doctor of Philosophy, the City University of New York.

1994

This manuscript has been read and accepted for the Graduate Faculty in Physics in satisfaction of the dissertation requirement for the degree of Doctor of Philosophy.

2/2/94
Date

Robert Alfano
Chairman of Examining Committee

2/3/94
Date

Edward K. Ivon
Executive Officer

Dr. W. Cai

Dr. J. Gersten

Dr. R. Marino

Dr. R. J. Seymour

Dr. K. Shum

Dr. F. W. Smith

Supervisory Committee

The City University of New York.

ABSTRACT

Electron Spin Polarization and Relaxation in GaAs and GaAs/$Al_xGa_{1-x}As$ Quantum Wells

by

Hsieh Shin Chao

Advisor: Professor Robert R. Alfano

In this thesis, I have investigated the spin relaxation mechanism and the operating momentum relaxation scattering mechanism in bulk GaAs and quantum wells by time resolved luminescence measurements.

The determinations of these two relaxation mechanisms were made from the comparisons between measurements and theoretical calculations of several parameters including temperature, carrier density, and carrier energy. In these calculations, special attention was paid to the density of states because of the dimensionality change when dimensionality changes. It turned out that all results from measurements involving different parameters lead to the same conclusions for the spin relaxation mechanism and momentum relaxation mechanism.

The effective spin relaxation mechanism was observed to be independent of the dimensionality but it is temperature dependent. At high temperatures (T>80K), the D'yakonov-Perel' mechanism is effective while at low temperatures (T<80K), the Bir-Aronov-Pikus mechanism is effective. The operating momentum relaxation scattering was determined to be the acoustic phonon scattering.

Acknowledgments

I would like to thank my advisor Dr. Robert R. Alfano for his guidance and support that made such unique disciplinary research possible. My gratitude also goes to Dr. L. J. Sham, Dr. Nate Ockman, and Dr. Wei Cai for their helpful discussion and suggestions. I want to thank Dr. H. Morkoc for providing quantum wells samples and Dr. Y. Takiguchi and Mr. M. Cavicchia for technical assistance. I also want to thank Ms Megan for her excellent secretarial service and Mr. H. C. Gi for the kindness of allowing me the access to his personal computer on which most of the typing of this thesis was done.

Without the support and patience from my wife, the work of this thesis would have been much harder. Two years ago, she was diagnosed with breast cancer and had multi-operation surgery. Right after she was out of hospital she insisted on leaving me for home in order to provide me with a decent study environment in which I could concentrate while working on this thesis. Also, I am greatly indebted to the Physics faculty at CCNY, especially to Prof. M. Lax, Prof. M. Sarachik, and Prof. V. Chung. They provided me with the medical insurance when my original insurance was terminated for unknown reason and my wife was still in the hospital.

Because of their help, I gained a little space to take a breath at that desperate moment. It would have been impossible for me to deal with the huge medical bill without their help.

At last, great appreciation goes to my parents. Even though they are not able to see the completion of my studies today, their encouragement motivated my advanced education. My mother and father died in 1984 and 1987, respectively, while I was in the middle of this research. This thesis is dedicated to them.

Table of Contents

Lists of Tables

List of Figures

CHAPTER ONE

INTRODUCTION

1.1 Background

"Spin" is one of the fundamental characteristics of electrons. A spin polarized electron source is already being widely used in a number of experiments in high energy physics and low energy diffraction in solid state and atomic physics. However, little work on spin polarization and relaxation has been done in a two dimensional (2D) quantum confined system. Dimensionality reduction from 3D to 2D varies not only the density of states but also the electronic band structure - the degeneracy of heavy hole and light hole at Γ is lifted. It is possible that the variation might introduce new physics into the spin dynamics. This is what motivated the research.

The idea for this investigation comes from the fact that polarized optical information can be transferred from the exciting light source to the excited semiconductor material when polarized photons are absorbed, their momenta are transferred to the medium creating a specific orientation regarding the angular or linear momentum of the electrons in degenerate states. This is so called "optical orientation". Electron spin orientation is a direct consequence of angular momentum conservation.

The semiconductor material becomes a transient magnet in the spin polarization point of view. The oriented electrons can not hold the

orientation for too long because the subsequent scattering dephases their orientation in the course of energy relaxation. There are several proposed spin dephasing mechanisms which will be discussed in the section on spin depolarization in Chapter 2. At recombination, the polarized luminescence can be observed if the spin polarization still exists.

The orientation of electron spin can be detected by measuring the luminescence which is also polarized. In the case of electron spin orientation, optical excitation with right hand circular (RHC) (or left hand circular (LHC)) polarization results in a photoluminescence containing both polarizations, RHC and LHC, however the intensities of two polarized luminescence are different not only having different intensities but having different temporal profiles.

The process of electron spin orientation is schematically described in Figure 1-1, 1-2, and 1-3 for sequential cases which happens before excitation, orientation formation, and spin relaxation, respectively.

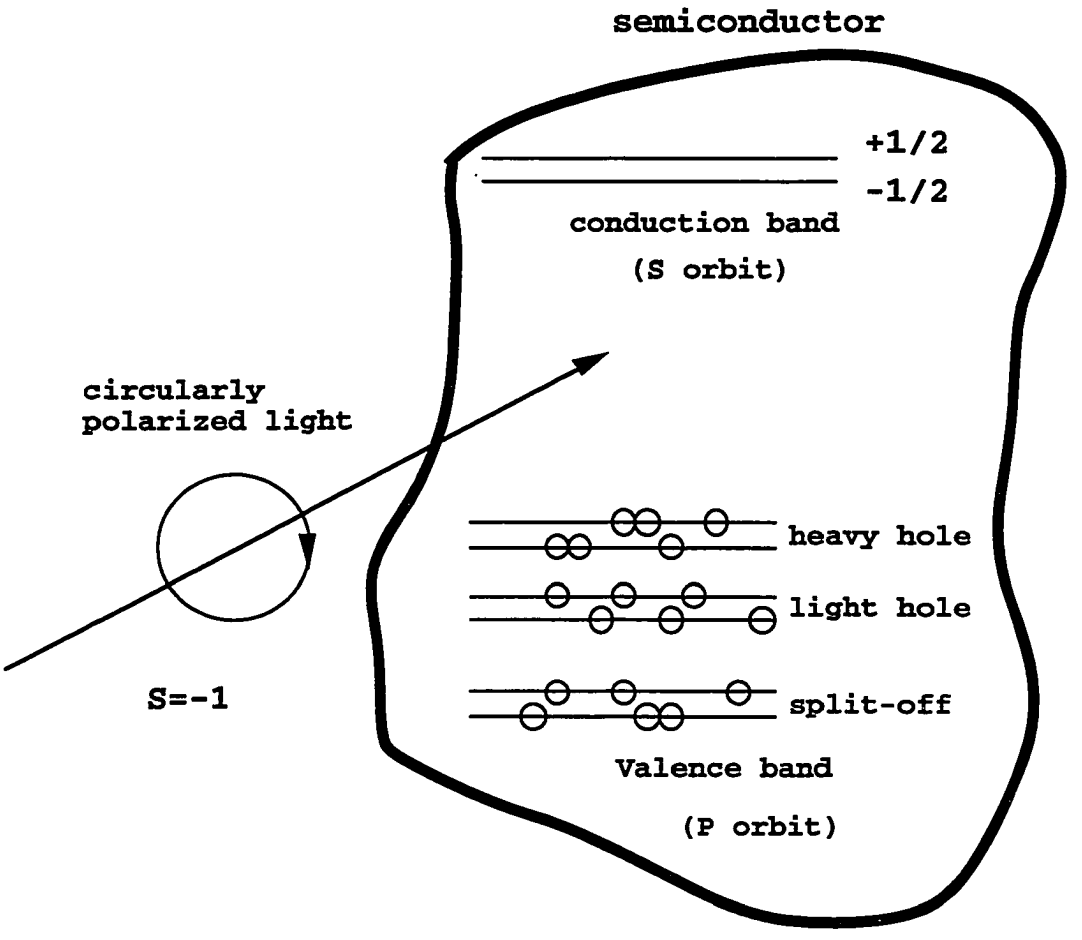

Figure 1-1. At $t = 0$, before the light interacts with the solid, electrons are all in the valence band without orientation.

Before excitation (Fig. 1-1) or at the moment of excitation, there are no electron in the conduction band. All the electrons are in the valence band with an even distribution in spin-up and spin-down states. The polarization of the optical excitation is chosen to be RHC. The photon's angular momentum is -1.

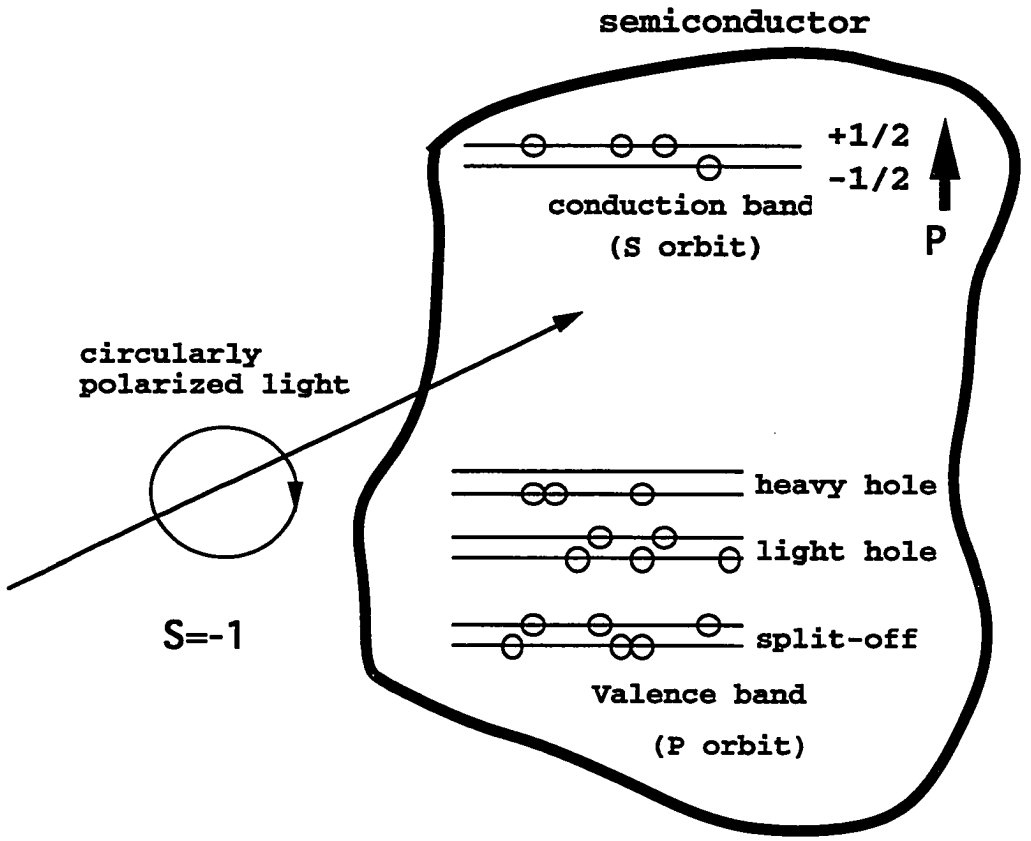

Figure 1-2. At $t > 0$, the optical polarization is transferred to the material creating spin orientation in the conduction band

After excitation (Fig. 1-2), the electrons are placed into the conduction band. The conduction band has two spin states. The energy splitting between them is very small. Due to unequal transition possibilities (selection rules) to these spin states from heavy hole and light hole bands in the valence band, the electron spin populations are different in spin-up and spin-down states resulting a net internal magnetic field

$M = \sum_i m_i$ where $m_i = +\frac{e\hbar}{2m_e c}$ or $-\frac{e\hbar}{2m_e c}$ is the electron magnetic moment.

The semiconductor is similar to a transient magnet.

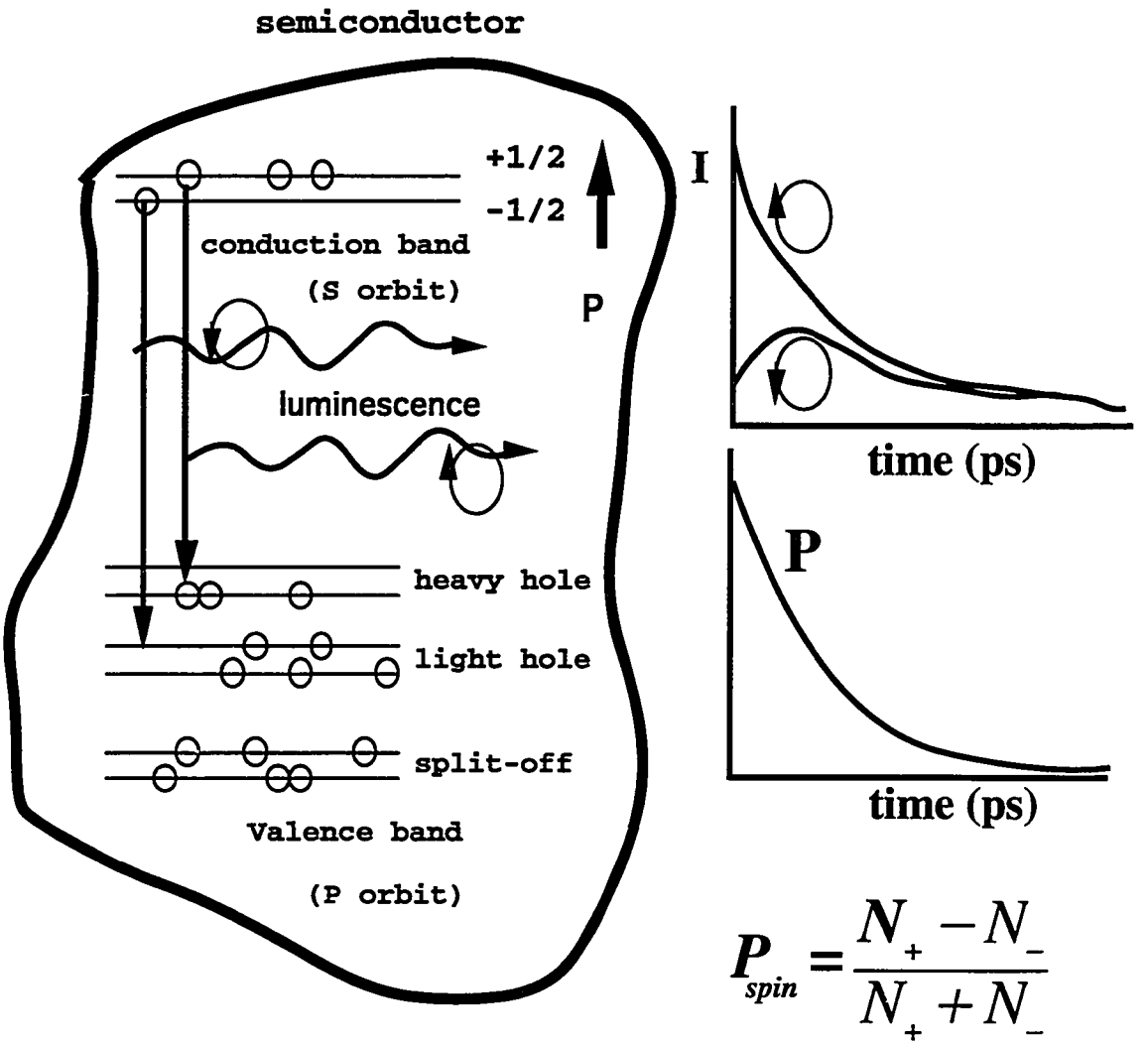

Figure 1-3. At recombination, electrons return to the valence band by emitting circularly polarized luminescence

In Fig. 1-3, the luminescence at recombination has two polarized components (S=+1, -1). They have different intensities levels and temporal profiles. The polarization is defined as $P = \frac{I_+ - I_-}{I_+ + I_-}$ where I_+ and I_- are the intensities of LHC and LHC components, respectively, of the luminescence.

1.2 History

In the early 1920's, the work on optical orientation was pioneered by Wood and Hanle[1, 2]. They observed the effect of a weak magnetic field on the polarization of the resonance fluorescence of mercury and sodium vapor. The importance of this work was not realized until 1949 when Brossel and Kastler[3] initiated a systematic investigation of this phenomenon and started a new research branch which we now call "optical pumping". The main outcome of the investigations of polarizing the different monochromatic radiation of mercury atom by Kastler and his coworkers was gaining a clear understanding and practical implementation of the fact that optical excitation results in a different population of degenerate or nearly degenerate sublevels which belong to levels coupled through a regular transition by optical excitation.

As an investigative tool, photoelectron spectroscopy turned out to be a powerful method for exploring the electronic structure of solids. The determination of the electronic energy bands E(**k**) is one of its successes. Much necessary information is obtained from the primary photoexcited electrons. However, not much attention is paid to the internal degree of

freedom of the electron "the spin" thereby failing to give a complete description of the state of the photoelectrons. The measurement of electron spin orientation with respect to a suitably chosen quantization direction can provide new insight into the electronic structure of a solid.

From the electron spectroscopic point of view a clear advantage of introducing the spin polarization in photoemission is the fact that electrons can be experimentally labeled by an additional quantity besides energy and momentum. In the investigation of semiconductor material structures involving degenerate bands or nearly degenerate bands it is difficult to identify the initial and final states of a transition without considering the factor of spin. However, with the additional information provided by the spin, the problem can be unambiguously simplified because the transitions from neighboring bands produce polarizations of opposite sign.

Electron spin polarization for a given transition depends on the symmetry of the wave functions involved. Apart from hybridization, it is independent of the form of crystal potential and the band parameters. For all the III-V zincblende semiconductor compounds, the direct-gap transition at Γ-point produces the same electron spin spectroscopy. GaAs is a special representative among them.

In 1968, Lampel and Fishman[4] proposed the optical approach to experimentally investigate spin relaxation of photogenerated electrons in semiconductors by using circularly polarized optical pumping technique by steady state measurements. In 1977, Fishman and Lampel[5] calculated the possible spin dephasing channels i.e. 1) the splitting of conduction band, 2) the spin-orbital interaction, 3) the hyperfine interaction with

nuclei of the host crystal and 4) the exchange interaction between electrons and holes. They also demonstrated experimentally the electron alignment in solids using circularly polarized light.

For crystals with zinc-blende structure, like GaAs, the selection rules specify that for the transition from the valence band maximum Γ_8 to the conduction band minimum Γ_6, three times as many electrons are excited to the preferred spin state as those to the antipreferred state depending on the exciting photon polarization. The time resolved polarization P of the photoemitted electrons depends on the initial polarization P_0 of the electrons in the conduction band and on all of the depolarizing processes[6-8] (scattering with phonons, impurities and other carriers or the precessional motion due to a internal pseudo-magnetic field or the exchange of spin states between electrons and holes) that take place before electrons recombine with holes. The initial polarization of the photoluminescence is the result of the optical orientation which occurs in the photoexcitation and thermalization processes.

Most of the theories for electron spin alignment and relaxation were developed in the 60's and 70's using steady state approaches. The experiments started in the 70's. Some researchers have done a great deal in this field. Among them, Ekimov and Safarov[9,10] (1971) measured the degree of spin polarization P (%) as a function of photoexcitation energy for p type GaAs with different doping concentration N_A Fishman and Lampel[5] (1977) also measured P (%) as a function of photoexcitation energy for p type GaAs with $N_A = 4 \times 10^{18}\, cm^{-3}$ at different temperatures combined with applied magnetic field. They also measured the spin

relaxation time as a function of temperature. They observed that the spin relaxation time τ_s is between $60ps$ and $350ps$ and $\tau_s \sim T^{-1/2}$. They also found that the spin exchange splitting of the $1s$ exciton $\Delta_{x,1s} \approx 0.1meV$ and the spin depolarization at high kinetic energy $(200-300meV)$ can be explained by the splitting of the conduction band.

A new experimental era using time-resolved photoluminescence technique was pioneered by Seymour and Alfano[11] in 1980. They first measured spin relaxation time using the temporal profile of the luminescence. This direct observation of spin relaxation makes the investigation more reliable and accurate. Later they measured the spin relaxation time[12] as a function of photogenerated e-h density ($N = 5\times10^{17}$ to 10^{19} cm^{-3}) for p type GaAs with different doping concentration ($N_A = 6\times10^{16}$ to $1.1\times10^{18}cm^{-3}$) by using short laser pulse excitation. They showed that $\tau_s \sim N^{-0.63}$. K. Zarrouati et. al[13]. (1987) measured the spin relaxation time as a function of temperature of p doped GaAs ($N_A = 10^{16}$ to $10^{19}cm^{-3}$). They discovered a categorization for the predominate spin relaxation mechanisms under different conditions. The conclusion was that at low temperature and high doping concentration, the Bir-Aronov-Pikus (BAP) spin exchange mechanism is important while at high temperature and low doping concentration, the D'yakonov-Perel' (DP) conduction band splitting interaction mechanism is important. Generally speaking, the spin relaxation time τ_s decreases as the temperature increases. Spin polarization (%) decreases as the exciting photon energy increases. When a magnetic field is applied, the polarization (%) decreases with increasing **B** field. As for the doping

concentration N_A, it seems that τ_s is short for concentrated electrons (heavily doped or photogenerated).

H. Chao[14], the author of this thesis, first measured the spin relaxation time of GaAs quantum wells in 1988 and found that τ_s in quantum wells is much shorter than that in bulk material. D. D. Awschalom et al. have done some measurements on dilute magnetic semiconductor $Cd_{1-x}Mn_xTe$ quantum wells manifesting magnetic carriers confined in the quantum well and showing the inability of 2D system to support the long-range spin-glass order. They also found a multi component decay process with the initial component extremely fast ($\sim 1ps$). Most recently, T. C. Damen[15] (1991) measured the spin relaxation time of electrons, holes and excitons in quantum wells by using p-doped, n-doped and undoped GaAs/AlGaAs at low excitation intensity. They proved the theoretical prediction made by L. J. Sham[16] of incomplete hole spin relaxation in quantum wells and showed that the hole spin relaxation time in GaAs wells was around 4 ps. The information of the previous research are briefly summarized in Table 1-I.

Table of spin relaxation time measured in the past

	τ_s	Samples	References
Fisherman & Lampel	500 - 50 ps (2K -80K)	p doped bulk GaAs ($4 \times 10^{18} cm^{-3}$)	1. G. Lampel, Phys. Rev. Lett. 64, p.491 (1968) 2. G. Fishman and G. Lampel, Phys. Rev. B 16 p.820 (1977)
Seymour & Alfano	50 ps 80K	p doped bulk GaAs ($7 \times 10^{17} cm^{-3}$)	R. J. Seymour and R. R. Alfano, Appl. Phys. Lett. 37(2) p.231 (1980)
Chao & Alfano	< 50 ps	undoped GaAs/GaAlAs q. w. 55Å, 90Å, at low T (20K) high photo-carrier density ($10^{19} cm^{-3}$)	H. Chao, K. S. Wong, R. E. Alfano, Unlu and Morkoc, J. SPIE 942 p.215 (1988)
Zarrouati et. al.	10 ns to 100 ps (τ_s measured as functions of T and n_p)	p doped bulk GaAs (10^{16} - $3 \times 10^{18} cm^{-3}$)	K. Zerrouati, F. Fabre, G. Bacquet, J. Bandet, J. Frandon and G. Lampel, D. Paget, Phys. Rev. B 37(3) p.1334 (1987)
Damen et. al.	$\tau_s(e)$ = 150 ps $\tau_s(h)$ = 4 ps $\tau_s(x)$ = 50 -150 ps (0.2 - 50mW)	p doped GaAs/GaAlAs q. w. n doped GaAs/GaAlAs q. w. intrinsic GaAs/GaAlAs q. w. Low photo-carrier density ($10^{11} cm^{-2}$)	1. T. C. Damen, Karl Leo, Jagdeep Shah and J. E. Cunningham, Appl. Phys. Lett. 58(17) p.1902 (1991) 2. T. C. Damen, Luis Vina, J. E. Cunningham and Jagdeep Shah, Phys. Rev. Lett. 67(24) p.3432 (1991)

Table I-1 Table of the past work on spin

1.3 Thesis statement

The objective of this thesis is to investigate which factors are introduced into the spin dynamics of electrons while their degree of freedom is reduced from 3D to quasi-2D. The approach of the investigation is to study the dependence of spin relaxation time on temperature, carrier energy, and photogenerated carrier concentration in 2D and 3D GaAs using circularly polarized optical pumping and time resolved photo-luminescence measurement by a synchroscan streak camera system.

The physics questions which are of importance in this study are as follows:

1. Does the dimensionality variation cause the spin depolarization mechanism to change ?

2. What physical parameters cause the degree of the spin polarization to change ?

3. How does the spin relaxation rate change with the reduction of degree of freedom (3D to 2D)?

4. What is the most effective scattering mechanism causing carrier momentum relaxation ?

5. What is the temperature dependence on the spin relaxation dynamics of 2D systems ?

6. What is the effect of the carrier density on the spin relaxation dynamics ?

1.4 Applications of spin polarized carriers (SPC)

The method of optical orientation combined with the optical detection of polarized electron-hole carriers and excitons provides a possibility to measure band structure parameters with extremely high precision, and to study picosecond/subpicosecond-scale processes occurring in a system of free carriers and excitons. Optical orientation studies have led to the development of a very sensitive method for the optical detection of magnetic resonance. This permits one to observe resonance in very thin epitaxial semiconducting films. It also provides experimentalists with a very efficient source of polarized electrons.

The polarized electron beams can be applied in various fields such as atomic, solid state and high-energy physics. The discovery of optical spin orientation, a new label of states, has allowed us to experimentally determine the hybridization of energy bands which is an important property of the electronic states, but is impossible to derive from simple energy-and-angle photoemission. This might be the most significant application of optical spin orientation in academic applications. SPC also can be applied in the field of communication and computation playing the role of message carrier. Electron spin system is a binary (bi-level) system which is similar to (1, 0) or (high, low) signals but it provides a faster processing capability, therefore it may be important in developing new

communication and optical computation devices with smaller size and shorter response times.

As far as the optical memory device is concerned, spin is the smallest unit indicating the magnetic property of the material. The Ising model of spin glasses states that there are two spin ground states separated by a barrier. These two lowest energy states correspond to two opposite spin states. The height of the energy barrier determines the memorizing period (stability) of the material. Generally speaking, the memorizing period is in the time domain of hundreds of years.

So, the spin polarized signal is very useful in implementing the new generation of communication and computation devices because all the binary signals can eventually be replaced by SPC. Furthermore, the present electron-based system has a limit on the size, for example, 0.1 micron of diameter is considered as the limit of the operating chips because of the complexity.

From a recent research report[17], SPC can be built in a chip with the dimension reduced 1000 times from the limit (0.1 micron). This allows the operating time to be 1000 times shorter. "The 21st century could run on spin polarization..... It could be the answer to the diminishing-size dilemma of semiconductors", said Dr. Gary A. Prinz, a solid-state physicist at the Naval Research Laboratory in Washington D. C.; and "Spin could be the basis for a new generation of devices...." said Dr. David D. Awschalom, a physicist at the University of California at Santa Barbara are the best words to describe the importance of spin polarization in the future.

Dr. Mark Johnson, a physicist at Bellcore, devised a *spin transistor*[17] of conductive metals. His world's first demonstration of spin injection showed that the highly structured magnetism was mobil in a new and unforeseen way. He found that the spins of electrons in an electric current were ordered, or polarized, as they passed through a magnetic film and the polarization was kept when the current was carried into non magnetic material. His experimental results have shown very interesting phenomena that the smaller the size, the more efficiently it works.

1.5 Organization of thesis

This thesis is organized into eight chapters. In Chapter 1, general information is provided including background, previous research results, thesis statement, and the major applications of spin dynamics.

In Chapter 2, theories about the spin polarization formation and dephasing mechanisms will be described. In the first section brief information about GaAs band structure is provided. The second section is on spin polarization. In this section, the selection rules, transition probabilities, and the relation between initial degree of spin polarization and carrier thermalization are covered. Spin depolarization is discussed in section [2.3] where three proposed major relaxation mechanisms (DP, EY, and BAP) are discussed. The mathematical equations for each mechanism are also presented in this section. A brief discussion of scattering, the major factor causing spin and momentum relaxation, is discussed first in the section. It leads to the idea of a determination of the effective carrier

momentum relaxation scattering mechanism from the measurement of spin relaxation time. The spin relaxation rate equations, from which the spin relaxation time constant is obtained, are derived in the [2.4]. The theoretical calculation on the temperature and carrier concentration dependence of spin relaxation time in 2D and 3D are presented in [2.6]. The variation of photogenerated carrier density between 3D and 2D systems is in [2.7].

General information relevant to experiments is collected in Chapter 3. It includes experimental setups, data analysis strategy, samples used in this research project, and some preliminary testing results.

In Chapters 4, the most effective scattering mechanism responsible for the carrier momentum relaxation is determined to be the acoustic phonon scattering from the temperature dependent data through a new approach. This conclusion is consistent with the results of both the carrier energy dependence and carrier concentration dependence data presented in Chapter 5 and Chapter 6, respectively.

The details of the characteristics of the temperature dependence of the spin relaxation time in bulk and quantum wells were discussed and compared in Chapter 7. Chapter 8 concludes the thesis by making some suggestions for future work.

1.6 References

1. W. Happer, ***Rev. Mod. Phys. 44 169*** (1972)

2. E. B. Aleksandrov, ***Sov. Phys. Usp 15 436*** (1973)

3. A. Kastler, ***Science 158 214*** (1967)

4. G. Lampel, ***Phys. Rev. Lett. 64, 491*** (1968)

5. G. Fishman and G. Lampel, ***Phys. Rev. B 16 820*** (1977)

6. M. I. D'yakonov and V. I. Perel, ***Sov. Phys. JETP 38, 177*** (1974)

7. Y. Yafet, ***Solid State Phys. 15, 371*** (1963)

8. G. L. Bir, A. G. Aronov, and G. E. Pikus, ***Sov. Phys. JETP 42, 705*** (1976)

9. A. I. Ekimov and V. I. Safarov, ***Zh. Eksp. Teor. Fiz. Pis'ma 13 251*** (1971)

10. A. I. Ekimov and V. I. Safarov, ***Zh. Eksp. Teor. Fiz. Pis'ma 13 700*** (1971)

11. R. J. Seymour and R. R. Alfano, ***Appl. Phys. Lett. 37(2) 231*** (1980)

12. R. J. Seymour, M. R. Junnarkar, and R. R. Alfano, ***Phys. Rev. B 24 3623*** (1981)

13. K. Zerrouati, F. Fabre, G. Bacquet, J. Bandet, J. Frandon and G. Lampel, D. Paget, ***Phys. Rev. B 37(3) 1334*** (1987)

14. H. Chao, K. S. Wong, R. E. Alfano, Unlu and Morkoc, ***J. SPIE 942 215*** (1988)

15. T. C. Damen, Karl Leo, Jagdeep Shah and J. E. Cunningham, ***Appl. Phys. Lett. 58(17) 1902*** (1991)

16. T. Uenoyama and L. J. Sham, ***Phys. Rev. Lett. 64(25) 3070*** (1989)

17. Mark Johnson, ***Science 260 320*** (1993)

CHAPTER TWO

THEORY

2.1 Band structure

To understand the nature of semiconductors one must consider what happens when similar atoms are brought together to form a solid such as a crystal. As two similar atoms approach each other the wave functions of the electrons begin to overlap. To satisfy Pauli's exclusion principle, the states of all spin-paired electrons acquire energies which are slightly different from their values in the isolated atom. Thus if N atoms are packed within a range of interaction what really exists is a band of states instead of a discrete level as in the isolated atom. The energy distribution of the states depends strongly on the inter atomic distance. It is illustrated in Figure 2-1 for an assemblage of carbon atoms. As a result of state mixing, the energy of electrons are distributed in two energy bands. It should be noted that the higher energy (2P) band sometimes merges with the lower energy band (2S) for long inter atomic distance. However, at the actual lattice constant, two bands are separated by an energy gap. In the gap, there are no allowed states. The lower band, which is normally completely filled with electrons, is called the valence band. The upper band, which contains no electrons, is called the

conduction band. If an electron were placed in this band, it can acquire a net drift under the influence of an electric field.

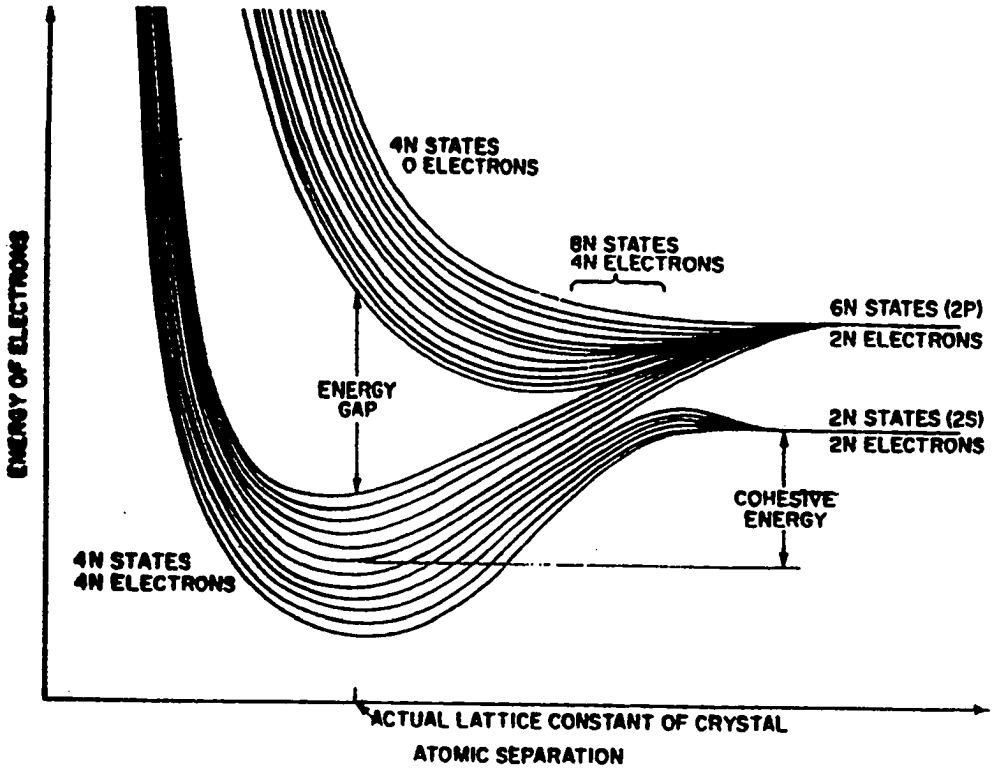

Figure 2-1. Energy banding of allowed levels in diamond as a function of spacing between atoms

It is the size of the energy gap and the relative availability of electrons that determine whether a solid is metal, semiconductor, or insulator. For semiconductors, the energy gap usually extends over less than 3 eV and the density of electrons in the upper band (or of holes in the lower band) is usually less than $10^{20}cm^{-3}$. By contrast, in a metal the upper band is populated with electrons far above the energy gap and the electron concentration is of the order of $10^{23}cm^{-3}$. Insulators, on the other hand, have a large energy gap, usually greater than 3 eV, and have a

negligible electron concentration in the upper band (and practically no holes in the lower band).

GaAs is direct-gap material in which the bottom of the conduction band and the top of the valence band are located at the center of the Brillouin zone (Γ-point)[1,2]. The energy band structure of GaAs is drawn in Fig. 2-2.

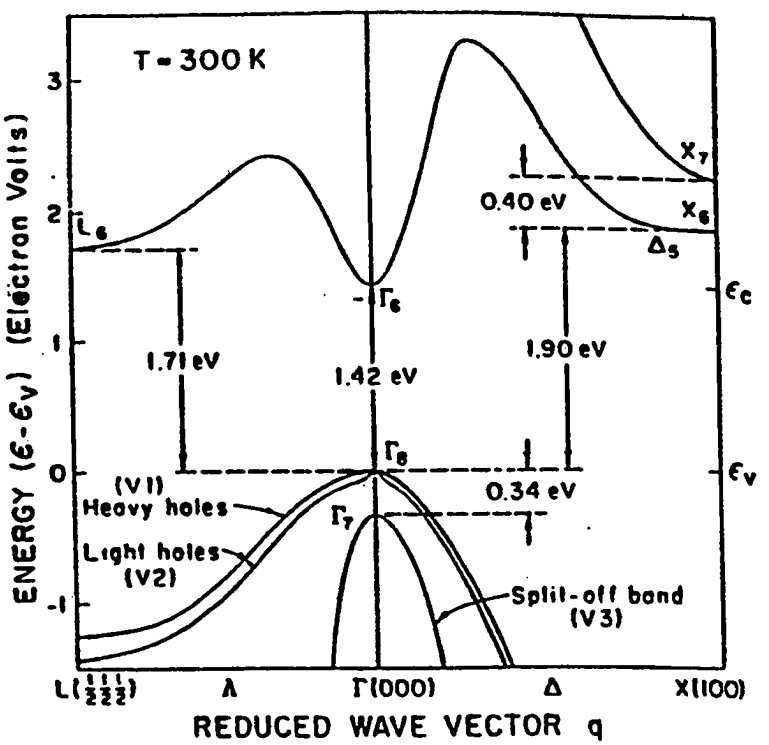

Figure 2-2. In GaAs, variation of energy with wave vector for the uppermost part of the valence band system and for the lowest sets of conduction band minima. Energy gaps at room temperature are shown in the diagram.

This chapter starts with the discussion of the band structure of the semiconductor samples. The eigen functions and the energies of electrons

with electron spin taken into account will be presented for conduction band, heavy hole valence band, light hole valence band, and split-off valence band. Then the selection rules which creates the spin polarization are provided. The effect on the degree of spin polarization from carrier thermalization will also be discussed. Carrier spin relaxation mechanisms are listed and briefly described in the next section.

The rate equation governing the spin evolution will be related to the experimental strategy -- ultrafast pulse excitation combined with time resolved luminescence measurement by a streak camera. It is necessary to say a few words about scattering in the last section because it is the major effect causing spin relaxation.

2.1.1 Conduction band

The electron state in the conduction band can be described by[3]

$$\Psi_{k,m} = u_m \exp(i\vec{k}\cdot\vec{r}), \qquad m = \pm\frac{1}{2} \tag{2.1}$$

where the Bloch amplitude $u_{\pm 1/2}$ correspond to the different spin states:

$$u_{+1/2} = S\uparrow, \qquad u_{-1/2} = S\downarrow \tag{2.2}$$

Here S denotes the coordinate part of the S-type Bloch amplitude which is invariant under symmetry transformations of the crystal. Figure 2-3 shows the S wave electron distribution. Near the Γ-point the energy can be expressed in terms of momentum $\vec{k}$ and effective mass m_e as

$$E_c(\vec{k}) = \frac{\hbar^2 k^2}{2m_e} \tag{2.3}$$

where $\hbar = h/2\pi$, h is Plank's constant.

The Hamiltonian of electron in conduction band[4] can be written as

$$H = \frac{\hbar^2 k^2}{2m_e} + \frac{\hbar}{2}\sigma \cdot \Omega(\vec{k}) \tag{2.4}$$

where σ is the Pauli matrix and $\Omega(\vec{k})$ is a vector whose magnitude is proportional to k^3. The X component of Ω can be written as

$$\Omega_x(\vec{k}) = \alpha\hbar^2 (m_e\sqrt{2m_eE_g})^{-1} k_x(k_y{}^2 - k_z{}^2) \tag{2.5}$$

where α is a dimensionless coefficient indicating the intensity of spin splitting, for GaAs, $\alpha = 6\times 10^{-2}$. The k^3 term in Eq. (2.5) is due to the absence of an inversion center which, obviously, can be treated as an effective magnetic field acting on the electron spin and the magnitude of this interaction is a function of momentum $\vec{k}$. It is obvious that the vector Ω is always perpendicular to $\vec{k}$.

2.1.2 Heavy hole and light hole band

The wave function of electrons near the top of the valence band can be written as

$$\Psi_{k,m} = e^{i\vec{k}\cdot\vec{r}} \sum_{\mu} \left(\chi_{m,\mu}(\vec{k}) u_{\mu}^{3/2} \right), \quad m = \pm\frac{1}{2}, \ \pm\frac{3}{2} \tag{2.6}$$

where m is the z-component of angular momentum $j = 3/2$. $m = \pm 3/2$ represent heavy hole band (hh), and $m = \pm 1/2$ represent the light hole band (lh). The explicit formulae for the Bloch amplitudes can be given as

$$u^{3/2}_{+3/2} = -\frac{\sqrt{2}}{2}(X + iY)\uparrow$$

$$u^{3/2}_{-3/2} = +\frac{\sqrt{2}}{2}(X + iY)\downarrow$$

$$u^{3/2}_{+1/2} = -\frac{\sqrt{3}}{3}[\frac{\sqrt{2}}{2}(X + iY)\downarrow + \sqrt{2}Z\uparrow]$$

$$u^{3/2}_{-1/2} = +\frac{\sqrt{3}}{3}[\frac{\sqrt{2}}{2}(X - iY)\uparrow + \sqrt{2}Z\downarrow] \qquad (2.7)$$

Here X, Y, and Z are the p-type coordinate part of the Bloch amplitudes which transform as coordinates X, Y, and Z. Figure 2-3 shows the P wave electron distribution.

The energy and the coefficient $\chi_{m,\mu}$ are obtained by solving the equation

$$H\chi_m = \varepsilon_\mu \chi_m \qquad (2.8)$$

where χ_m is a column matrix of coefficients $\chi_{m,\mu}$. H is the Hamiltonian of Eq. (2.4). For simplicity the spherical approximation, proposed by Luttinger in 1956[5], is often applied by neglecting the warping of the constant energy surfaces. Luttinger's Hamiltonian can be expressed as

$$H = \frac{\hbar^2}{2m_o}(\gamma_1 + \frac{5}{2}\gamma)k^2 - \frac{\hbar^2}{m_o}\gamma(\vec{k}\cdot\boldsymbol{J})^2,$$

$$\gamma = (2\gamma_2 + 3\gamma_3)/5 \qquad (2.9)$$

where γ_1, γ_2, γ_3 are Luttinger's parameters, and j_x, j_y, j_z are 4x4 matrices corresponding to the angular momentum. Under this approximation the energy of the heavy holes and the light holes are isotropic and they are given by

$$\varepsilon_{\pm 3/2} = \hbar^2 k^2 / m_{hh}, \quad \varepsilon_{\pm 1/2} = \hbar^2 k^2 / m_{lh} \tag{2.10}$$

where m_{hh}, m_{lh} are the effective masses of heavy hole and light hole respectively.

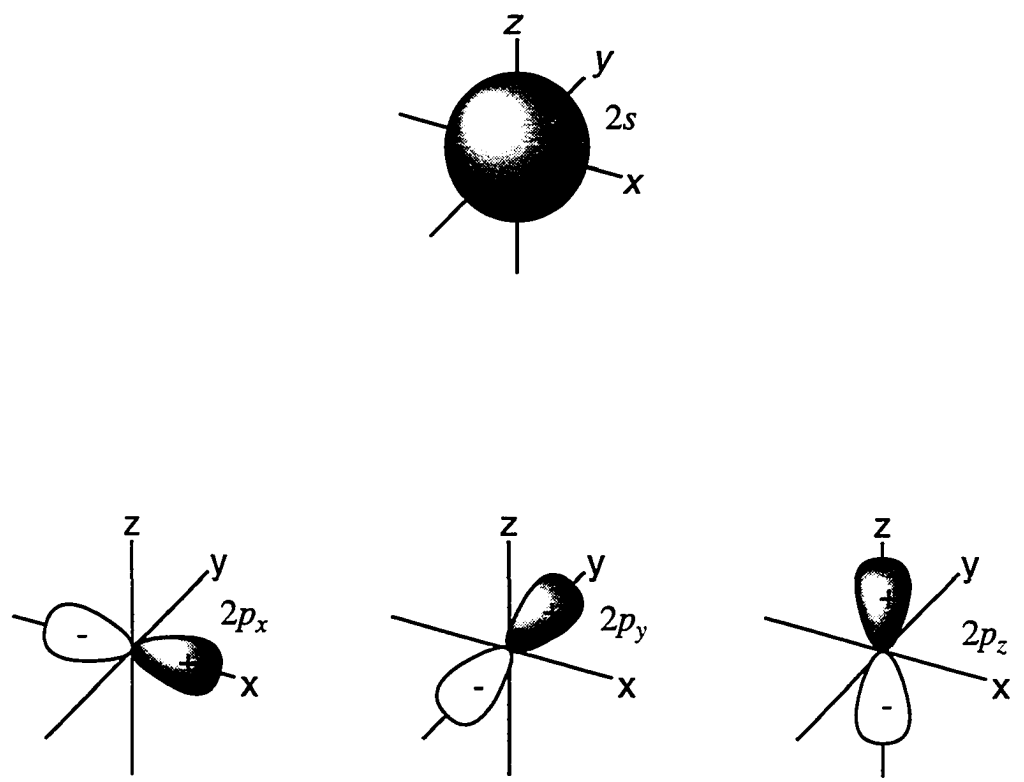

Figure 2-3. Spatial distribution of electrons of s- function and p-function (X, Y, Z).

The coefficient $\chi_{m,\mu}(\vec{k})$ is now the function of $\vec{k}$ only. It can be rewritten as

$$\chi_{m,\mu} = D^{3/2}_{m,\mu}(\theta, \varphi, \phi) \tag{2.11}$$

where θ and φ are the polar angles of $\vec{k}$ and ϕ is the arbitrary phase of the wave function.

2.1.3 Split-off band

By spherical approximation, the wave function of electron in the split-off (Δ) band is analogous to Eq. (2.6) and it can be expressed as

$$\Psi_{k,m} = e^{i\vec{k}\cdot\vec{r}} \sum_{\mu} \left(D^{1/2}_{m,\mu}(\theta, \varphi, \phi) u^{1/2}_{\mu} \right) \tag{2.12}$$

where $m = \pm\frac{1}{2}$ are the projection of the angular momentum on the direction of $\vec{k}$. The eigenfunctions can be expressed as

$$u^{1/2}_{+1/2} = -\frac{\sqrt{3}}{3}[(X + iY)\downarrow + Z\uparrow]$$

$$u^{1/2}_{-1/2} = +\frac{\sqrt{3}}{3}[-(X - iY)\uparrow + Z\downarrow] \tag{2.13}$$

As the energy increases to a level comparable to the spin-orbit splitting, Δ, mixing of the light hole band and the split-off band occurs[7] and then nonparabolicity of light hole band will be observed. This is beyond the subject of spin dynamics and will not be discussed further here.

The wave functions of the different states are summarized and listed below:

Conduction band

$$\left|c,\ \frac{1}{2},+\frac{1}{2}\right\rangle=\left|S\uparrow\right\rangle \qquad \left|c,\ \frac{1}{2},-\frac{1}{2}\right\rangle=\left|S\downarrow\right\rangle$$

Heavy hole

$$\left|v,\ \frac{3}{2},+\frac{3}{2}\right\rangle=\left|(1/\sqrt{2})(X+iY)\uparrow\right\rangle$$
$$\left|v,\ \frac{3}{2},-\frac{3}{2}\right\rangle=\left|(1/\sqrt{2})(X-iY)\downarrow\right\rangle$$

Light hole

$$\left|v,\ \frac{3}{2},+\frac{1}{2}\right\rangle=(1/\sqrt{3})\left|(1/\sqrt{2})(X+iY)\downarrow\right\rangle+\sqrt{2/3}\left|Z\uparrow\right\rangle$$

$$\left|v,\ \frac{3}{2},-\frac{1}{2}\right\rangle=(1/\sqrt{3})\left|(1/\sqrt{2})(X-iY)\uparrow\right\rangle+\sqrt{2/3}\left|Z\downarrow\right\rangle$$

Split-off

$$\left|\Delta,\ \frac{1}{2},+\frac{1}{2}\right\rangle=(\sqrt{2/3})\left|(1/\sqrt{2})(X+iY)\downarrow\right\rangle-1/\sqrt{3}\left|Z\uparrow\right\rangle$$

$$\left|\Delta,\ \frac{1}{2},-\frac{1}{2}\right\rangle=(\sqrt{2/3})\left|(1/\sqrt{2})(X-iY)\uparrow\right\rangle-1/\sqrt{3}\left|Z\downarrow\right\rangle$$

where $i=\sqrt{-1}$ was used.

2.2 Selection Rules

For direct interband transitions, there is a correspondence between a quantum transition from state i to state f and a classical dipole with frequency $\omega_{if} = (E_f - E_i)/\hbar$ and the amplitude of the dipole moment is equal to the transition matrix element

$$P_{i,f} = \langle i|P|f\rangle \tag{2.14}$$

where P is the dipole moment operator, i and f stand for initial and final states respectively.

In III-V semiconductors like GaAs, the non-zero transition matrix elements between S-type and p-type wave functions are

$$\begin{aligned} \langle S|P|X\rangle &= p\hat{x} \\ \langle S|P|Y\rangle &= p\hat{y} \\ \langle S|P|Z\rangle &= p\hat{z} \end{aligned} \tag{2.15}$$

and because the two and only two spin states, $|\uparrow\rangle, |\downarrow\rangle$ are orthogonal to each other therefore we also have

$$\langle \uparrow|P|\downarrow\rangle = \langle \downarrow|P|\uparrow\rangle = 0 \tag{2.16}$$

Since the total angular momentum must be conserved, therefore, the transition selects appropriate initial and final states. The initial and final states are determined by the type (polarization) of the excitation, for example,

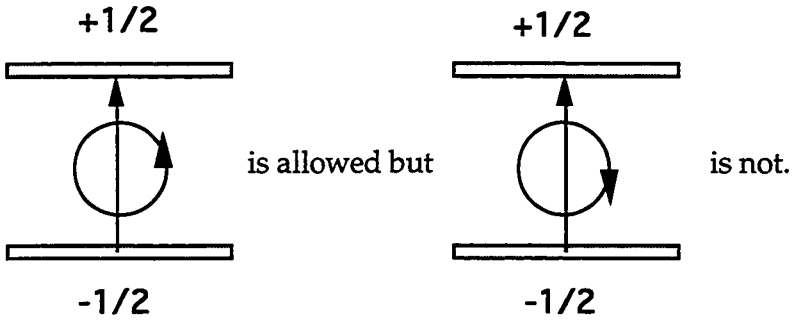

The transition probability associated with each transition can be calculated from the wave functions of the initial and the final states and it is demonstrated in the next section [2.2.1].

2.2.1 The calculation of the transition probability and the determination the type of the dipole moment associated with the transition

Three examples of detail calculation of the transition probability and the type of the transition dipole moment were given in Equations (2.17), (2.18), and (2.19) for $\left\langle c,\frac{1}{2},+\frac{1}{2}\middle|P\middle|v,\frac{3}{2},+\frac{3}{2}\right\rangle$, $\left\langle c,\frac{1}{2},-\frac{1}{2}\middle|P\middle|v,\frac{3}{2},-\frac{1}{2}\right\rangle$, and $\left\langle c,\frac{1}{2},+\frac{1}{2}\middle|P\middle|v,\frac{3}{2},-\frac{1}{2}\right\rangle$. The first example is the transition between the spin-up conduction band and the spin-up heavy hole band; the second example is between the spin-down conduction band and the spin-down light hole band. Both transitions have the same initial and final spin states. The third example is the transition between spin-up conduction band and spin-down light hole band. The initial and final spin states of the third example are opposite.

Example 1 Heavy hole (+3/2) to conduction band (+1/2).

$$\left\langle c,\frac{1}{2},+\frac{1}{2}\middle|P\middle|v,\frac{3}{2},+\frac{3}{2}\right\rangle$$
$$=1/\sqrt{2}\,\langle S|P|X\rangle+i\,1/\sqrt{2}\,\langle S|P|Y\rangle=1/\sqrt{2}\,p(\hat{x}+i\hat{y}) \tag{2.17}$$

Example 2 Light hole (-1/2) to conduction band (-1/2).

$$\left\langle c,\frac{1}{2},-\frac{1}{2}\middle|P\middle|v,\frac{3}{2},-\frac{1}{2}\right\rangle=\sqrt{2/3}\langle S|P|Z\rangle=\sqrt{2/3}p(\hat{z}) \tag{2.18}$$

Example 3 Light hole (-1/2) to conduction band (+1/2).

$$\left\langle c,\frac{1}{2},+\frac{1}{2}\middle|P\middle|v,\frac{3}{2},-\frac{1}{2}\right\rangle$$
$$=(1/\sqrt{3})(1/\sqrt{2})\langle S|P|X\rangle-i(1/\sqrt{3})(1/\sqrt{2})\langle S|P|Y\rangle \tag{2.19}$$
$$=1/\sqrt{6}\,p(\hat{x}-i\hat{y})$$

All transitions between the conduction band and the valence bands can be summarized in the list below:

$$\left\langle c,\frac{1}{2},\pm\frac{1}{2}\middle|P\middle|v,\frac{3}{2},\pm\frac{3}{2}\right\rangle=p\frac{1}{\sqrt{2}}(\hat{x}\pm i\hat{y})$$
$$\left\langle c,\frac{1}{2},\pm\frac{1}{2}\middle|P\middle|v,\frac{3}{2},\mp\frac{3}{2}\right\rangle=0$$
$$\left\langle c,\frac{1}{2},\pm\frac{1}{2}\middle|P\middle|v,\frac{3}{2},\pm\frac{1}{2}\right\rangle=p\frac{\sqrt{2}}{\sqrt{3}}\hat{z} \tag{2.20}$$
$$\left\langle c,\frac{1}{2},\pm\frac{1}{2}\middle|P\middle|v,\frac{3}{2},\mp\frac{1}{2}\right\rangle=p\frac{1}{\sqrt{6}}(\hat{x}\mp i\hat{y})$$
$$\left\langle c,\frac{1}{2},\pm\frac{1}{2}\middle|P\middle|\Delta,\frac{1}{2},\pm\frac{1}{2}\right\rangle=-p\frac{1}{\sqrt{3}}\hat{z}$$
$$\left\langle c,\frac{1}{2},\pm\frac{1}{2}\middle|P\middle|\Delta,\frac{1}{2},\mp\frac{1}{2}\right\rangle=p\frac{1}{\sqrt{3}}(\hat{x}\mp i\hat{y})$$

hh-c transitions are represented by two circular dipole moments, clockwise and counterclockwise, rotating in the plane perpendicular to $\hat{k}$. lh-c transitions are represented by two linear dipoles oscillating along the direction of $\hat{k}$ and two circular dipoles rotating in the plane perpendicular to $\hat{k}$. hh-c transitions are similar to lh-c but with the different transition probabilities.

A schematic diagram is plotted in Figure 2-4 to summarize the entire picture of transitions between conduction band and valence band given by Eq. (2.20). In the figure, the pattern overlapped with the transition arrow line is the type of dipole moment, linear or circular, and the number around the pattern is the associated transition probability.

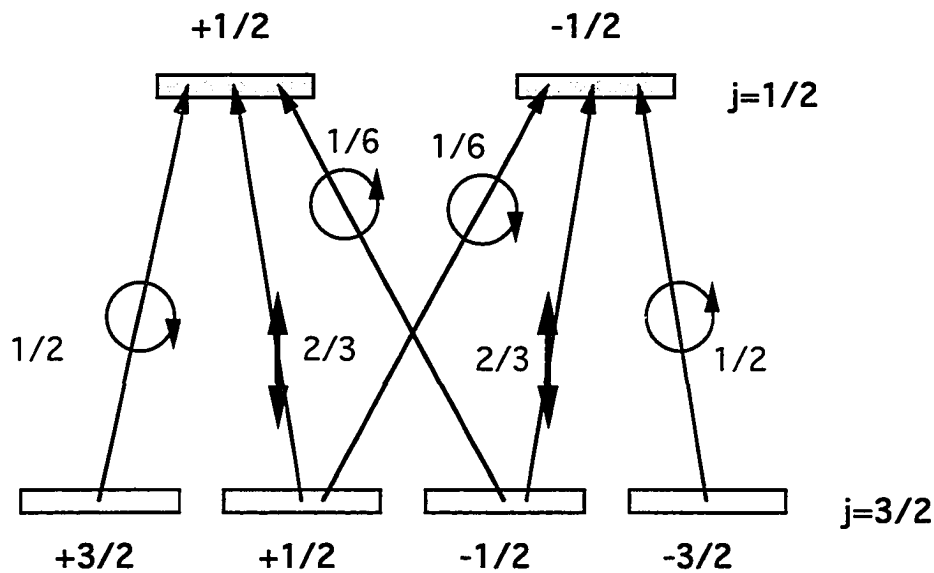

Figure 2-4. Possible transitions between conduction band and valence band.

2.2.2 The calculation of the initial degree of spin polarization

From Figure 2-4, the spin polarization, P_{spin}, of the electrons in the conduction band can be calculated by using $p_{spin} = \frac{N_+ - N_-}{N_+ + N_-}$, where N_+ and N_- are the electron spin population of spin-up and spin-down states, respectively. In the case of an $s = -1$ (s is the phonon's angular momentum) optical excitation, due to the difference of transition probability, it results in $N_+ = 3N_-$. Therefore $p_{spin} = \frac{3-1}{3+1} = 50\%$. For the degree of spin polarization observed in the luminescence, P_{spin} depends on the material. In bulk material, heavy hole and light hole bands are degenerate at the zone center (Γ) therefore the observed spin polarization can be calculated as follows

$$p_{spin}^{bulk} = \frac{[1/2 \cdot 3 + 1 \cdot 1/6] - [3 \cdot 1/6 + 1 \cdot 1/2]}{[1/2 \cdot 3 + 1 \cdot 1/6] + [3 \cdot 1/6 + 1 \cdot 1/2]}$$

$$= \frac{[3/2 + 1/6] - [1/2 + 1/2]}{[3/2 + 1/6] + [1/2 + 1/2]}$$

$$= \frac{4}{16} = 25\%$$

where $[1/2 \cdot 3 + 1 \cdot 1/6]$ and $[3 \cdot 1/6 + 1 \cdot 1/2]$ are the intensities of $s = -1$ and $s = +1$ luminescence. On the other hand, in quantum wells, the degeneracy of is lifted, if the optical pumping of $s = -1$ involved only the heavy hole band, therefore, the spin polarization p_{spin}^{qw} becomes

$$p_{spin}^{qw} = \frac{1/2 - 1/6}{1/2 + 1/6}$$

$$= \frac{2}{4} = 50\%$$

Therefore, the degree of spin polarization can be increased by changing the material structure.

2.3 Spin depolarization mechanisms

The general theory of electron spin relaxation in metals and semiconductors has been developed by Overhauser[8] (1953), Elliott[9] (1954), and Yafet[10] (1963). There are two major groups of explanation for spin relaxation. The first category consists of various magnetic interactions which connect states of opposite spin and directly result in spin change. These magnetic interactions are generally slow and spin flip through these interactions is thought of as the result of spin state admixture. For quick interactions, mixing of opposite spins arises from the spin-orbit interaction of $\vec{k} \cdot \vec{p}$ type and the lifting of Kramer's degeneracy due to the lack of inversion symmetry in the zinc blende structure.

The starting point of the general theory is the assumption that quasi thermal equilibrium is established through scattering (e-e, e-phonon) much faster than the momentum relaxation, energy relaxation, and spin relaxation processes because the e-e scattering and e-phonon scattering times are much shorter than these processes. e-e scattering results in a carrier distribution while the e-phonon scattering is responsible for the energy relaxation.

The electron spin, momentum, and energy relaxation are parallel processes. Among them, momentum and spin relaxation are directly

related through scattering such as acoustic phonon deformation scattering, piezoelectric scattering, ionized impurity scattering, and optical phonon scattering.

By virtue of the fast scattering, three major mechanisms are believed to be responsible for spin relaxation from a phenomenological point of view. The discussion will begin with a general picture of scattering which is the major reason for spin and momentum depolarization.

2.3.1 Scattering[11, 12]

A real crystal is not a perfect crystalline solid and the imperfections impede the free motion of carriers. The imperfections are in the form of crystal defects, foreign impurity atoms, and lattice vibrations. It is the last kind alone that relaxes the carrier energy, although all three kinds relax the carrier momentum. The electron-phonon interaction will be discussed now in detail.

The scattering probability $S(\boldsymbol{k},\boldsymbol{k}')$ from the initial state $(E_k,\vec{k})$ to the final state $(E_{k'},\vec{k}')$ is given by[11]

$$S(\boldsymbol{k},\boldsymbol{k}') = (2\pi/\hbar)|M(\boldsymbol{k},\boldsymbol{k}')|^2 \delta(E_k - E_{k'} \pm \Delta E) \qquad (2.21)$$

where $M(\boldsymbol{k},\boldsymbol{k}')$ is the matrix element for the particular scattering and ΔE is the energy change due to the absorption or emission of phonons. The matrix element $M(\boldsymbol{k},\boldsymbol{k}')$ is expressed as

$$M(\boldsymbol{k},\boldsymbol{k}') = \int_{V_c} X_{n_{q',k'}} \Delta V X_{n_{q,k}} \, d\Omega \qquad (2.22)$$

where V_c is crystal volume, ΔV is the scattering potential in the crystal, $d\Omega$ is a volume element, and $X_{n_{q,k}}$ and $X_{n_{q',k'}}$ are the representations of the wave functions for the electron-phonon systems before and after the scattering, respectively. In the equation, an assumption has been made that the phonon occupation number for the wave vector q changes from $n_{q,k}$ to $n_{q',k'}$ and $n_{q',k'} = n_{q,k} \pm 1$.

The scattering potential ΔV is due to the displacement of the lattice atoms from their equilibrium position when the lattice vibrates. In nonpolar semiconductors the vibration causes a perturbation in the crystal potential called the deformation potential. It is proportional to the relative displacement of the neighboring atoms in the case of small displacement. For acoustic phonon, the deformation potential in the first-order approximation is[13]

$$\Delta V = E_1 \nabla \bullet \boldsymbol{u} \tag{2.23}$$

for optical phonons that in the zero-order approximation is[14]

$$\Delta V = D_o \boldsymbol{u} \tag{2.24}$$

where $\boldsymbol{u}$ is the displacement of the lattice atoms and E_1 and D_o are the deformation constants.

For polar materials, the relative displacement of the atoms produces additional potentials due to the redistribution of the charges associated with the ions. The acoustic phonons produce, in addition to the deformation potential, a potential giving rise to the phenomenon of piezoelectricity which may be expressed in a simplified form as[15]

$$\Delta V = (eh_{pz}/iq\varepsilon)\nabla \bullet \boldsymbol{u} \tag{2.25}$$

where h_{pz} is an averaged constant derived from the piezoelectric tensor, q is the phonon wave number, ε is the permittivity. The optical phonons produce polarization potentials given by[16]

$$\Delta V = (e\omega_0/q)[(\rho/\varepsilon_o)(K_\infty^{-1} - K_s^{-1})]^{1/2}\boldsymbol{u} \tag{2.26}$$

where ω_0 is the optical phonon frequency, ρ is the mass density, K_∞^{-1} and K_s^{-1}, respectively, are the dielectric constants for very high and very low frequencies, ε_o is the free space permittivity.

The scattering matrix elements were calculated for various scattering mechanisms and they are provided in Table 2-I.

Table 2-I Square of matrix element of various scattering mechanisms

scattering mechanism	*square of matrix element*
acoustic phonon deformation potential	$E_1^2\hbar\omega_q(n_q + 1/2 \pm 1/2)(2V_c\rho s^2)^{-1}$ ω_q: phonon frequency, n_q: phonon occupation number S: longitudinal acoustic velocity
piezoelectric	$e^2h_{pz}\hbar(n_q + 1/2 \pm 1/2)(2V_c\varepsilon^2\rho\omega_q)^{-1}$
nonpolar optical phonon	$D_o^2\hbar(n_0 + 1/2 \pm 1/2)(2V_c\rho\omega_o)^{-1}$ ω_o: optical phonon frequency, n_0 : optical phonon occupation number
polar intervalley phonon	$\hbar e^2\omega_o(K_\infty^{-1} - K_s^{-1})(n_0 + 1/2 \pm 1/2)(2V_c\varepsilon_o q^2)^{-1}$
ionized impurity	$e^4(\lvert\boldsymbol{k} - \boldsymbol{k}'\rvert^2 + 1/\lambda^2)^{-2}(V_c{}^2\varepsilon^2)^{-1}$ $\boldsymbol{k}, \boldsymbol{k}'$: electron wave vectors before and after scattering
Alloy	$2V_o\alpha_1(1-\alpha_1)E_{ab}^2V_c^{-1}$ α_1 : fraction of atoms of one type E_{ab}: scattering potential

The type of scattering strongly affects the relaxation processes in semiconductors such as energy relaxation, momentum relaxation, and spin relaxation. The three relaxations are simultaneous processes. Among them, the momentum relaxation and spin relaxation are parallel processes. They are directly related and strongly affect each other.

The various scattering processes will be related to the carrier momentum relaxation in the following section and the most effective scattering mechanism responsible for the momentum relaxation will be determined in Chapter 4. This information of momentum relaxation is important because the spin relaxation time is generally a function of momentum relaxation time.

2.3.2 Momentum relaxation

The momentum of the free carriers is distributed equally in all directions in the absence of external forces and the average value is zero. The carriers gain momentum when an external force $\boldsymbol{F}$ is applied. The gained momentum relaxes to zero through the scattering processes when the force is withdrawn. This phenomenon of momentum relaxation is related to the statistical property of carriers and is usually discussed on the basis of the Boltzmann equation. When the external force $\boldsymbol{F}$ is applied, the distribution $f(\boldsymbol{k})$ can be expressed as

$$\frac{\partial f(\boldsymbol{k})}{\partial t} = -\frac{\boldsymbol{F}}{\hbar}\cdot\nabla_k f(\boldsymbol{k}) - \frac{V_c}{8\pi^3}\times$$

$$\int\{f(\boldsymbol{k})[1-f(\boldsymbol{k}')][S(\boldsymbol{k},\boldsymbol{k}')] - f(\boldsymbol{k}')[1-f(\boldsymbol{k})][S(\boldsymbol{k}',\boldsymbol{k})]\}d\boldsymbol{k}' \qquad (2.27)$$

The average momentum in the direction of $\hat{i}$ (direction of the external force F) at energy E corresponding to the wave vector k is

$$\hat{i}\, p(E) = \hat{i} \int \hbar k_i f(k) dk_\theta dk_\phi \, [\, f(k) dk_\theta dk_\phi \,]^{-1}$$

where $dk_\theta dk_\phi$ is an element of the surface area perpendicular to k and k_i is the $\hat{i}$-component of k. By multiplying Eq. (2.27) with $\hbar k_i dk_\theta dk_\phi$ and integrating, we have

$$\frac{\partial p(E)}{\partial t} = (\frac{F}{\hbar}) I_1 - \frac{p(E)}{\tau_p(E)} \tag{2.28}$$

where $$I_1 = \int [\, \partial f(k)/\partial k_i \,] \hbar k_i dk_\theta dk_\phi \, [\, f(k) dk_\theta dk_\phi \,]^{-1}$$

$$\tau_p(E) = \int \hbar k_i f(k) dk_\theta dk_\phi \, [\, \hbar k_i \partial_c f(k) dk_\theta dk_\phi \,]^{-1}$$

$\partial_c f(k)$ is written for the integral term in Eq. (2.27). Eq. (2.28) indicates that the average momentum changes with the time constant $\tau_p(E)$, therefore, $\tau_p(E)$ is defined as the momentum relaxation time. $\tau_p(E)$ depends on the form of $f(k)$ which is a function of both the scattering term and the force term.

The calculation of the momentum relaxation time has been performed by B. R. Nag[11] for various types of scattering. It includes acoustic phonon deformation potential scattering, piezoelectric potential scattering, impurity scattering, and nonpolar optical phonon scattering. The normalized momentum relaxation time ($\tau_{ac}, \tau_{al}, \tau_{pz}, \tau_{op}, \tau_{imp}$) of various scattering mechanisms are plotted in Figure 2-5 for a concentration of 10^{19} cm^{-3}. The equations from which curves in Figure 2-5 were calculated are listed in Table 2-II.

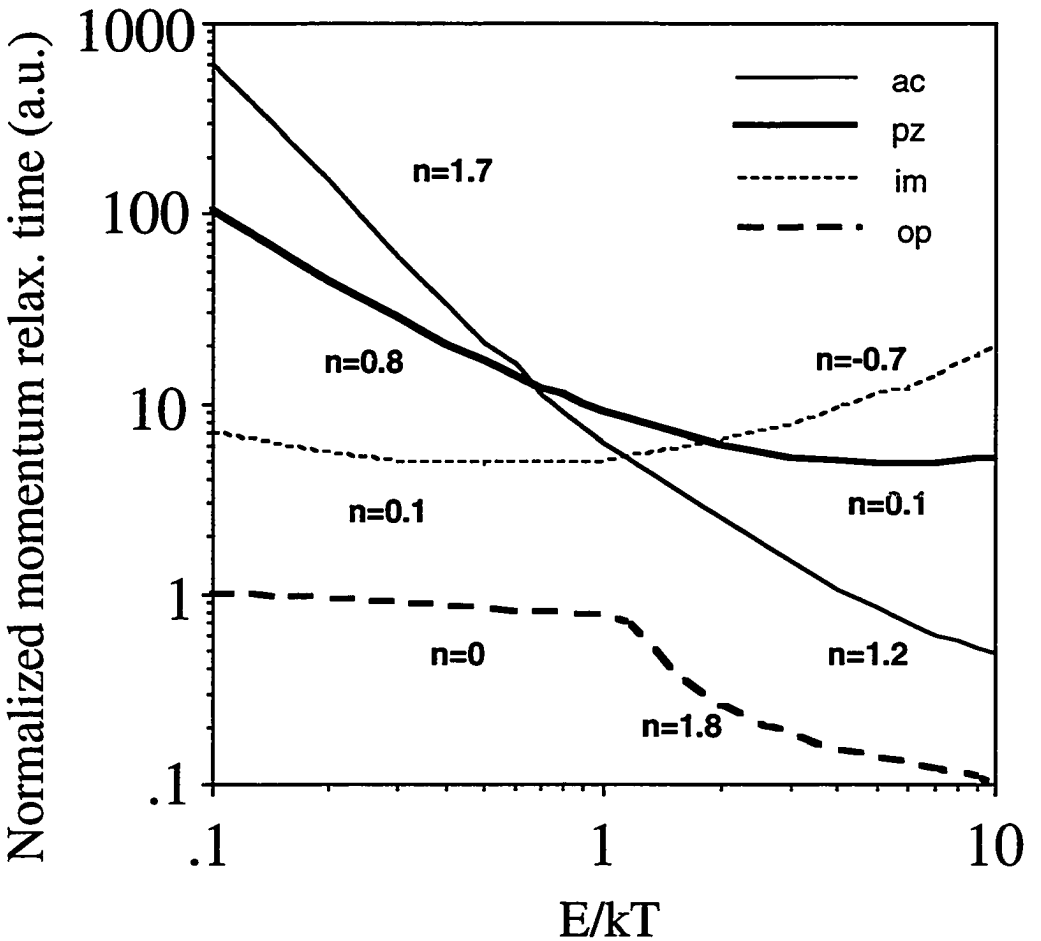

Figure 2-5 Energy dependence of the normalized momentum relaxation time for various scattering mechanisms including acoustic phonon deformation potential (ac), piezoelectric (pz), ionized impurity (im), and non-polar optical phonon. Values of n are indicated for two regions, $E/kT > 4$, and $E/kT < 4$.

In Figure 2-5, the labeled n represents the energy dependence of $\frac{1}{\tau_p}$ for each scattering, in other words, $\tau_p \sim (E/kT)^{-n}$. By approximation, the energy dependence of τ_p is assumed to be unchanged in each temperature regime separated by T=80K. The average carrier energy of

my experiments is between $20-35meV$. At T=80K, it is equivalent to the point of $E/kT=4$.

Table 2-II Table of equations from which the normalized momentum relaxation time for various scattering mechanisms were calculated.

Acoustic phonon deformation potential scattering	$\tau_{ac}=(3\pi^{1/2}/4)(300/T_L)^{3/2}\tau_0^{ac}F_{ac}(x)$ $\tau_0^{ac}=2(2\pi)^{1/2}\rho\hbar^4 s^2[E_I^2 m_*^{3/2}(300k_B)^{1/2}]^{-1}$ $F_{ac}(x)=x^{-1/2}[1-4(S_c/x)+6(S_c/x)^2\ln(1+x/S_c)$ $-2(S_c/x)^2(1+S_c/x)^{-1}]^{-1}$
Alloy scattering	$\tau_{al}=(3\pi^{1/2}/4)(300/T_L)^{3/2}\tau_0^{al}F_{al}(x)$ $\tau_0^{al}=(2\pi)^{1/2}\hbar^4[3V_o\alpha_I(1-\alpha_I)E_{ab}^2 m_*^{3/2}(300k_B)^{1/2}]^{-1}$ $F_{al}(x)=F_{ac}(x)$
Piezoelectric scattering	$\tau_{pz}=(3\pi^{1/2}/8)(300/T_L)^{1/2}\tau_0^{pz}F_{pz}(x)$ $\tau_0^{pz}=16(2\pi)^{1/2}\varepsilon^2\hbar^2\rho s^2[3e^2\hbar_{pz}^2 m_*^{1/2}(300k_B)^{1/2}]^{-1}$ $F_{pz}(x)=x^{-1/2}[1-2(S_c/x)\ln(1+x/S_c)$ $+(S_c/x)(1+S_c/x)^{-1}]^{-1}$
Non-polar optical phonon scattering	$\tau_{op}=(3\pi^{1/2}/2)(300/T_L)^{1/2}\dfrac{[\exp(\theta_o/T_L)-1]}{[\exp(300/T_L)-1]}\tau_0^{op}F_{op}(x)$ $\tau_0^{op}=2(2\pi)^{1/2}\rho\hbar^3\omega_o[\exp(300/T_L)-1][3D_o^2 m_*^{3/2}(300k_B)^{1/2}]^{-1}$ $F_{op}(x)=[\sqrt{x+\theta_o/T_L}$ $+H(x-\theta_o/T_L)\exp(\theta_o/T_L)\sqrt{x-\theta_o/T_L}]^{-1}$
Impurity scattering	$\tau_{imp}=(\pi^{1/2}/8)(300/T_L)^{3/2}\tau_0^{imp}F_{imp}(x)$ $\tau_0^{imp}=2^7(2\pi)^{1/2}\varepsilon^2 m_*^{1/2}(300k_B)^{3/2}(N_i e^4)^{-1}$ $F_{imp}(x)=x^{3/2}[\ln(1+x/S_c)-(1+S_c/x)^{-1}]^{-1}$

In Table 2-II, $x=E/kT$, $S_c\sim N^{1/3}$ is the screening factor and N is the carrier concentration.

The reason for the polar optical phonon scattering being excluded from the calculation of the momentum relaxation time is because of the difficulty in defining this quantity with mathematical equations. It involves two things, first, the polar optical phonon scattering is not elastic

($E_{ph} = 36meV$) (see Fig. 2-6); secondly, the scattering rate for polar optical phonon scattering depends on the angle between the initial and final directions of momentum (Fig. 2-7).

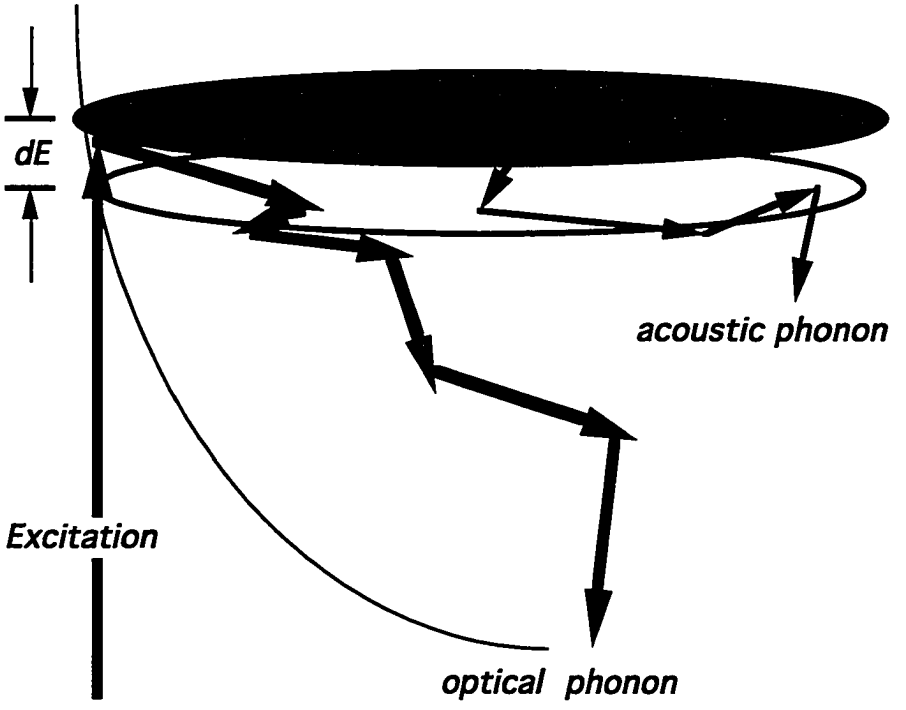

Figure 2-6 Comparison between optical and acoustic phonon scattering in the aspect of energy

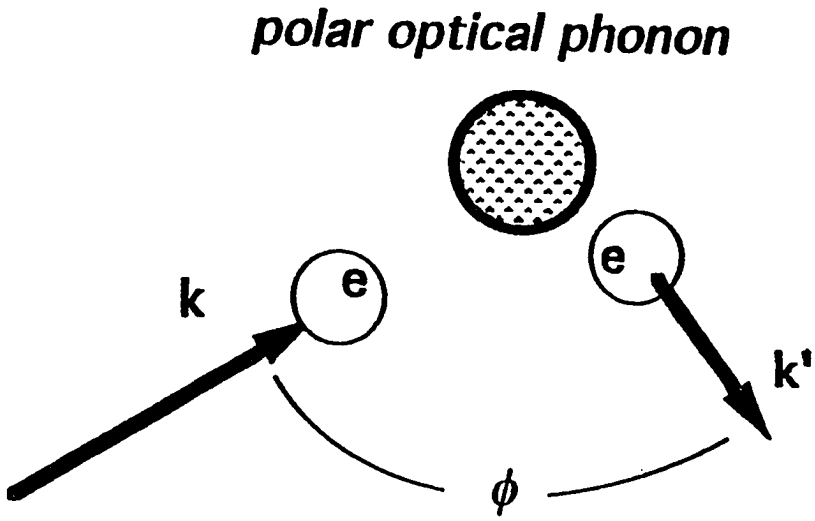

Figure 2-7 The scattering probability of the optical phonon scattering is a function of the scattering angle ϕ between k and k'

2.3.3 Elliot-Yafet (EY) Mechanism

Elliot[9] and Yafet[10] have consider the effect of spin-orbit coupling on normal electron-phonon and electron-impurity scattering. In a simpler fashion, one can write the spin relaxation rate as the momentum scattering rate times the probability of the event that reverses spin

$$\frac{1}{\tau_s(E)} = \frac{\left|M_{\bar{k}'\downarrow,\bar{k}\uparrow}\right|^2}{\left|M_{\bar{k}'\uparrow,\bar{k}\uparrow}\right|^2} \frac{1}{\tau_p(E)} \tag{2.29}$$

where τ_p is the momentum relaxation time, $M_{\bar{k}'\downarrow,\bar{k}\uparrow}$ and $M_{\bar{k}'\uparrow,\bar{k}\uparrow}$ are the matrix elements for spin flip and no spin flip transitions, respectively. Fishman and Lampel[17] calculated the spin relaxation rate due to this mechanism and found

$$\frac{1}{\tau_s(E)} = \frac{32}{27}\left[1-\frac{m_c}{m_o}\right]\frac{1+\eta/2}{1+2\eta/3}\frac{\eta}{1+\eta}\left[\frac{E}{E_g}\right]^2\frac{1}{\tau_p(E)} \qquad (2.30)$$

where $\eta = \frac{\Delta}{E_g}$. For this mechanism, the spin relaxation rate increases with an increasing momentum relaxation rate, contrary to the characteristic of the precessional relaxation mechanism to be discussed next. Figure 2-8 schematically describes the spin relaxation due to the spin non-conserved scattering between electrons and other particles.

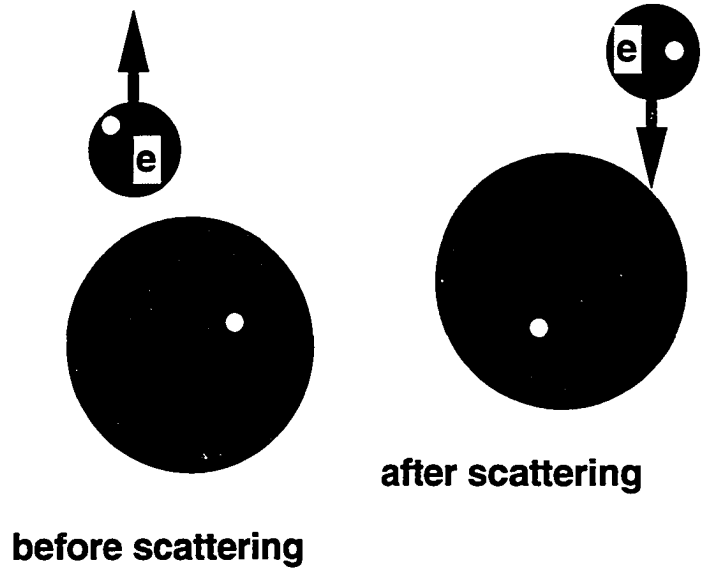

Figure 2-8 Schematic description of the EY spin relaxation mechanism. Electron's spin state varies due to scattering.

2.3.4 D'yakonov-Perel' (DP) Mechanism

This mechanism was originally proposed by D'yakonov[18,19] and Perel'[19,20] (1971). It is based on the effect of the removal of Kramer's degeneracy on carrier scattering which results in the conduction band splitting. This splitting can be viewed as a pseudomagnetic field that causes a precession of the electron spin. Because the magnitude of this effective magnetic field depends on the electron wave vector (~ k^3), it leads to a precession vector $\omega(\vec{k})$ that also depends on the wave vector. As the electron is scattered, not only $\omega(\vec{k})$ undergoes random variations in magnitude and direction but this random variation in the precession of the electron spin leads to the spin depolarization.

D'yakonov and Perel' calculated the relaxation rate for this process as a function of electron energy and found that

$$\frac{1}{\tau_s(E)} = \frac{2}{3}\omega^2\tau_c(E) \tag{2.31}$$

where $\tau_c(E)$ is the effective collision time at energy E. In equation (2.31), the Larmour frequency is expressed as a function of energy, $\omega^2(E)$. It is the angular average of $\omega^2(\vec{k})$ (see Fig. 2-9). For isotropic scattering $\tau_c = \tau_p$ while for anisotropic scattering $\tau_c = \tau_p/6$. In this thesis, τ_c will be replaced by τ_p in order to link the spin relaxation to the momentum relaxation.

From Eq. (2.31) we can see that as the collision rate increases (decreases), this mechanism becomes less effective (more effective). This is because the spin vectors do not precess significantly in the period of

time between two consecutive collisions. Fishman and Lampel[17] (1977) have shown that

$$\omega^2 = \frac{16}{315}\left(\frac{\Delta}{\hbar}\right)^2 \frac{B'}{\hbar^2/2m_o}\left(1-\frac{m_c}{m_o}\right)\frac{1}{(1+\eta)(1+2\eta/3)}\left(\frac{m_c}{m_o}\right)^2\left(\frac{E}{E_g}\right)^3 \qquad (2.32)$$

where B' is the conduction band splitting. For GaAs, $B' = 10\hbar^2/2m_o$. This mechanism becomes more important at higher energies because of the cubic dependence of the electron energy.

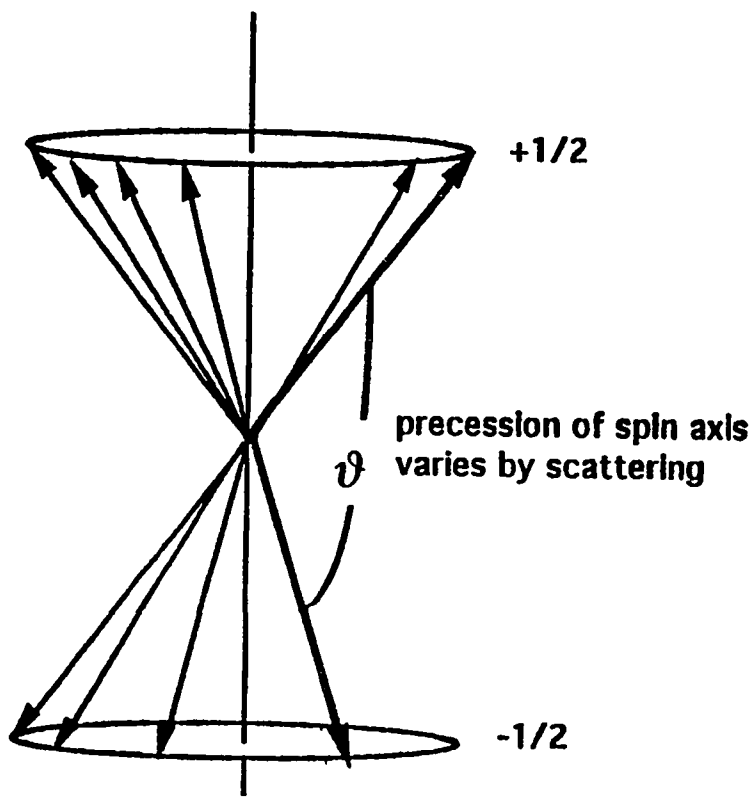

Figure 2-9. Schematic description of the DP spin relaxation mechanism

2.3.5 Bir-Aronov-Pikus (BAP) Mechanism

The electron-hole interaction can be expected to lead to electron spin relaxation because the holes do not retain spin alignment for long.

Bir, Aronov, and Pikus[20,21] (1976) have considered a spin exchange interaction between electrons and holes. In the treatment involving magnetic interactions, it is found that the electron exchanges spin with a hole. The Hamiltonian of the quasi-short range exchange interaction is expressed as[22]

$$H_{exch} = A_{exch} V \boldsymbol{J} \cdot \boldsymbol{S} \delta(\vec{r}) \tag{2.33}$$

where V is the crystal volume, $\boldsymbol{J}$ is the hole angular momentum, $\boldsymbol{S}$ is the electron spin, $\vec{r}$ is the relative distance between electron and hole. The constant A_{exch} is the exchange coupling between the periodic parts of the electron and hole wave functions. In the case of high photogenerated carrier concentration the screening length is less than the first Bohr radius. Under this approximation, the spin relaxation rate can be derived as

$$\frac{1}{\tau_s(E)} = N_h \left[\frac{\sqrt{(5\pi)}}{8} \frac{\Delta_{x,1S}}{E_{x,1S}} a_{x,1S}\right]^2 \left[\frac{2E}{m_e}\right]^{1/2} \tag{2.34}$$

where $a_{x,1S}$ is the first order Bohr radius, $\Delta_{x,1S}$ is the exchange splitting of the $1S$ state of the exciton, N_h is the hole concentration, $E_{x,1S}$ is the binding energy of the $1S$ state exciton. Figure 2-10 schematically describes the spin exchange interaction between electrons and holes.

As the given optical selection rules indicated in the last section, the transition matrix elements of a certain circularly polarized dipole moment, presuming clockwise, are producing three times as many electrons in the spin-up state as in the spin-down state. The spin polarization p is defined as the ratio of the electron spin population

difference over the total electron spin population which is expressed as $P = \frac{N_+ - N_-}{N_+ + N_-}$.

To start the analysis of spin dynamics, it is assumed that electrons of either spin state are in thermal equilibrium with the other. There also exists a possibility that electrons of a given spin state can go to the opposite spin state through a weak interaction.

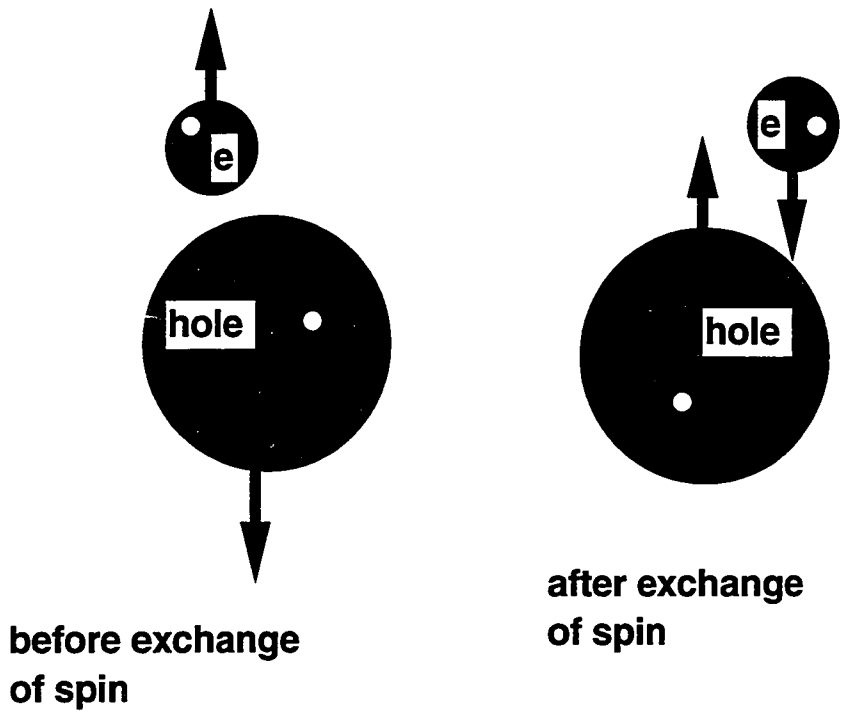

Figure 2-10. Schematic description of the BAP spin relaxation mechanism. Electron exchanges its spin with hole's.

Since holes relax their spin polarization much faster than electrons there will be no spin polarized electrons if this exchanging interaction persists.

2.4 Rate equations

The evolution of photogenerated electrons $(+\frac{1}{2}, -\frac{1}{2})$ in the conduction band are described by these 2 conjugate rate equations[23]:

$$\frac{dN_+}{dt} = -\frac{N_+}{\tau_r} - \frac{N_+}{\tau_{sf}} + \frac{N_-}{\tau_{sf}} \tag{2.35}$$

$$\frac{dN_-}{dt} = -\frac{N_-}{\tau_r} - \frac{N_-}{\tau_{sf}} + \frac{N_+}{\tau_{sf}} \tag{2.36}$$

where N_+, N_- are the carrier population of spin up and spin down states, respectively, τ_r is the carrier life time, and τ_{sf} is the carrier spin flip time. The solution to the rate equations (2.35) and (2.36) are

$$N_+(t) + N_-(t) = [N_+(0) + N_-(0)]\exp(-t/\tau_r) \tag{2.37}$$

$$N_+(t) - N_-(t) = [N_+(0) - N_-(0)]\exp(-t/\tau_r - 2t/\tau_{sf}) \tag{2.38}$$

and

$$N_+(t) = N_+(o)[\exp(-t/\tau_s - 2t/\tau_{sf}) + \exp(-t/\tau_r)] \tag{2.39}$$

$$N_-(t) = N_-(o)[\exp(-t/\tau_s) - \exp(-t/\tau_r - 2t/\tau_{sf})] \tag{2.40}$$

The time resolved spin polarization is described by

$$P_{spin}(t) = \frac{N_+(o) - N_-(o)}{N_+(o) + N_-(o)}\exp(-t/\tau_S)$$

$$= P_{spin}(o)\exp(-t/\tau_S) \tag{2.41}$$

Here, a new parameter τ_S is defined as $\tau_S = \tau_{sf}/2$. Obviously, the initial degree of spin polarization $P_{spin}(o)$, the spin relaxation time τ_S

and the recombination life time τ_r can be obtained from direct time-resolved measurements. This excite-and-see experimental strategy has been applied by Seymour and Alfano[24] in 1980.

2.5 Comparison between the steady state measurements and the time resolved measurements.

In the course of this thesis, there are many comparisons made between the spin relaxation times measured by steady state method and those by time resolved method. The comparison is meaningful if the spin relaxation times obtained by different methods are basically the same. This is the purpose for doing this comparison.

The derivation for the time resolved measurements has been done in the previous section. The derivation for the steady state measurements is given as the following:

Starting from the same rate equations (2.35) and (2.36)

$$\frac{dN_+}{dt} = -\frac{N_+}{\tau_r} + \frac{N_-}{\tau_{sf}} - \frac{N_+}{\tau_{sf}}, \qquad \frac{dN_-}{dt} = -\frac{N_-}{\tau_r} + \frac{N_+}{\tau_{sf}} - \frac{N_-}{\tau_{sf}} \tag{2.42}$$

the ratio of $(dN_+/dt - dN_-/dt)$ to $(dN_+/dt + dN_-/dt)$ can be rewritten as

$$\frac{dN_+/dt - dN_-/dt}{dN_+/dt + dN_-/dt} = \frac{(N_+ - N_-)(1/\tau_r + 2/\tau_{sf})}{(N_+ + N_-)\,1/\tau_r} \tag{2.43}$$

The numerical value of equation (2.43) can be calculated because of the generation rate of dN_+/dt is three times as big as $dN\_/dt$. Therefore, we have

$$\frac{dN_+/dt - dN\_/dt}{dN_+/dt + dN\_/dt} = \frac{3-1}{3+1} = 0.5 \tag{2.44}$$

Since spin polarization is defined as $P = \frac{N_+ - N\_}{N_+ + N\_}$ it can be rewritten as

$$P = 0.5\frac{1/\tau_r}{1/\tau_r + 2/\tau_{sf}} = 0.5\frac{\tau_{sf}/2}{\tau_{sf}/2 + \tau_r} \tag{2.45}$$

In the steady state[25], τ_s is determined from the steady state polarization P and

$$P = 0.5\frac{\tau_s}{\tau_s + \tau_r} \tag{2.46}$$

It is clearly that equations (2.45) and (2.46) are identical if $\tau_s = \tau_{sf}/2$. The steady state and time resolved method result in the same spin relaxation time τ_s.

2.6 The temperature and carrier concentration dependencies of the spin relaxation time.

The spin relaxation rate due to the various mechanisms were given as a function of carrier energy E. However the band of luminescence is too narrow to provide the information about E dependence of the spin relaxation time. Fortunately, dependencies of temperature, T, and carrier concentration, N, are available allowing a wide range of investigation.

To use them as the parameters in the analysis, a mathematical process is necessary. This process is essentially an averaging integral with respect to energy by taking the density of states and the distribution function into account. The temperature and the carrier concentration dependencies are provided by the result of this integration.

This integration can be expressed as[23]

$$\frac{1}{\tau_s(T,N)} = \frac{\int [1/\tau_s(E)]\rho(E)f(E,T)dE}{\int \rho(E)f(E,T)dE} \tag{2.47}$$

where $\rho(E)$ and $f(E,T)$ are the density of states and the Fermi-Dirac distribution, respectively. The standard form and the solution of a j-order Fermi integral can be expressed as

$$\int_0^\infty \frac{(E/k_BT)^j dE/k_BT}{1+exp(E-\varepsilon_F)/k_BT} = \frac{(\varepsilon_F/k_BT)^{j+1}}{j+1} \tag{2.48}$$

where ε_F and k_B are the Fermi energy and Plank's constant, respectively. The result of the integral is a function of T and ε_F which is also a function of carrier concentration N. To practically perform the integral, the energy dependence of the spin relaxation time must be known. Equations (2.29) and (2.31) have shown that the spin relaxation times for D'yakonov-Perel' (DP) mechanism and Elliot-Yafet (EY) mechanism are functions of momentum relaxation time τ_p therefore the energy dependence of τ_p have to be predetermined. The energy dependence of τ_p depends on the scattering mechanism. However, which mechanism is responsible for momentum relaxation but it is still unclear. From the approximately linear dependencies of τ_p on E/kT seen in Figure 2-5, τ_p can be expressed as

$$\tau_p(E,T) \sim (E/kT)^{-n} \tag{2.49}$$

where n is a scattering dependent parameter. The numerical value of the parameter n will be experimentally determined. As soon as it is determined, the effective scattering mechanism causing momentum relaxation can be identified. The details will be discussed in chapter 4 "Determination of the effective scattering mechanism causing momentum relaxation".

Since τ_p is assumed to be a function of energy, equation (2.47) can be performed for D'yakonov-Perel' mechanism. The calculation of the temperature and carrier density dependencies in a 3D systems is performed as

$$[\tau_s]^{-1}_{3D(DP)} \sim \int \frac{(E/E_g)^3 \tau_p E^{0.5} dE}{1+exp(E-\varepsilon_F/kT)} \Big/ \int \frac{E^{0.5} dE}{1+exp(E-\varepsilon_F/kT)}$$

since $\tau_p \sim (E/kT)^{-n}$

$$\sim (kT)^{4.5} \int \frac{(E/kT)^{3.5-n} d(E/kT)}{1+exp(E-\varepsilon_F/kT)} \Big/ (kT)^{1.5} \int \frac{(E/kT)^{0.5} d(E/kT)}{1+exp(E-\varepsilon_F/kT)}$$

by the approximation given in equation (2.49), $[\tau_s]^{-1}_{3D(DP)}$ can be expressed as a ratio of two ordered Fermi integrals with the orders equal to $3.5-n$ and 0.5 for the numerator and denominator, respectively. Therefore,

$$[\tau_s]^{-1}_{3D(DP)} \sim (kT)^3 (\varepsilon_F/kT)^{4.5-n} / (\varepsilon_F/kT)^{1.5}$$

after simplifying,

$$[\tau_s]^{-1}_{3D(DP)} \sim \varepsilon_F{}^{3-n} kT^n \sim N^{2-0.67n} \tag{2.50}$$

By the same approach, the calculation of the temperature and carrier density dependencies in a 2D systems is performed as

$$[\tau_s]^{-1}_{2D(DP)} \sim \int \frac{(E/E_g)^3 \tau_c dE}{1+exp(E-\varepsilon_F/kT)} \Big/ \int \frac{dE}{1+exp(E-\varepsilon_F/kT)}$$

since $\tau_p \sim (E/kT)^{-n}$

$$[\tau_s]^{-1}_{2D(DP)} \sim (kT)^4 \int \frac{(E/kT)^{3-n} d(E/kT)}{1+exp(E-\varepsilon_F/kT)} \Big/ (kT) \int \frac{d(E/kT)}{1+exp(E-\varepsilon_F/kT)}$$

by the approximation given in equation (2.49), $[\tau_s]^{-1}_{2D(DP)}$ can be expressed as a ratio of two ordered Fermi integrals with the orders equal to $3-n$ and 0 for the numerator and denominator, respectively. Therefore,

$$[\tau_s]^{-1}_{2D(DP)} \sim (kT)^3 (\varepsilon_F/kT)^{4-n} / (\varepsilon_F/kT)$$

after simplifying,

$$[\tau_s]^{-1}_{2D(DP)} \sim \varepsilon_F{}^{3-n} kT^n \sim N^{3-n} \tag{2.51}$$

For EY mechanism, the spin relaxation time was given as a function of energy in equation (2.29). The calculation of the temperature and carrier density dependencies in a 3D systems is performed as

$$[\tau_s]^{-1}_{3D(EY)} \sim \int \frac{(E/E_g)^2 \, 1/\tau_c \, E^{1/2} dE}{1+exp(E-\varepsilon_F/kT)} \Big/ \int \frac{E^{1/2} dE}{1+exp(E-\varepsilon_F/kT)}$$

since $\tau_p \sim (E/kT)^{-n}$

$$\sim (kT)^{3.5} \int \frac{(E/kT)^{2.5+n}\, d\,E/kT}{1-exp(E-\varepsilon_F/kT)} \Big/ (kT)^{1.5} \int \frac{(E/kT)^{1/2}\, d\,E/kT}{1-exp(E-\varepsilon_F/kT)}$$

by the approximation given in equation (2.49), $[\tau_s]^{-1}_{3D(EY)}$ can be expressed as a ratio of two ordered Fermi integrals with the orders equal to $2.5+n$ and 0.5 for the numerator and denominator, respectively. Therefore,

$$[\tau_s]^{-1}_{3D(EY)} \sim (kT)^2 \frac{(\varepsilon_F/kT)^{3.5+n}}{(\varepsilon_F/kT)^{1.5}}$$

after simplifying,

$$[\tau_s]^{-1}_{3D(EY)} \sim \varepsilon_F{}^{2+n} (kT)^{-n} \sim N^{1.33+0.67n} (kT)^{-n} \qquad (2.52)$$

The calculation of the temperature and carrier density dependencies in a 2D systems is performed as

$$[\tau_s]^{-1}_{2D(EY)} \sim \int \frac{(E/E_g)^2\, 1/\tau_c\, dE}{1-exp(E-\varepsilon_F/kT)} \Big/ \int \frac{dE}{1-exp(E-\varepsilon_F/kT)}$$

since $\tau_p \sim (E/kT)^{-n}$

$$\sim (kT)^3 \int \frac{(E/kT)^{2+n}\, d\,E/kT}{1-exp(E-\varepsilon_F/kT)} \Big/ (kT) \int \frac{d\,E/kT}{1-exp(E-\varepsilon_F/kT)}$$

by the approximation given in equation (2.49), $[\tau_s]^{-1}_{2D(EY)}$ can be expressed as a ratio of two ordered Fermi integrals with the orders equal to $2+n$ and 0 for the numerator and denominator, respectively. Therefore,

$$[\tau_s]^{-1}_{2D(EY)} \sim (kT)^2 \frac{(\varepsilon_F/kT)^{3+n}}{(\varepsilon_F/kT)}$$

after simplifying,

$$[\tau_s]^{-1}_{2D(EY)} \sim \varepsilon_F{}^{2+n}(kT)^{-n} \sim N^{2+n}(kT)^{-n} \tag{2.53}$$

For BAP mechanism, the spin relaxation time is given as a function of energy in equation (2.34). The calculation of the temperature and carrier density dependencies in a 3D systems is performed as

$$[\tau_s]^{-1}_{3D(BAP)} \sim \int \frac{(E)^{0.5}(E)^{0.5}dE}{1+exp(E-\varepsilon_F/kT)} \Big/ \int \frac{(E)^{0.5}dE}{1+exp(E-\varepsilon_F/kT)}$$

since $\tau_p \sim (E/kT)^{-n}$

$$\sim (kT)^2 \int \frac{(E/kT)d(E/kT)}{1+exp(E-\varepsilon_F/kT)} \Big/ (kT)^{1.5} \int \frac{(E/kT)^{0.5}d(E/kT)}{1+exp(E-\varepsilon_F/kT)}$$

by the approximation given in equation (2.49), $[\tau_s]^{-1}_{3D(BAP)}$ can be expressed as a ratio of two ordered Fermi integrals with the orders equal to 0.5 and 0 for the numerator and denominator, respectively. Therefore,

$$[\tau_s]^{-1}_{3D(BAP)} \sim (kT)^{0.5}(\varepsilon_F/kT)^2/(\varepsilon_F/kT)^{1.5}$$

after simplifying,

$$[\tau_s]^{-1}_{3D(BAP)} \sim \varepsilon_F{}^{0.5}T^0 \sim N^{0.34} \tag{2.54}$$

The calculation of the temperature and carrier density dependencies in a 2D systems is performed as

$$[\tau_s]^{-1}_{2D(BAP)} \sim \int \frac{(E)^{0.5}\,dE}{1+exp(E-\varepsilon_F/kT)} \Big/ \int \frac{dE}{1+exp(E-\varepsilon_F/kT)}$$

since $\tau_p \sim (E/kT)^{-n}$

$$\sim (kT)^{1.5} \int \frac{(E/kT)^{0.5}\,d(E/kT)}{1+exp(E-\mathcal{E}_F/kT)} \Big/ (kT) \int \frac{d(E/kT)}{1+exp(E-\mathcal{E}_F/kT)}$$

by the approximation given in equation (2.49), $[\tau_s]^{-1}_{2D(BAP)}$ can be expressed as a ratio of two ordered Fermi integrals with the orders equal to 0.5 and 0 for the numerator and denominator, respectively. Therefore,

$$[\tau_s]^{-1}_{2D(BAP)} \sim (kT)^{0.5} (\mathcal{E}_F/kT)^{1.5} / (\mathcal{E}_F/kT)$$

after simplifying,

$$[\tau_s]^{-1}_{2D(BAP)} \sim \mathcal{E}_F{}^{0.5} T^0 \sim N^{0.5} \qquad (2.55)$$

There are some points that should be made from the results of the Fermi integral performed for 3D and 2D systems.

1. The temperature dependence of the spin relaxation time does not vary corresponding to the dimensionality variation. Normally, when the dimensionality of a system reduces from 3 to 2, the density of states, $\rho(E)$, varies; it is a function of energy depending on the dimensionality. In 3D, $\rho(E)_{3D} \sim \sqrt{E}$; in 2D, $\rho(E)_{2D} \sim E^0$. Since the density of states is not a function of temperature and it is the same in both the denominator and numerator therefore they cancel each other out. The other reason is

because the *variation* of the temperature dependencies, in the denominator and numerator, are coherent due to the dimensionality change.

The difference of the density of states can not affect the result of the integral when the dimensionality of the system of interest reduces from 3 to 2. The same temperature dependence is seen. For the carrier density dependence, it comes from the fact that the Fermi energy ε_F is a function of it. The result of the integral contains the Fermi energy.

When it is related to the carrier concentration, different equations must be applied. They are $N_{3D} \sim \varepsilon_F^{1.5}$ and $N_{2D} \sim \varepsilon_F$ for 3D and 2D respectively. This is the decisive point giving a different carrier density dependence for 2D and 3D.

The temperature and the carrier density dependencies of τ_s are summarized and given in Table 2-III and Table 2-IV, respectively.

Table 2-III Table of theoretical temperature dependencies of τ_s for various combinations of spin relaxation mechanism and momentum relaxation scattering

	acoustic phonon	piezoelectric	impurity	non-polar optical phonon
DP	$T^{-n-1.5}$	$T^{-n-0.5}$	$T^{-n-0.5}$	$T^{-n+1.5}$
EY	$T^{+n-1.5}$	$T^{+n-0.5}$	$T^{+n-0.5}$	$T^{+n+1.5}$
BAP	T^0	T^0	T^0	T^0

Table 2-IV Theoretical carrier concentration dependence of τ_s. Where n is a parameter used in the Fermi integral representing the energy dependence of the momentum relaxation time $\tau_p \sim (E/kT)^{-n}$.

	3D (bulk)	2D (Q.W.)
BAP	$N^{-0.34}$	$N^{-0.5}$
DP	$N^{-2+0.67n}$	N^{-3+n}

2.7 The variation of photogenerated carrier concentration in bulk and in quantum wells from the same excitation.

Carrier concentration is one of the experimental variables used in the investigation of the carrier spin dynamics. The spin relaxation time has been calculated to be a function of carrier concentration. The dependence on carrier concentration is different for different relaxation mechanisms.

The calculation of the carrier concentration generated by assuming single photon absorption involves many things such as the power of the pulse, the pulse width, e-e scattering time, photon energy, the total number of states, the exciting spot size, the absorption depth ..... and a lot more. Generally speaking the intensity of the exciting laser pulse decreases as the pulse makes its way through the sample by following an exponential decay pattern. It is expressed as $I(x) = I(0)exp(-x/\alpha)$ where $I(0)$ is the pulse intensity at the front surface and α is the absorption depth.

For simplicity, the number of photo-generated carrier is calculated by dividing the energy of the pulse by a single photon energy. The volume of the photogenerated carrier depends on the exciting spot size and the absorption depth. Since the power of the pulse decreases, the carrier concentration will not be a constant but possibly an exponentially decreasing quantity as the pulse penetrates deeper into the sample. When measurements are made, the luminescence comes out from everywhere the carriers were generated in the sample. The diffusion of carrier may not be rapid enough (10^7m/s) to reach a equilibrium concentration therefore the time resolved profile is the sum of all the luminescence of different concentrations at different physical locations. The spin relaxation time has been measured as a function of carrier concentration by Seymour and Alfano[26] in 1981 and it was observed that $\tau_s \sim N^{-0.63}$.

Now, let us consider a multi-layer sample. Each layer may have a different spin relaxation temporal profile because of the different photo-generated carrier density in each layer. The front layers definitely have a higher concentration than the back layers. The front layers relax spin much faster than the back layers because spin relaxation time depends on the carrier concentration[24] to the power of -0.63, For simplicity, the spin relaxation is described as a single exponentially decay process. Assuming the initial spin polarization of each layer to be independent of the physical location (depth) from where the luminescence is emitted, $P_i = P$, the overall spin polarization temporal profile can be expressed as

$$P_{all}(t) = \sum_i N_i P_i \, exp(-t/\tau_{si}) \qquad (2.56)$$

Since the carrier concentration N decays exponentially, therefore, the concentration of the i_{th} layer N_i can be written as $N_i = N_0 exp(-id)$ by assuming the absorption depth α is 1. We have

$$P_{all}(t) = P\sum_i N_0 exp(-id) exp(-t/\tau_{si}) \tag{2.57}$$

after simplifying,

$$P_{all}(t) = N_0 P\sum_i exp(-id - t/\tau_{si}) \tag{2.58}$$

where d is the thickness of each layer, $\tau_{si} = \tau_{s0}[exp(-id/\alpha)]^{-0.63}$ is the spin relaxation time constant of the i_{th} layer with τ_{s0} the spin relaxation time of the front layer.

A theoretical calculation has been done for two ultimate cases, thin 100Å quantum well and thick 20 μm bulk material. The data are presented in Figure 2-11 plotted in the semi-log scale for easier observation and comparison. It indicates that the former case of quantum well has a much shorter relaxation time constant than that of the later case of thick bulk material. A diagram in Figure 2-12 schematically demonstrates how the carrier concentration and τ_s change spatially. The darkness of the volume is the index of the carrier concentration in that volume. Four luminescence pictures indicate the spin relaxation process slows down as the photo generated carrier concentration decreases.

The spin relaxation times are also calculated as a function of the depth measured from the front surface at where the laser pulses enter. It can be observed that the spin relaxation time of a certain layer, τ_{si},

exponentially increases corresponding to the increase of the depth. Computed results are presented in Figure 2-13.

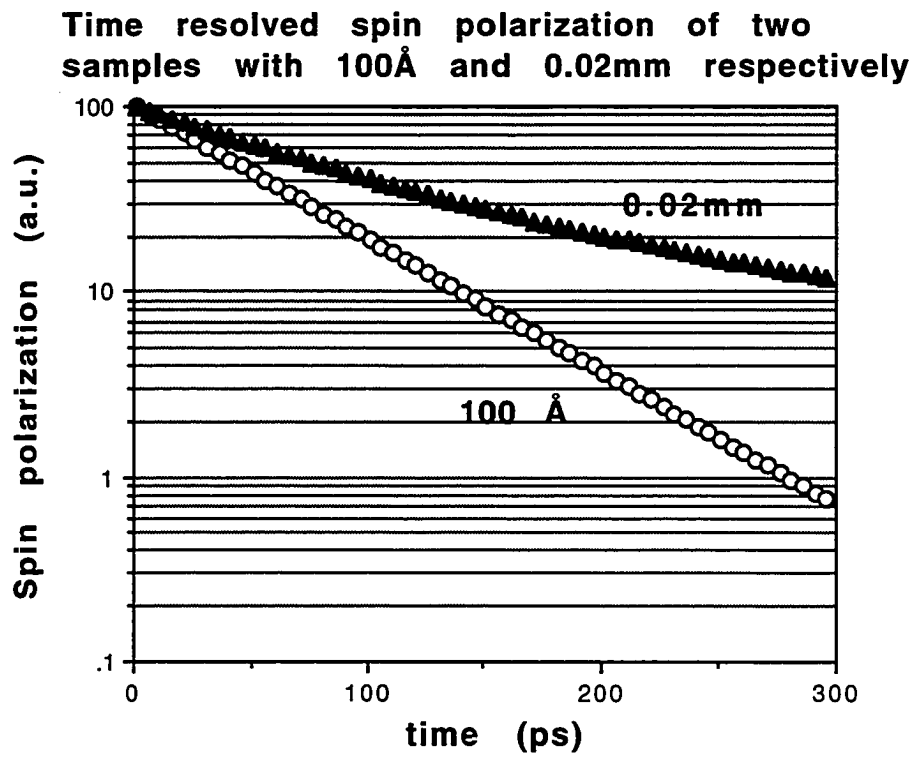

Figure 2-11. The theoretical calculation of the temporal evolution of the spin polarization. The painted triangle is for the sample of 20 μm, circle is for the sample with 100 Å thickness. The spin relaxation at the front layer is assumed to be 60 ps.

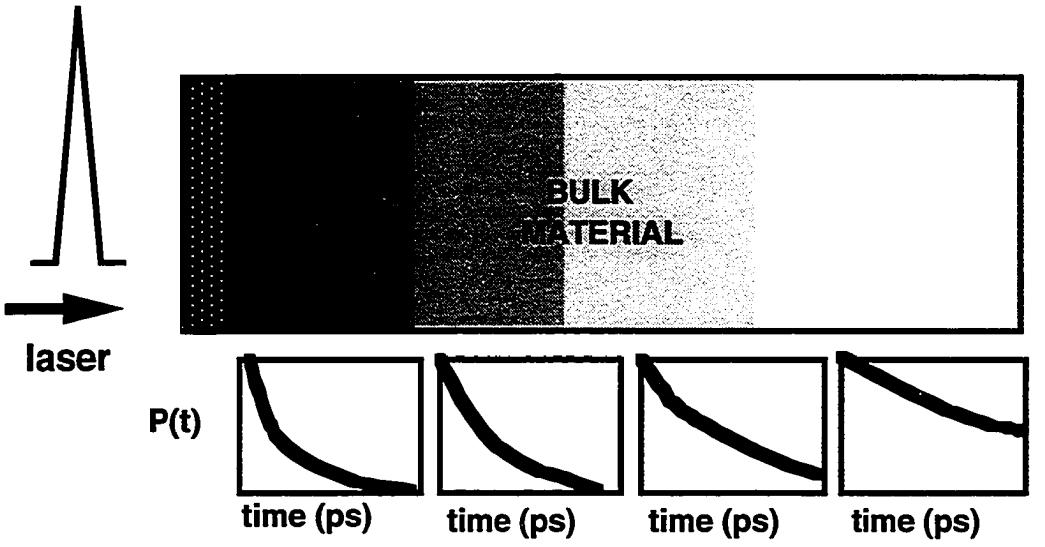

Figure 2-12. A schematic description for the change of the spin relaxation time as a function of the depth measured from the front surface at where the laser pulses enter. The spin relaxation slows down corresponding to the decrease of carrier concentration when going deeper. It is a result from the dependence of the spin relaxation time on the carrier density.

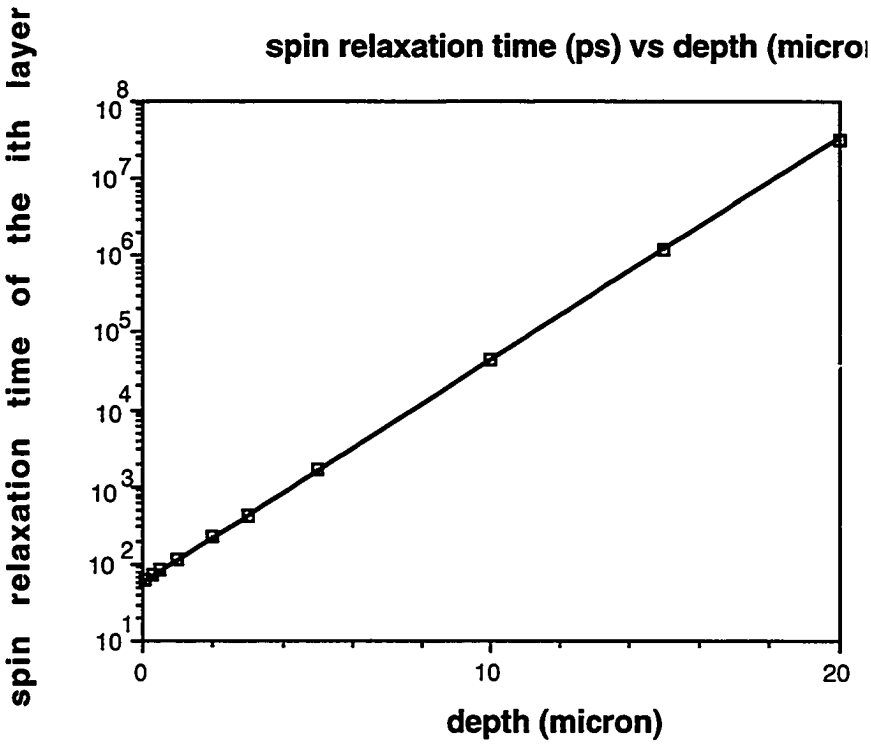

Figure 2-13. A theoretical calculation of the spin relaxation time as a function of the physical location at where the luminescence is generated. The depth is measured from the front surface where the laser pulses enter.

2.8 Photogenerated Carrier Concentration in 2D system

The pumping power of laser pulse of *750nm* line was *50nJ/pulse* and the total number of photons $N_{photon} = \frac{E_{laser}}{h\nu}$.

$$N_{photon} = \frac{50 \times 10^{-9}(joule) \times 10^{7}(erg/joule)}{1.6 \times 10^{-12}(erg/eV) \times 1.65(eV/photon)} = 1.8 \times 10^{11} \text{ photons}$$

The pulse width was *300fs*. The diameter of the focused spot was *0.4mm* (see Figure 2-14)

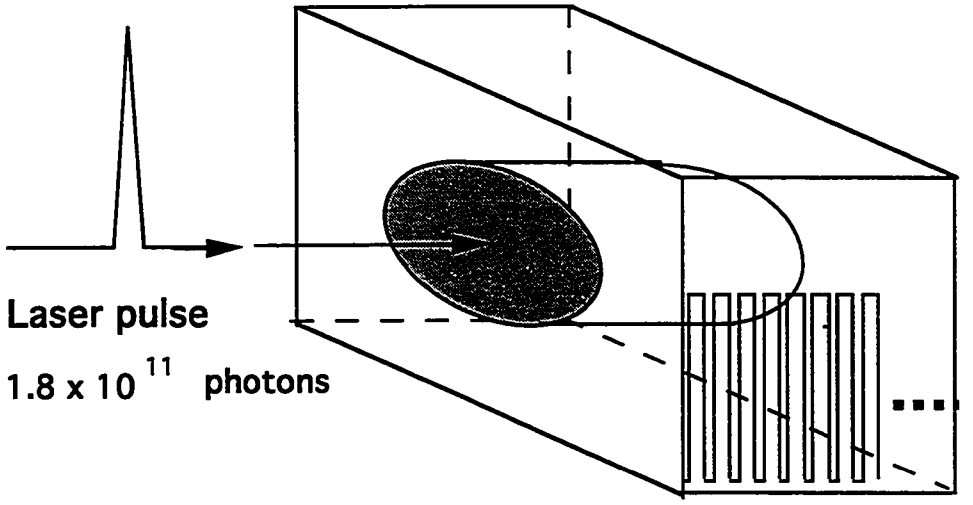

Figure 2-14 Region of the well structure. The total number of wells is 55.

The sample I used was a multi quantum well structure with the well size 55-Å, the gap energy between the conduction band minimum and valence band maximum is measured to be 1.61eV (*770nm*). The volumetric density of photogenerated carriers n_e is calculated as

$$n_e = \frac{N_{photon} \times f}{V} \tag{2.55}$$

where $f = \int_0^a e^{-x/L} dx$ is the absorption efficiency for the exciting laser pulse. The parameters used in the integral are $L \sim 1\mu m$ the effective absorption length and $a = 55Å \times 50 = 2750Å$ is the sum of the width of all wells (Note: We assume that there is no absorption in the barrier region). The volume of the active absorption region is $V = a \cdot \pi r^2$ where $r = 200\mu m$ is the laser spot size.

According to the parameters given above, we estimated that the average carrier volumetric concentration was $n_e^V \sim 10^{18} cm^{-3}$. The

equivalent surface concentration is $n_e^S \sim 10^{12} cm^{-2}$. In the next section, we calculate the available states.

2.8.1 Fermi Energy, ε_F, vs. Excess Pumping Energy, E_{ex}

At the moment of optical pulse excitation, the carriers created in the conduction band will form a pulse-like distribution (δ-function). A few femtoseconds later, electrons redistribute due to the electron-electron scattering which does not change the total energy of the system. Some electrons will be scattered to lower energy levels and some electrons will be scattered to higher energy levels. This electron-electreon scattering does not involve phonon emission therefore no energy loss and consequently, the energy remains unchanged. Because the electron-electron interaction is much faster than the electron-phonon interaction, electrons photoexcited by a strong laser pulse quickly form a Fermi-Dirac distribution in a very short time ($t < 10\,ps$) without losing energy.

For simplicity, at $T = 0°K$, the relation between the exciting energy and Fermi energy can be obtained from the calculation as

$$E_{k,total} = n_e \cdot (E_{ph} - E_{g,eff}) = \int_0^{\varepsilon_F} E_c \cdot \rho(E_c)\, dE_c = \frac{\varepsilon_F^2 \rho}{2} \quad ,$$

$$E_{ph} = E_{ex} + E_{g,eff} \quad , \text{ and}$$

$$E_{g,eff} = E_g + E_q \quad , \tag{2.59}$$

where $E_{k,total}$ is the total kinetic energy of photoexcited electrons, n_e is the number of photoexcited electrons, E_{ph} is the excitation photon energy, E_g is the gap energy, E_q is the quantization energy, ε_F is Fermi

energy, and $\rho(E)$, a constant in 2D, is the density of states and the derivation of $\rho(E)$ is given in the next section. If the 2D electron states are fully filled by the photoexcited electrons the distribution of electrons is a Fermi-Dirac distribution and the Fermi energy ε_F can be estimated by using Eq. (2.59). The relation between the excess energy $E_{ph} - E_{g,eff}$ and Fermi energy ε_F can be rewritten as

$$\varepsilon_F{}^2 = \frac{2 \cdot n_e \cdot (E_{ph} - E_{g,eff})}{\rho} \tag{2.60}$$

Since $n_e = \rho \cdot \varepsilon_F$, we have

$$\varepsilon_F = 2(E_{ph} - E_{g,eff}) \tag{2.61}$$

In equation (2.61), $E_{ph} = 1.65eV$ and $E_{g,eff} = 1.61eV$, the excess energy is $E_{ph} - E_{g,eff} = 40meV$, In my case of optical pumping, the Fermi energy $\varepsilon_F = 80meV$ (see Eq. (2.61). A schematic description is given in Figure 2-15.

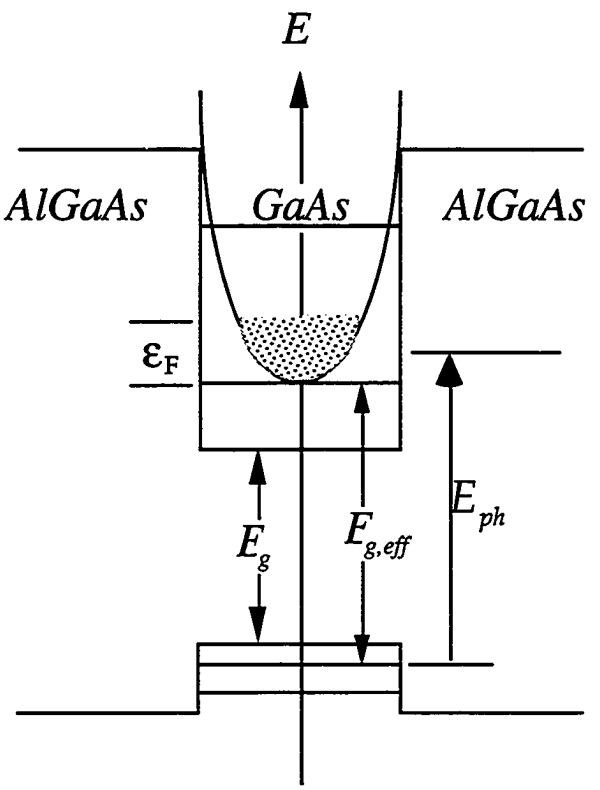

Figure 2-15 Figure of the carrier distribution and the energy structure

To find the density of states in a 2D system, we start with $\psi = C exp(i\vec{k}\cdot\vec{r})$ - as a solution to Schrodinger's equation

$$-\frac{\hbar^2}{2m}\nabla^2\psi = E\psi \quad . \tag{2.62}$$

where $k = 2\pi n/L$ and $n = 1,2,3,4,.....$, and $\Delta k = 2\pi/L$. We can also obtain $k = \sqrt{2mE/\hbar^2}$ and $dk = mdE/\hbar\sqrt{2mE}$ from the relation $E = \frac{\hbar^2 k^2}{2m}$. The 2D density of states ρ_{2D} is defined as the number of states between k and $k + dk$ per unit volume. Each state occupies $(2\pi/L)^2$ in k space. The 2D density of states has been calculated to be a constant and it can be expressed as

$$\rho_{2D} = \frac{m}{2\pi\hbar^2} = 1.38 \times 10^{10} cm^{-2} meV^{-1} \quad (2.63)$$

The energy gap E_g^{Γ} of $Al_xGa_{1-x}As$ and $GaAs$ can be calculated by using Equation (2.64) where x is the Aluminum composition.

$$E_g^{\Gamma}(x) = 1.425 + 1.155x + 0.37x^2 \quad (2.64)$$

In calculation, $x = 0.35$ and $x = 0$ were used for the case of $Al_{0.35}Ga_{0.65}As$ and $GaAs$, respectively. The well depth is calculated to be $450meV$. The quantization energy is calculated to be $80meV$. The excitation energy is $35 - 40meV$ more than the effective gap energy. This energy barrier of $450meV$ can keep all the photogenerated carriers ($10^{12} cm^{-2}$) in the well.

In my experiments, the Fermi-Dirac distribution formed at low temperatures remains until the electrons recombine with holes because Pauli exclusion principle prohibits emission of optical phonons. The $e-h$ recombination time is in the nanosecond regime. Therefore, at the time of measurement of luminescence, the concentration of the photoexcited carriers can be considered as unchanged.

In the case of continuous wave (cw) pumping, which usually generates carriers with very low density, the electron dynamics is different. It takes a long time for the system to reach the steady state, allowing the emission of phonons, and as a result, the total energy is not conserved. Before the system reaches the steady state, the energy decreases resulting in a much lower Fermi energy level.

The concept of "electron concentration" used in this thesis is the concentration of electrons photogenerated by a single pulse. The concentration is estimated in the first few hundreds of picoseconds. After about a nanosecond the electron concentration decays to zero until next pulse arrives. The average concentration over one period is much lower than the concentration generated by a single pulse.

2.8.2 Saturation of carriers

According to the above estimations given in Equations (2.61) and (2.63), there are $\varepsilon_F \cdot \rho = 1.1 \times 10^{12} cm^{-2}$ allowed electron states per unit area. The carrier density produced by photo-pumping is about $10^{12} cm^{-2}$. Absorption saturation should not be a serious problem where similar photo-generated carrier concentrations have been used in other publications[27,28]. In these cases, the photogenerated carrier density used by others in the wells were $0.8-2 \times 10^{12} cm^{-2}$ [27] and $10^{15} - 5 \times 10^{18} cm^{-3}$ [28], respectively.

2.8.3 Carrier saturation of a low intensity pumped 3D system

The density of states of a 3D system ρ_{3D} is given in Eq. (2.65)

$$\rho_{3D}(E) = \frac{1}{2\pi^2}\frac{1}{\hbar^3}(2m^*)^{3/2}E^{1/2}$$

$$= 5.83 \times 10^{37} E^{1/2} cm^{-3} erg^{-1} \qquad (2.65)$$

For a Fermi-Dirac distribution, there are two conditions to be satisfied. (1). The total number of carriers in the conduction band must be equal to the total number of electrons excited; (2). The energy must be conserved. The first condition can be expressed as Equation (2.66)

$$n_e = \frac{1}{2\pi^2}\frac{1}{\hbar^3}(2m^*)^{3/2}\int_0^\infty \frac{E^{1/2}dE}{exp(E-\varepsilon_F/kT)+1} \tag{2.66}$$

by Eq. (2.48),

$$n_e = \frac{1}{2\pi^2}\frac{1}{\hbar^3}(2m^*)^{3/2}(\frac{\varepsilon_F}{kT})^{3/2}\frac{(kT)^{3/2}}{3/2} \tag{2.67}$$

The second condition can be expressed by Eq. (2.68)

$$n_e \cdot (E_{ph}-E_{g,eff}) = \frac{1}{2\pi^2}\frac{1}{\hbar^3}(2m^*)^{3/2}\int_0^\infty \frac{E^{1/2}\times EdE}{exp(E-\varepsilon_F/kT)+1}$$

$$= \frac{1}{2\pi^2}\frac{1}{\hbar^3}(2m^*)^{3/2}\left(\frac{\varepsilon_F}{kT}\right)^{5/2}\frac{kT^{5/2}}{5/2} \tag{2.68}$$

By ratioing Eq. (2.68) to Eq. (2.67), we have

$$\varepsilon_F = \frac{5}{3}(E_{ph}-E_{g,eff}) \tag{2.69}$$

The total number of available states is $N = \frac{1}{3\pi^2}\frac{1}{\hbar^3}(2m^*)^{3/2}E^{3/2}$, for the case of $40meV$ excess energy, $N = 1.36\times 10^{18}cm^{-3}$. The carrier concentration calculated is $10^{18}cm^{-3}$. Carriers are not saturated.

The 2D case can be done in the same fashion by assuming a carrier temperature T. In fact, the same result that $\varepsilon_F = 2(E_{ph}-E_{g,eff})$ will be obtained.

To reach the saturation, a very intense pulse must be applied and it becomes the case involving phonon emission. The mechanism is different and saturation concentration is very high. In the case of fat pulse excitation then the carrier relaxation time $t_{relaxation}$ is compatible to the

pulse duration $t_{duration}$. An effective factor of absorption ($f = \frac{t_{duration}}{t_{relaxation}}$) should be considered while calculating the photoexcited carrier density.

2.9 References

1. Sadao Adachi, ***J. Appl. Phys. 58(3) R1*** (1985)

2. J. S. Blakemore, ***J. Appl. Phys. 53(10) R123*** (1982)

3. "***Optical Orientation***", Chapter 2, edited by F. Meier and B. P. Zakharchenya, Elsevier Science Publishers B. V. (1984)

4. G. Dresselhaus, ***Phys. Rev. 100 580*** (1955)

5. J. M. Luttinger, ***Phys. Rev. 102 1030*** (1956)

6. A. R. Edmond, "***Angular momentum in Quantum Mechanisms***" Princeton Univ. Press, New York (1957)

7. E. D. Kane, ***J. Phys. Chem. Solid 1 82*** (1956)

8. A. W. Overhauser, ***Phys. Rev. 89 689*** (1953)

9. R. J. Elliott, ***Phys. Rev. 96, 2661*** (1954)

10. Y. Yafet, ***Solid State Phys. 15, 371*** (1963)

11. B. R. Nag, "***Semiconductors Probed by Ultrafast Laser Spectroscopy***", Vol. I, edited by R. R. Alfano, Academic Press, New York, Chapter 1, 3 (1984)

12. Esther M. Conwell, "***High Field Transport in Semiconductors***", Academic Press, New York, Chapter 3 (1967)

13. J. Bardeen and W. Shockley, ***Phys. Rev. 80 72*** (1950)

14. W. A. Harrison, ***Phys. Rev. 104 1281*** (1956)

15. A. R. Hutson, ***J. Appl. Phys. 32 2287*** (1961)

16. H. Ehrenreich, ***J. Phys. Chem. Solids 2 131*** (1957)

17. G. Fishman and G. Lampel, ***Phys. Rev. B 16 820*** (1977)

18. M. I. D'yakonov and V. I. Perel', ***Sov. Phys. JETP 33, 1053*** (1971)

19. M. I. D'yakonov and V. I. Perel, ***Sov. Phys. JETP 38, 177*** (1974)

20. G. L. Bir, A. G. Aronov, and G. E. Pikus, ***Sov. Phys. JETP 42, 705*** (1976)

21. G. L. Bir, G. E. Pikus, A. S. Skal, ***Sov. Phys. Semicond. 8 715*** (1974)

22. "***Optical Orientation***", Chapter 3, edited by F. Meier and B. P. Zakharchenya, Elsevier Science Publishers B. V. (1984)

23. E. J. Johnson, R. J. Seymour and R. R. Alfano, "***Semiconductors Probed by Ultrafast Laser Spectroscopy***", Vol. II, Chapter 19, edited by R. R. Alfano, Academic Press, New York, (1984)

24. R. J. Seymour and R. R. Alfano, ***Appl. Phys. Lett. 37(2) 231*** (1980)

25. K. Zerrouati, F. Fabre, G. Bacquet, J. Bandet, J. Frandon and G. Lampel, D. Paget, ***Phys. Rev. B 37(3) 1334*** (1987)

26. R. J. Seymour, M. R. Junnarkar, and R. R. Alfano, ***Phys. Rev. B 24 3623*** (1981)

27. A. L. Powell, C. C. Button, J, S. Roberts, and P. I. Rockett, ***Phys. Rev. Lett. 67(21) 3010*** (1991)

28. J. F. Ryan, R. A. Taylor, A. J. Turberfield, and Angela Maciel, ***Phys. Rev. Lett. 53(19) 1841*** (1984)

CHAPTER THREE

EXPERIMENT METHODS

Measurements made as a function of time are so called "time-resolved" measurements[1-3]. When a semiconductor sample is exposed to an intense light source, e.g., a laser pulse, the electrons in a semiconductor are excited. The electrons gain energy and they are elevated to the conduction band. The conduction electrons can not hold this extra energy for a long time because they will experience scattering with other particles or even with themselves almost immediately following the optical excitation. The various scattering processes cause energy, momentum, and spin relaxations. Excitation followed by various relaxations is the major events to investigate and they are best studied by time-resolved measurements which include photoluminescence and absorption (or transmittance).

In ultrafast laser spectroscopy, the research attention is focused on the processes taking place in a very short period of time, generally speaking, in the picosecond or subpicosecond time domain.

In the course of my thesis, time-resolved photoluminescence measurements was applied as an experimental tool.

This chapter consists of ten sections. [3.1] briefly introduces the time resolved luminescence measurements; [3.2] describes the experimental setups; [3.3] through [3.5] talk about the process of data including acquisition, averaging, calculation, and fitting; [3.6] discusses the difficulties experienced in the course of this thesis; [3.7] gives the sample characteristics; [3.8] explains the flow of research; [3.9] provides with some preliminary results; [3.10] is references.

3.1 Time resolved luminescence measurements

There are several different techniques used to perform the time-resolved photoluminescence measurements. Optical gating[4,5], and streak camera[6] are the most commonly used methods. The function of the first two categories comes from the idea of time-space conversion and the constant speed of light. It takes 1 picosecond for the light to travel over 0.3 mm. From the experimental point of view, 1 picosecond is too fast to measure but 0.3 mm is a measurable quantity. With an optical gate (shutter) controlled by a light pulse traveling within a fixed distance, the measurement can be accurately made at any expected moment. The streak camera works like an extremely fast oscilloscope with storage capability and the operational time resolution can be as high as few picosecond.

Optical (Kerr) gating consists of a Kerr active medium located between two crossed-polarizers. Under the intense electric field of the laser pulse, the Kerr active medium experiences an induced birefringence. As a result, the transmitted light becomes elliptically polarized and passes

partly through the second polarizer. As far as the timing is concerned, light can pass the Kerr gate while it is temporally coincident with the intense laser pulse that opens the gate. The laser pulse can select a certain portion of the temporal profile of the photo-luminescence. The time resolution of this optical gating method depends on the laser pulse duration. Optical gating can provide very good time resolution as long as the gating pulse duration is very narrow.

The streak camera is the most widely used in the direct photo-luminescence measurements. Photon-electron-photon conversion is the major operational principle. Photoelectrons are emitted when light strikes the photocathode. The emitted electrons are deflected by an applied ramp voltage which causes the electrons to be transversely streaked across a phosphorescent screen at the same time they are accelerated towards the anode. The photoelectrons released at different times from the photocathode strike the phosphorescent screen at different positions causing a track with a spatial intensity profile directly proportional to the incident temporal intensity profile of the luminescence.

With connection to a Wollaston prism, a streak camera can simultaneously measure the temporal profiles of luminescence of opposite polarizations. A streak camera also can be used by coupling it to a spectrograph to produce a 2-dimensional array providing both temporal and spectral characteristics of the photoluminescence. The detail of the operation of streak camera will be discussed in [3.2.4].

3.2 Experimental setups

The experiments were performed using subpicosecond pulse excitation and time resolved photoluminescence (PL) streak camera techniques[7].

Two laser systems, CPM dye laser and tunable dye laser, have been used to generate two exciting energies in this research plan. The exciting wavelengths are 620nm (above bandgap) and 750nm (close-to bandgap) lines. Both exciting lines can be generated from the CPM dye laser system with high exciting intensity level at 20 Hz repetition rate. The tunable dye laser system generates 750 nm line with low exciting intensity level at 82 MHz.

3.2.1 CPM dye laser system

The laser source system consists of a CPM dye laser[8], a 4 stages optical amplifier, a double-prism pulse compressor, super-continuum generator, and synchronous amplification.

CPM dye laser and Optical amplifier

CPM stands for Colliding Pulse Mode-locking. This CPM laser system is shown in Figure 3-1, 3-2, and 3-3. In Figure 3-1, Rh6G is functioning as the laser active medium and DODCI is functioning as the mode locking medium. Rh6G is pumped at the threshold by an Ar^+ laser. The laser cavity is in a ring configuration the emitting light from Rh6G will go in opposite directions. DODCI absorbs weak light when it is not

saturated and it transmits when saturated. Because of this special character, a light spike which has high enough intensity can bleach the DODCI and pass through. The spike then gets amplified and sharpened in the cavity.

In order to have the most efficient mode locking, DODCI is located at exactly 1/4 of the entire cavity length from Rh6G. Because of its very short recovering time, DODCI, a saturable absorber, performs like an organic optic shutter with 1 ns recovery time. The wings of pulse which have very low intensities will be eliminated and the light pulse will be squeezed to be very narrow. The mode locking is accomplished in DODCI because the random phased light cancels out, only the mode-locked light can pass.

The output pulse from the CPM laser has a 60 fs pulse width and 3 pJ/pulse. It passes through 4 amplifiers following the CPM laser. The total amplification through all the amplifiers is 10^5. The dye in the first cell is Sulfarhodamine B (SRB). The other three cells are filled with Sulfarhodamine 640. (SR640). The pumping light for the amplifiers at 530 nm is the second harmonic of a Q-switched Nd:YAG laser. The details of the laser are given in the theses of Dr. A. Katz[11] and Dr. M. Yan[12].

Compressor and Continuum generator

The laser pulse after passing through the amplifiers has a power of 0.3 mJ and the wavelength is 620 nm. The generation of the 750 nm line is accomplished through the combination of pulse compression, supercontinuum generation and synchronous pumping techniques. The

0.3 mJ pulse of 450 fs in width is sent into a 2-layer double-prism compressor. The principle of pulse compression is to balance the (positive) chirp by an equal amount of optical path in glass (negative). The width of the output pulse becomes 110fs. The pulse losing 50% of the original energy on compression is focused (f=5 cm) on a 5mm methanol cell and a broad band spectrum is then generated.

The 750 nm excitation line is selected from the continuum by a 10nm narrow band filter and is amplified in a 1 cm cell of LDS 750 pumped by the 530 nm line of 90 - 100 mJ/pulse in power from Nd:YAG (the second harmonic of YAG). The 530 nm line is focused through a 25 cm cylindrical lens. The amplified 750 nm line is 0.4 μJ/pulse. The amplification is 15-20. The optical density of LDS 750 is measured to be 0.4 in a 500 mm cell. The details of the laser are given in the thesis of Dr. M. Yan[12].

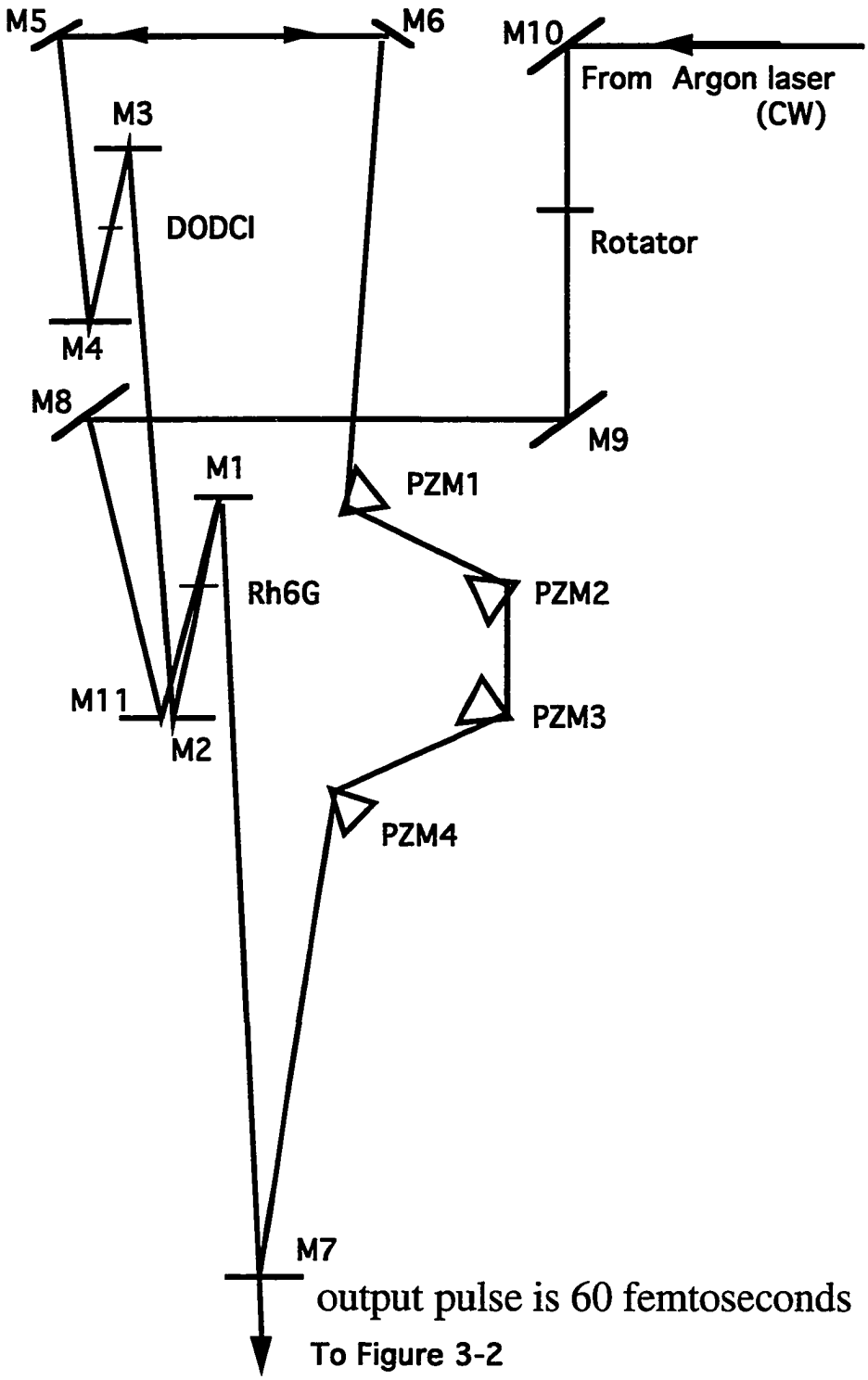

Figure 3-1. Colliding Pulse Mode-locking ring dye laser

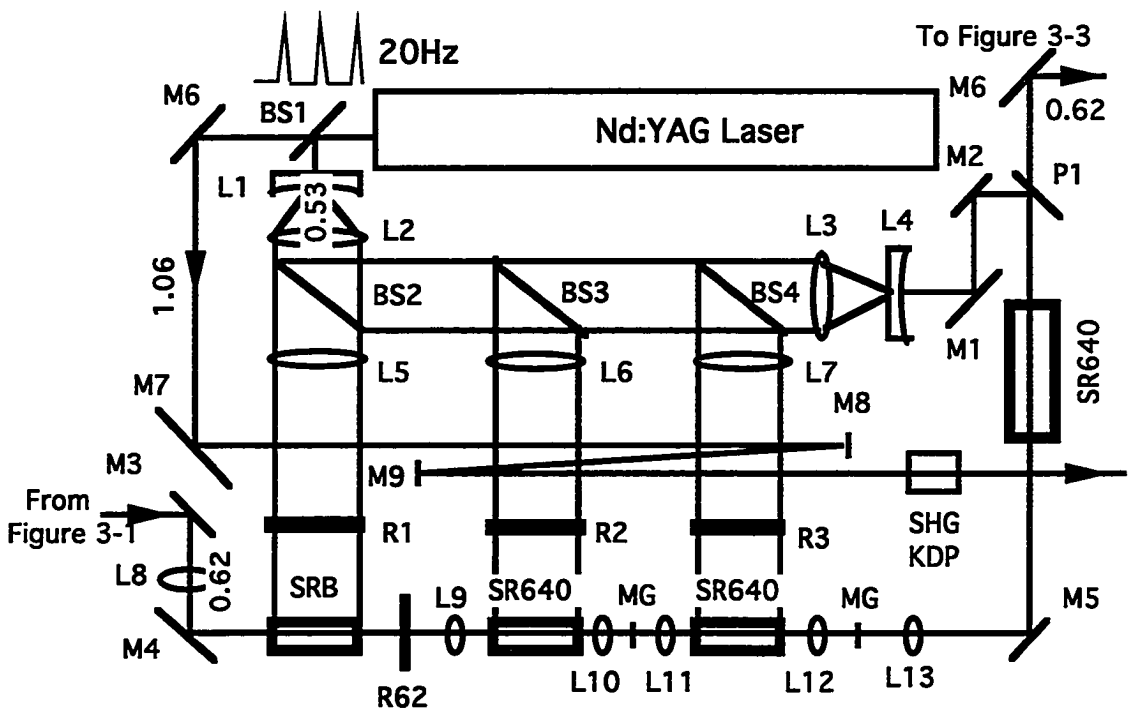

Figure 3-2. Amplifier system following the CPM dye laser. Details are given in references [11] and [12].

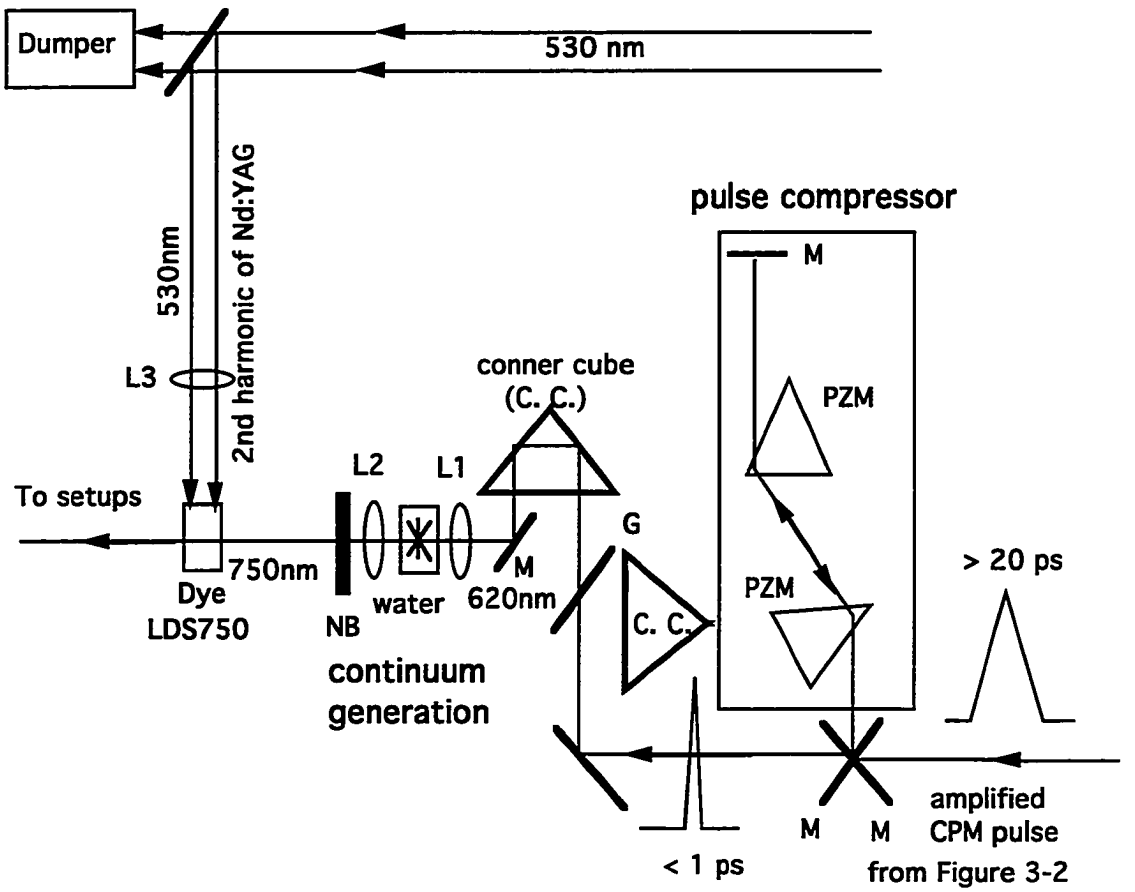

Figure 3-3. Diagram of pulse compression, supercontinuum generation, and amplification of the selected wavelength, 750 nm line. Details are given in reference [12].

3.2.2 Tunable dye laser

The low density experiments are conducted by using a system consisting of a synchronously pumped dye laser (Figure 3-4), a spectrometer with 1nm resolution and a 10 ps time resolution 2D streak camera. The 2D streak camera here allows user to open 512 vertical and

512 horizontal detecting windows. A 1D streak camera only has 2 vertical detecting windows.

The pumping light source for the dye, LDS 750, is a cw mode locking Nd:YAG laser with an acousto-optic crystal driven at 41MHz which is the resonant vibrational frequency of quartz. The output from Nd:YAG laser at the 1.06 mm line is 90-100 ps in width and the average power is 8W. A pulse compressor (glass fiber, grating) reduces the pulse width down to 4 ps with average power of 4.5 W and then the second harmonic (530 nm) is generated in KTP. The 530 nm line output has 800 mW of power.

The dye cavity length which determines laser pulse repetition rate is designed to match with the pumping rate. The repetition rate is 82 MHz. The output laser pulse at 750 nm line is 100mW in power and 400-500 fs in width.

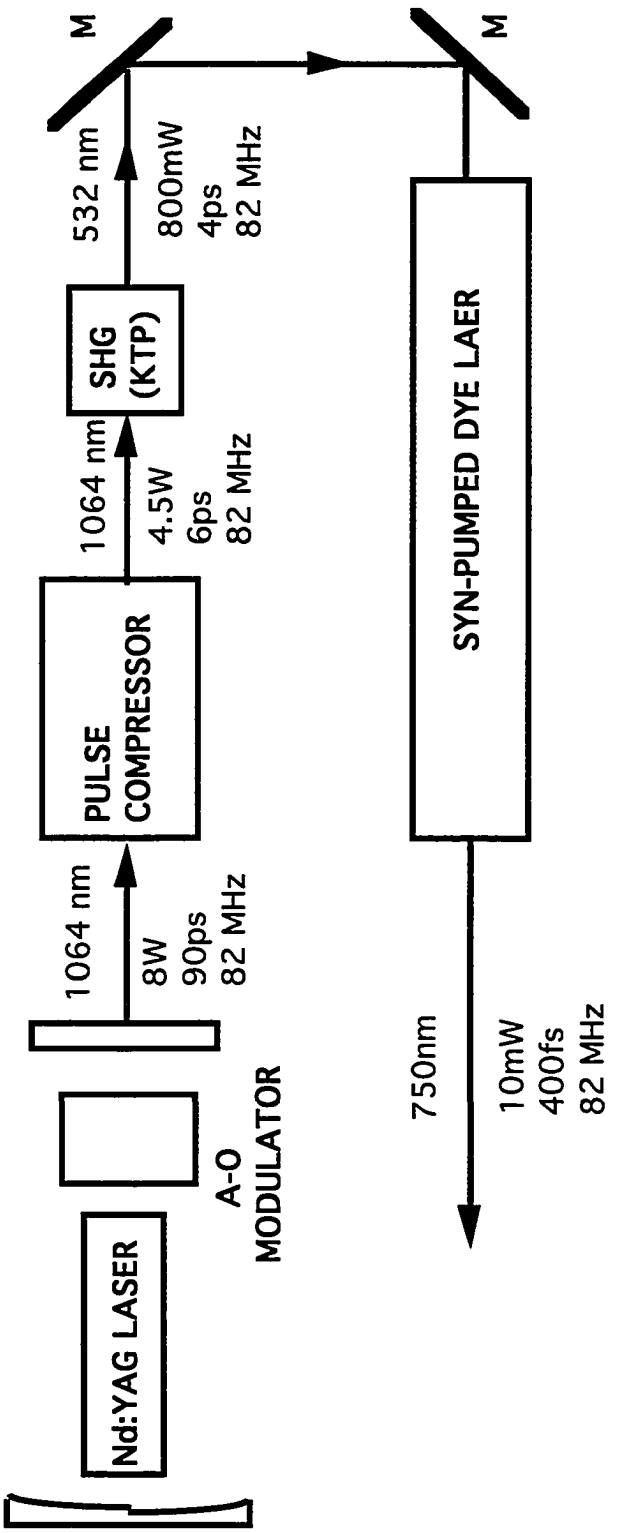

Figure 3-4. Diagram of tunable dye laser system

3.2.3 Optical arrangement for the time resolved measurement with streak camera

The optics of the setup consists of 3 mirrors, 3 lenses, 2 quarter wave plates, 1 linear polarizer, 1 thin glass slide, 1 glass wedge, and a Wollaston prism. The relative positions of these parts are drawn in Figure 3-5.

The excitation pulse first encounters a glass wedge, 8% of the light is reflected at the surface to generate a coherent prepulse and the rest passes through. The prepulse is used as a time reference in data averaging and it indexes the electronic jittering. A pair of quarter wave plates ($\lambda/4$) are used to convert the optical polarization between linear and circular. One, located along the exciting path, converts the linearly polarized incoming pulse to be circularly polarized; the other, located along the luminescence path converts the circularly polarized luminescence to be linearly polarized. Both are located in front of the Helium dewar. The incident angle of excitation is around 10^{o}, therefore, the measurements are basically for front luminescence. The Wollaston prism is used to spatially separate the vertically (V) and horizontally (H) polarized components.

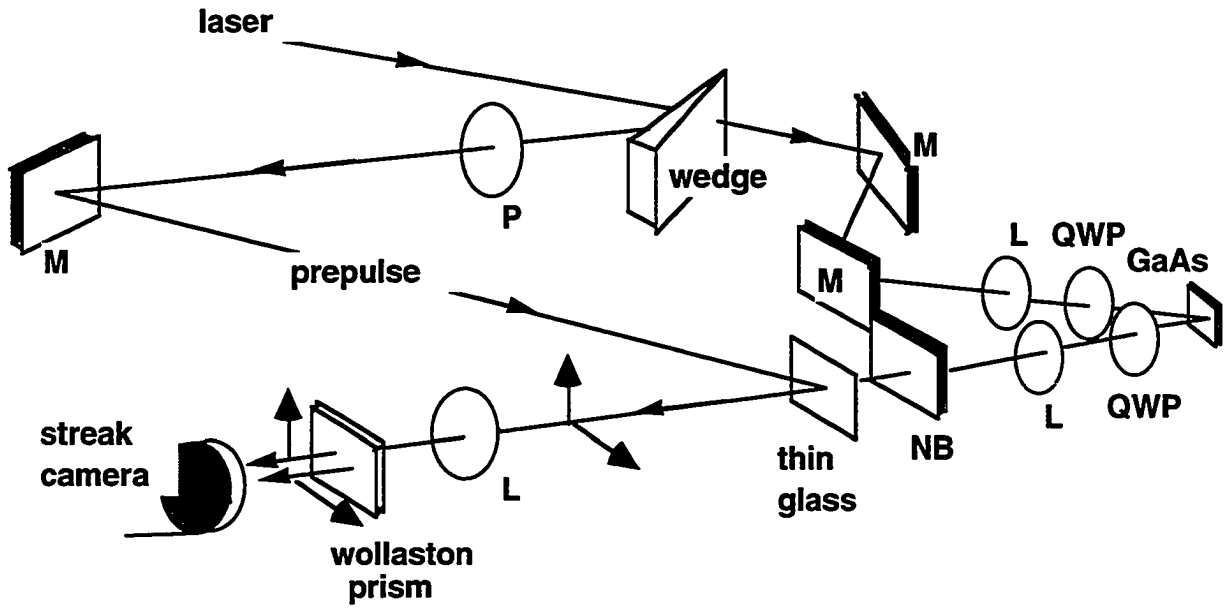

Figure 3-5. Experimental setups for the simultaneous detection of both polarized luminescence. M, L, QWP stand for mirror, lens, and quarter wave plate, respectively.

This setup can be modified to have both energy and temporal resolution in one measurement. The 1D streak camera with Wollaston prism in the simultaneous measurement setups are replaced by a 2D streak camera connected with a spectrometer and a depolarizer when both spectral and temporal resolution are required in one measurement. This new setup is schematically demonstrated in Figure 3-6.

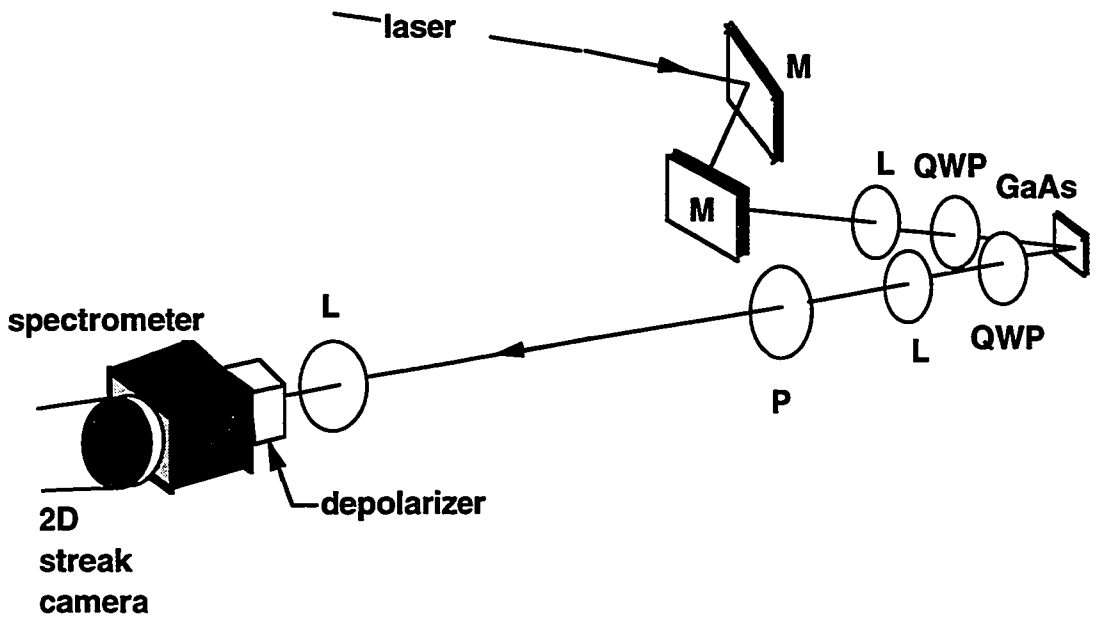

Figure 3-6. Experimental setups for measurements with energy-and-time resolution.

Low temperature and vacuum techniques are also involved in my measurements. High vacuum for experiments is provided by a diffusion pump operating at pressure under 10^{-3} torr. Low temperature measurements are made in a cold finger Helium dewar (Janis, model ST). The temperature controller is made by Lake Shore Cryotronics (model DRC 80C).

3.2.4 Streak camera

The entire set of the streak camera that I used consists of five parts: streak unit (HAMAMATSU synchroscan streak unit M1955), SIT camera,

temporal analyzer, camera controller, and monitor. Among them, the streak tube is the major detective device in the streak camera.

The fast scanning (sweeping) device in the synchroscan unit is triggered by the escaping light split off from the exciting laser pulses running at 120 MHz in my experiments. The triggering signal is detected by a fast diode. The time taken by the triggering signal traveling through the cable to the streak camera unit must match the time taken by optical signal (exciting pulse) traveling in the air before it reaches the sample. The electric triggering runs periodically but the optical signal only comes up at certain time, in order to detect the entire fast-changing luminescence signal a delay cable box is therefore necessary. The principle of operation of a streak tube is discussed with a schematic diagram provided in Figure 3-7 in the next paragraph. The interior of a streak tube (HAMAMATSU N1357) is drawn in Figure 3-8.

In Figure 3-7, fluorescence from the optically excited sample is collected through the entrance slit and the input optics forms the incident image of the fluorescence on the photocathode plane at one end of the streak tube. The equivalent electronic image then will be generated and the electrons are accelerated by the accelerating electrode next to the photocathode and enter the deflecting field. A pair of deflecting plates are installed to create the deflecting field. At the moment when electrons are passing through the deflecting field, a high speed ramp voltage is applied to the plates to deflect the electrons vertically from top to bottom. This sweep must be synchronized to the time when electrons pass through.

After the deflecting field, the deflected electron image is projected to the multi-channel plate (MCP). It is electronically magnified and then applied to the phosphor screen. At here, the electronic image is converted back into an optical image. The secondary optical image is then going through the output relay lens system entering the next part which is the SIT camera. During the operation, the deflecting field has converted the temporal information into spatial information and a flowing image (bright streak) will be seen on the TV monitor. The bright streak runs vertically from the top to the bottom following the time axis (Y). A calibration for the streak rate at each channel on the time axis is necessary because the rate is not constant. The streak rate calibration will be discussed in [3.4].

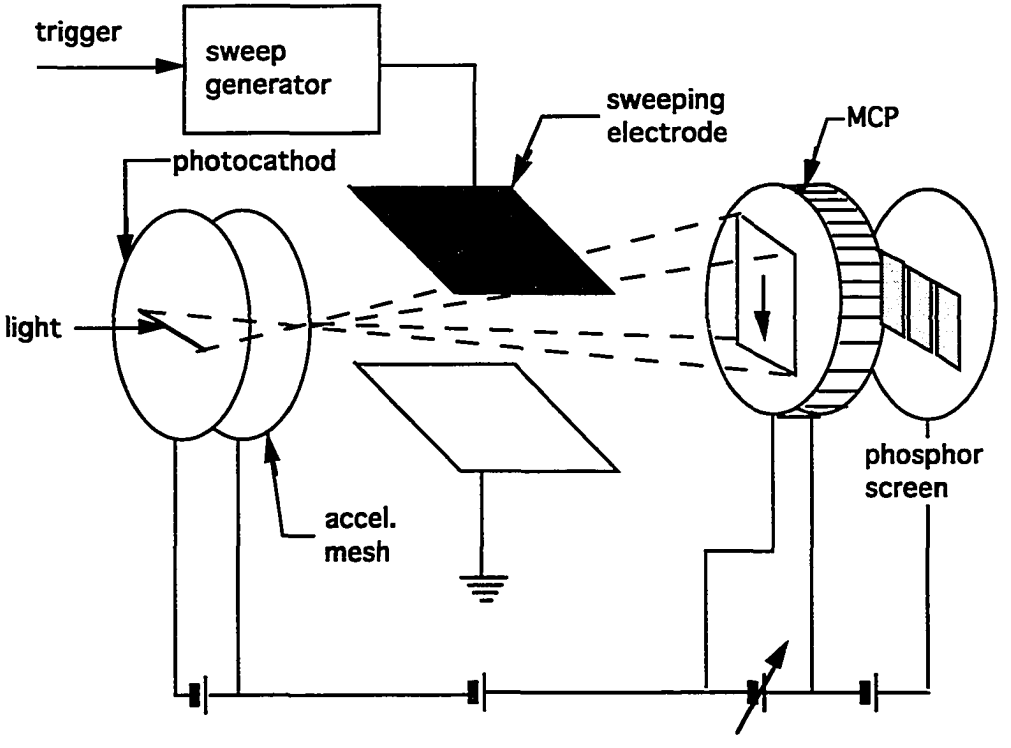

Figure 3-7. *Schematic diagram of the operation of a streak tube*

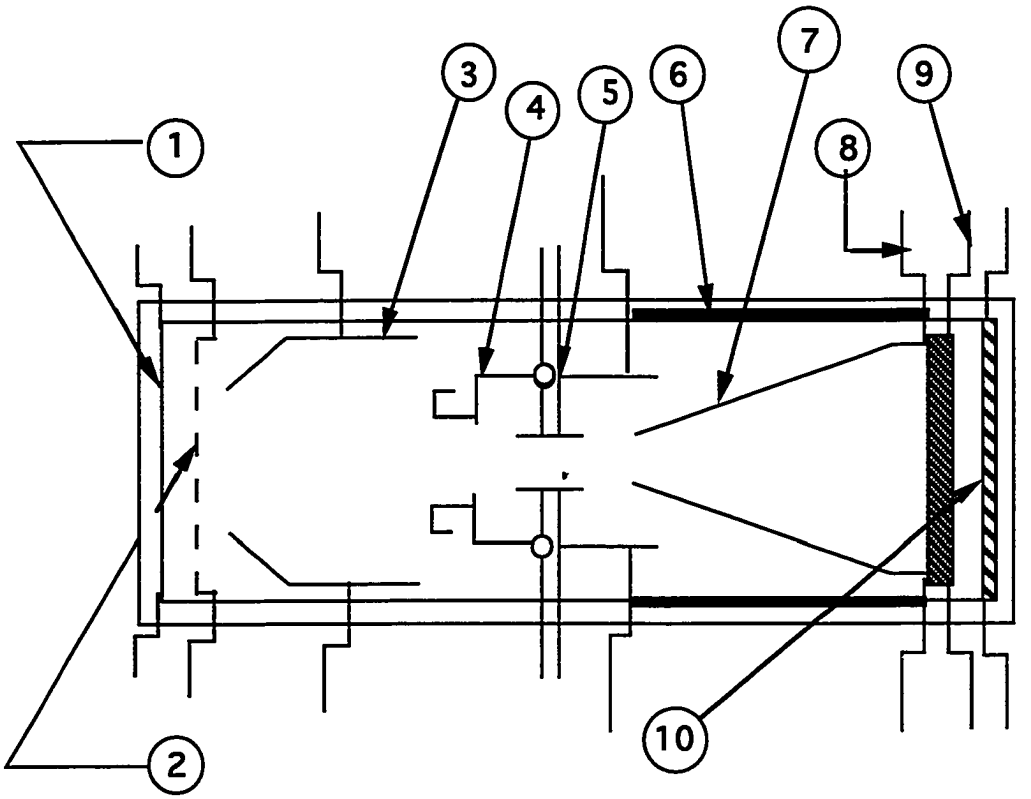

1. Photocathode (-10kV)
2. Mesh electrode (-8.5kV)
3. Focusing Electrode (-8.7kV)
4. Anode (0V)
5. Deflecting plate
6. Wall anode
7. Cone electrode (0V)
8. Micro-Channel Plate input electrode (0V)
9. MCP output electrode (+0.5 to 1 kV)
10. Fluorescent sereen (+3.5 to 4 kV)

Figure 3-8. Cross section diagram of the interior of a streak tube N1357

3.3 Data acquisition and Averaging

In the temporal analyzer (TA) of the 1D streak camera, data are collected and organized based on the pre-set conditions selected at the very beginning. In case 20 frames are chosen at the acquisition then the TA will accumulate 20 frames of data and what is displayed is the averaged of 20 frames. Generally speaking, it takes 30 ms to complish 1 frame of data. The data transfer from the TA to an IBM computer is done through an interface routine <SPINRAW>. After transferring, the data is stored on floppy disk in the format of numbers like a 16 x 16 matrix. For each experimental condition, at least 10 measurements were made and an averaging routine <SPINAVE> was written to average the data files. This routine reformats and average data based on the temporal coordinate of the prepulse. The noise level is greatly reduced in the averaged data file.

In the TA of the 2D streak camera, the data organization (acquisition, accumulation, averaging...) is similar to that of 1D except for the format. The managing routine <TA> has many modes for all different purposes of use. Data stored in the minicomputer of the TA is structured like a 3D image. Each data point has 3 coordinates, intensity and two other variables. In my case, they are energy and time. To be more specific, the horizontal axis is energy and the vertical axis is time.

Data reformation can be done by running the ANALYZE MODE of <TA> in which horizontal and vertical windows were selected for relevant part of the data images. The next step after data selection is data translation from binary to ASCII code. Then data can be recognized by

IBM routines and the following work is just exactly what has been applied in using the 1D streak camera.

The major difference between the operation of a 1D and a 2D streak camera is the simultaneity and multi-resolution of energy and time. The choice of which streak camera to use is based on the purpose of experiment.

3.4 Data calculation

During the mathematical operations, two necessary steps must be included. Window balancing improves the accuracy of data by lifting the unequal detector sensitivity between two windows, and streak rate calibration linearizes the nonlinearity of time scale.

Window balance In the streak camera, sometimes the sensitivity of the two detecting windows may vary. By applying correction coefficients to the intensities in both windows, the unequal sensitivity can be balanced. This is the so called "window balance". To determine the correcting coefficient in my experiments, the intensities of the V-component and H-component of a 45° polarized beam were measured in both windows. Theoretically, intensities of these two components were supposed to be equal, however, due to the unequal detector sensitivity, the intensity in window 2 was 85-93% of that in window 1.

Figure 3-9 shows the setup to test the balancing coefficient.

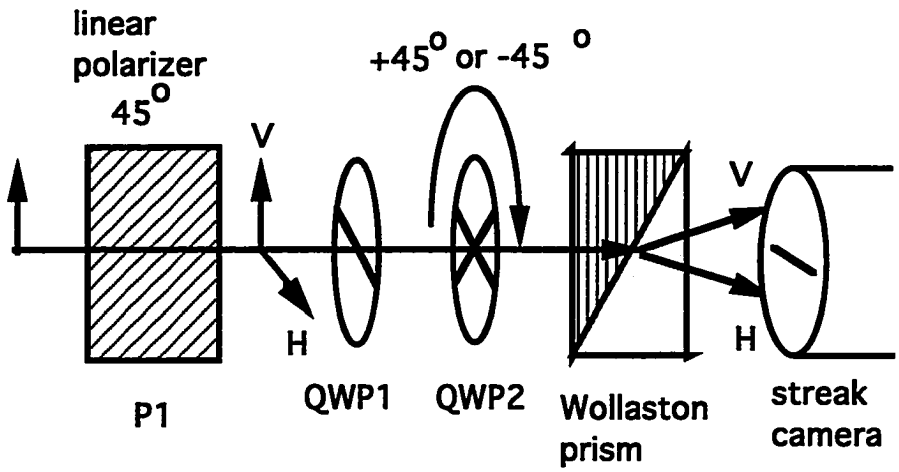

Figure 3-9. The setup to test the window balancing coefficient.

Suppose I_V, I_H, I_1, I_2, are the intensity of the vertical component, the intensity of the horizontal component, the intensity detected by widow 1, the intensity detected by window 2, respectively, C_1, C_2 are the intensity correction factors for window 1 and window 2, respectively. Obviously, we have $I_1 = C_1 I_V$ and $I_2 = C_2 I_H$ for the condition such that the optical axis of QWP2 is perpendicular to that of QWP 1, otherwise, we have $I_1 = C_1 I_H$ and $I_2 = C_2 I_V$ if the optical axis of QWP2 is parallel to that of QWP 1.

Let's define the ratio of the signal detected by window 1 to that of window 2 as

$$R_{perp} = \frac{I_1}{I_2} = \frac{C_1 I_H}{C_2 I_V} \text{ for the perpendicular case} \qquad (3.1)$$

$$R_{para} = \frac{I_1}{I_2} = \frac{C_1 I_V}{C_2 I_H} \text{ for the parallel case} \qquad (3.2)$$

By multiplying R_{para} to R_{perp} we have

$$R_{perp} \cdot R_{para} = \frac{C_1 I_H}{C_2 I_V} \cdot \frac{C_1 I_V}{C_2 I_H} = (\frac{C_1}{C_2})^2 \qquad (3.3)$$

By taking the ratio of R_{perp} to R_{para} we have

$$R_{perp} / R_{para} = \frac{C_1 I_H}{C_2 I_V} \Big/ \frac{C_1 I_V}{C_2 I_H} = (\frac{I_H}{I_V})^2 \qquad (3.4)$$

The window balance can be obtained from equation (3.3) by using

$$WB = \frac{C_1}{C_2} = \sqrt{R_{perp} \cdot R_{para}} \qquad (3.5)$$

and numerical value of R_{perp} / R_{para} in the equation (3-4) indicates whether I_V and I_H are equal. For example, if one measurement gives

$$R_{perp} = 0.874 \quad \text{and} \quad R_{para} = 0.881$$

then the window balance, $WB = 0.878$ and the ratio of the H-component to the V-component, $\frac{I_H}{I_V} = 0.996$. Result of the measurement for the signal ratio, $\frac{I_H}{I_V}$, and the window balance factor, WB, are provided in Figure 3-10 and 3-11, respectively.

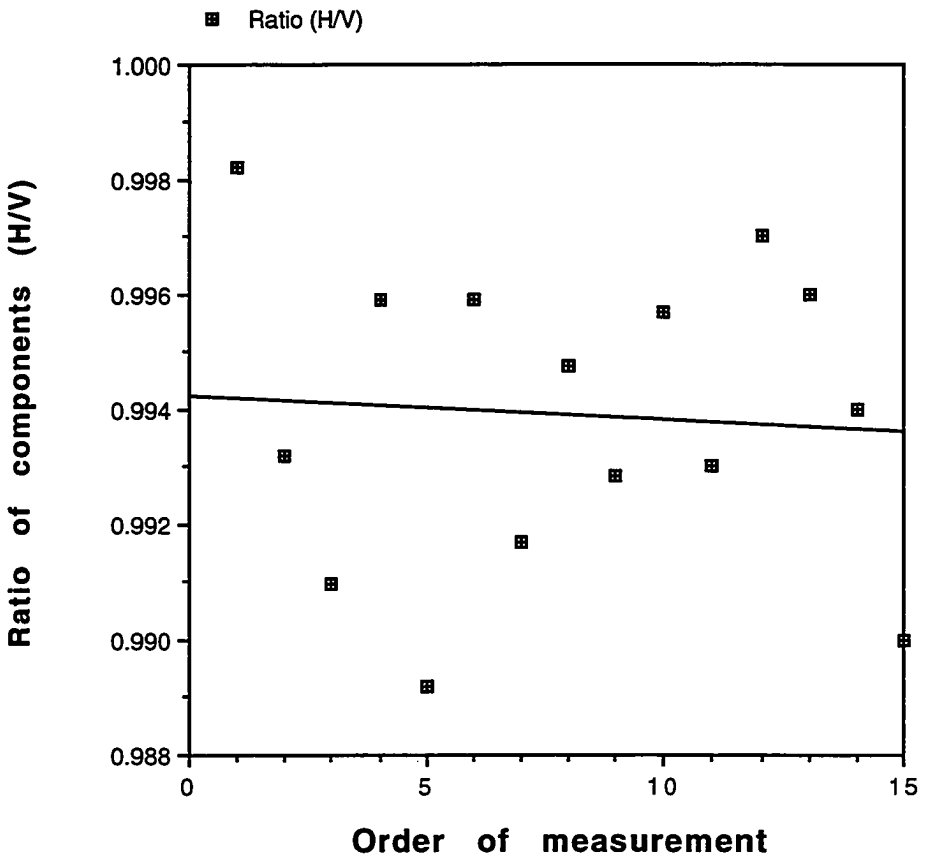

Figure 3-10 Ratio of horizontal component (H) to vertical component (V). The solid line is a least square fit to the data points

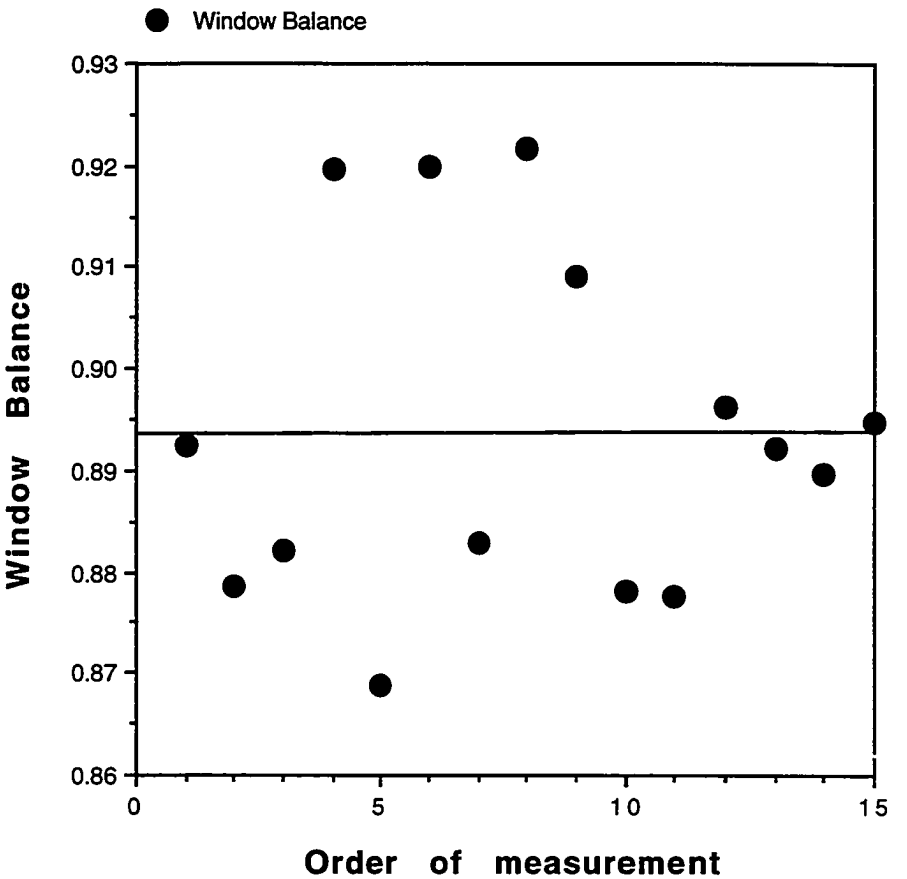

Figure 3-11 Window balance ($\frac{C_1}{C_2}$) (see Eq. 3.5)

Streak rate calibration The streak unit (M1955) provides four operational streak rates (0.3ns, 1ns, 2ns, 5ns/15mm). Those rates, indicated on the panel, are the averaged rates over all channels. In fact, the rate at each channel is not the same. They follow some rate distributions. Unfortunately, the rate distributions are also different for the given four

rates. Therefore, calibration of the streak rate at each channel is quite important. A software <STRIKCAL> was written for the streak rate calibration. (see Appendix)

The calibration is done by using an etalon with a piece of metal with fixed thickness "spacing d" located between two semitransparent mirrors with transmission coefficient T. The calibrating pulses produced in this manner make up a train of pulses separated in a time $\Delta t=2d/c$, where c is the speed of light. The intensity profile of the train is a decaying exponential with each subsequent peak reduced by $(1-T)^2$. For each round trip of the pulse between mirrors, a light pulse of intensity $I_k=I_0(1-T)^{2k}$ is produced, for k=0,1,2,3....n. Since $I_k/I_{k+1}=1/(1-T)^2=$ constant, the envelope of the peaks of the pulses follows a single exponential decay as $I = I_0 exp\{[t/\Delta t]\ell n(1-T)^2\}$, where the time between peaks $t=k\Delta t$. The peaks are used to calibrate the time axis and correct for the intensity variations. The sweep rate per channel $\Delta t/\Delta X$ versus the channel number X is used to calibrate the time base of the streak camera where ΔX is the number of channels between peaks and Δt is fixed for a given etalon mirror-spacing.

In calibration, the calibrator has to adjust the optical delay to move the pulse train in order to have the pulse train cover as many channels as possible. In Figure 3-12, the streak rate calibration setup is drawn. In Figure 3-13, four typical calibration curves are plotted for different streak rate.

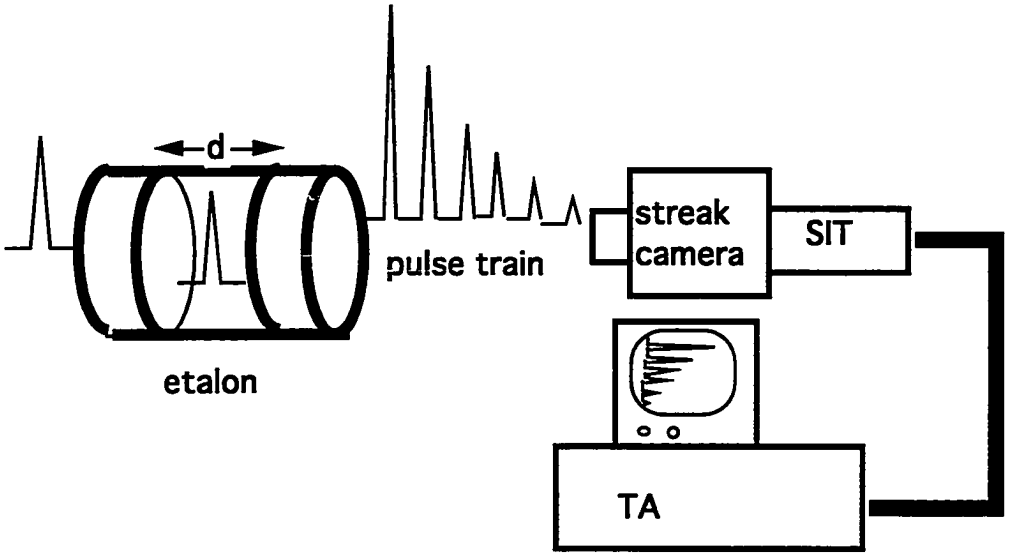

Figure 3-12. Diagram of the streak rate calibration setup

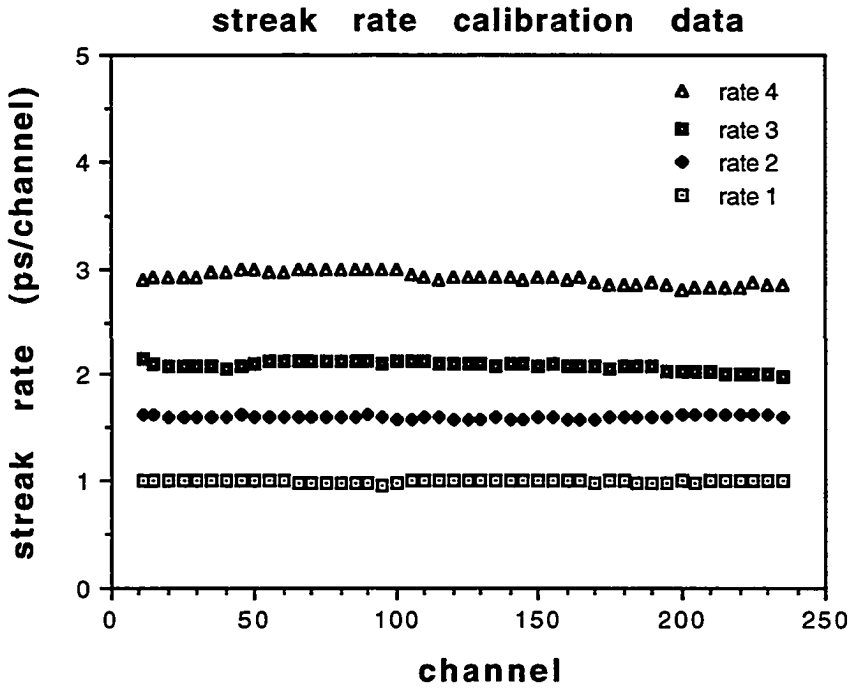

Figure 3-13. Calibrated streak rate of each channel (ps/channel)

Spin polarization calculation A routine named <CACUSPIN> (see Appendix) was written for calculating the time resolved spin polarization profile from which the degree of spin polarization and the spin relaxation time can be determined. In running this routine, the V- and H-components along with their sum, difference and ratio are all visible. They are all shown simultaneously on the monitor to provide a clear picture for comparison. In the calculation, the data were balanced by the correcting factor determined previously and the data files are in the format of 6 x 256 matrices.

3.5 Fitting

The spin depolarization time constant, τ_s, provides us with a great deal of information such as the spin and momentum relaxation mechanisms; the temperature dependence of τ_s; the carrier concentration dependence of τ_s; and how quantum confinement affects the spin relaxation. To determine the spin relaxation time constant, τ_s, time-resolved spin polarization data were fit with a single exponential decay model which is the simplest theoretical prediction. This job was done by the software <SPINFIT>. (see Appendix)

Generally speaking, there are two strategies to analyze (fit) the time resolved spin polarization data in order to determine the spin relaxation decay time constant. They are :

1. **Dual fitting (DF):** This method applies two time constants, τ_r and τ_s, to simultaneously fit the two oppositely polarized time-resolved luminescence components without calculating the spin polarization.

2. **Single fitting (SF):** This method applies one time constants, τ_s, to fit the time resolved spin polarization profile obtained from calculations.

To obtain τ_s, the fittings by using Eq. (2.28), (2.29) to these two time resolved luminescence, (DF), introduces higher percentage error and consumes twice the amount of time compared to the other fitting strategy, (SF), in which τ_s is obtained from fitting to the spin polarized temporal profile by using Eq. (2.30). The major drawback of DF strategy is the inconsistency of the fitting parameters between two conjugate luminescence for the pair of fitting constants determined from one luminescence curve may not fit the other. From another point of view, dual fitting fits the luminescence therefore the initial degree of spin polarization is invisible but in the single fitting, the initial degree of spin polarization is an important fitting parameter.

The itemized comparison between two fitting strategies regarding initial spin polarization, time consumed for fitting, and the fitting consistency are listed in Table 3-I.

From Table 3-I, single exponential fitting has more advantages, therefore, it was the fitting strategy I used. In fitting the time resolved spin polarization, tremendous fluctuation of spin polarization due to dividing over a small number was seen in the tail regime ($t > 400ps$) where the luminescence is very weak. Therefore, more attention was paid to the

front, where the luminescence is intense. The τ_s obtained from this fitting was compared to the other relevant data with systematic similarities and variations.

Table 3-I The itemized comparison between two fitting strategies

	Single fitting	Dual fitting
Direct observation of initial spin polarization	**yes**	**no**
Time required to perform the fitting	**short**	**long**
Worry about fitting constant's consistency	**no**	**serious**

The fitting limitation is determined by the time resolution of the luminescence which, for the most of the measurements, is around 25-45 picoseconds. In this thesis, all the spin relaxation time constants are limited to be longer than 25 picoseconds.

3.6 Experimental difficulties

During the course of this thesis it was noted that a clear-cut spin polarization data curve was difficult to obtain. The polarized luminescence components are always look pretty, however, the luminescence from TA must be averaged to smooth out the noise and be mathematically processed to obtain the spin polarization. To judge

whether the spin polarized signal is good for analysis, based on the look of photoluminescence, is impossible at the moment of measurement. For the same experimental condition, normally ten or more files were taken for averaging. Therefore, this is time consuming.

Large noise levels in the spin polarization temporal profiles are another difficult. The worse noise level among the accepted data introduced a 35% error percentage to the spin polarization time (average is 20%). Anything with an error percentage higher than 35% was neglected. Based on this fact, less than 50% of the measurements are available for fitting.

3.7 Samples

There are four samples used in the measurements. Due to the complexity of the measurement, it is impossible to measure all samples for every experiment. Sample slection was based on the similarities (except the compared factor) for each comparison and the observed signal intensity. The characteristics of the selected samples were summaried in Table 3-II.

Table 3-II Semiconductor samples used in the measurements

Type (n, p, i)	type	Other characteristic	Experiments done varying
p	3D Bulk	p=7x1017 cm^{-3}	T, N(low T), E_{ex}
i	2D (55Å)	x=0.3 (Al)	T, N
i	2D (90Å)	x=0.3 (Al)	T
p	2D (40Å)	stressed (Si) p=10^{18} cm^{-3} x=0.35 (Al)	T, E_c

where i stands for intrinsic, E_{ex} and E_c are the exciting energy and carrier energy, respectively.

3.8 Flow chart of the research

The approach of this research is from two directions, *theory* (calculation of Fermi integrals) and *experiment* (time resolved luminescence using streak camera). The variables chosen to investigate electron spin dynamics are *temperature (T), energy (E_C), and concentration (N).* The results from each direction are compared to the corresponding part from the other. The conclusions are made based on these comparisons.

Spin relaxation mechanisms depend on momentum relaxation. The spin relaxation times were expressed as a function of momentum relaxation times. Knowing momentum relaxation scattering is equally

important to knowing spin relaxation and they will be determined simultaneously.

There is an approximation made to simplify the calculation, namely, $\tau_p \sim (E/kT)^{-n}$, where the variable n depends on the type of scattering for momentum relaxation. These types include acoustic phonon (ac) scattering, piezoelectric (pz) scattering, impurity (im) scattering, optical phonon (op) scattering. The result of calculations will depend on n.

As a matter of fact, investigations using every dependence (path T, path N, and path E_C (see Fig. 3-14)) can provide information about the spin relaxation and momentum relaxation scattering mechanisms.

All three paths are tested and *identical* information about the spin relaxation mechanism and momentum relaxation scattering is expected from different path.

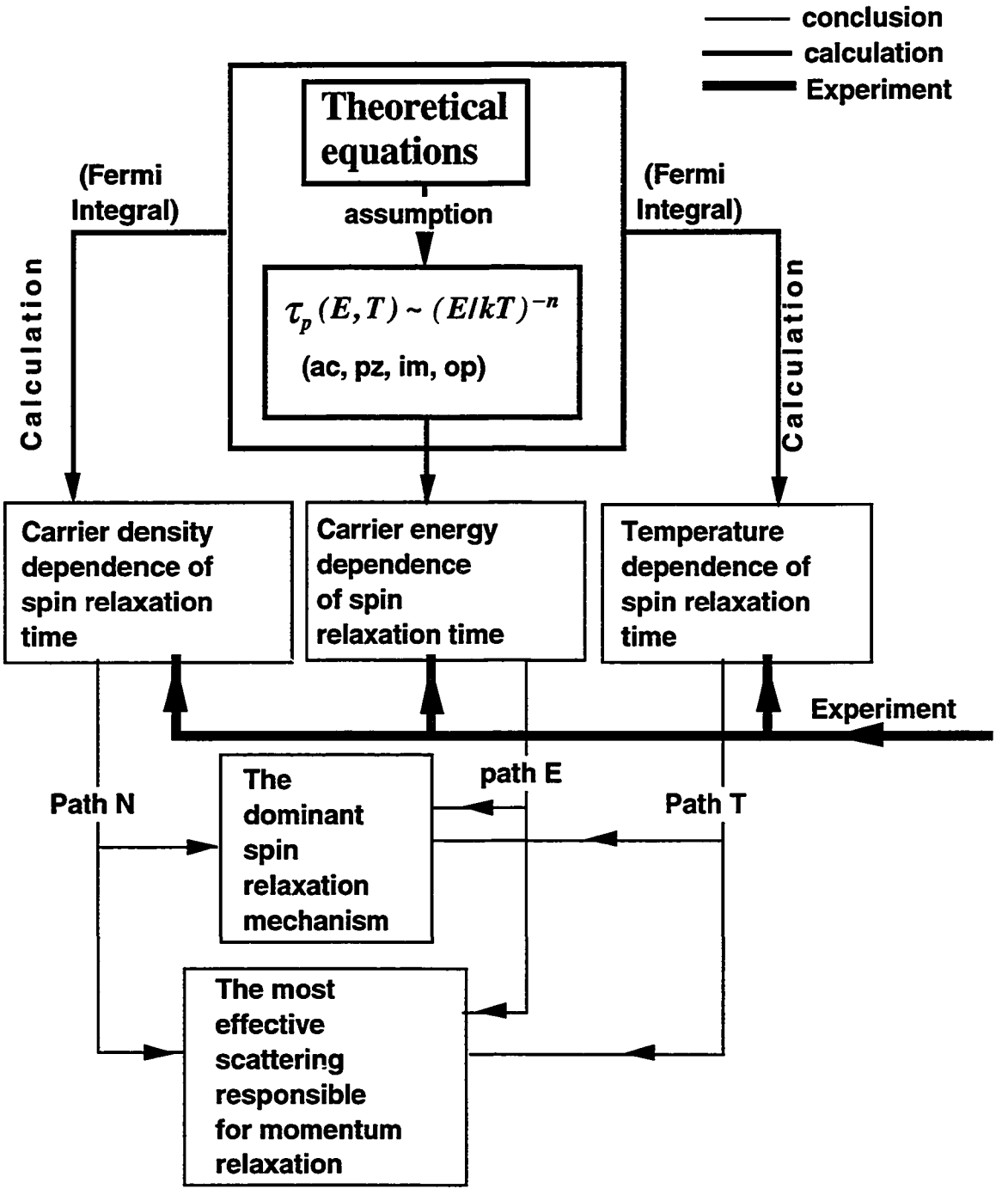

Figure 3-14. Flow chart of the logic of the thesis

3.9 Preliminary calibration testing results

3.9.1 Degree of circular polarization of the exciting laser pulse

In all my experiments, the exciting laser pulses are circularly polarized. They are converted from linear polarization by a quarter wave plate at suitable wavelength. In order to have a high degree of spin polarized signal a highly circularly polarized excitation must be guaranteed. Before starting the measurements, the degree of circular polarization of the excitation was tested. The setup to test the circular polarization consists of a photodiode, 2 linear polarizers, and 1 quarter wave plate of the wavelength to be tested. The arrangement of testing optics drawn in Figure 3-15, 3-16, 3-17. The procedures of checking the degree of circular polarization are described as the following:

Step 1. Align two linear polarizers (P1, P2) and the photodiode with the beam path.

Step 2. Rotate P2 to make it perpendicular to P1. If P1 is perpendicular to P2 then the transmission should be almost zero. Then fix P1 and P2 at this orientation. (see Fig. 3-15)

Step 3. Locate the quarter wave plate between P1 and P2.

Step 4. Rotate the quarter wave plate until the transmission intensity becomes maximum then fix the quarter wave plate at this orientation. (see Fig. 3-16)

Step 5. Loose P2 and rotate it. Take record of the transmission at different orientation of P2. (see Fig. 3-17)

Step 6. Plot out the record.

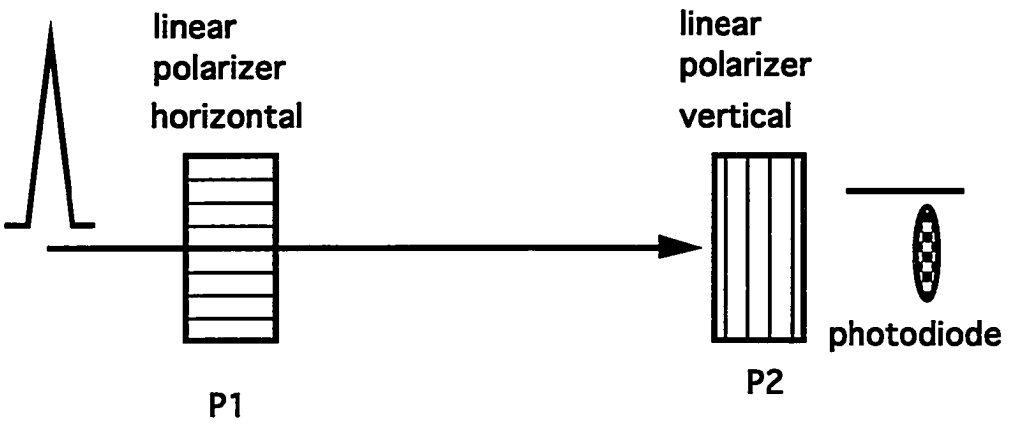

Figure 3-15. The initial arrangement of the setup for testing the circular polarization of the excitation.

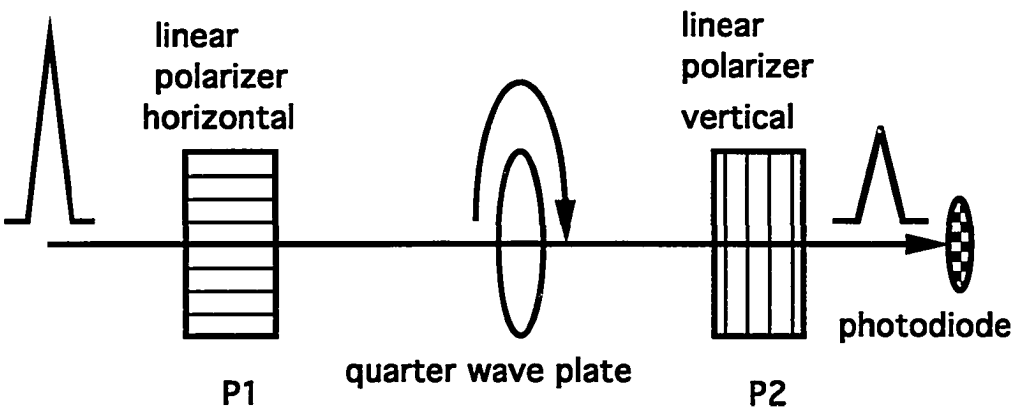

Figure 3-16. The arrangement of the testing setup after the quarter wave plate was introduced.

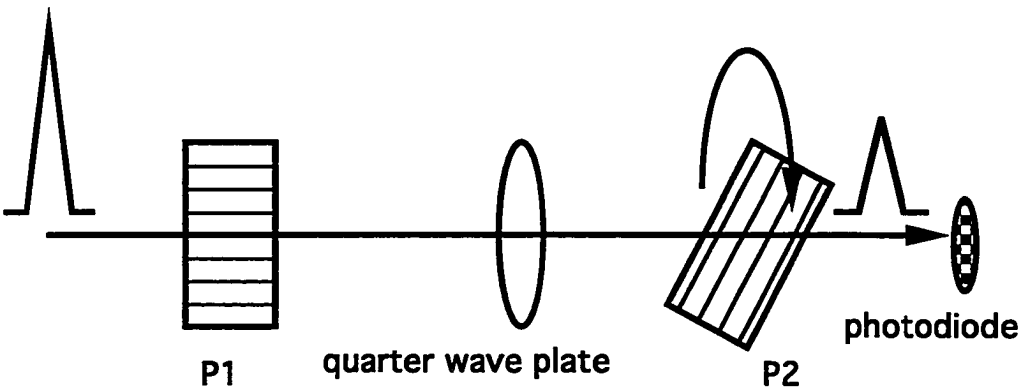

Figure 3-17. The arrangement of the setups during testing

If the intensity of transmission keeps constant, then the circular polarization is perfect. The deviation of my measured intensity of the transmitted laser is 5% as a function of P2's orientation. The transmitted intensity varies over an order of 3 without the $\lambda/4$ located between P1 and P2. The testing results are presented in Figure 3-18.

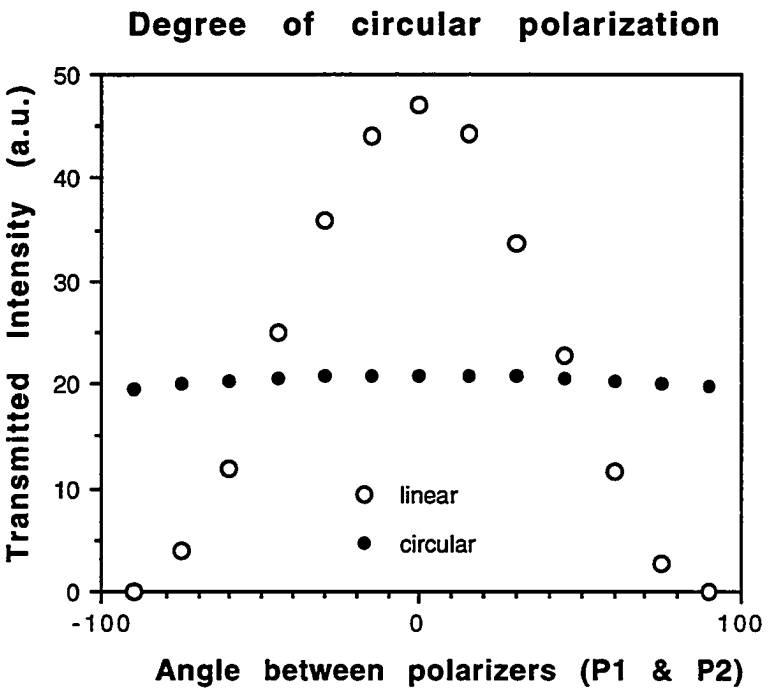

Figure 3-18. The transmitted laser (750 nm) intensity measured as a function of the orientation of linear polarizer P2, where the empty circles are for the measurements made without the quarter wave plate $\lambda/4$ located between P1 and P2, painted circles are for those made with $\lambda/4$.

3.9.2 Variation of the initial degree of spin polarization.

Measurements of spin relaxation time were done in a p-doped ($p=7x10^{17}cm^{-3}$) bulk GaAs at several temperatures (80K - 200K). The sample was excited by two energies, 750nm line (close to bandgap) and 620 nm line (above bandgap).

The goal of these measurements is to confirm the availability and the accuracy of the experimental setup which is used in the course of this thesis. The experimental results should provide information about the difference made by the two pumping energies.

The major difference observed concerns the degree of initial spin polarization. In the case of an excitation energy close to the band gap energy, an initial spin polarization of 26% was observed; while in the case of an excitation energy much larger than the bandgap energy, the initial spin polarization was only 13%. The results were compared to the data obtained by Garbuzov et al[10]. A good agreement is found.

As far as the spin relaxation times are concerned, they showed exactly what was found by Zarrauti el al. from steady state measurements. The numerical values of τ_s measured using two different pumping energies followed the same temperature dependence in the measured temperature regime (80K to 200K). They are also in agreement with Zarrauti's results[9]. τ_s drops from 350ps at 80K to 130ps at 200K. The estimated mathematical expression can be written as $\tau_s \sim T^{-2.8}$. Data are compared to that obtain by Zarrauti et al. and are plotted in Figure 3-19. Each individual time resolved spin relaxation curve is plotted in Figure 3-

20. The degrees of initial spin polarization determined from the curves presented in Figure 3-20 are summarized in Figure 3-21. Figure 3-22 provides the comparison between my data and the results measured by Garbuzov et al.. The agreement on the degree of spin polarization as a function of pumping energy is apparent.

The reason for the spin polarization drop in the neighborhood of the energy equal to the bandgap energy plus the split-off energy is believed to be the involvement of split-off band and the multiscattering effect during the thermalization.

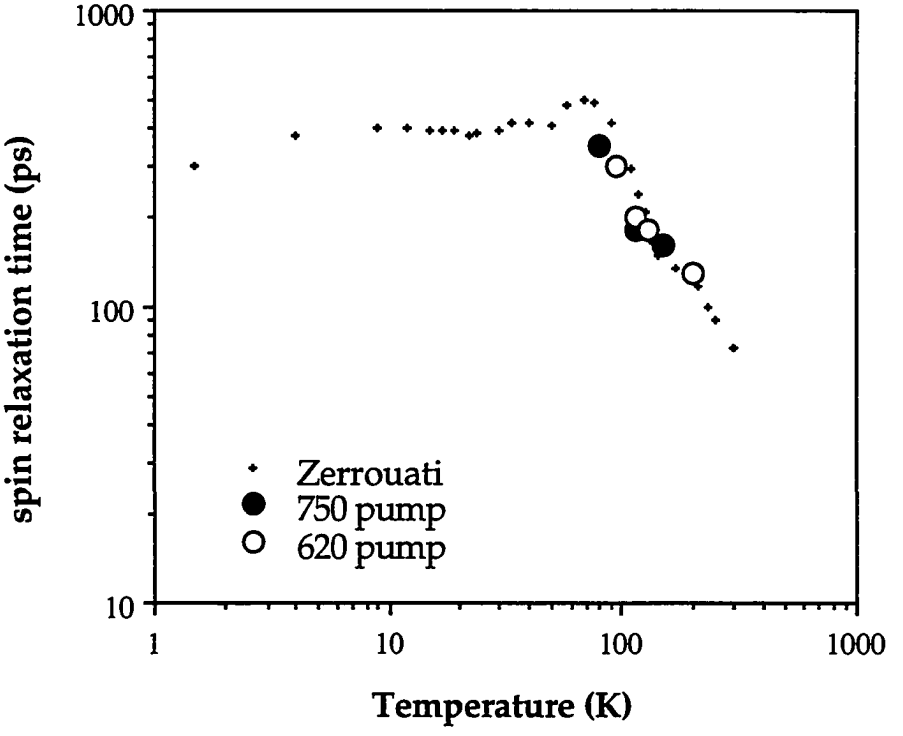

Figure 3-19. The temperature dependent spin relaxation time of bulk GaAs. Data indicated that $\tau_s \sim T^{-2.8}$. The temperature dependence of spin relaxation time in the tested temperature regime is in a very good agreement with that measured by Zerrouati et al[9].

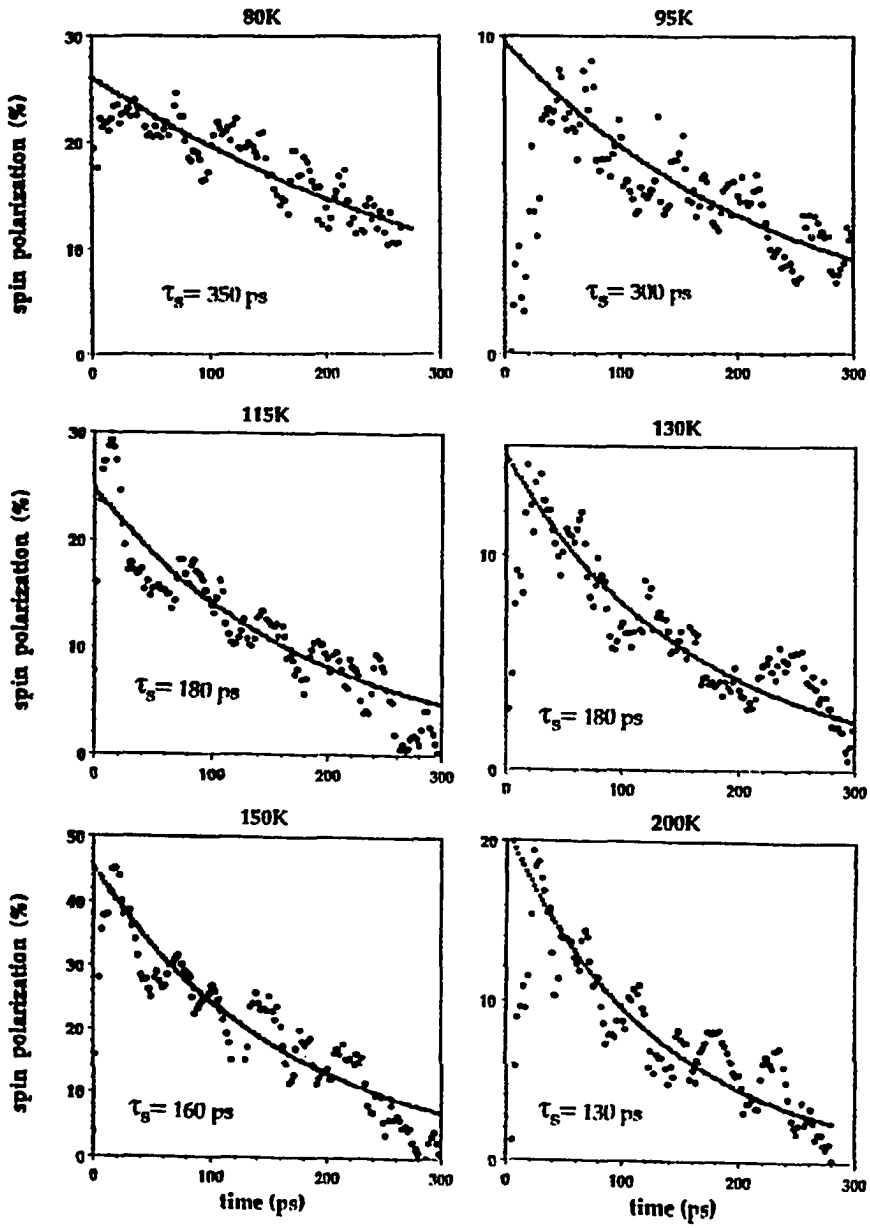

Figure 3-20. The time resolved spin polarization data measured in bulk GaAs. Figures on the right are for 620nm line excitation while the figures on the left are for 750nm line excitation. τ_s refers to the fitted values of spin relaxation times.

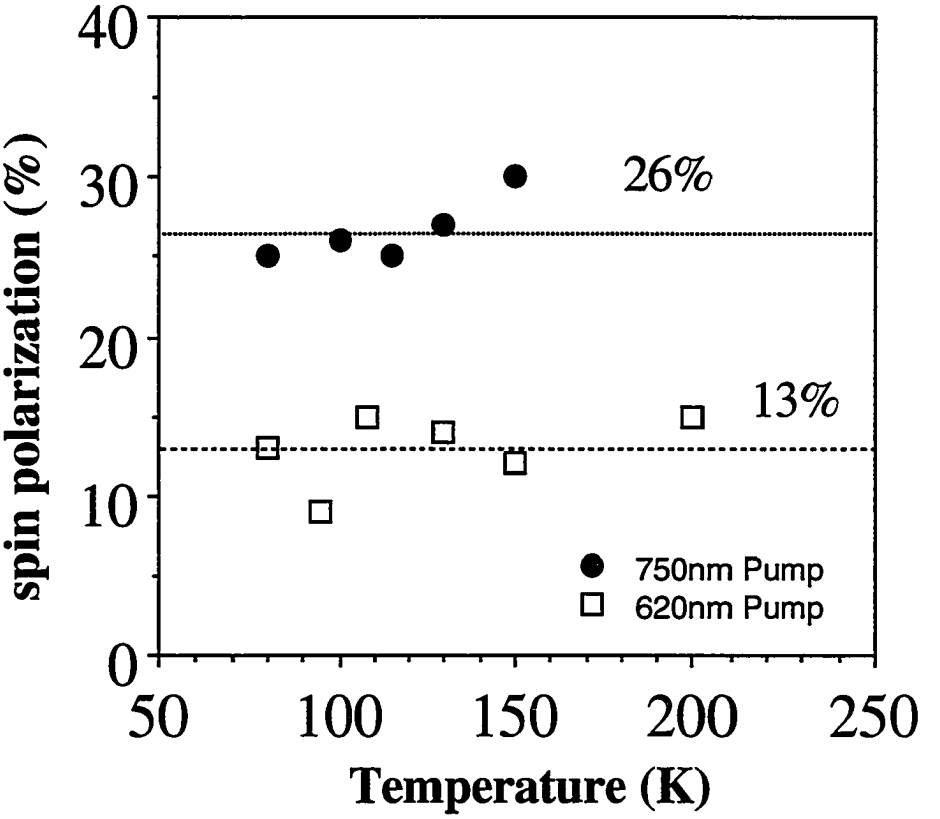

Figure 3-21. The initial degree of spin polarization summarized from Figure 3-20. It is clear that 750nm excitation line results in a high degree (26%) while the 620nm line results in a lower degree (13%).

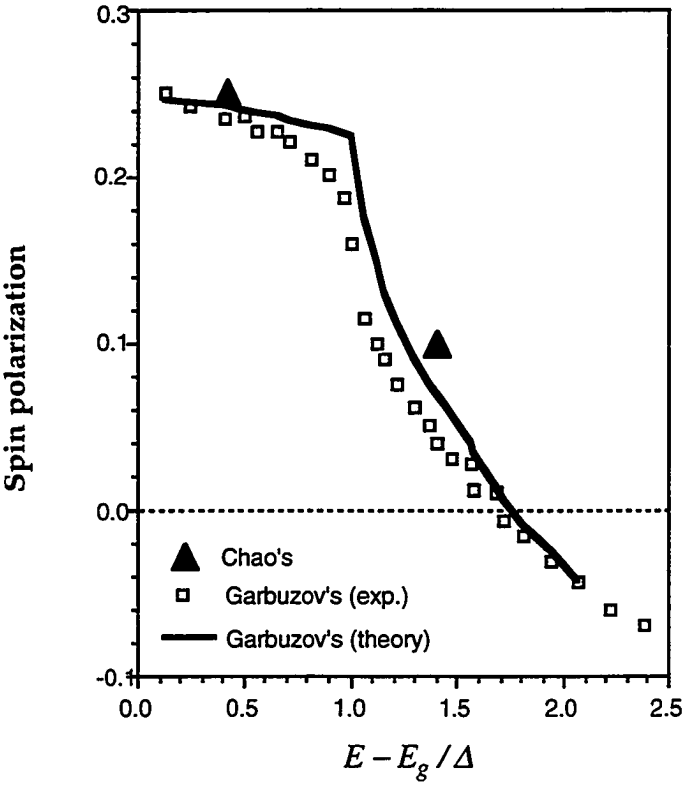

Figure 3-22. A comparison between Chao's data and the results measured by Garbuzov et al.[10].

3.9.3 Reversal of the sign of the spin polarization without varying either the degree of spin polarization or the spin relaxation time

Based on the theory of electron spin polarization given in [2.4], it is obvious that the effect of right-hand and left-hand circularly polarized light on producing the electron spin polarization in the conduction band is *anti-symmetric*. This means that when right-hand circularly polarized light is used as excitation, spin polarization is $+\frac{1}{2}$, while left-hand circularly polarized light creates $-\frac{1}{2}$ spin polarization, When the exciting polarization reverses, the spin polarization only changes sign without changing its magnitude. Furthermore, the spin relaxation time is also the same. This is one of the important characteristics of spin dynamics and it was tested by measuring the spin polarization of the photoluminescence in the bulk GaAs with both circularly polarized excitations.

A measurement of spin polarization reverse was performed in a bulk GaAs sample at 200K. The spin polarization temporal profile of each circularly polarized excitation is given in Figure 3-23. Data indicated an inversion of the sign without changing either the magnitude of the degree of polarization or the spin relaxation time very much. The degree of spin polarization and the spin relaxation time were measured to be 30% and 135 ps, respectively.

Figure 3-23. (a) The temporal profile of spin polarization from a sample excited by S=-1 laser pulses. (b) The temporal profile of spin polarization from a sample excited by S=+1. Where S is the angular momentum of the exciting pulse.

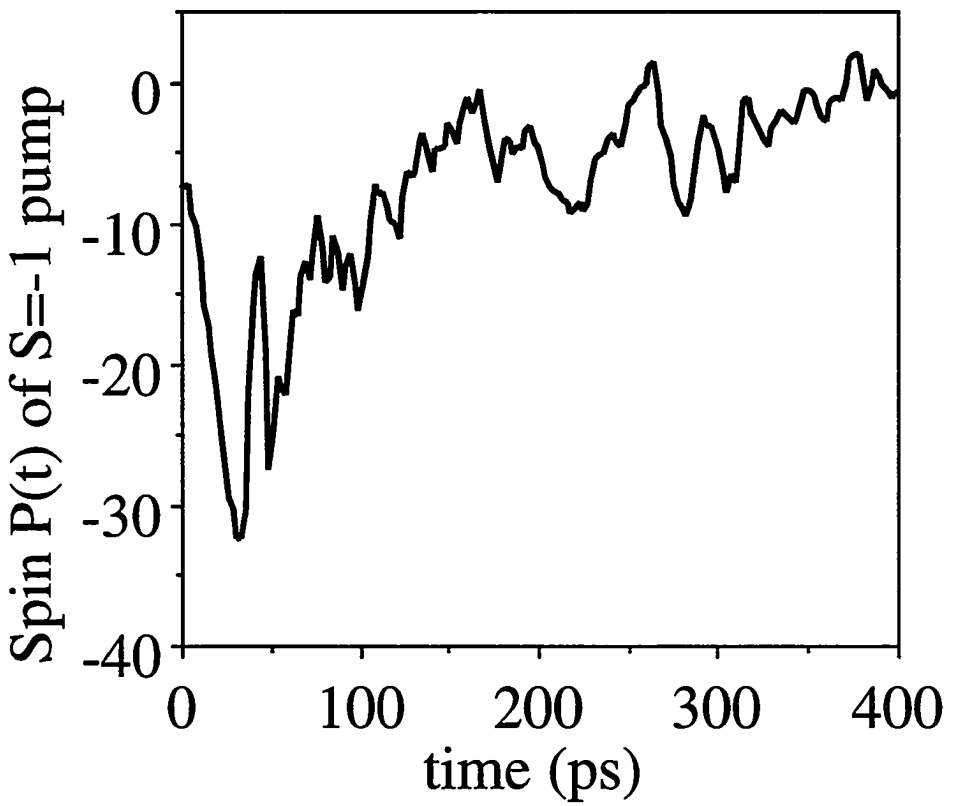

Figure 3-23 (a)

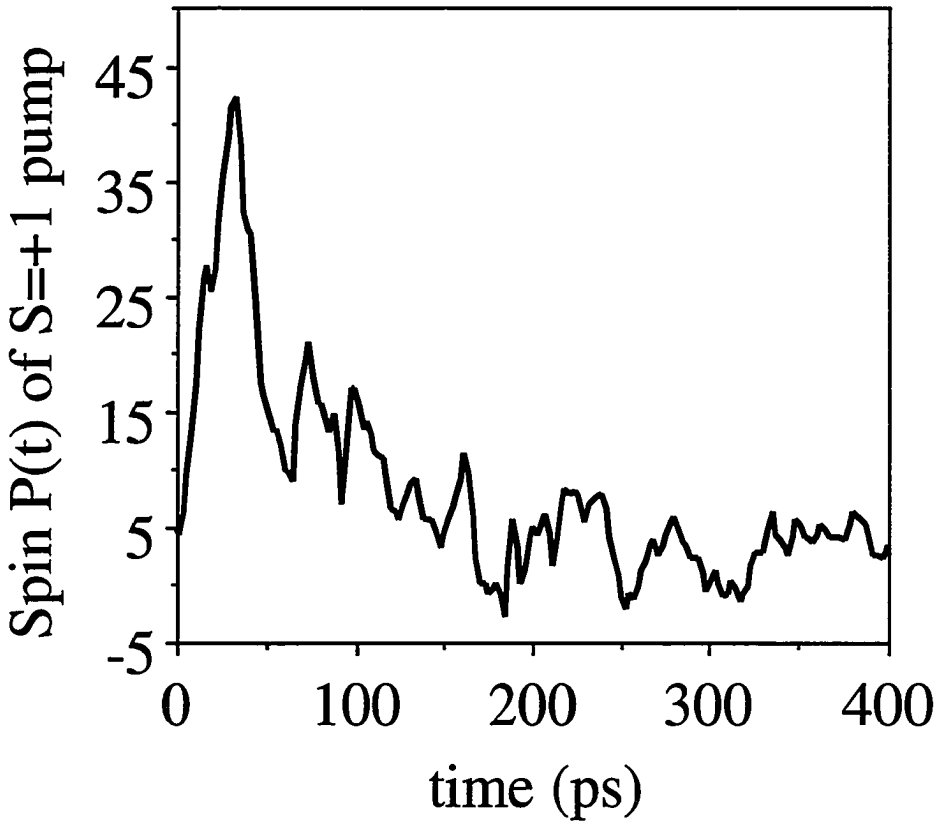

Figure 3-23 (b)

3.10 References

1. K. Shum, M. R. Junnarkar, H. Chao, R. R. Alfano, and H. Morkoc, ***Phys. Rev. B 37 8923*** (1988)

2. Jagdeep Shah, B. Deveaud, T. C. Damen, W. T. Tsang, A. C. Gossard, and Lugli, ***Phys. Rev. Lett. 59 2222*** (1987)

3. H. Chao, K. S. Wong, R. E. Alfano, Unlu and Morkoc, ***J. SPIE 942 215*** (1988)

4. P. P. Ho, "***Semiconductors Probed by Ultrafast Laser Spectroscopy***", Vol. II, edited by R. R. Alfano, Academic Press, New York, Chapter 25, (1984)

5. Jagdeep Shah, T. C. Damen, B. Deveaud, and D. Block, ***Appl. Phys. Lett. 50 1307*** (1987)

6. N. Schiller, Y. Tsuchiya, E. Inuzuka, Y. Suzuki, K. Kinoshita, K. Kamiya, H. Iida, and R. R. Alfano, ***Optical Spectra June*** (1980)

7. C. V. Shank, ***Science 219 (4588) 1027*** (1983)

8. A. Katz, H. Chao, M. Yang, Y. Budansky, A. Gorokhovsky, L. Kalpaxis, and R. R. Alfano, "***CPM femtosecond laser system user's guide***" IUSL internal documentary

9. K. Zerrouati, F. Fabre, G. Bacquet, J. Bandet, J. Frandon and G. Lampel, D. Paget, ***Phys. Rev. B 37(3) 1334*** (1987)

10. D. Z. Garbuzov, R. I. Dzhioev, L. M. Kanskaya, and V. G. Fleisher, ***Fiz. Tverd. Tela 14 1720*** (1972)

11. A. Katz, "***Subpicosecond time resolved absorption and transient grating in GaAs***", Ph.D. thesis (1989)

12. M. Yan, "***Ultrafast spectroscopy in conjugated organic and biological meterials***", Ph.D. thesis (1993)

CHAPTER FOUR

DETERMINATION OF THE MECHANISMS FOR CARRIER MOMENTUM RELAXATION AND SPIN RELAXATION IN GaAs AND GaAs/AlGaAs QUANTUM WELLS

Achievement

The dominant mechanisms for carrier momentum relaxation and spin relaxation were obtained from the temperature dependent data of electron spin relaxation time in GaAs and GaAs/AlGaAs quantum wells. It was found that, at high temperatures (T>80K), the electron momentum relaxation arises mainly from acoustic phonon deformation potential scattering and the electron spin relaxation is due to D'yakonov-Perel mechanism.

4.1 Introduction

As previously stated, carriers posses two types of alignment, linear momentum and angular momentum. These two properties are involved in the relaxation of photoexcited hot carriers and may be important for ultra small scale optical memory elements. Momentum relaxation[1,2] is the fastest carrier randomization process in semiconductors. Upon absorption of photons with appropriate energy, the electrons are photoexcited from the valence bands to the conduction band. These electrons will be localized at well defined points in phase space with wave vector **k** and in effect are oriented[3,4].

Scattering with other carriers, these photoexcited electrons will be scattered to another point **k'** in phase space in a very short period of time. After multiple scattering, the carriers will reach an isotropic momentum distribution. The momentum relaxation time describes how rapidly the photo-oriented momenta become randomly distributed. There are several scattering processes such as impurity scattering, nonpolar optical phonon scattering, piezoelectric potential scattering and acoustic phonon scattering to randomize momentum.

Theoretical calculations have been performed by B. R. Nag[1] who showed the dependence of the momentum relaxation time on E/kT. Most recently, T. Uenoyama[5] used the acoustic phonon interaction model with the spin mixing of the hole band to successfully derive the incomplete hole spin relaxation. The dominant mechanism for electron momentum relaxation has not yet been satisfactorily determined.

In turn, carrier angular spin orientation is a second and related type of optical orientation in semiconductors. This orientation can create a local distribution of magnetic moment lasting for a period of time equal to τ_s which is defined as the spin relaxation time. The relaxation processes of these two types of alignment are parallel, the spin relaxation time τ_s is a function of the momentum relaxation time τ_p (for DP and EY mechanisms) as they are correlated through collisions. The main scattering mechanism responsible for the momentum relaxation may be determined from the measurements of the spin relaxation time.

In this chapter, the mechanisms for carrier momentum relaxation and spin relaxation is determined. The determination is through a comparison between the theoretical calculation and the experimental result.

4.2 Theoretical calculation of the temperature dependence of τ_s

The theoretical temperature dependencies of τ_s for each proposed spin relaxation mechanism (DP, EY, and BAP) were calculated and tablized in Table 4-I. The calculation was performed for various couplings of momentum scattering mechanism with spin relaxation mechanism. In the calculation, equations provided in Table 2-III were used for each spin relaxation mechanism. The numerical values of n, provided in Figure 2-5, were used for each momentum scattering mechanism. For the DP and EY mechanisms the dependence was calculated to be a function of

n, while for the BAP mechanism that was independent of n therefore is independent of scattering processes.

4.3 Experimental methods

The experimental approach adopted is to measure the time resolved spin polarized luminescence at various temperatures. The effective momentum relaxation mechanism and the dominating spin relaxation mechanism are determined by comparing the theoretical calculation to the experimental results of the temperature dependence. The variable of n provides the information of the effective scattering process responsible for momentum relaxation while the temperature dependence itself reveals the dominating spin relaxation mechanism.

The setup used to perform the experiments was the simultaneous detection setup which consists of a CPM ring dye laser followed by four synchronously pumped amplifiers, a pulse compressor and a continuum generation cell. A $300fs$-narrow 750nm pulse was used as the exciting source and an 1D streak camera system with $20ps$ resolusion was used to measure the polarized luminescence. The spin relaxation time was measured in GaAs/AlGaAs quantum wells with well thickness L_Z=55Å and 90Å at several temperatures between 4K and 150K. The photogenerated carrier density is estimated to be ~ $10^{18}cm^{-3}$.

4.4 Experimental results

The time resolved spin polarization measured in two different temperature regimes are presented in Figure 4-1(a)-(c) and 4-2(a),(b) for 55Å and 90Å, respectively. The temperature dependencies of τ_s for the bulk material, 90Å and 55Å wells are plotted in Figure 4-3. In this figure, data of τ_s in the bulk material were measured by K. Zerrouati[6] *et al.*. From the presented data two temperature dependencies are observed in different regimes separated by T=80K. The spin relaxation seems to be dominated by two mechanisms depending on temperature. The temperature dependencies of the spin relaxation time are small at T<80K. They are $\tau_s \sim T^{0.1}$ in bulk material, $\tau_s \sim T^{-0.38}$ in 90Å wells and $\tau_s \sim T^{-0.45}$ in 55Å wells. The salient feature occurs above 80K, where $\tau_s \sim T^{-2.8}$ is observed for all two wells and bulk material. This is in agreement with the theory

4.5 Discussion

The effective momentum relaxation scattering process was determined by comparing the theoretical calculation with the experimental results of the temperature dependence. The calculation was performed by using the equations listed in Table 4-I with different values of n, given in Figure 2-5, for various scattering and spin relaxation mechanisms. The calculated results are also listed in Table 4-II. In comparison, at low temperatures (T<80K), several overlapping mechanisms occur with small and similar temperature dependencies. It

would be difficult to obtain the dominating mechanisms for momentum and spin relaxation in this temperature regime. At high temperatures (T<80K), there is only one type of coupling gives a large and similar numerical value of the temperature dependence of τ_s. In this case, the calculated temperature dependence of the spin relaxation time is -3.2 while the measured is -2.8 ± 0.2. It is the D'yakonov-Perel' mechanism which randomizes the spin orientation and the acoustic phonon deformation potential scattering which randomizes the linear momentum orientation. The details of the characteristic of the temperature dependence of τ_s will be discussed in Chapter 7. The experimental results are in agreement with the theoretical predictions. The physical reason for the acoustic phonon dominating the momentum relaxation over the optical phonon at temperatures above 80K is related to the energy conservation since the momentum relaxation is an energy invariant relaxation hence the momentum relaxation time, τ_p, is a function of energy. Based on this fact, the momentum relaxation scattering should be elastic which is not the case of the optical phonon scattering[1]. Optical phonon scattering contributes mainly to energy relaxation.

4.6 Conclusion

In conclusion, from the temperature dependence of the carrier spin relaxation time τ_s, the electron-acoustic deformation potential scattering was determined to be the most effective scattering mechanism for electron momentum relaxation in the high temperature regime (T>80K).

4.7 References

1. B. R. Nag, "***Semiconductors Probed by Ultrafast Laser Spectroscopy***", Vol. I, edited by R. R. Alfano, Academic Press, New York, Chapter 1, 3 (1984)

2. Esther M. Conwell, "***High Field Transport in Semiconductors***", Academic Press, New York, Chapter 3 (1967)

3. "***Optical Orientation***", edited by F. Meier and B. P. Zakharchenya, Elsevier Science Publishers B. V. (1984)

4. E. J. Johnson, R. J. Seymour and R. R. Alfano, "***Semiconductors Probed by Ultrafast Laser Spectroscopy***", Vol. II, edited by R. R. Alfano, Academic Press, New York, Chapter 19, 199 (1984)

5. T. Uenoyama and L. J. Sham, ***Phys. Rev. Lett. 64(25) 3070*** (1989)

6. K. Zerrouati, F. Fabre, G. Bacquet, J. Bandet, J. Frandon and G. Lampel, D. Paget, ***Phys. Rev. B 37(3) 1334*** (1987)

Table 4-I Theoretical temperature dependencies of $\tau_s \sim T^x$ calculated from all combinations of spin relaxation mechanism and scattering processes. The numbers in the top-left corner box are the temperature dependencies measured from experiments.

Experimental T-Dependence High T:-2.8±0.2 (for all) Low T:-0.1(bulk),-0.38(90Å), -0.45(55Å)		**Theoretical Temperature Dependence (x)**		
		D'yakonov Perel'	Elliot Yafet	Bir Aronov Pikus
Deformation potential	T>80K	**-3.2**	**0.2**	**0**
	T<80K	**-2.7**	**-0.3**	**0**
Piezoelectric	T>80K	**-1.3**	**0.3**	**0**
	T<80K	**-0.6**	**-0.4**	**0**
Optical phonon	T>80K	**-0.6**	**-0.4**	**0**
	T<80K	**0.2**	**-1.2**	**0**
Impurity	T>80K	**1.5**	**1.5**	**0**
	T<80K	**-0.3**	**3.3**	**0**

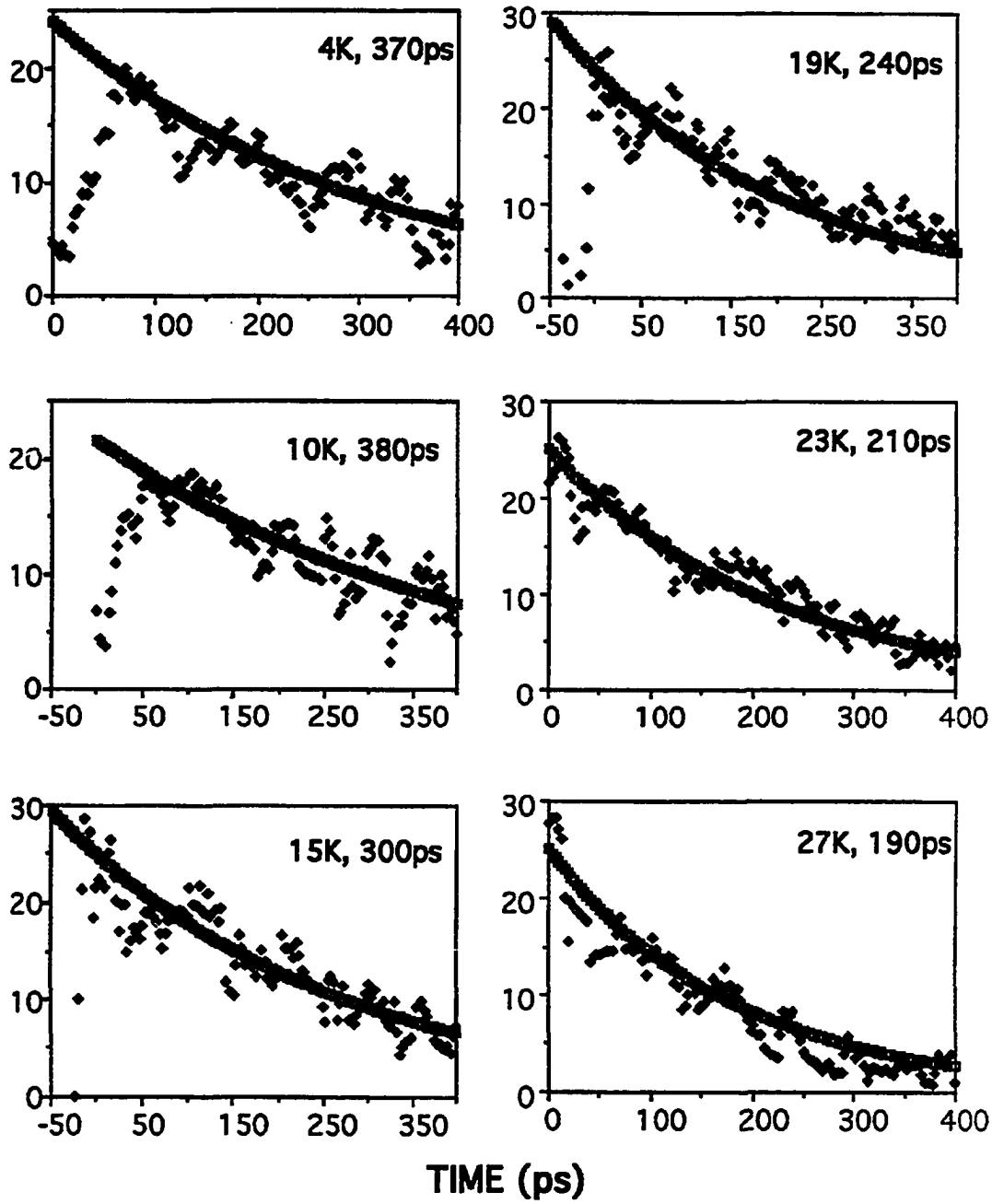

Figure 4-1(a) Time resolved spin polarizations (%) measured at various temperatures (4K to 27K) from a 55Å quantum well sample. The fitted spin relaxation times appear next to the temperatures.

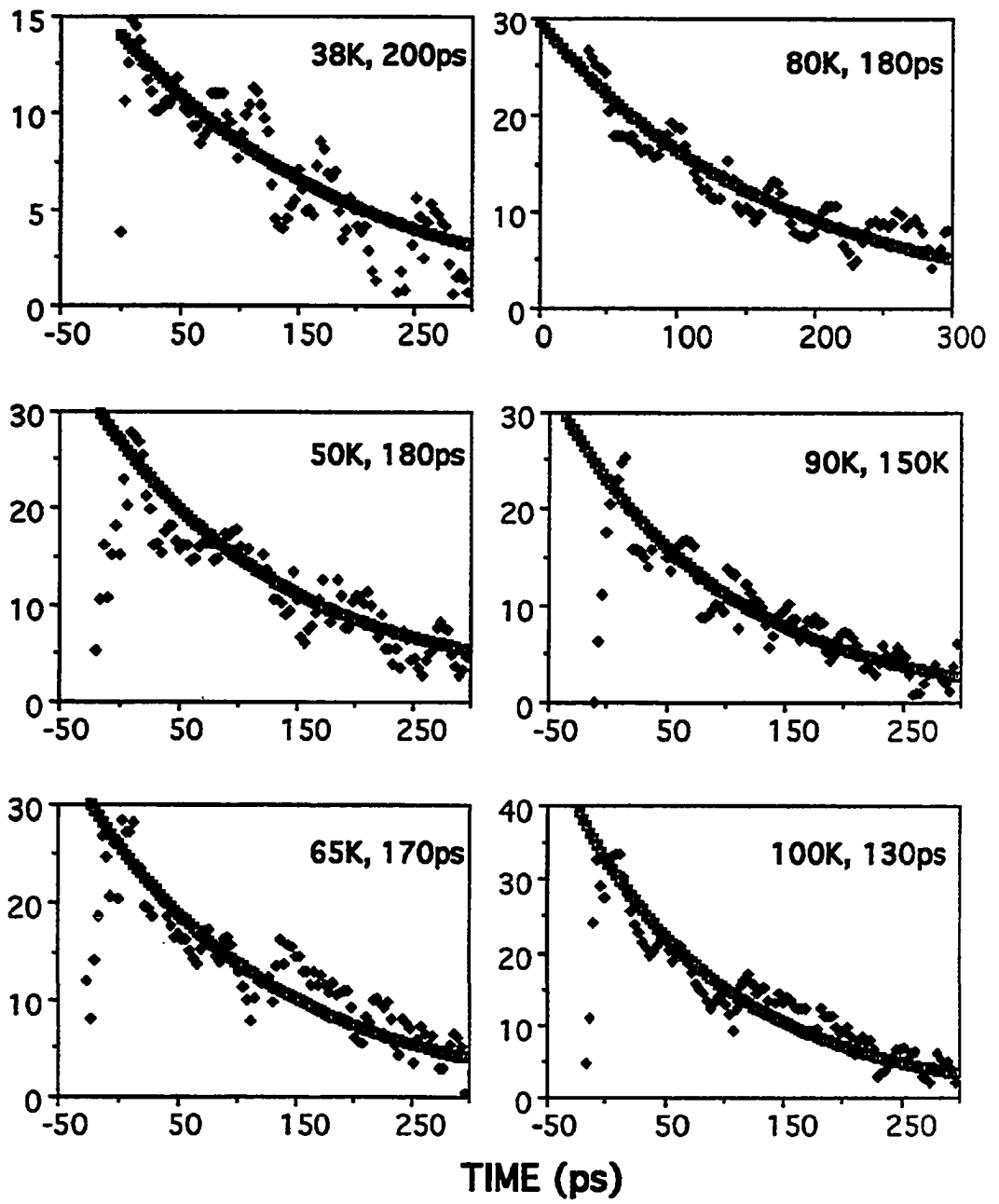

Figure 4-1(b) Time resolved spin polarizations (%) measured at various temperatures (38K to 100K) from a 55Å quantum well sample. The fitted spin relaxation times appear next to the temperatures.

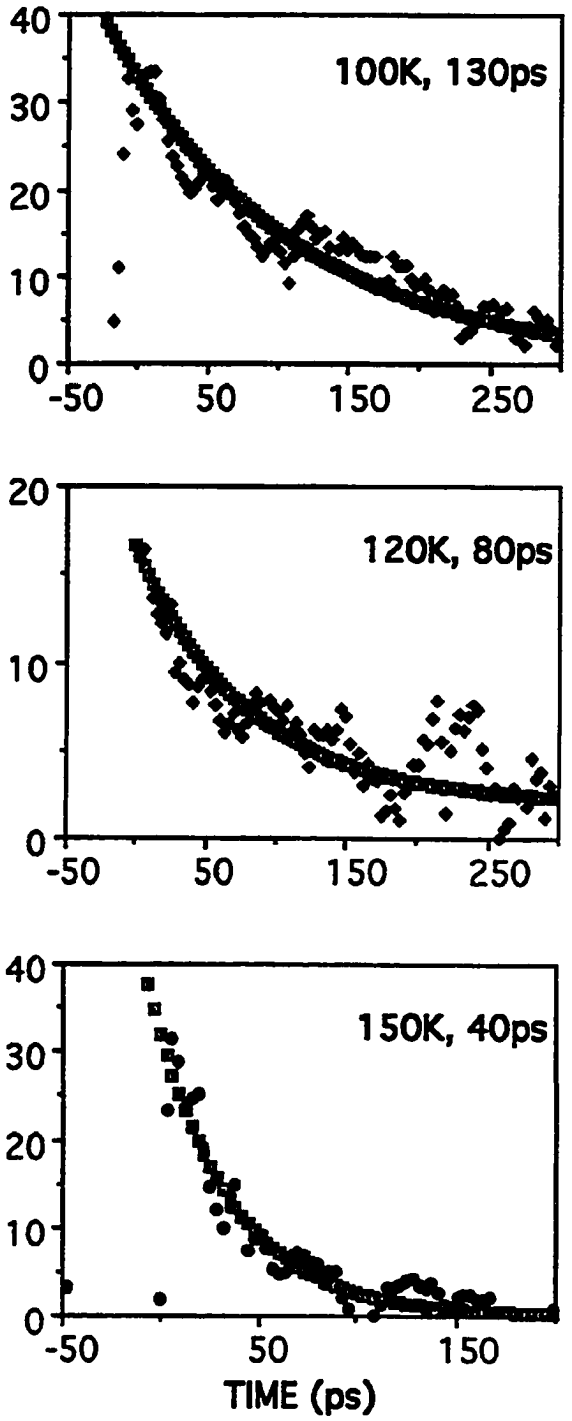

Figure 4-1(c) Time resolved spin polarizations (%) measured at various temperatures (100K to 150K) from a 55Å quantum well sample. The fitted spin relaxation times appear next to the temperatures.

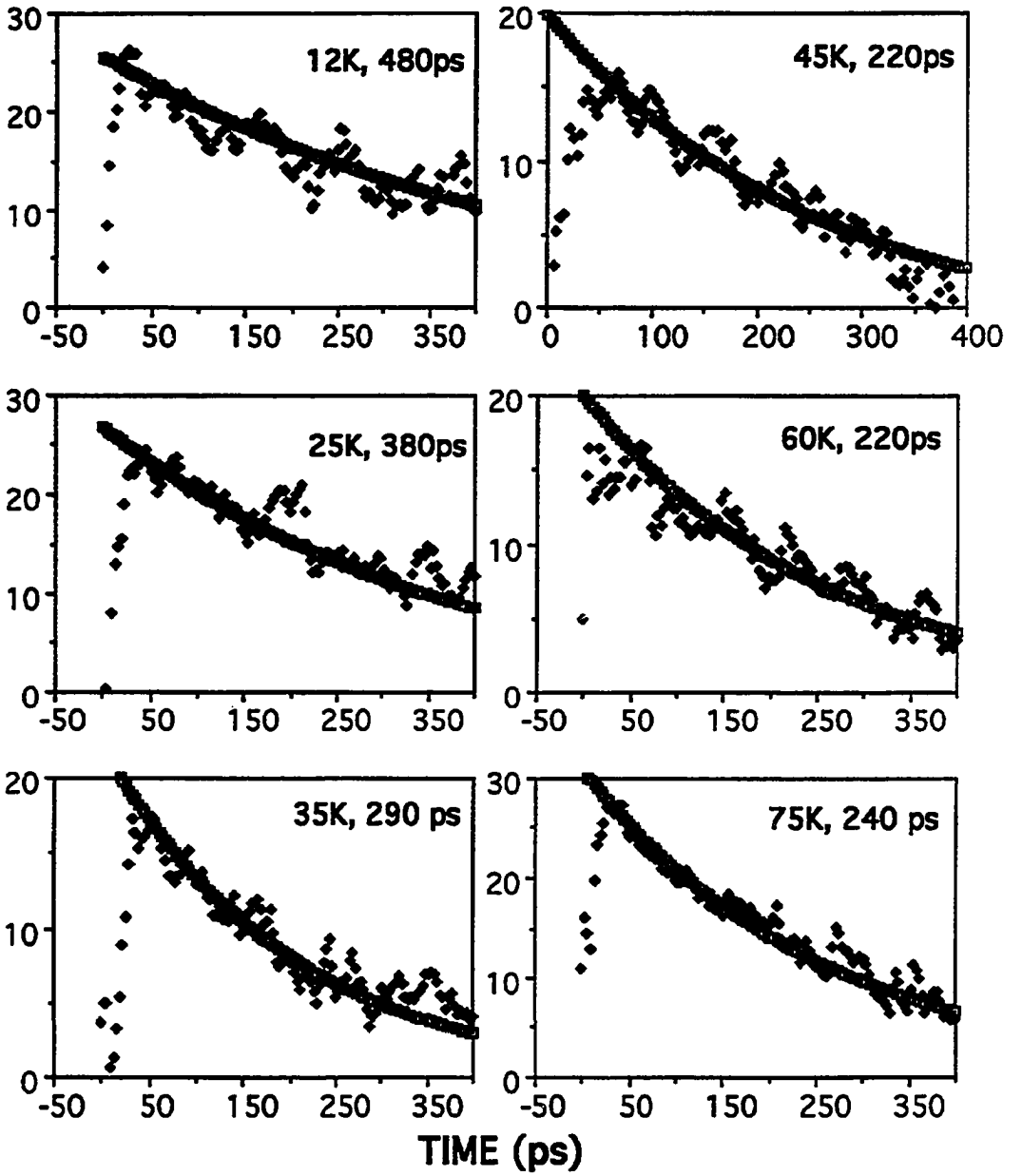

Figure 4-2(a) Time resolved spin polarizations (%) measured at various temperatures (12K to 75K) from a 90Å quantum well sample. The fitted spin relaxation times appear next to the temperatures.

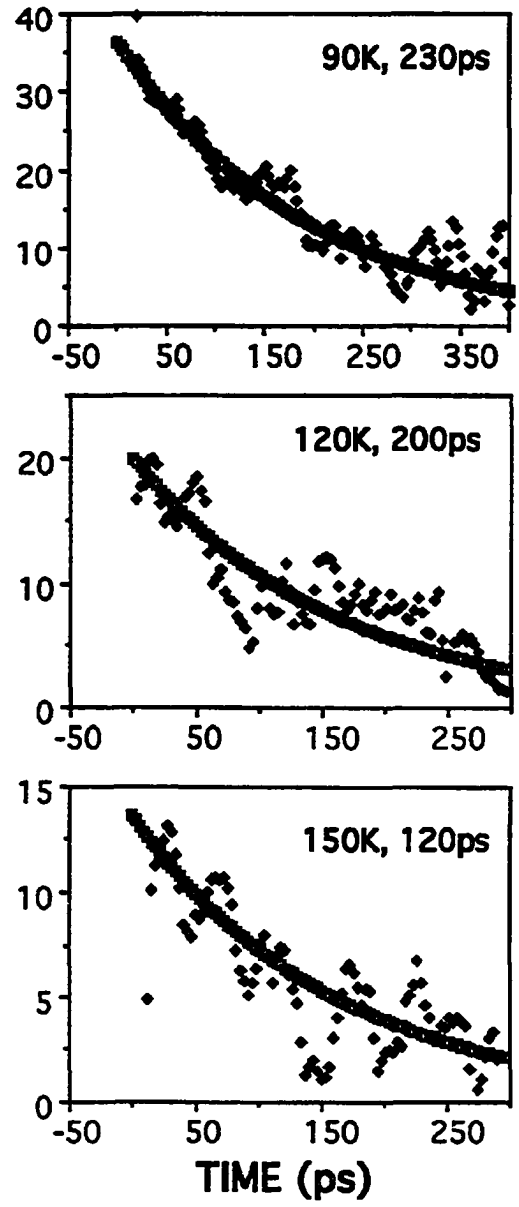

Figure 4-2(b) Time resolved spin polarizations (%) measured at various temperatures (90K to 150K) from a 90Å quantum well sample. The fitted spin relaxation times appear next to the temperatures.

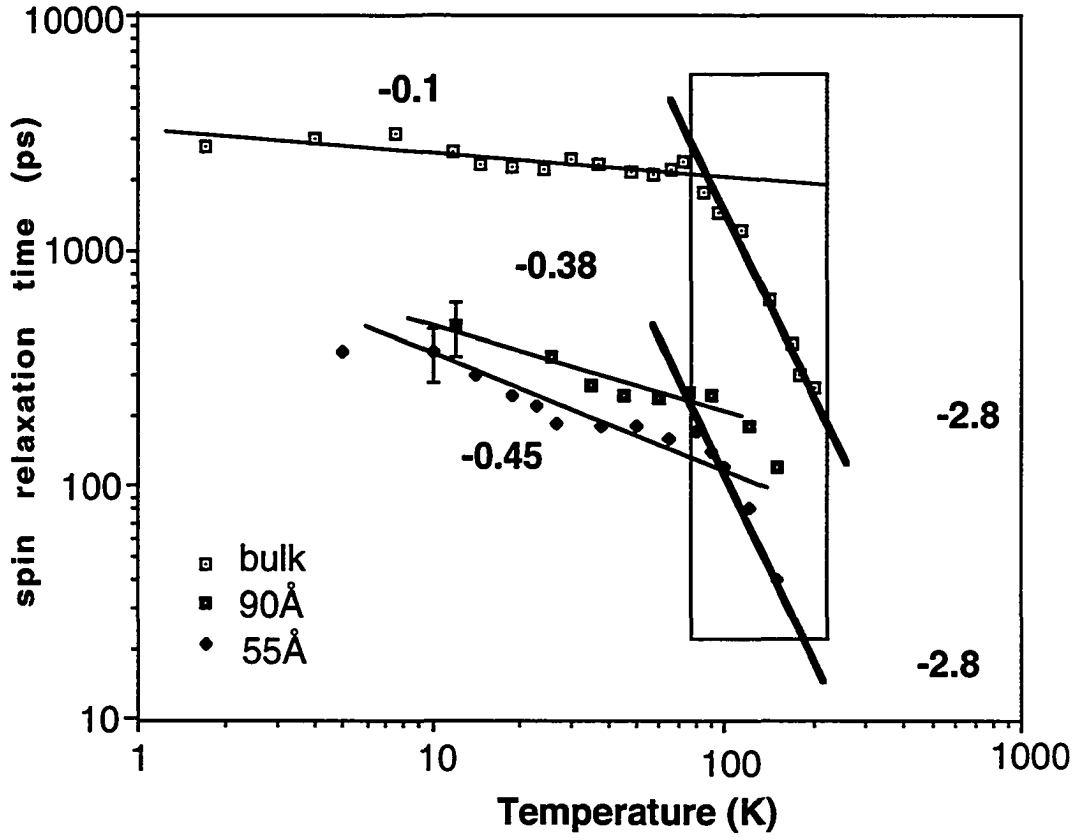

Figure 4-3 The temperature dependencies of the spin relaxation time. Data in the blocked section are applied in the analysis determining the operational scattering process responsible for the momentum relaxation. The spin relaxation times of bulk was obtained from ref. [1].

CHAPTER FIVE

CARRIER ENERGY DEPENDENCE OF SPIN RELAXATION TIME

Achievement

A study of the carrier energy dependence of the spin relaxation time in a stressed 40Å GaAs/AlGaAs quantum wells was performed at two temperatures (20K and 200K). The experimental data agrees with the Bir-Aronov-Pikus spin relaxation mechanism at 20K while agrees with the D'yakonov-Perel' spin relaxation mechanism at 200K.

5.1 Background

In the previous chapter, the mechanism of momentum relaxation and spin relaxation have been determined in the high temperature regime. The mechanism in the low temperature regime has not been uniquely determined due to the multiple possibilities.

Spin relaxation time is related to the scattering time which depends on carrier energy and carrier density. The equations of the spin relaxation time were all written as functions of energy[1-2]. In this paper, the carrier energy dependence of spin relaxation time of electrons was studied in a stressed GaAs quantum wells with 40Å well thickness in order to determine the mechanisms responsible for the momentum relaxation and spin relaxation, respectively.

5.2 Theory

There are five major mechanisms[3-8] proposed to account for the conduction band electron spin depolarization in semiconductors. They are 1. the D'yakonov and Perel' (DP) mechanism, 2. the Elliot and Yafet (EY) mechanism, 3. the Bir-Aronov-Pikus (BAP) mechanism, 4. the interaction between electronic spin $\boldsymbol{S}$ and a nuclear spin $\boldsymbol{I}$, and 5. the Kleinman and Miller (KM) mechanism. The first three mechanisms were discussed in Chapter 2, the last two mechanisms will be discussed as the following.

The fourth mechanism[8] of the spin relaxation is the interaction between an electronic spin S and a nuclear spin I. This mechanism is similar to that electrons exchange their spin with the nucleus'. Awschalom *et al*[9]. have made low temperature measurements in $Cd_{1-x}Mn_xTe$. Their time resolved data support the concept of a bound magnetic polaron. The lifetime of this process is extremely long (~10^{-6} sec) compared to that of the BAP and DP mechanisms (~10^{-10} to 10^{-12} sec), therefore, it will not be discussed further.

The fifth mechanism is the Kleinman and Miller (KM) mechanism[5]. It considers a virtual annihilation of a colliding electron-hole pair producing a virtual photon which is again absorbed and produces a second electron-hole pair. The electron of the second pair will be holding the opposite spin to the original. This interaction results in a spin relaxation with the rate expressed as

$$\frac{1}{\tau_s} = \frac{1}{\tau_o} \quad \text{for} \quad kT << \varepsilon_F$$

$$\frac{1}{\tau_s} = \frac{1}{\tau_o}\frac{N_A}{4}\left(\frac{2p\hbar^2}{MkT}\right)^{3/2} \quad \text{for} \quad kT >> \varepsilon_F \qquad (5.1)$$

where $\frac{1}{\tau_o} = \frac{22}{9}\left(\frac{e^2 p^2 n_{gap} E_g}{m_o \hbar^2 c^3}\right)$, $M = m_e + m_h$, ε_F is Fermi energy, N_A is the doping density, p is electron momentum ($p^2 m_0^{-1} = 13eV$), and $n_{gap} = 3.6$ is the index of refraction at the energy gap. The difference of this mechanism from the others is that this mechanism provides a non-vanishing spin relaxation time at zero temperature and, obviously, the relaxation constant does not depend on energy.

Generally speaking, two competing group of mechanisms for the spin relaxation have emerged. The mechanism involves the magnetic interactions which connect states of opposite spin resulting in direct spin flips is generally slow while the mechanism involves the spin-orbit interaction, $\vec{k} \cdot \vec{p}$, and the lifting of Kramer's degeneracy due to the lack of inversion symmetry is rapid. Among the faster mechanisms are the DP and EY mechanisms. Among the slow mechanisms are the BAP mechanism and hyperfine coupling. The KM mechanism is undefined under this categorization.

The carrier energy E_c is defined as $E_c = \frac{hc}{\lambda} - E_{g,eff}$ where $E_{g,eff}$ is the energy difference between the conduction band minimum and the valence band maximum. It is the sum of the gap energy, E_g, and the quantization energy E_q. λ, h, and c are the pumping wavelength, Plank's constant, and speed of light, respectively. A schematic description of $E_{g,eff}$ is provided in Figure 5-1. The carrier's energy dependence of the spin relaxation time for each mechanism except for the hyperfine coupling are listed in Table 5-I. It should be noted that $\tau_p \sim (E_c/kT)^{-n}$ has been assumed to represent the energy dependence of the momentum relaxation time. The numerical value of n for various scattering processes[10] are given in Table 5-II. The theoretical calculation of the energy dependence of τ_s for various coupling of scattering mechanism and spin relaxation mechanism in two temperature regimes is given in Table 5-III.

5.3 Experiments

The energy dependent spin relaxation times were measured at various emission energies because the thermal equilibrium of excited carriers is established much more rapidly than the spin relaxation processes. The sample is a modulation Be-doped multiple GaAs/AlGaAs wells grown on Si with well size L_Z=40Å[11]. In this stressed material, E_{lh}, the light hole band maximum energy, is lower than E_{hh}, the heavy hole band maximum energy, because of unequal band shrinkage. The effective gap energies $E_{g,eff} = E_c - E_{lh}$ was calculated to be $1.54eV$ and $1.485eV$ at 20K and 200K, respectively (see Figure 5-2 and 5-3). The measurements were performed by using the dual resolution (time and energy) setups which consists of a synchronously pumped tunable dye laser with output at 750 nm and a 2D streak camera with 15 ps time resolution. The photogenerated carrier density is around $5x10^{16}$ cm^{-3}. The repetition rate is 82 MHz. The luminescence from the 40Å GaAs quantum wells is detected by the 2D streak camera. The streak camera was connected to a spectrometer with 0.2 nm spectral resolution in order to obtain the energy dependence. Oppositely polarized luminescence components were alternately detected. Measurements were made at temperatures of 20K and 200K. The time resolved carrier spin polarization profile at certain carrier energy was obtained by integrating all the luminescence in a (vertically) selected window along the time axis. In this paper, each vertical window covers 20 horizontal channels which approximately equals to 4 nm.

There are two advantages to use this setup. The high repetition rate of excitation allows low intensity excitation (carrier density ~ $10^{11}cm^{-2}$) avoiding the complexity of the carrier dynamics in the very high density case. The combination of 2D streak camera and spectrometer provides both energy and temporal dependencies in one measurement.

5.4 Results

Figure 5-4 shows a typical 2-dimensional image stored in the 2D streak camera system. The luminescence spectrum at 20K and 200K are drawn in Figure 5-2 and 5-3, respectively. The x coordinates of the dark squares are the emission energies at which the spin relaxation times were obtained. In Figure 5-2, four emission energies (or carrier energies) were selected, they are at 1.54eV (τ_s=110ps), 1.555eV (τ_s=80ps), 1.574eV (τ_s=60ps), and 1.56eV (τ_s=52ps). In Figure 5-3, five emission energies (or carrier energies) were selected, they are at 1.503eV (τ_s=82ps), 1.507eV (τ_s=73ps), 1.515eV (τ_s=51ps), 1.533eV (τ_s=22ps), and 1.545eV (τ_s=16ps).

The salient feature of this 2-dimensional image is the simultaneous access to the temporal and energy dependencies of the spin relaxation time. Figure 5-5 shows the four selected examples of the time resolved spin polarization measured at T=20K. Figure 5-6 shows the five selected examples of the time resolved spin polarization measured at T=200K.

The energy dependencies of the spin relaxation time measured at 20K and 200K are displayed in Figure 5-7 and 5-8, respectively. From Figure 5-7 and Figure 5-8, the energy dependencies of the spin relaxation

time were estimated to be $\tau_s(E_c) \sim E_c^{-0.52\pm0.08}$ and $\tau_s(E_c) \sim E_c^{-1.38\pm0.15}$ at 20K and 200K, respectively.

The degrees of initial spin polarization at two measured temperatures were also plotted and presented in Figure 5-9 and 5-10 for 20K and 200K, respectively. High degrees of initial spin polarization (>40%) can be observed in Fig. 5-10.

5.5 Discussion

The carrier spin dephasing mechanism was determined by matching the various calculated energy dependencies of the spin relaxation time (given in Table 5-III) to the dependencies obtained from measurements at two temperature regimes (Figure 5-7, 5-8). We found that, at high temperature (200K), only DP mechanism and the deformation potential acoustic phonon scattering coupling gives a numerical value of the energy dependence with a power of *1.3* which is satisfactorily close to the experimental result of the energy dependence with the power of 1.38 ± 0.15. For 20K, it seems that the BAP mechanism coupled with all the listed scattering processes provides the best numerical value of *0.5* which best matches to the experimental result of 0.52 ± 0.08. Therefore, for carriers in quantum wells, the BAP mechanism is dominating the spin relaxation at low temperatures while the DP mechanism is dominating at high temperatures. This conclusion of the dominating spin relaxation mechanism at low temperatures was not able to be reached by the previous temperature dependent measurements.

The salient features in this study are the two fold determinations - determination of the dominating spin relaxation mechanism (DSRM) as the BAP mechanism at low temperatures and the DP mechanisms at high temperatures and also determination of the operational momentum relaxation scattering process (OMRSP) as the acoustic phonon deformation potential scattering at high temperatures. Both determinations (DSRM and OMRSP) made this time at high temperatures are in agreement with the determination made from the temperature dependent measurements[12] previously. The operational momentum relaxation scattering process at low temperatures can not be determined by this method because the BAP mechanism is independent of the scattering mechanism.

The spin dynamics affected by the stress due to the unequal expansion coefficient between GaAs and Si can be studied in two aspects, the initial degree of spin polarization and the spin relaxation time. It was found that the initial degree of spin polarization is increased (see Figure 5-10) while the spin relaxation time, by comparing to the measurements of 55Å, is shortened, as expected, at 20K due to quantum confinement. The reason for the high degree of initial spin polarization observed in this internally stressed material is from the hole band splitting in the valence band[11]. This splitting reduces the interaction between heavy holes and light holes resulting high degree of spin polarization.

For spin relaxation time, since the major effects of the stress, band splitting, is in the valence band, the electrons in the conduction band are lightly affected. The shorting in the spin relaxation time is mainly due to

the quantum confinement. Different electron spin relaxation mechanism due to the stress is not expected.

5.6 Conclusion

In conclusion, in quantum wells, the DP mechanism and the deformation potential scattering are repeatedly determined to be the dominant spin relaxation mechanism and the operational momentum relaxation scattering mechanism, respectively, at 200K. This is in agreement with the previous conclusion obtained from the temperature dependent measurements. The BAP mechanism is first determined to be the dominant spin relaxation mechanism at 20K.

5.7 References

1. E. J. Johnson, R. J. Seymour and R. R. Alfano, "***Semiconductors Probed by Ultrafast Laser Spectroscopy***", Vol. II, edited by R. R. Alfano, Academic Press, New York, Chapter 19, 199 (1984)

2. "***Optical Orientation***", edited by F. Meier and B. P. Zakharchenya, Elsevier Science Publishers B. V. (1984)

3. M. I. D'yakonov and V. I. Perel', ***Sov. Phys. JETP 33, 1053*** (1971)

4. G. L. Bir, A. G. Aronov, and G. E. Pikus, ***Sov. Phys. JETP 42, 705*** (1976)

5. D. A. Kleinman and R. C. Miller, ***Phys. Rev. Lett. 46(1) 68*** (1981)

6. R. J. Elliott, ***Phys. Rev. 96, 2661*** (1954)

7. Y. Yafet, ***Solid State Phys. 15, 371*** (1963)

8. A. Abragam, "***The Principles of Nuclear Magnetism***", Oxford University Press, London, (1961)

9. D. D. Awschalom, J. M. Hong, L. L. Chang, and G. Grinstein, ***Phys. Rev. Lett. 59 1733*** (1987)

10. B. R. Nag, "***Semiconductors Probed by Ultrafast Laser Spectroscopy***", Vol. I, edited by R. R. Alfano, Academic Press, New York, Chapter 1, 3 (1984)

11. K. Shum, Y. Takiguchi, J. M. Mohaidat, R. R. Alfano, K. Adomi and H. Morkoc, ***Phys. Rev. B 44(8) 4044*** (1991)

12. Hsieh Shin Chao and R. R. Alfano, (in preparation)

Table 5-I The calculated energy dependence of spin relaxation time for the major relaxation mechanisms where $\tau_p \sim (E_c/kT)^{-n}$ has been used in the calculation.

τ_s	Energy dependence
D'yakonov-Perel'	$E_c^{\,n-3}$
Elliot-Yafet	$E_c^{\,-2-n}$
Bir-Aronov-Pikus	$E_c^{\,-0.5}$
Kleinman-Miller	$E_c^{\,0}$

Table 5-II The numerical values of n for various scattering processes including acoustic phonon deformation potential, piezoelectric, optical phonon, and ionized impurity in different temperature regimes. The results of calculation of $\tau_p(E/kT)$ was presented in Figure 2-5. Detail calculation was given in ref. 12.

n	Low Temperatures	High Temperatures
Deformation potential	1.15	1.6
Piezoelectric	-0.05	0.75
Nonpolar optic phonon	-0.76	0
Ionized Impurity	1.2	0

Table 5-III Theoretical energy dependencies of τ_s ($\tau_s \sim E_c^x$). Calculation was applied for all couplings of the spin relaxation mechanism and the scattering processes. The numerical values given in the box at top-left corner are the energy dependencies obtained from experiments which are given in Figure 5-7 and 5-8.

Exp. E-Dependence (x) High T: -1.38±0.15 Low T: -0.52±0.08		**Theoretical E-Dependence (x)**			
		DP	EY	BAP	KM
Deformation potential	T=200K	**-1.4**	**-3.6**	**-0.5**	**0**
	T=20K	**-1.85**	**-3.5**	**-0.5**	**0**
Piezoelectric	T=200K	**-2.25**	**-2.75**	**-0.5**	**0**
	T=20K	**-3.05**	**-1.95**	**-0.5**	**0**
Optical phonon	T=200K	**-3**	**-2**	**-0.5**	**0**
	T=20K	**-3.76**	**-1.24**	**-0.5**	**0**
Impurity	T=200K	**-3**	**-2**	**-0.5**	**0**
	T=20K	**-1.8**	**-3.2**	**-0.5**	**0**

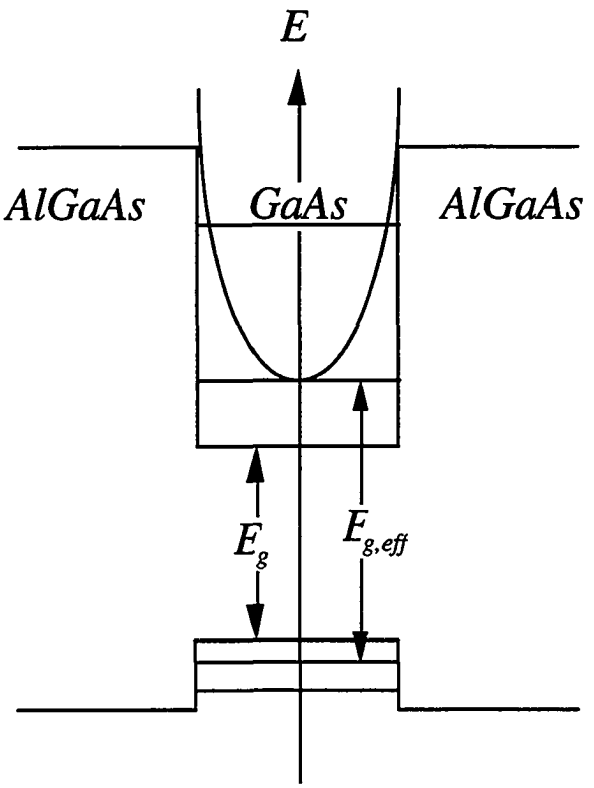

Figure 5-1 The effective gap energy $E_{g,eff} = E_e - E_{lh}$ in a well.

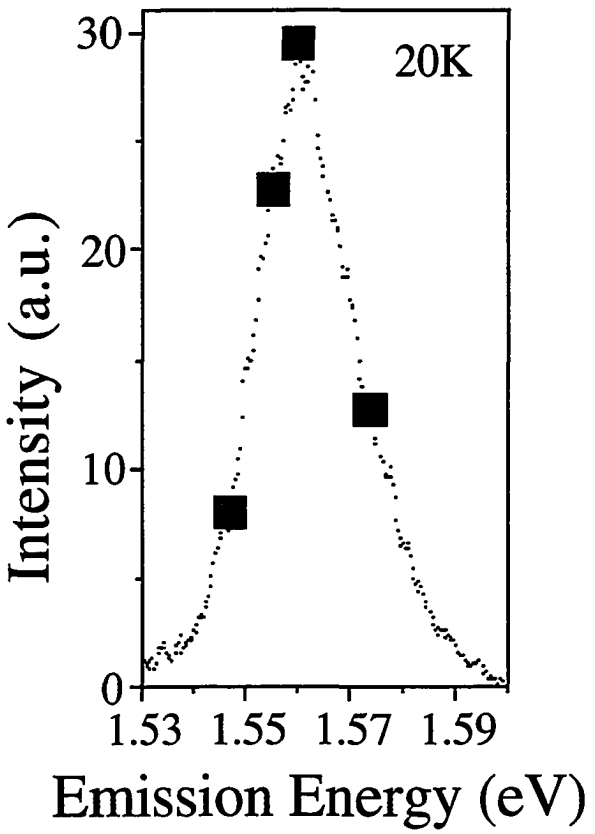

Figure 5-2 The luminescence spectrum at 20K. The black squares mark the emission energies at which the spin relaxation times were measured and compared in order to determine the energy dependence of τ_s.

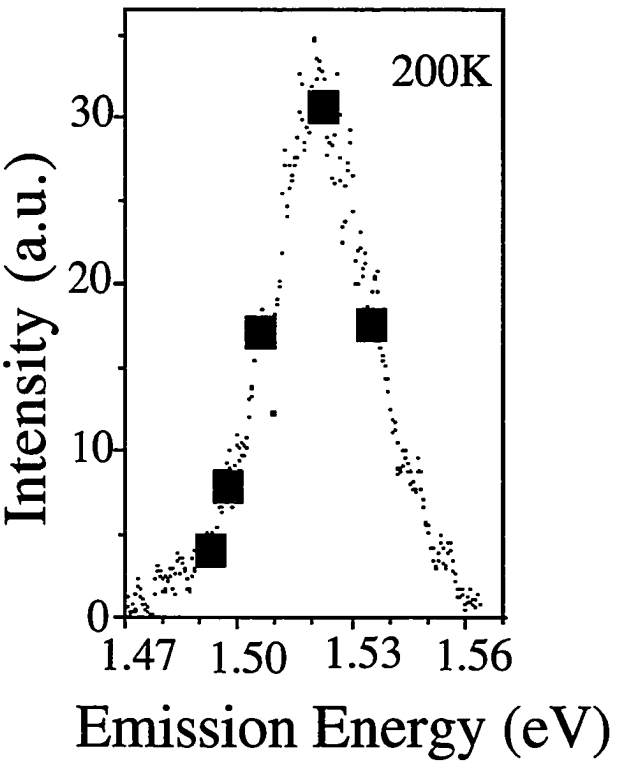

Figure 5-3 The luminescence spectrum at 200K. Carrier energy higher than 1.535 eV was not presented because of the limitation of the time resolution.

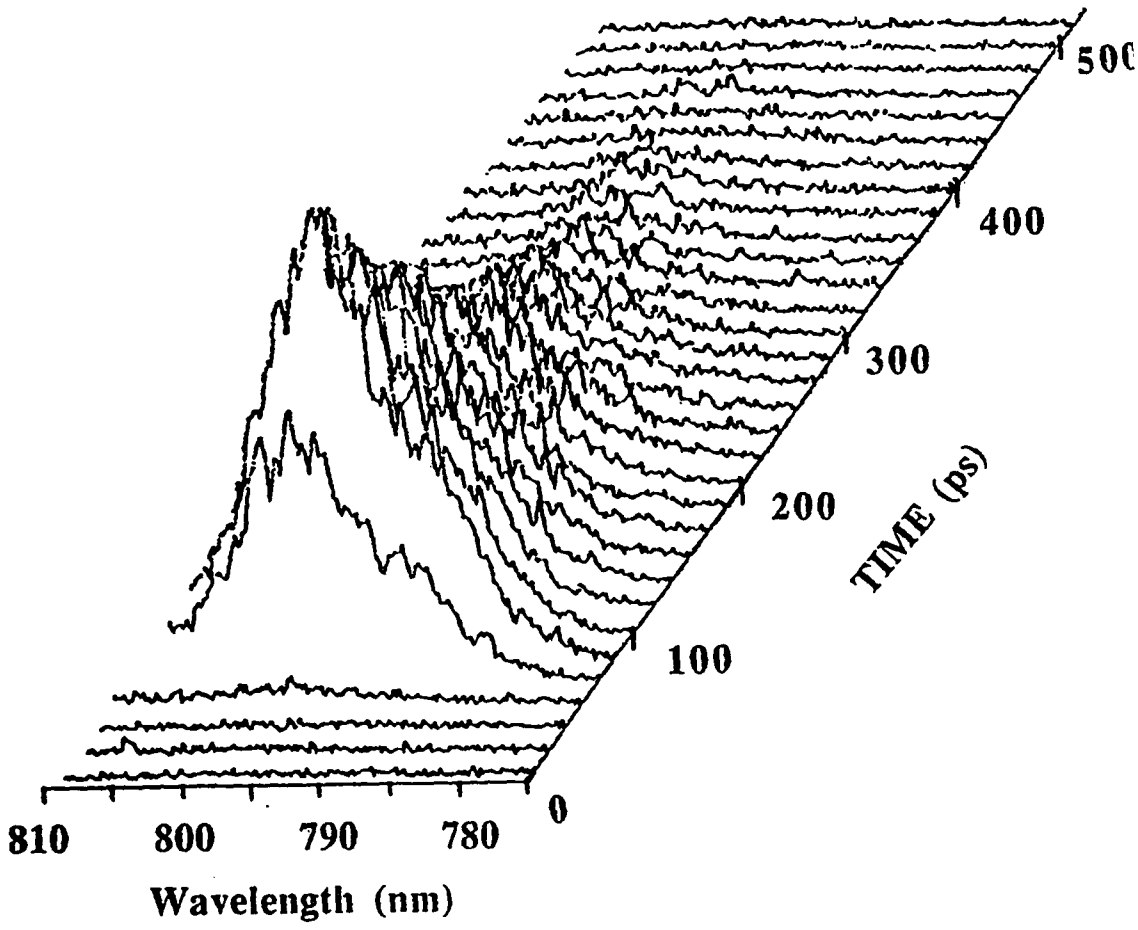

Figure 5-4 The typical luminescence image stored in the 2D streak camera system. X-axis represents the emission energy; Y-axis represents time.

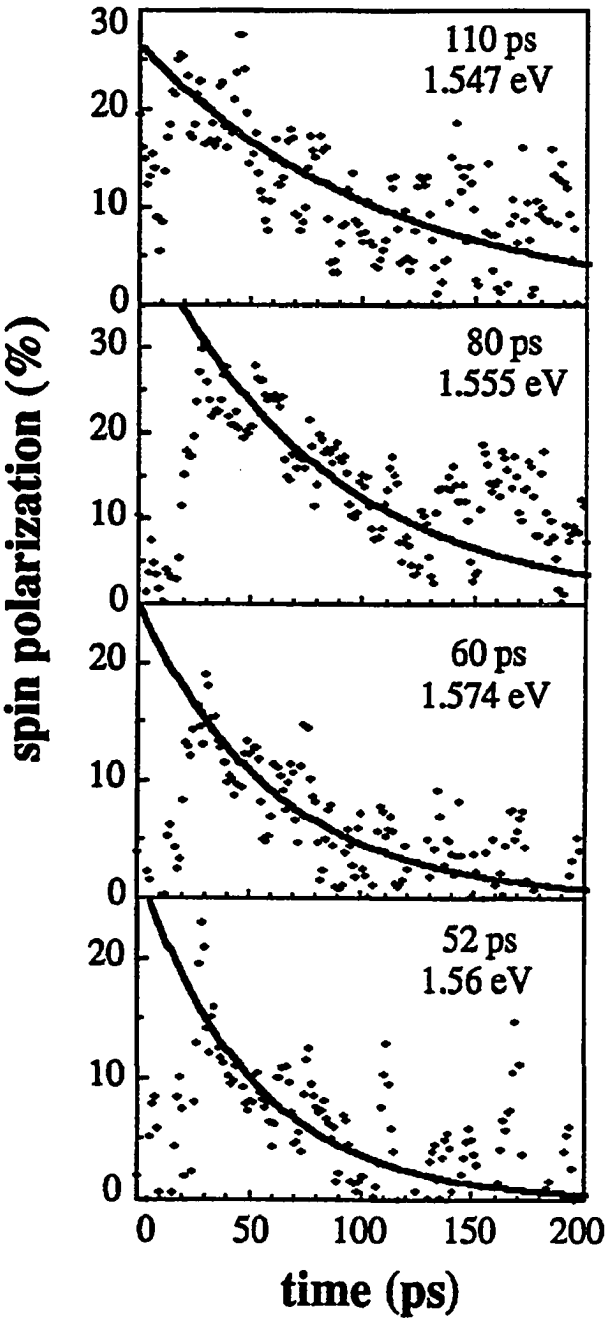

Figure 5-5 Five typical time resolved spin polarization profiles measured at 20K foremission energies at 1.547eV, 1.555eV, 1.574eV, and 1.56eV, respectively. The corresponding spin relaxation times were fitted to be 110ps, 80ps, 60ps, and 52ps respectively. Y-axis is spin polarization.

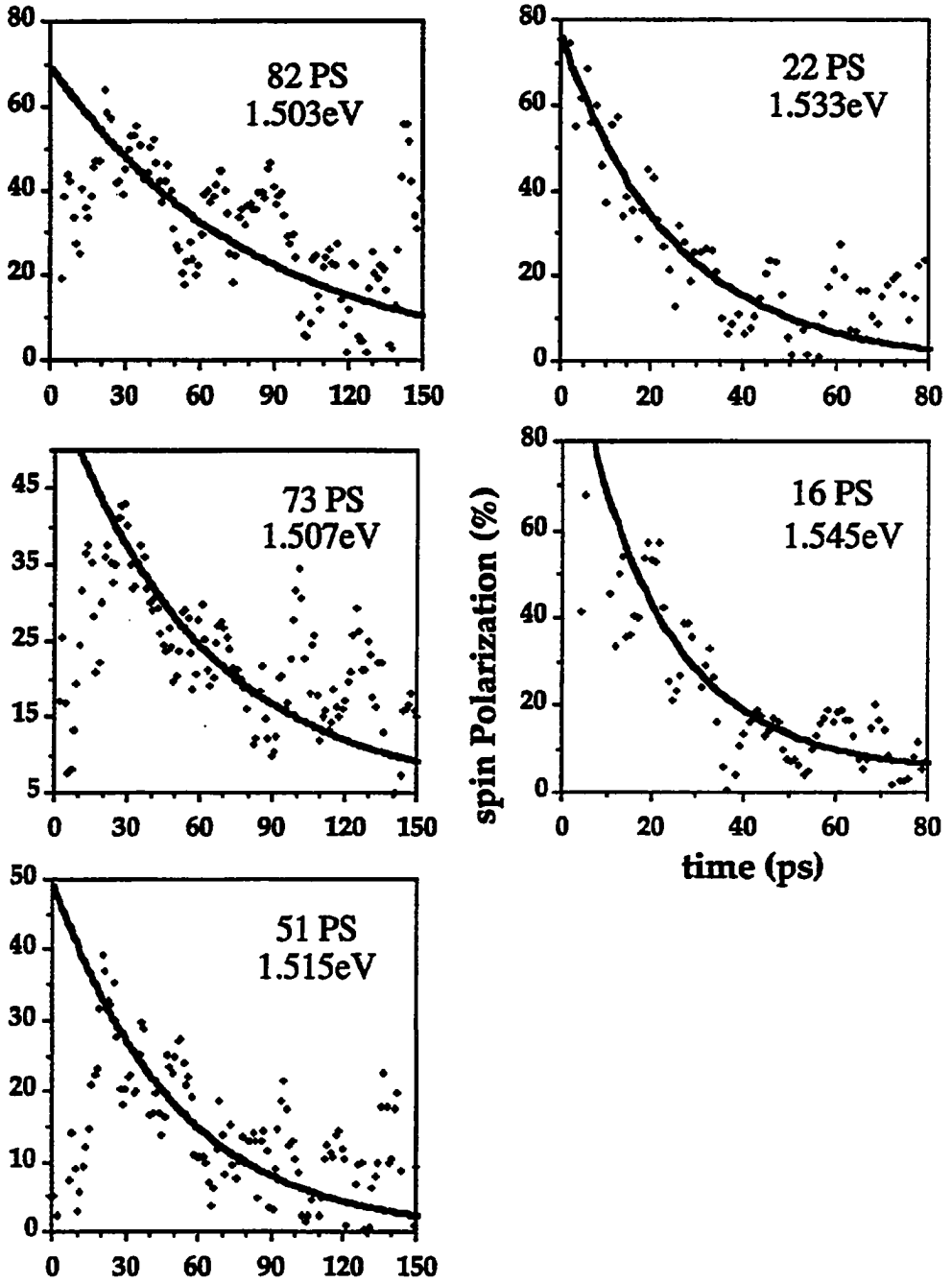

Figure 5-6 Four typical time resolved spin polarization measured at 200K for emission energies at 1.503eV, 1.507eV, 1.515eV, 1.533eV, and 1.545eV, respectively. The corresponding spin relaxation times were fitted to be 82ps, 73ps, 51ps, 22ps, and 16ps respectively.

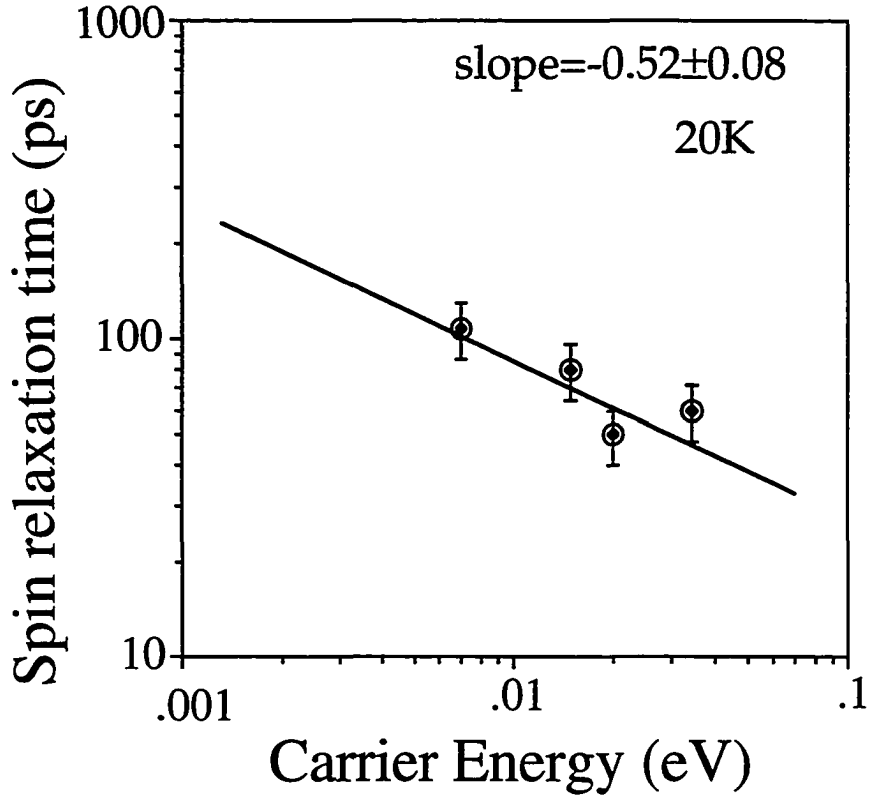

Figure 5-7 The spin relaxation time measured as a function of carrier's energy at 20K. The energy dependence, is measured to be -0.52±0.08. Therefore, $\tau_s \sim E_c^{-0.52\pm0.08}$.

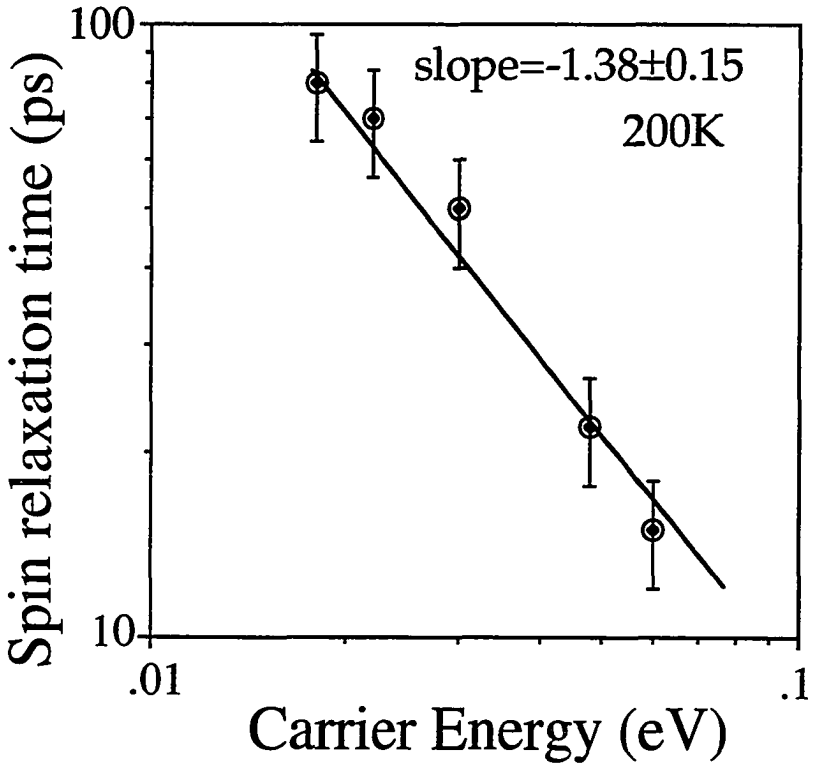

Figure 5-8 The spin relaxation time measured as a function of carrier's energy at 200K. The energy dependence is measured to be -1.38±0.15. Therefore, $\tau_s \sim E_c^{-1.38\pm0.15}$.

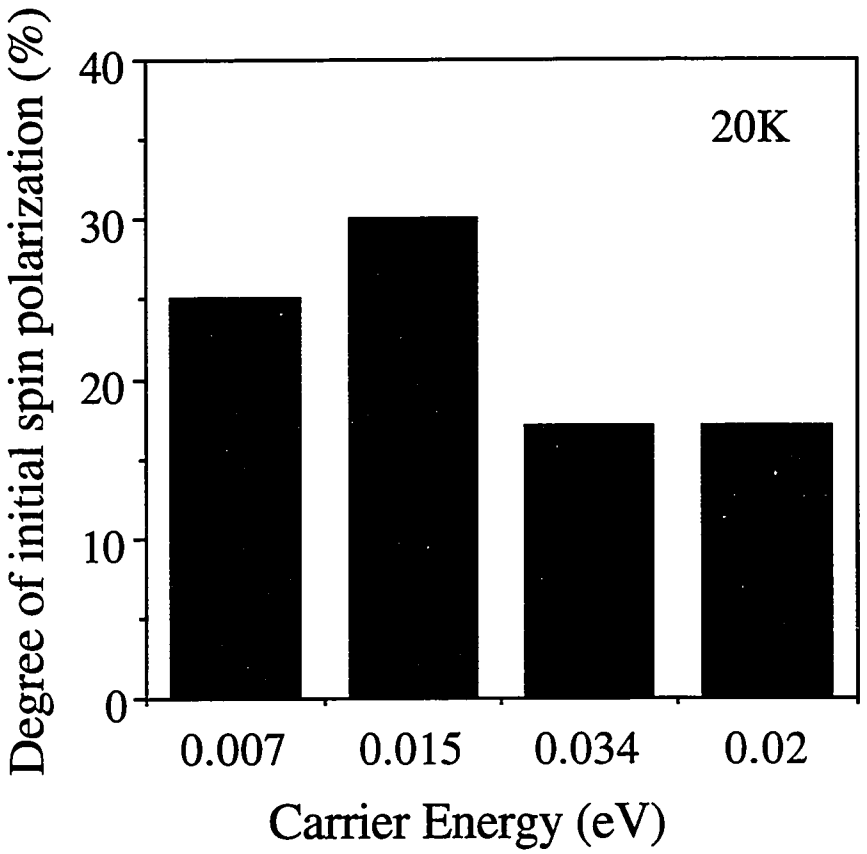

Figure 5-9 The initial degree of spin polarization at various carrier energies measured at 20K.

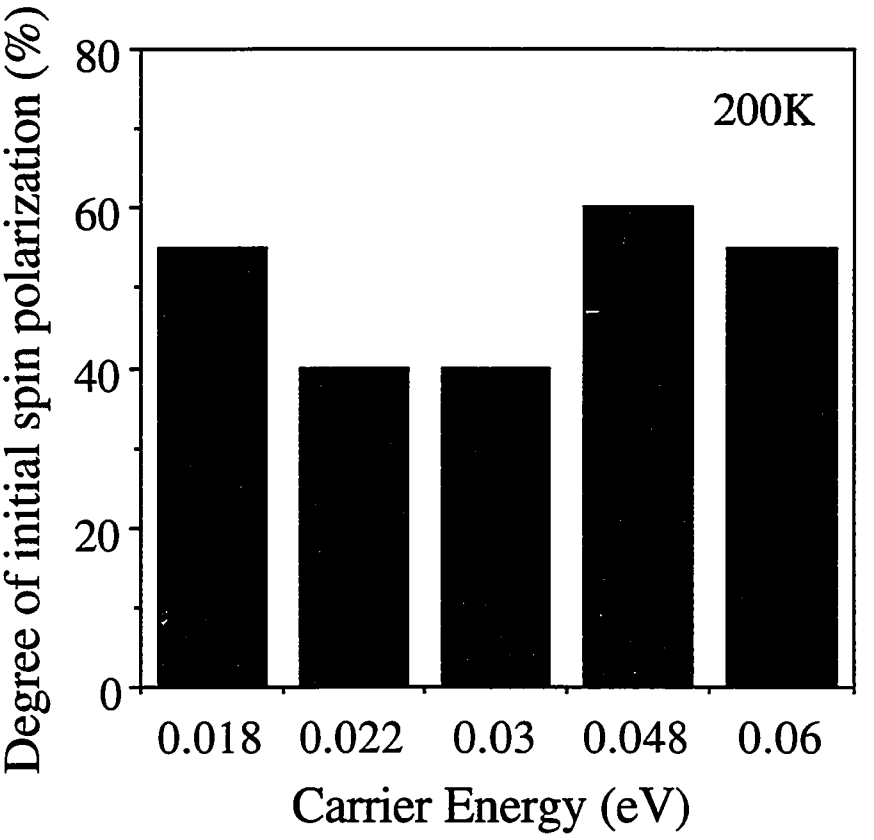

Figure 5-10 The initial degree of spin polarization at various carrier energies measured at 200K.

CHAPTER SIX

CARRIER DENSITY DEPENDENCE OF SPIN RELAXATION TIME

Achievement

The spin relaxation times in GaAs and 55-Å GaAs/AlGaAs wells were measured as functions of carrier concentration N at various temperatures. In this study, the carriers were photogenerated with densities ranging between $7x10^{16}$ and $10^{18}cm^{-3}$. The carrier concentration dependencies of τ_s were observed in bulk GaAs as $\tau_s \sim N^{-0.32}$ at T=40K, the carrier concentration dependencies of τ_s were observed as $\tau_s \sim N^{-0.42}$ and $\tau_s \sim N^{-1}$ for 55Å quantum wells, at T=20K, and T=100K respectively.

The dominating mechanism for carrier spin relaxation was determined. It is found that the Bir-Aronov-Pikus (BAP) mechanism dominates at 20K and 40K for quantum wells and bulk GaAs, respectively; while the D'yakonov-Perel' (DP) mechanism dominates at 100K.

The operational spin relaxation mechanism is also determined to be the deformation potential scattering at high temperatures (T>80K). Both determinations are in agreement with the previous determinations from the temperature and carrier energy dependencies.

6.1 Background

In Chapter 4 and 5, the temperature and energy dependencies were studied in two dimensionalities (3D and 2D). The BAP mechanism was determined to be effective at low temperatures and the DP mechanism is effective at high temperatures. In this paper, we studied the dependence of τ_s on carrier concentration in order to confirm the dominating spin relaxation mechanism by different approach.

6.2 Theory

The carrier density plays an important role in the spin relaxation process because the spin relaxation time depends on scattering time which is a function of concentration. The first time resolved measurement on carrier concentration dependence of τ_s was performed by Seymour and Alfano[1]. They measured the carrier density ($7\text{x}10^{17}$ to 10^{19}cm^{-3}) dependence of τ_s in p-doped bulk GaAs at 70-100K and found $\tau_s \sim N^{-0.63}$. They also determined the DP mechanism was the effective spin relaxation mechanism for their experimental condition.

The theoretical carrier concentration dependence of τ_s in 2D and 3D have been obtained from the energy dependence through Fermi integrals. The results were list in Table 2-IV. In Table 2-IV, the variable n is the energy dependence of the momentum relaxation time and it plays a role of fitting parameter for the determination on the effective spin and linear momentum relaxation mechanisms. The momentum relaxation time has been calculated, as a function of energy, by B. R. Nag[2] for various

scattering mechanisms (see Figure 2-5). From this figure, the numerical values of n can be obtained. By using the appropriate value of n, the concentration dependence of τ_s for every spin relaxation mechanism involving with each scattering mechanism can be calculated. Table 6-I presented the result soft this calculation.

The effective spin relaxation mechanism can be determined by comparing the theoretical calculation with the experimental results.

6.3 Experiments

The measurements were performed using both bulk and quantum well (L_Z=55Å) GaAs samples. Bulk sample was measured at temperature of 40K. The quantum well sample was measured at two temperatures, 20K and 100K. The simultaneous detection setups is used. The excitation wavelength is 750nm. The photogenerated carrier concentrations were in a range between $7x10^{16}$ to $10^{18}cm^{-3}$.

6.4 Results

The spin relaxation times τ_s of bulk GaAs measured at 40K can be expressed as $\tau_s \sim N^{-0.23\pm0.04}$, while for the quantum wells, τ_s can be expressed as $\tau_s \sim N^{-0.37\pm0.05}$ and $\tau_s \sim N^{-0.91\pm0.13}$ at 20K and 100K, respectively. Data of three carrier density dependent measurements at different temperatures were respectively plotted in Figure 6-1, 6-2, and 6-3. For a easy comparison, Table 6-II summarized these carrier concentration

dependencies from experiments. The time resolved spin polarization curves for bulk GaAs at 40K, 55Å quantum wells at 20K, and 55Å quantum wells at 100K were plotted in Figure 6-1(a), 6-2(a), and 6-3(a), respectively. The carrier concentration dependencies of each previous case were correspondingly plotted in Figure 6-1(b), 6-2(b), and 6-3(b), respectively. The carrier concentration dependence of the spin relaxation time of bulk GaAs at high temperatures (70K-100K) was measured by Seymour *et al.*[1]. They reported $\tau_s \sim N^{-0.63}$ and determined the dominating spin relaxation mechanism was the DP mechanism.

6.5 Discussion

By comparing Table 6-II to Table 6-I, it is found that the carrier concentration dependence of τ_s for bulk GaAs at 40K and quantum well GaAs/AlGaAs at 20K both agree with the prediction of BAP mechanism while the carrier concentration dependence of τ_s of quantum well GaAs/AlGaAs at 100K agrees with the prediction of DP mechanism. It indicates that the dominating spin relaxation mechanism in the specific temperature regime is independent of the dimensionality.

The most effective mechanism dominating the spin relaxation in quantum wells in two temperature regimes, T<80K and T>80K, has been studied previously[3-4] by using the temperature and the energy dependencies. From temperature dependence[3], the DP mechanism and the deformation potential scattering were respectively determined to be the effective spin relaxation mechanism (ESRM) and the momentum relaxation scattering mechanism (MRSM) at high temperatures. The

ESRM and the MRSM were not able to be determined at low temperatures due to several numerically overlapped temperature dependencies which agreed with the experimental data.

From carrier's energy dependence[4], the DP mechanism and the deformation potential scattering were repeatedly determined to be the ESRM and MRSM at high temperatures. Furthermore, the BAP mechanism was first determined to be the ESRM at low temperatures. However, the MRSM was still uncertain because the BAP mechanism is independent of the scattering. In this carrier concentration dependence, the same results are obtained.

Generally speaking the experimental results are in agreement with the theory. To explain why the spin relaxation time shortens as carrier concentration increases, the fundamental equations (2.27) - (2.32) are recalled and it will be discussed in each temperature regime from an energy point of view. The energy of a photoexcited electronic system can be described by its Fermi energy, ε_F. ε_F is a function of carrier concentration, n_{2D} or n_{3D}, as $\varepsilon_F \sim n_{2D}$ and $\varepsilon_F \sim (n_{3D})^{2/3}$ depending on the dimensionality.

6.5a Low Temperature (T<80K)

At low temperatures, because of the effectiveness of the BAP mechanism, the spin relaxation rate, τ_s^{-1}, is proportional to the square root of the carrier energy. For highly concentrated system, Fermi energy is high resulting fast relaxation. It is true for both 2D and 3D systems.

6.5b High Temperature (T>80K)

At high temperatures, DP mechanism is effective, the carrier energy dependence of the spin relaxation rate, τ_s^{-1}, can be written as $\tau_s^{-1} \sim E^{1.3}$. when concentration is high, Fermi energy is high hence the spin relaxation rate is high. In the above calculation, the deformation potential scattering has been assumed to be the effective scattering causing momentum relaxation. The momentum relaxation time due to the acoustic phonon deformation potential scattering, τ_p^{ac}, can be expressed as[2]

$$\tau_p^{ac}(x) \sim \left[1-4(S_c/x)+6(S_c/x)^2 \ln(1+x/S_c)-2(S_c/x)^2(1+S_c/x)^{-1}\right]^{-1} \quad (6.1)$$

where $x = E/kT$, and $S_c \sim N^{1/3}$ is the screening coefficient. τ_p^{ac} versus N is drawn in Figure 6-4 for $x = 0.1$. τ_p^{ac} can be expressed as $\tau_p^{ac} \sim N^{0.6}$ in the concentration regime from 10^{16} to 10^{19}cm^{-3}. Obviously, when the carrier concentration increases, the momentum relaxation time increases, however, the spin relaxation time τ_s, of the dominating DP mechanism, is inversely proportional to τ_p, therefore, spin relaxation becomes rapid as concentration increases. We can also derive the carrier concentration dependence of ω, the Armor frequency. Since $\tau_s \sim N^{-0.91}$ was obtained from experiments, we can write $\omega \sim N^{-0.15}$ indicating that the frequency of precession depends very weakly on the carrier concentration. It is in agreement with the theory.

In Figure 6-4, a maximum τ_p^{ac} was observed at a critical concentration N_c around 10^{20}cm^{-3}. It results an increase of the spin relaxation time corresponding to an increase of carrier concentration in the high density regime with $N > N_c$ opposite to what was observed

previously at low density regime with $N < N_c$ where the spin relaxation time decreases corresponding to an increase of carrier concentration.

6.6 Conclusion

The effective spin relaxation mechanism is determined from the carrier concentration dependence of the spin relaxation time. It is found that the BAP mechanism is effective at low temperatures while the DP mechanism is effective at high temperatures for both the bulk and quantum wells. For the momentum relaxation scattering, acoustic phonon deformation potential scattering is determined to be effective at high temperatures. The same conclusion has been obtained from the previous temperature and energy dependencies.

6.7 References

1. R. J. Seymour, M. R. Junnarkar, and R. R. Alfano, ***Phys. Rev. B 24 3623*** (1981)

2. B. R. Nag, "***Semiconductors Probed by Ultrafast Laser Spectroscopy***", Vol. I, edited by R. R. Alfano, Academic Press, New York, Chapter 1 (1984)

3. Hsieh Shin Chao and R. R. Alfano, (unpublished, see Chapter 4 of this thesis)

4. Hsieh Shin Chao and R. R. Alfano, (unpublished, see Chapter 5 of this thesis)

Table 6-I Calculated carrier density dependence of $\tau_s \sim N^x$ for various combinations of spin relaxation mechanism and momentum relaxation mechanism. The calculations were performed in two temperature regimes separated by T=80K.

Concentration dependence (x)			DP		EY		BAP	
			3D	2D	3D	2D	3D	2D
AC	high T	n=1.7	-0.86	-1.3	-2.47	-3.7	-0.34	-0.5
	low T	1.2	-1	-1.5	-2.34	-3.5	-0.34	-0.5
PZ	high T	0.8	-1.46	-2.2	-1.87	-2.8	-0.34	-0.5
	low T	0.1	-1.8	-2.7	-1.53	-2.3	-0.34	-0.5
IM	high T	0.1	-1.93	-2.9	-1.4	-2.1	-0.34	-0.5
	low T	-0.7	-2.2	-3.3	-1.13	-1.7	-0.34	-0.5
OP	high T	0	-2	-3	-1.33	-2	-0.34	-0.5
	low T	1.8	-0.8	-1.2	-2.54	-3.8	-0.34	-0.5

Table 6-II. Experimental results of the carrier concentration dependencies of τ_s. The measurement of bulk GaAs done at 70-100K (**) was performed by Seymour[3] *et al.*.

	3D (bulk)	2D (Q.W.)
Low temperature	$N^{-0.233\pm0.04}$ (40K)	$N^{-0.37\pm0.05}$ (20K)
High temperature	$N^{-0.63**}$ (70-100K)	$N^{-0.91\pm0.13}$ (100K)

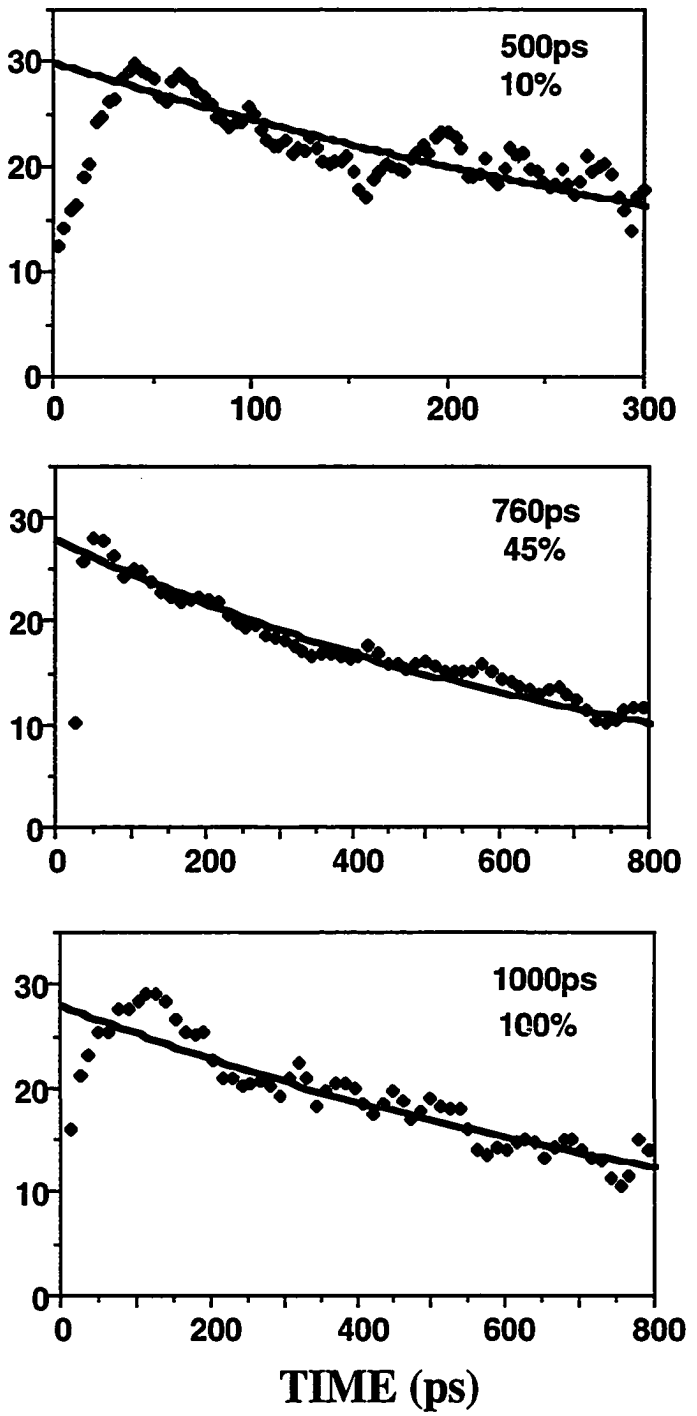

Figure 6-1(a) Time resolved spin polarization measured at various carrier concentrations for bulk GaAs measured at 40K. The fitted spin relaxation times apprear on the top of concentration percentage. 100% refers to a concentration of $10^{18}cm^{-3}$.

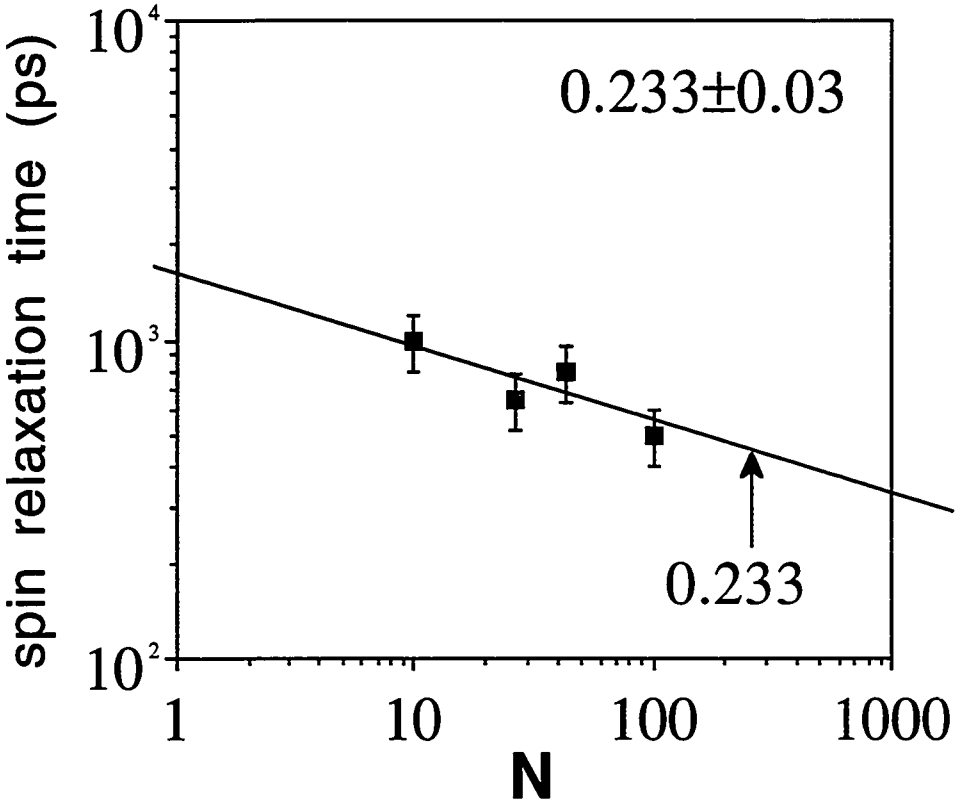

Figure 6-1(b) Spin relaxation times plotted as a function of carrier concentration for bulk GaAs measured at 40K. This result shows that $\tau_s \sim N^{-0.233\pm0.03}$. The unit of N on the X-axis is 10^{16} cm^{-3}.

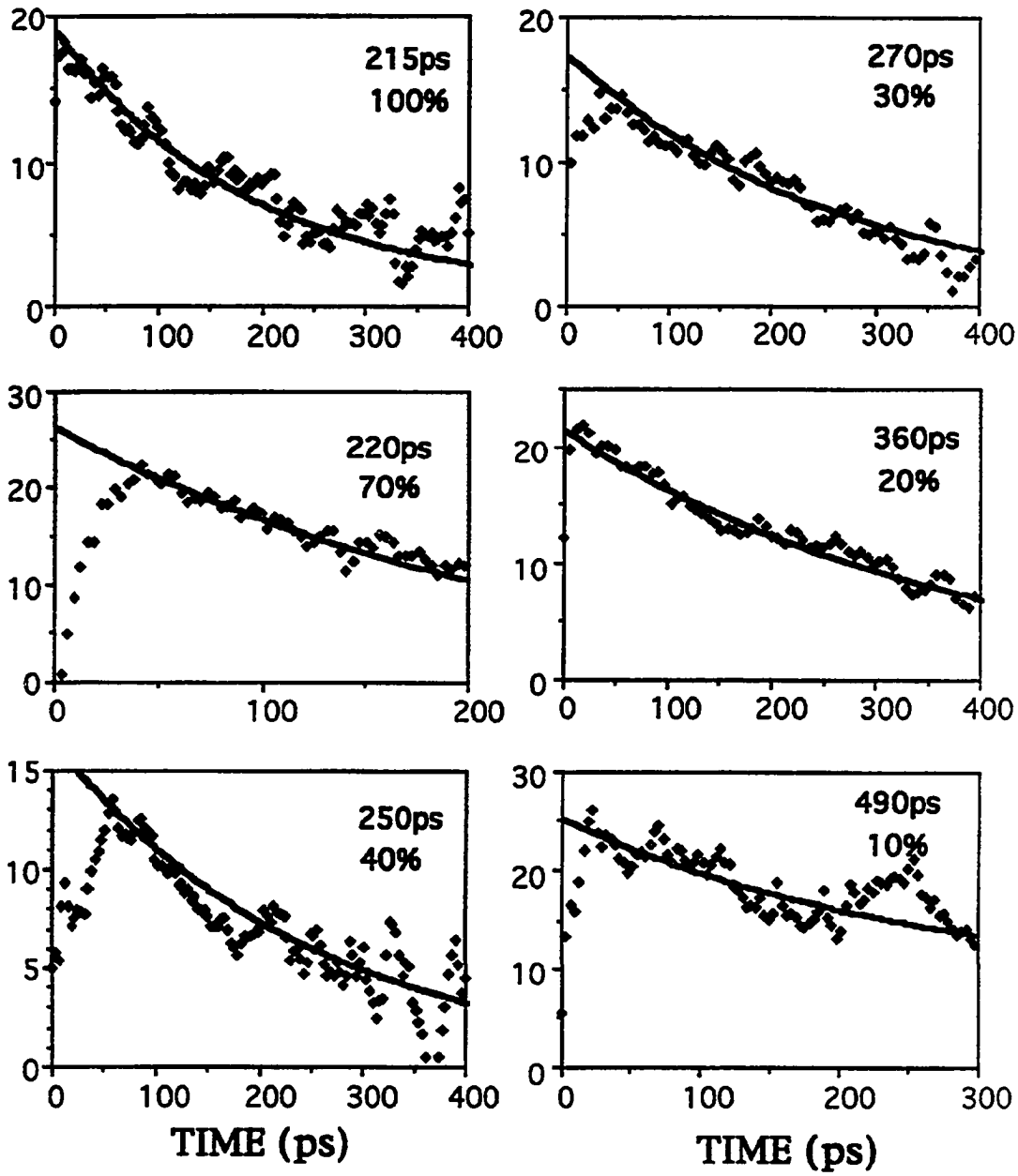

Figure 6-2(a) Time resolved spin polarization measured at various carrier concentrations for 55Å wells measured at 20K. The fitted spin relaxation times apprear on the top of concentration percentage. 100% refers to a concentration of $10^{18}cm^{-3}$.

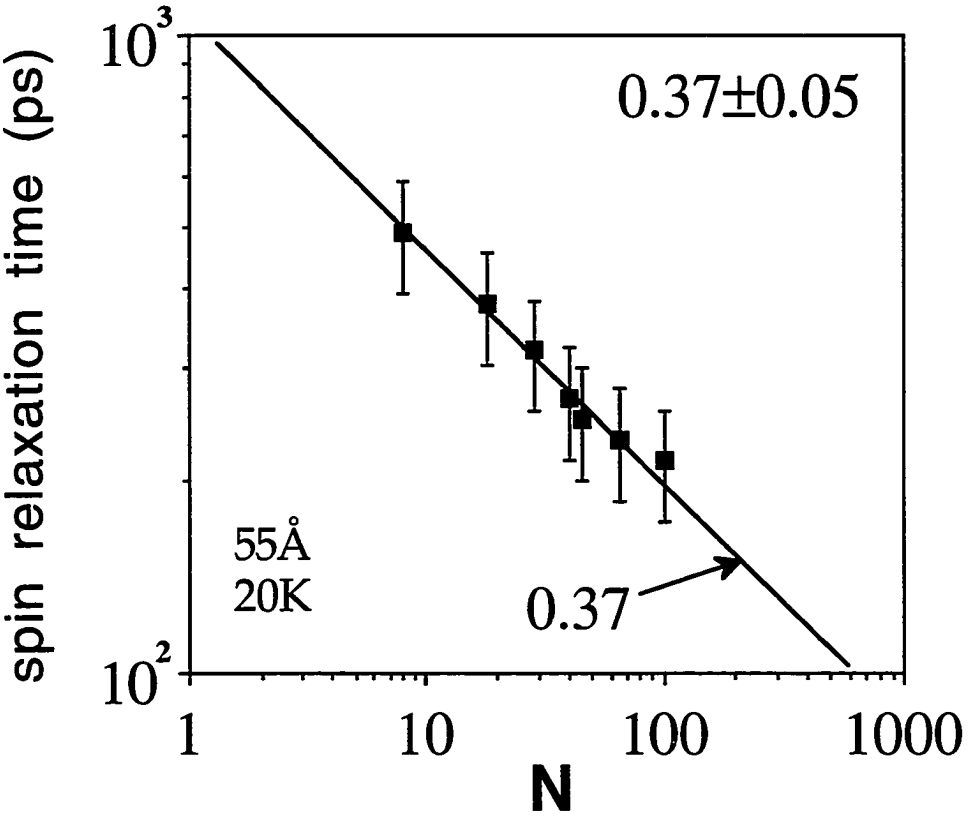

Figure 6-2(b) Spin relaxation times plotted as functions of carrier concentration for 55Å wells measured at 20K. This result shows that $\tau_s \sim N^{-0.37\pm0.05}$. The unit of N is 10^{16} cm^{-3}.

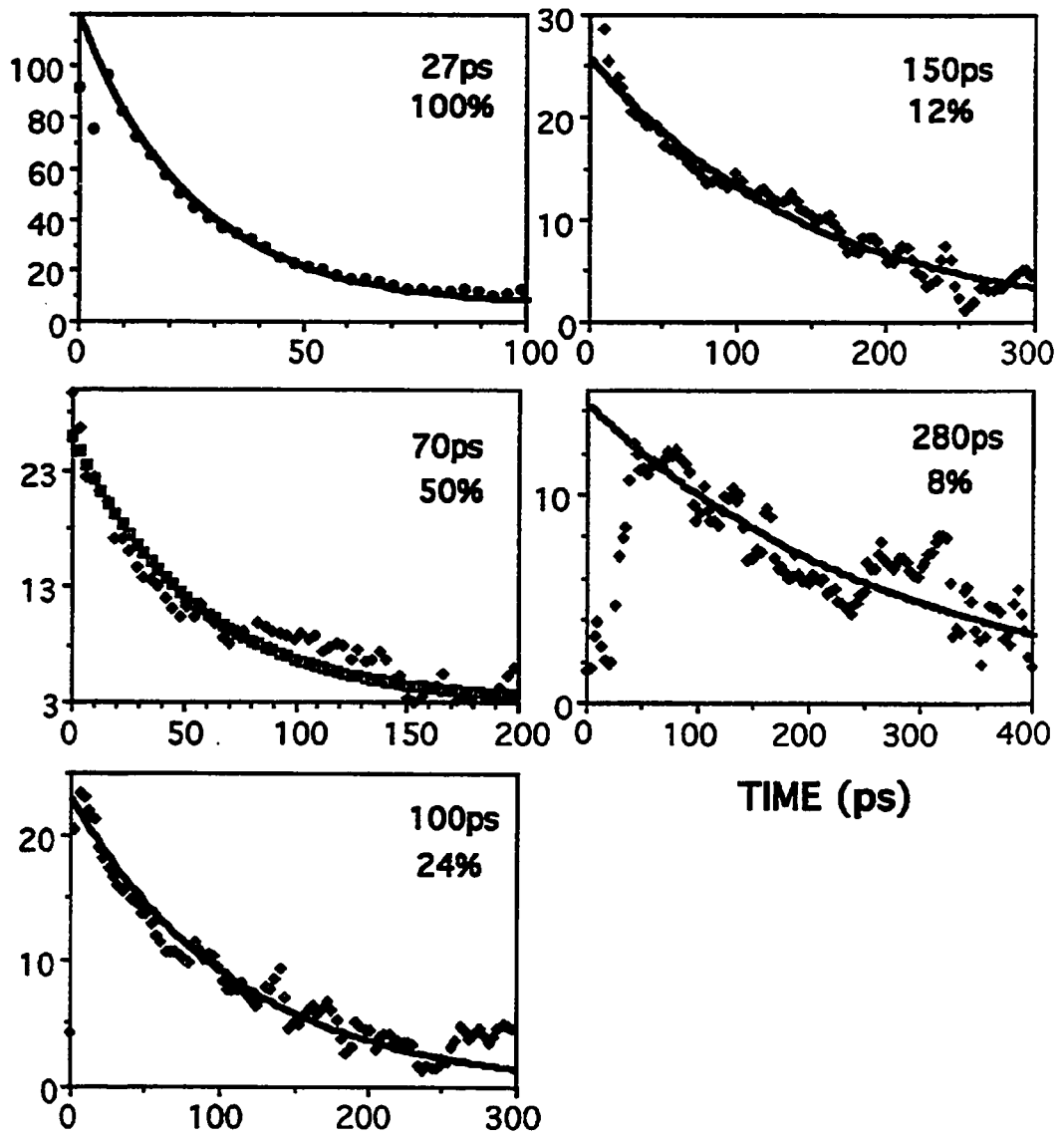

Figure 6-3(a) Time resolved spin polarization measured at various carrier concentrations for 55Å wells measured at 100K. The fitted spin relaxation times apprear on the top of concentration percentage. 100% refers to a concentration of $10^{18}cm^{-3}$.

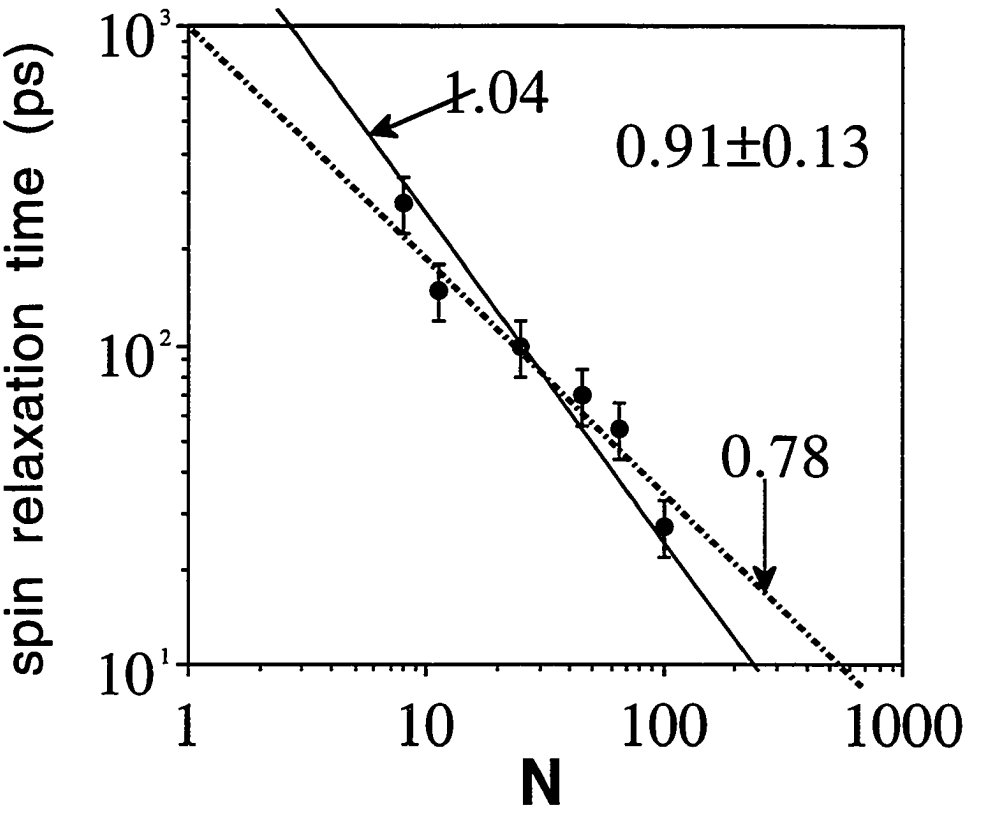

Figure 6-3(b) Spin relaxation times plotted as functions of carrier concentration for 55Å wells measured at 100K. This result shows that $\tau_s \sim N^{-0.91\pm0.13}$. The unit of N is 10^{16} cm^{-3}.

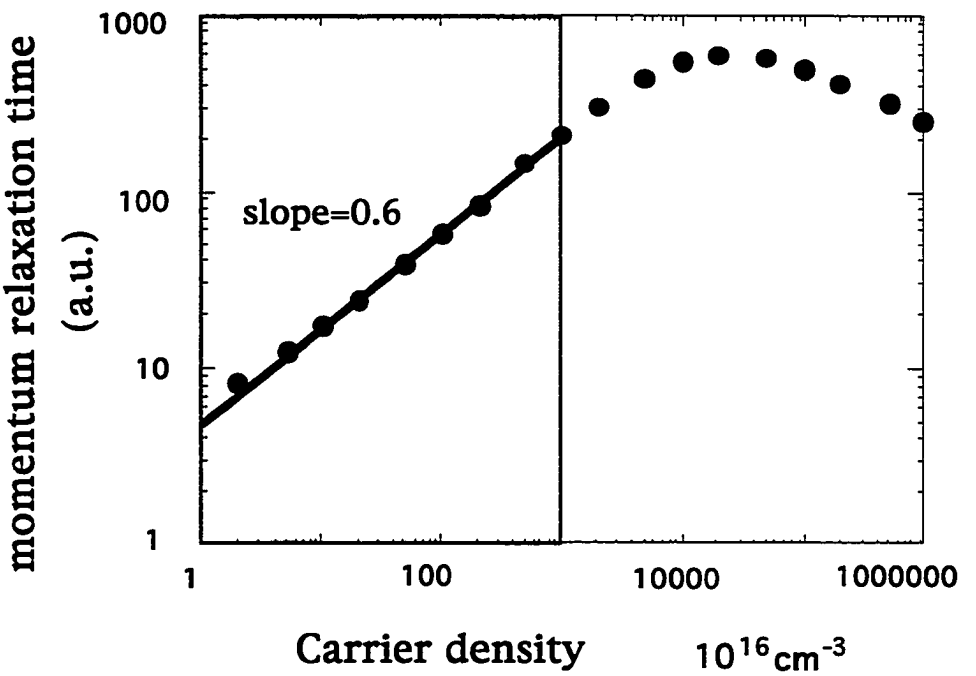

Figure 6-4 The momentum relaxation times calculated as a function of carrier concentration due to deformation potential scattering. Calculation is based on Eq. (6.1). The X axis is carrier density N in unit of $10^{16}cm^{-3}$ and the Y axis is the momentum relaxation time in arbitrary unit. The momentum relaxation times in the shaded area can be expressed as $\tau_p^{ac} \sim N^{0.6}$.

CHAPTER SEVEN

THE TEMPERATURE DEPENDENCE OF CARRIER SPIN RELAXATION TIME

Achievement

The temperature dependence of electron spin relaxation time was studied in bulk GaAs and GaAs/AlGaAs quantum wells. It is observed that spin relaxation times in 55Å quantum wells are ten times shorter than those in the bulk. A dual dependence on temperature is also observed in two temperature regimes separated by T=80K. It is because of two different mechanisms which are operational in those temperature regimes, respectively.

7.1 Background

The experimental results of temperature dependence of τ_s has been seen in Chapter 4 where the high temperature carrier spin relaxation mechanism and momentum relaxation scattering were determined to be the DP mechanism and the deformation potential scattering from the temperature dependence of τ_s. In this chapter, the characteristics of temperature dependence of τ_s in different dimension and at temperatures will be studied.

7.2 Theory

The process of spin relaxation were discussed in many research reports[1-4]. Several competing mechanisms have been proposed to account for the spin relaxation based on different interactions experienced by the carriers. The competition among them was studied by the various dependencies of τ_s, for example, the temperature dependence, the carrier energy dependence, the carrier concentration dependence, and the dimensionality dependence. From the experimental results of these dependencies, the BAP mechanism[3] is determined to be dominating the electron spin relaxation at low temperatures while the DP mechanism[4] is dominating at high temperatures.

The temperature dependence is obtained from the calculations of Fermi integral. In the calculations, the 3D and 2D density of states (ρ_{3D}, ρ_{2D}) have been used respectively. However, the integral results in the same temperature dependencies for both dimensions. It is because of the independence of the density of states on temperature.

The T-dependencies of τ_s in both dimensions were calculated to be $\tau_s^{BAP}(T) \sim T^0$ and $\tau_s^{DP}(T) \sim T^{-n-1.5}$ for the BAP mechanism and the DP mechanism, respectively, where n is the energy dependence of momentum relaxation time. By comparing to the experimental results, n can be determined to be 1.3 and this is most similar to the acoustic phonon deformation potential scattering which has $n = 1.7$. The calculation was performed based on the non degenerate electron system.

7.3 Experiments

The same simultaneous detection experimental setups was discussed in Chapter 4.

7.4 Results

In Figure 4-1, the temperature dependent spin relaxation times in bulk material and two quantum wells were plotted. It showed $\tau_{s(b)} \sim T^{-0.1}$ for T<80K and $\tau_{s(b)} \sim T^{-2.8}$ for T>80K, $\tau_{s(qw90)} \sim T^{-0.38}$ and $\tau_{s(qw55)} \sim T^{-0.45}$ for T<80°K, and $\tau_{s(qw55)} \sim T^{-2.8}$ for T> 80°K, where $\tau_{s(b)}$, $\tau_{s(qw90)}$, and $\tau_{s(qw55)}$ represented the spin relaxation times of bulk material, 90Å wells, and 55Å wells, respectively. There are two salient features that should be emphasized. First, the spin depolarization time τ_s depends on the dimensionality of the sample that $\tau_{s(b)}$ is longer than $\tau_{s(qw90)}$ which is longer than $\tau_{s(qw55)}$ at the same temperature in both temperature regimes. Secondly, the depolarization

times, from all three samples, are functions of temperature with clearly different dependencies in two temperature regimes.

The temperature dependencies of τ_s of three dimensionalities changed from $\tau_{s(b)} \sim T^{-0.1}$ in the bulk through $\tau_{s(qw90)} \sim T^{-0.38}$ in 90Å wells to $\tau_{s(qw55)} \sim T^{-0.45}$ in the 55Å wells in the low temperature regime (T<80K); while $\tau_s \sim T^{-2.8}$ held for all samples in the high temperature regime (T>80K). In other words, the temperature dependence is invariant when dimensionality reduces at high temperatures.

It has been seen from the experimental results given in Figure 4-1, the temperature dependencies for all three samples are weak at low temperatures and are similar to the BAP mechanism; while the dependence is strong at high temperatures and is similar to the DP mechanism. There is no sign from my temperature dependent data showing the agreement with the EY theoretical prediction. From the other measured dependencies on the carrier energy and carrier concentration the predomination by the EY mechanism has not been seen either.

7.5 Discussion

The dual temperature dependent feature shown in Figure 4-I indicates that there are two different mechanisms, which involves different temperature dependencies, dominating in different temperature regimes.

From the previous experimental results obtained from the carrier concentration dependence, the carrier's energy dependence, along with the

dual temperature dependent feature observed this time, it is confirmed that the BAP mechanism dominates spin relaxation at low temperatures and the DP mechanism dominates at high temperatures. The physical meaning of this result can be explained as the following. At low temperatures, electron and hole associate to form an exciton enhancing the exchange interaction, therefore, the BAP mechanism is effective. The DP mechanism replaces the BAP mechanism to be effective at high temperatures because exciton dissociates by gaining thermal energy and the spin exchange interaction between electron and hole is greatly reduced.

7.5a Low temperature regime (T<80K)

At T<80K, the BAP mechanism is dominating and $\tau_s \sim T^0$ is theoretically predicted. The temperature dependencies were experimentally observed as $\tau_{s(b)} \sim T^{-0.1}$, $\tau_{s(qw90)} \sim T^{-0.38}$, and $\tau_{s(qw55)} \sim T^{-0.45}$. In the bulk, it is roughly in consistent with the theory while in the quantum wells, not only the numerical values of the T-dependence did not satisfactorily match the theory but they depend on dimensionality. The reason for this disagreement is the possible degeneracy of electrons in the quantum wells.

To determine whether the electrons are degenerate or not, we can compare the Fermi temperature T_F with the lattice temperature T. If $T_F > T$, then the electrons are considered degenerate. There is one thing to be noted that Fermi energy, $\varepsilon_F = k_B T_F$, is a function of carrier concentration n. In 3D system, $\varepsilon_F \sim n^{2/3}$ while in 2D system, $\varepsilon_F \sim n$. Therefore, the Fermi temperature of quantum wells is strongly affected by the carrier concentration and the carriers in the quantum wells are easy to become degenerate if they are highly concentrate. In Chapter 3, high carrier concentration generation

was demonstrated in the thin well. Without taking carrier diffusion into account, Figure 7-1 plotted the spin relaxation time, τ_s, as a function of the sample thickness from 100Å to 10μm. τ_s was estimated from fitting to curves drawn in Figure 2-11.

The experimental condition results in the $\varepsilon_F = 75meV$ above the bottom of the Γ-valley. This amount of Fermi energy is equivalent to a temperature at $850^\circ K$ which is higher than the lattice temperature I had in the experiments. The quantum well samples are likely degenerate. For degenerate system the temperature dependencies of τ_s was calculated and expressed as [5]

$$\frac{1}{\tau_s} = \frac{3}{\tau_o}\frac{v_e}{v_B}\frac{k_B T}{\varepsilon_F}|\Psi(o)|^4 N_p a_B{}^3 \sim T^{3/2} \qquad (7.1)$$

where τ_o is a constant related to the strength of exchange splitting of the exciton ground states; $|\Psi(o)|$ is the Sommerfeld factor; a_B is the exciton Bohr radius; $v_B = \hbar/\varepsilon_F a_B$ is exciton Bohr velocity; $v_e = \sqrt{3k_B T/m_e^*}$ is the velocity of thermalized electrons; N_p is the density of holes. Obviously, τ_s of the degenerate electrons depends on T stronger than that of non degenerate electrons. This explains why $\tau_{s(qw90)} \sim T^{-0.38}$ and $\tau_{s(qw55)} \sim T^{-0.45}$. The temperature dependencies in wells do not numerically match the theoretical prediction of the temperature dependence to a power of $3/2$ because the degeneracy might be only partial.

7.5b High temperature regime (T>80K)

In high temperature regime, the DP mechanism, which involves the randomization of the electron's spin axis through precessional-scattering, is

effective. The theoretical temperature dependence is $\tau_s \sim T^{-3.2}$ but $\tau_s \sim T^{-2.8}$ was experimentally observed.

The large numerical difference of τ_s ($\tau_{s(b)}(T):\tau_{s(qw55)}(T) = 10:1$) observed between the bulk and two wells is attributed to the variation of the carrier concentration in the samples. As what has been mentioned earlier in the discussion of the section of low temperatures thin wells generally have highly concentrated carriers hence have high energy. Since $\tau_s \sim E^{-1.3}$, a conclusion from the carrier's energy dependence, the bulk sample with low concentration has long τ_s while the thin wells with high concentration will have short τ_s.

The observed strong temperature dependencies, namely, $\tau_s \sim T^{-2.8}$ are true for the bulk and wells in this temperature regime. It indicates that the temperature dependencies do not change as a result of the dimensionality changes. This is in agreement with the theoretical calculations given in Table 2-III which shows that the T-dependencies of all three mechanisms are independent of the dimensionality.

7.6 Conclusion

In conclusion, the temperature dependence of electron spin depolarization time in both bulk GaAs and quantum wells is observed. It shows that two different mechanisms are dominating the spin depolarization in different temperature regime. It is true for both quantum wells and bulk GaAs.

The e-h spin exchange mechanism (BAP) is dominating at low temperatures (T<80K); the precessional mechanism (DP) is dominating at low temperatures (T>80K).

Because of the excitonic effect (for T<80K) and electron degeneracy (for T>80K), spin relaxation time is shorter in quantum wells than in the bulk.

7.7 References

1. E. J. Johnson, R. J. Seymour and R. R. Alfano, "***Semiconductors Probed by Ultrafast Laser Spectroscopy***", Vol. II, edited by R. R. Alfano, Academic Press, New York, Chapter 19, 199 (1984)

2. G. E. Pikus and A. N. Titkov, "***Optical Orientation***", Chapter 3, edited by F. Meier and B. P. Zakharchenya, Elsevier Science Publishers B. V. (1984)

3. G. L. Bir, A. G. Aronov and G. E. Pikus, ***Sov. Phys. JETP 42, 705*** (1976)

4. M. I. D'yakonov and V. I. Perel, ***Sov. Phys. JETP 38, 177*** (1974)

5. K. Zerrouati, F. Fabre, G. Bacquet, J. Bandet, J. Frandon and G. Lampel, D. Paget, ***Phys. Rev. B 37(3) 1334*** (1987)

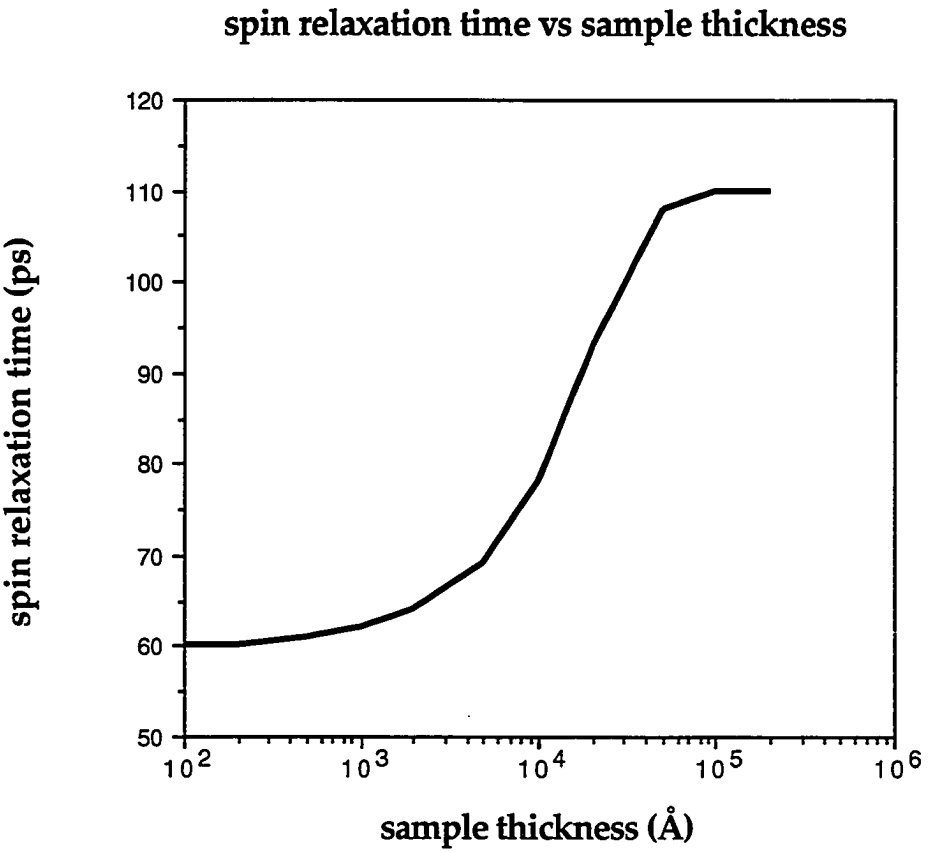

Figure 7-1 A theoretical prediction of the spin relaxation time as a function of the sample's thickness. In the calculation, carrier diffusion was not included.

CHAPTER EIGHT

CONCLUSIONS

Ultrafast pulse excitation and time resolved measurements has been used to investigate electron spin depolarization. Electron spin depolarization has many possible mechanisms. Each mechanism becomes dominating under certain conditions. In order to determine the operational spin relaxation mechanism I investigated the spin relaxation times, τ_s, at different lattice temperatures, carrier energies, and carrier concentrations.

In the course of this thesis, the scattering process which is responsible for the momentum relaxation has also been investigated. It is important to identify the operational momentum relaxation scattering process because the spin relaxation and the momentum relaxation are parallel processes.

The spin relaxation times measured as functions of temperature, carrier energy, and carrier concentration provided much useful information in determining the operational carrier spin relaxation mechanism and the operational scattering process responsible for the carrier momentum relaxation.

The scattering causing momentum relaxation was determined, in the high temperature regime (T>80K), to be the acoustic phonon deformation

potential scattering. The determination was made based on the experimental results from all measurements depending on temperature, carrier energy, and carrier concentration. In the low temperature regime (T<80K), the momentum relaxation scattering process can not be determined because of the dominating spin relaxation mechanism, the Bir-Aronov-Pikus mechanism, is independent of the momentum relaxation. It involves an spin exchange interaction between electrons and holes.

For spin relaxation at high temperatures, the D'yakonov-Perel mechanism was determined to be dominant. This result is in agreement with all measurements.

It was observed that τ_s in the bulk material is much longer than that in the 2-dimensional wells. In the bulk material, τ_s was seen in the nanosecond domain while in the wells, τ_s was less than few hundred picoseconds depending on the temperature. For the difference of the numerical values of τ_s between the bulk GaAs and GaAs/$Al_xGa_{1-x}As$, it is due to the strong excitonic effect and high Fermi temperature in low and high temperature regimes, respectively. Strong excitonic effect results in fast spin exchange interaction and high Fermi temperature results in a high Larmor frequency. Both effects speed up the electron spin relaxation.

For the dominating spin relaxation mechanism, it is the same for 2D and 3D. Therefore, the dimensionality change does not change the spin relaxation mechanism.

The salient feature of this thesis is that the results from all types of measurements lead to the same conclusion in determining the operational

spin relaxation mechanism and the effective momentum relaxation scattering mechanism which is that the operational spin relaxation mechanism is the BAP mechanism at low temperatures while it is the DP mechanism which is operational at high temperatures. For the scattering causing momentum relaxation, the acoustic phonon scattering is dominant.

8.1 Future directions

The work done in this thesis is just the tip of an iceberg. More measurements need to be conducted to obtain more information about this complicated-but-useful field. Additional attention should be paid to the spin polarization which was not deeply involved in this thesis. Spin polarization could be greatly enhanced by modifying the structure of the polarized material (narrowing down the well or applying stress) and by carefully selecting the excitation energy and the detection band linewidth (resonant pumping and detecting the luminescence from a recombination to one hole band, say, only e-hh). The other direction of the continuing research in the future should be in the direction of the improvement on the quality of equipment or the development of new detection technique. A tunable excitation laser source with stable output and a jitter free and sensitive detector will be highly appreciated.

The advantage of taking electron spin characteristic into account is that the measurements related to electron spin are more reliable because they provide detailed information from a deeper electronic level which is not considered by non-spin measurements. Today, the electronic properties of

semiconductors are widely applied in technological advances. Research on transport and optical properties have been explored with a great depth. This fundamental property of electron, "spin", is still far from understood. It deserves our attention.

APPENDIX

In this chapter of appendix, there contains five computer programs written for various purposes for the completion of this thesis. The specific function of each routine is (listed in the order of appearance) calibration, data transfer, averaging, calculation, and fitting.

All programs are running in Quick BASIC. All instructions are included in the routine. Runner just have to follow the program. For most of the routines, source file name is the only input and the storage file with results from the specific operation of that program is the output.

The following program <STRKCALI.BAS> calibrats the streak rate of each of the streak camera.

```
REM ========== STREAK RATE CALIBRATION ==========
   CLEAR
   SCREEN 2
   LOCATE 6, 1: PRINT "16th-240th CHANNEL ARE CALIBRATED"
   PRINT "PULSE INTENSITY MUST BE HIGHER THAN 20"
   PRINT "USE LOWER CHARACTER "
   PRINT "SET COMMUNICATION MODE (mode com2:96,n,8,2,p)  "
   PRINT "    ": INPUT "PRESS KEY <CR> TO CONTINUE.....", G$

   DIM STAC(10)
   DIM Y(260, 16)
   DIM TB(260)
   DIM Q(260): DIM R(260, 2)
   DIM QL(260)
   DIM AC$(25)
   DIM T$(256)
REM ========== PRESET PARAMETERS ==========
50  CLS : CLEAR
   LOCATE 15, 1
   INPUT "Enter flight-time of etlon (ps)   ", TD
   GOSUB 200
   LOCATE 14, 1
   PRINT "Standard Time Interval :"; TD
110 GOSUB 300                          'Input data from TA, translates and shows    '
   LOCATE 15, 1
   INPUT "Accept the data ? (y/n, default=y)  ", ANS$          'data selection      '
   GOSUB 200
   IF ANS$ = "n" THEN GOTO 110
   GOSUB 530                           'Sorting pulses and printing out      '
   GOSUB 610                           'Streak rate calculation and display  '
REM ========== OPERATION SELECTION ==========
150 LOCATE 15, 1
    PRINT "Continue to take pulse-trains .....1"
   PRINT "Stop taking shots and start to average .....2"
    PRINT "Ready for next RATE .....3"
   LOCATE 20, 1
   INPUT "Enter Selection (1,2,3)    ", S
   GOSUB 200
   IF S = 1 THEN GOTO 110                          'Continue shots  '
   IF S = 2 THEN GOSUB 720                         'start average   '
   IF S = 3 THEN GOSUB 900: GOTO 50                'next rate       '
   DRAW "bm300,100"

200 FOR L = 15 TO 20
   LOCATE L, 1
   PRINT "                                "
   NEXT L
   RETURN
REM ========== DATA ACQUISITION ==========
300 OPEN "com2:9600,n,8,2,rs,cs,ds,cd,lf" FOR RANDOM AS #1
   'OPEN "scrn:" FOR OUTPUT AS #2
   PRINT "activate digital output of streak camera "
   FOR i = 1 TO 22
   INPUT #1, AC$(i)
   'PRINT #2, AC$(I)
```

```
   NEXT i
   CLOSE 1
REM ═══════════ DATA ORGANIZATION & DISPLAY ═══════════
   FOR M = 7 TO 22
   FOR j = 1 TO 16
   N = (M - 7) * 16 + j
   T$(N) = LEFT$(AC$(M), 4 * j)
   T$(N) = RIGHT$(T$(N), 4)
   QL(N) = VAL(T$(N))
   NEXT j
   NEXT M
   GOSUB 400
   DRAW "bm330,190"
   DRAW "r257 u80 l257 d80"
   DRAW "bm331,190"
   FOR x = 1 TO 256
   h = QL(x) * .3
   DRAW "nu=" + VARPTR$(h)
   DRAW "bm+1,+0;"
   NEXT x
   RETURN
400 DRAW "bm330,190"
   FOR x = 1 TO 257
   h = 80
   DRAW "c0;"
   DRAW "nu=" + VARPTR$(h)
   DRAW "bm+1,+0;"
   NEXT x
   DRAW "c1;"
   RETURN
REM ═══════════ PULSE PEAK LOCALIZATION ═══════════
530 P = 0
   FOR C = 3 TO 254
   IF QL(C) < 20 THEN GOTO 600
   IF QL(C - 2) - QL(C - 1) > 0 THEN GOTO 600
   IF QL(C - 1) - QL(C) > 0 THEN GOTO 600
   IF QL(C) - QL(C + 1) < 0 THEN GOTO 600
   IF QL(C + 1) - QL(C + 2) < 0 THEN GOTO 600
   P = P + 1: STAC(P) = C
   LOCATE 15, 1: PRINT P; " pulse at  "; STAC(P)
   LPRINT P; " pulse at  "; STAC(P); " with Intensity"; QL(C)
600 NEXT C
   RETURN
REM ═══════════ MEASUREMENT STATISTICS ═══════════
610 FOR N = 1 TO P - 1
   FOR x = STAC(N) TO STAC(N + 1) - 1
   CD = STAC(N + 1) - STAC(N)
   TB(x) = TB(x) + 1
   IF TB(x) > 12 THEN LOCATE 22, 1
   PRINT "CHANNEL"; x; "HAS BEEN COVERED"; TB(x); "TIMES !"
   IF CD = 0 THEN GOTO 620
   Y(x, TB(x)) = TD / CD
620 NEXT x
   NEXT N
REM ═══════════ SCALING & PLOTTING ═══════════
   MIN = Y(STAC(2), 1) * .85
   MAX = Y(STAC(2), 1) * 1.15
```

```
   SCALE = 50 / (MAX - MIN)
   DRAW "bm330,105"
   DRAW "r257 u50 l257 d50"
   DRAW "bm331,105"
   FOR x = 1 TO 256
   h = TB(x) * 3
   DRAW "nu=" + VARPTR$(h)
   DRAW "bm+1,+0;"
   NEXT x
   DRAW "bm330,50"
   DRAW "r257u50l257d50"
   FOR x = 1 TO 256
   i = 330 + x
   j = 50 - (Y(x, TB(x)) - MIN) * SCALE
   PSET (i, j)
   NEXT x
   RETURN
720 FOR x = 1 TO 256
   IF TB(x) = 0 THEN GOTO 730
   FOR S = 1 TO TB(x)
   R(x, 0) = R(x, 0) + Y(x, S)
   NEXT S
   R(x, 0) = R(x, 0) / TB(x)
   PRINT x, R(x, 0)
730 NEXT x

   DRAW "bm50,50"
   DRAW "r257u50l257d50"
   FOR x = 1 TO 256
   i = 50 + x
   j = 50 - (R(x, 0) - MIN) * SCALE
   PSET (i, j)
   NEXT x
REM ========== STORAGE FILE NAME INPUT ==========
   LOCATE 15, 1
   INPUT "Enter RATE filename  ", FILE$
   OPEN FILE$ FOR OUTPUT AS #2
   FOR x = 16 TO 240
   PRINT #2, R(x, 0), TB(x)
   NEXT x
   LOCATE 15, 1
   PRINT "Data have been saved in "; FILE$
795 CLOSE
   RETURN

REM ========== FRAME PLOTTING ROUTINE ==========
810 CLS
   DRAW "bm330,190"
   DRAW "r255 u50 l255 d50 u50"
   FOR x = 1 TO 5
   DRAW "br50"
   DRAW "nd50
   NEXT x
   DRAW "bm326,130"
   DRAW C0$
   DRAW "bm+38,0"
   DRAW C5$: DRAW C0$
```

```
    DRAW "bm+30,0"
    DRAW C1$: DRAW C0$: DRAW C0$
    DRAW "bm+30,0"
    DRAW C1$: DRAW C5$: DRAW C0$
    DRAW "bm+25,0"
    DRAW C2$: DRAW C0$: DRAW C0$
    DRAW "bm+25,0"
    DRAW C2$: DRAW C5$: DRAW C0$
    DRAW "bm330,190"

900 FOR i = 1 TO 256
    TB(i) = 0
    NEXT i
    RETURN
REM ========== STREAK RATE DISPLAY ==========
970 FOR x = 2 TO 255
980 h = TB(x) * 3
990 DRAW "nu=" + VARPTR$(h)
995 DRAW "bm+1,+0;"
1000 NEXT x
1010 RETURN
```

The following program <SPINRAW2.BAS> transfers the time resolved integrated (T.R.I.) luminescence data from the streak camera to the IBM personal computer.

```
REM == ROUTINE OF DATA TRANSFER (streak camera to IBM ) ==========
100 CLEAR : CLS : SCREEN 2
110 LOCATE 5, 1
113 PRINT "This program transfers raw data from TA to PC and store in a file"
120 PRINT "Output filename is automatically generated by program  "
130 PRINT "Set T-switch to C"
131 PRINT "Communication mode setting : mode com2:96,n,8,2,p"
132 PRINT "Floppy disk takes 110 files only, at that point, a warning sound will be on": PRINT "    "
134 PRINT "TURN ON PRINTER"
140 PRINT "  ": INPUT "Read above and press return to continue .....    ", G$
150 DIM AC$(25)
160 INPUT "enter filename (w/d) (a:jun011)  ", FILE$              'giving initial data filename'
170 OPEN "com2:9600,n,8,2,rs,cs,ds,lf" FOR RANDOM AS #1  'open data interfacing port '
180 OPEN "scrn:" FOR OUTPUT AS #2                                  'open monitor screen          '
190 OPEN FILE$ FOR OUTPUT AS #3                                   'open storing data file       '
200 PRINT "activate digital output of streak camera "
210 FOR i = 1 TO 22
220 INPUT #1, AC$(i)
230 PRINT #2, AC$(i)                                          'data display on minitor      '
240 PRINT #3, AC$(i)                                         'data stored in the storing file     '
250 NEXT i
260 CLOSE
270 LPRINT "DATA HAVE SAVED IN "; FILE$; " FOR WINDOW "; RIGHT$(AC$(2), 1):
GOSUB 283
280 GOTO 170
283 PRINT "C0MPLETED FILE : "; FILE$
290 G = LEN(FILE$) - 7
300 L$ = LEFT$(FILE$, 7)
310 R$ = RIGHT$(FILE$, G)
320 DD = VAL(R$): ND = DD + 1
   fc = fc + 1
   IF fc = 110 THEN PRINT "Disk is almost full, REPLACE ANOTHER ONE !!" ELSE GOTO 330
REM ========== WARNING FOR FILE OVERFLOW ==========
   FOR i = 1 TO 10
   SOUND 3000, 10: SOUND 1000, 10
   NEXT i
325 PRINT "Press 1 to continue without resetting file-count   "
   PRINT "Press 2 to continue with resetting file-count (replace disk)  "
   PRINT "Press 3 to check number of files in the disk   "
   INPUT "enter code   ", cc
   IF cc = 2 THEN fc = 0
   IF cc = 3 THEN FILES "a:": INPUT "Enter a new file-count ", fc: GOTO 325
REM ========== GENERATING NEW FILE NUMBER ==========
330 ND$ = STR$(ND): LND = LEN(ND$) - 1
340 FILE$ = L$ + RIGHT$(ND$, LND)
350 PRINT "NEXT FILE NAME : "; FILE$
360 RETURN
```

The following program <SPNAVG.BAS> takes the average of multi T.R.I. luminescence data which were obtained under the same experimental conditions. The average is taken based on the temporal position of the prepulse.

```
REM ======= ROUTINE AVERAGES THE RAW DATA MULTI-FILES =======
  CLS
20 PRINT "This program is designed for SPINRAW data file average"
30 PRINT "The averaged file is generated by the system "
40 PRINT "Number of data points is fixed to 256"
50 PRINT "Maxium number of averaging file is 20"
60 PRINT "It translates string data into value"
80 DIM Q$(260), X(260)
90 DIM R(560), FL$(10)
  DIM T$(260), S(260)
  DIM B(1000), Q(590)
100 CLEAR : INPUT "enter window  ", WN$
120 F = 0
130 GOSUB 210
140 GOSUB 480
150 GOSUB 860
160 GOSUB 810
   GOSUB 1140
170 GOSUB 990
180 LOCATE 8, 1: INPUT "Job is done !! press <enter> .....", G$
190 GOTO 100
  REM ============ DATA FILE READ-IN SUBROUTINE ============
210 F = F + 1: PRINT "New file # ="; F
212 IF F > 1 THEN GOSUB 1300: GOTO 220
214 INPUT "enter the file name (with drive w/d)   ", FILE$
220 FL$(F) = FILE$: CLS : SCREEN 2
230 PRINT FILE$; " is RUNNING ! "
240 OPEN FILE$ FOR INPUT AS #2: C = 1
250 IF EOF(2) THEN CLOSE 2: GOTO 280
260 INPUT #2, Q$(C)
270 C = C + 1: GOTO 250
280 W$ = RIGHT$(Q$(2), 1): PRINT "Window = "; W$       'window checking & recording'
290 IF W$ = WN$ THEN GOTO 310
300 PRINT "Wrong window !!!": F = F - 1: GOTO 210
310 G = VAL(RIGHT$(Q$(4), 5))
320 IF F = 1 THEN OG = G
330 TAG = OG / G: PRINT "Gain="; G
335 PRINT "OG="; OG; "  TAG="; TAG

REM ================ DATA REFORMATION ================
340 FOR M = 7 TO 22
350 FOR J = 1 TO 16
360 L = (M - 7) * 16 + J
370 T$(L) = LEFT$(Q$(M), 4 * J)
380 T$(L) = RIGHT$(T$(L), 4)
390 Q(L) = TAG * VAL(T$(L))
400 NEXT J
410 NEXT M
412 LOCATE 5, 1: PRINT "                    "
420 RETURN
REM ========= DATA PLOTTING & PEAK SEARCHING ROUTINE =========
480 DRAW "bm325,180"
```

```
490 FOR X = 1 TO 256
500 Y = Q(X) * .4
510 DRAW "nu=" + VARPTR$(Y)
520 DRAW "bm+1,+0;"
530 NEXT X
540 DRAW "u108;l256;d108;r256;"
550 C = 50
560 DRAW "bm250,17;r375u13l375d13r138u13"
570 DRAW "bm250,33;r375u13l375d13"
580 DRAW "bm374,179"
590 DRAW "u106;"
600 LOCATE 15, 1: PRINT "key <r> move to the right"
610 LOCATE 16, 1: PRINT "key <l> move to the left"
620 LOCATE 19, 1: PRINT "key <d> to drop the file "
    LOCATE 20, 1: PRINT "key <f> for ending "
624 LOCATE 17, 1: PRINT "key <R> move to the right * 10"
626 LOCATE 18, 1: PRINT "key <L> move to the left * 10"
630 LOCATE 2, 34: PRINT "channel =  "
640 LOCATE 2, 51: PRINT "intensity =                "
650 LOCATE 2, 34: PRINT "channel = "; C
660 LOCATE 2, 51: PRINT "intensity = "; Q(C)
670 G = 106 - Q(C) * .4
680 C$ = INKEY$
690 LOCATE 4, 34: PRINT "MOVE THE LINE !                              "
700 LOCATE 4, 34: PRINT "                                             "
710 IF C$ = "r" THEN DRAW "c0;" ELSE GOTO 743
720 DRAW "nd=" + VARPTR$(G)
730 DRAW "c1;bm+1,+0;nd106;"
740 C = C + 1: GOTO 630
743 IF C$ = "R" THEN DRAW "c0;" ELSE GOTO 750
744 DRAW "nd=" + VARPTR$(G)
745 DRAW "c1;bm+10,+0;nd106;"
746 C = C + 10: GOTO 630
750 IF C$ = "l" THEN DRAW "c0;" ELSE GOTO 783
760 DRAW "nd=" + VARPTR$(G)
770 DRAW "c1;bm-1,+0;nd106;"
780 C = C - 1: GOTO 630
783 IF C$ = "L" THEN DRAW "c0;" ELSE GOTO 790
784 DRAW "nd=" + VARPTR$(G)
785 DRAW "c1;bm-10,+0;nd106;"
786 C = C - 10: GOTO 630
    'IF C$ = "d" THEN goto
790 IF C$ = "f" THEN RETURN
800 GOTO 680

REM ========== AVERAGING ROUTINE ==========
810 LOCATE 4, 34
820 INPUT "More file? (y/n, default=y) ", ANS2$
830 GOSUB 880
840 IF ANS2$ = "n" THEN LOCATE 6, 1 ELSE GOTO 850
   PRINT "Average has done with"; F; "files"
   RETURN
850 CLS : PRINT "Last file was "; FILE$: GOTO 130
860 LOCATE 6, 34: PRINT FILE$; "  PEAK REACHED AT "; C
870 PP = C: P(F) = C: RETURN
880 LOCATE 4, 34: PRINT "                                "
890 FOR X = 1 TO 220
```

```
900 R(X) = Q(PP + X - 8)
910 S(X) = R(X) + S(X)
930 NEXT X
940 LOCATE 15, 1
980 RETURN
REM ========== RESULTS STORAGE ROUTINE ==========
990 LOCATE 4, 34: INPUT "Store result in a file ? (y/n) ", ANS2$
1000 IF ANS2$ = "n" THEN LOCATE 4, 34 ELSE GOTO 1010
   INPUT "ARE YOU SURE ? (y/n)          ", A$
   IF A$ = "y" THEN RETURN
1010 IF ANS2$ = "y" THEN LOCATE 6, 34: INPUT "Enter filename (w/d/wo/e) ", FILE$
   IF LEN(FILE$) = 0 THEN GOTO 1010
1020 FFILE$ = FILE$ + ".W" + WN$
1030 OPEN FFILE$ FOR OUTPUT AS #1
   FOR N = 1 TO 220
1070 PRINT #1, S(N)
1080 NEXT N
1090 LOCATE 4, 34: PRINT "Data have saved in file "; FFILE$; "     "
1100 FOR B = 1 TO F
1110 LPRINT FL$(B), P(B)
1120 NEXT B
1130 LPRINT "AVERAGED RESULTS ARE IN "; FFILE$
   LPRINT "   "
   CLOSE : RETURN
1140 DRAW "bm325,180"
   FOR N = 1 TO 220
   S(N) = S(N) / F
   NEXT N
1150 FOR L = 1 TO 257
1160 DRAW "c0;nu110;bm+1,+0;"
1170 NEXT L
1180 DRAW "bm325,180"
1190 FOR N = 1 TO 220
1200 Y = S(N) * .4
1210 DRAW "c1"
1220 DRAW "nu=" + VARPTR$(Y)
1230 DRAW "bm+1,+0;"
1240 NEXT N
1250 DRAW "u108l220d108"
1260 RETURN
REM ========== NEXT FILE GENERATION ROUTINE ==========
1300 LNG = LEN(FILE$): N = LNG - 7
1310 RF$ = RIGHT$(FILE$, N)
1320 NRF = VAL(RF$) + 2: NRF$ = STR$(NRF)
1330 M = LEN(NRF$) - 1
1340 NFN$ = RIGHT$(NRF$, M)
1350 FILE$ = LEFT$(FILE$, 7) + NFN$
1355 PRINT "New file name is "; FILE$
1360 INPUT "Type to change new file name (default = no change) ", G$
1370 IF LEN(G$) = 0 THEN RETURN ELSE FILE$ = G$
1380 RETURN
```

The following program <CACUSPN.BAS> calculates the T.R. spin polarized by using the T. R. luminescence data which contain two oppositely polarized components. Spin polarization is calculated as $\rho(t) = \frac{I_+(t) - I_-(t)}{I_+(t) + I_-(t)}$ where $I_+(t)$ and $I_-(t)$ are the intensities of two oppositely polarized luminescence, respectively.

```
   REM ==== This routine calculates the time-resolved spin polarization ========
    SCREEN 9
    LOCATE 3, 1
    PRINT "****************************************** "
    PRINT "**                                          ** "
    PRINT "**   CORRECT FILE TITLE ON LINE 4000     ** "
    PRINT "**                                          ** "
    PRINT "****************************************** "
    PRINT " "
    INPUT "Press enter to continue .....", g$
    CLS
    LOCATE 2, 1
    PRINT "1. This routine calculates spin polarization and shows all the 4 "
    PRINT "   operational results (+,-,/,@) on screen     "
    PRINT "2. The original data file must be input from FLOPPY          "
    PRINT "3. The number of data points is fixed to 512                "
    PRINT "4. This routine is for IBM-MAC Translational format  "
    PRINT "5. This routine must run on 386 or higher machine"
    PRINT "6. Results will be saved in 3.5"diskette for MacPlot "
    PRINT "7. Storing Format :  (C:*.TRA)"
    PRINT "   T(ps)  w1   w2   Sum   Diff   Ratio   -Ratio"
    PRINT "   "
    PRINT "8. Background Correction and Window Balance runs at first   "
    PRINT "      "
    PRINT " "
    LOCATE 15, 1: COLOR 15: INPUT "Need print out ? (pass=y)", ans0$
    INPUT "Press enter to continue .....", g$
    CLS
REM============== DECLARATION ==============
    DIM q(560), q1(560), q2(560)
    DIM q01(560), q02(560), qt(560)
    DIM qd01(560), qd02(560)
    DIM Iq01(560), Iq02(560)
    DIM x(560), y(560)
    DIM z(560)
    DIM q100(560), q200(560)
    DIM M(560), P(560)

REM============== DATA INPUT ==============
1000 GOSUB 4000
    GOTO 1001
4000 FILETL$ = "sep83"
    PRINT FILETL$
    INPUT "Enter file number     ", N$
    FILE$ = FILETL$ + N$
    file1$ = "b:" + FILE$ + ".w1"
    file2$ = "b:" + FILE$ + ".w2"
4010 CLS
    OPEN file1$ FOR INPUT AS #1
    OPEN file2$ FOR INPUT AS #2
```

```
    C = 0: LOCATE 1, 1: PRINT file1$
4100 IF EOF(1) THEN CLOSE 1: n1 = C: GOTO 4300
    C = C + 1: INPUT #1, q01(C)
    'q01(C) = q01(C) / 1000
    'LOCATE 2, 1: PRINT C, q01(C)
    GOTO 4100
4300 C = 0: LOCATE 1, 1: PRINT file2$
4400 IF EOF(2) THEN CLOSE 2: n2 = C: GOTO 4500
    C = C + 1: INPUT #2, q02(C)
    'q02(C) = q02(C) / 1000
    'LOCATE 2, 1: PRINT C, q02(C)
    GOTO 4400
4500 IF n1 = n2 THEN nd = n1 ELSE GOTO 4600
    RETURN
4600 PRINT "Number of data does not match !!"
    CLS : GOTO 4000
REM============= PROGRAM STATEMENT ==============
1001 LOCATE 2, 1
    PRINT "This subroutine contains : 1. Background Correction "
    PRINT "                           2. Window Balance"
    PRINT "                           3. channel of Zero-time "
    PRINT "    "
    INPUT "press enter to continue and <s> to skip ..... ", g$
    CLS
REM ============= PARAMETERS PRESETTING ============
1003 M1 = 1: M2 = 1
    M01 = 1: M02 = 1
    EBWIN = 1
    BK1 = 0: BK2 = 0
    BK01 = 0: BK02 = 0
    dispX01 = 0: dispX1 = 0
    dispX02 = 0: dispX2 = 0
    Xpan = 0: Rscl = 0
    windo = 3
    'IF g$ = " " THEN GOTO 1003
    IF g$ = "s" THEN GOTO 1015

1010 GOSUB 1030
    GOSUB 1310
1015 FOR i = 1 TO 512
   q1(i) = q01(i)
   q2(i) = q02(i)
    NEXT i
    GOSUB 1700
    GOSUB 2500
1020 GOSUB 1100
1030 CLS
    FOR i = 1 TO 512
   q100(i) = q01(i)
   q200(i) = q02(i)
    NEXT i

1301 xminw = 0
    xmaxw = 512
    IF yminw = 0 THEN yminw = -3000
    IF ymaxw = 0 THEN ymaxw = 500000
```

```
REM ═══════════ MONITOR SCREEN DISPLAY ═══════════
 1302 LOCATE 5, 70: COLOR 3: PRINT "W1"
    LOCATE 5, 75: COLOR 4: PRINT "W2"
    LOCATE 5, 42: COLOR 5: PRINT sta1; "  "; sta2; "  "; sta3; "  "; sta4; "  "; sta5
    COLOR 15
    LOCATE 7, 58: PRINT "X:"; xminw; "-"; xmaxw
    LOCATE 8, 58: PRINT "Y:"; yminw; "-"; ymaxw
    LOCATE 9, 58: PRINT FILE$
    COLOR 5
    LOCATE 14, 26: PRINT "BK1="; BK01
    LOCATE 16, 26: PRINT "dTB="; dTB
    LOCATE 15, 26: PRINT "BK2="; BK02
    LOCATE 17, 26: PRINT "gndTB="; gndTB
    LOCATE 18, 26: PRINT "dispX1="; dispX01
    LOCATE 19, 26: PRINT "dispX2="; dispX02
    LOCATE 20, 26: PRINT "W1 Bal.="; M01
    LOCATE 21, 26: PRINT "W2 Bal.="; M02
    LOCATE 22, 26: PRINT "0-time CNL.="; CZO

    COLOR 15
    DRAW "bm330,330"
    DRAW "c15;u250r300d250l300"
    DRAW "bm330,280;c7;r300"
    DRAW "bm330,230;c7;r300"
    DRAW "bm330,180;c7;r300"
    DRAW "bm330,130;c7;r300"
    DRAW "bm390,330;c7;u250"
    DRAW "bm450,330;c7;u250"
    DRAW "bm510,330;c7;u250"
    DRAW "bm570,330;c7;u250"

    mt = 300 / (xmaxw - xminw)
    multiy = 250 / (ymaxw - yminw)
    rfx = 330
    rfy = 330 + yminw * multiy
    PSET (rfx, rfy), 2: DRAW "r300"
    FOR i = xminw TO xmaxw
    T = 330 + (i - xminw) * mt
    IF q01(i) < yminw THEN GOTO 1303
    IF q01(i) > ymaxw THEN GOTO 1303
    y1 = 330 - (q01(i) - yminw) * multiy
    PSET (T, y1), 3
1303 NEXT i
    FOR i = xminw TO xmaxw
    T = 330 + (i - xminw) * mt
    IF q02(i) < yminw THEN GOTO 1304
    IF q02(i) > ymaxw THEN GOTO 1304
    y2 = 330 - (q02(i) - yminw) * multiy
    PSET (T, y2), 4
1304 NEXT i
REM═══════════ CONTROL OF CURSOR ═══════════
    LOCATE 1, 41: PRINT "<l/L><r/R>.. cursor move/<A> .....recall"
    LOCATE 2, 41: PRINT "<1/2/B><Y><D><d/g/C/T>.... BC/dTB/gndTB"
    LOCATE 3, 41: PRINT "<X/W/I>.. PP align/Windo Bal./Initialize"
    LOCATE 4, 41: PRINT "<S/N/Z>... reScale /<0/f/F>. Ct0/finish"
    RETURN
1307 T = 330 + (i - xminw) * mt
```

```
    y1 = 330 - (q01(i) - yminw) * multiy
    y2 = 330 - (q02(i) - yminw) * multiy
    RETURN
1310 LOCATE 1, 41: PRINT "<l/L><r/R>.. cursor move "
    LOCATE 2, 41: PRINT "<1/2/B><Y><D><d/g/C/T>.... BC/dTB/gndTB"
    LOCATE 3, 41: PRINT "<X/W/I>.. PP align/Windo Bal./Initialize"
    LOCATE 4, 41: PRINT "<S/N/Z>... reScale /<F>. Ct0/finish"
    PRINT "                              "
1313 i = 50
    GOSUB 1307
    PSET (T, y1), 15
    PSET (T, y2), 15

1314 K$ = INKEY$
    LOCATE 16, 1: PRINT "Channel ="; i
    COLOR 3: PRINT q01(i); "       "
    COLOR 4: PRINT q02(i); "       "
    COLOR 1: PRINT q01(i) - q02(i); "     "
    COLOR 15
    IF K$ = "F" THEN GOTO 1475
    IF K$ = "r" THEN GOTO 1315
    IF K$ = "l" THEN GOTO 1315
    IF K$ = "R" THEN GOTO 1315
    IF K$ = "L" THEN GOTO 1315 ELSE GOTO 1316


1315 GOSUB 1307
    PSET (T, y1), 3: PSET (T, y2), 4
    IF K$ = "r" THEN i = i + 1: GOSUB 1307
    IF K$ = "l" THEN i = i - 1: GOSUB 1307
    IF K$ = "R" THEN i = i + 10: GOSUB 1307
    IF K$ = "L" THEN i = i - 10: GOSUB 1307
    PSET (T, y1), 15: PSET (T, y2), 15
    GOTO 1314
1316 IF K$ = "1" THEN BK1 = q01(i) ELSE GOTO 13164
    LOCATE 14, 26: COLOR 7: PRINT "BK1="; BK1
    COLOR 15
    GOTO 1314
13164  IF K$ = "d" THEN dTB = ABS(q01(i) - q02(i)) ELSE GOTO 1317
    XX = i
    IF q01(XX) > q02(XX) THEN B = 1
    IF q01(XX) < q02(XX) THEN B = 2
    LOCATE 16, 26: COLOR 7: PRINT "dTB="; dTB
    FOR i = 1 TO 512
    Iq01(i) = q01(i): Iq02(i) = q02(i)
    NEXT i
    FOR j = 1 TO 512
    IF B = 1 THEN q01(j) = q01(j) - dTB
    IF B = 2 THEN q02(j) = q02(j) - dTB
    NEXT j
    COLOR 15: CLS : GOSUB 1302
13165 SOUND 3000, 5: LOCATE 1, 1: INPUT "Need Retry   (y/n)   ", ReT$
    LOCATE 1, 1: PRINT "                                  "
    IF ReT$ = "y" THEN GOTO 13167
    IF ReT$ = "n" THEN B = 0: GOTO 1310
    GOTO 13165
13167 FOR i = 1 TO 512
```

```
    q01(i) = Iq01(i): q02(i) = Iq02(i)
    NEXT i
    dTB = 0: CLS
    GOSUB 1302
    GOTO 1310
1317 IF K$ = "2" THEN BK2 = q02(i) ELSE GOTO 13174
    LOCATE 15, 26: COLOR 7: PRINT "BK2="; BK2
    COLOR 15
    GOTO 1314
13174 IF K$ = "g" THEN GOTO 13176 ELSE GOTO 13178
13176 IF q01(i) >= q02(i) THEN gndTB = q02(i): BIG = 1
    IF q01(i) <= q02(i) THEN gndTB = q01(i): BIG = 2
    LOCATE 17, 26: COLOR 7: PRINT "gndTB="; gndTB
    COLOR 15
    GOTO 1314

13178 IF K$ = "I" THEN CLS  ELSE GOTO 1318
    GOSUB 4010
    GOTO 1003
1318 IF K$ = "B" THEN sta1 = 1 ELSE GOTO 13182
    FOR i = 1 TO 512
    q01(i) = q01(i) - BK1
    q02(i) = q02(i) - BK2
    NEXT i
    BK01 = BK01 + BK1
    BK02 = BK02 + BK2
    CLS
    GOSUB 1302
    GOTO 1310
13182 IF K$ = "C" THEN sta5 = 1 ELSE GOTO 13184
    FOR i = 1 TO 512
    Iq01(i) = q01(i): Iq02(i) = q02(i)
    NEXT i
    FOR i = 1 TO 512
    IF BIG = 1 THEN q01(i) = q01(i) - (dTB / (Xdi - 25) * i)
    IF BIG = 2 THEN q02(i) = q02(i) - (dTB / (Xdi - 25) * i)
    NEXT i
    CLS
    GOSUB 1302
    GOTO 13185

13184 IF K$ = "T" THEN sta5 = 1 ELSE GOTO 1319
131844 LOCATE 2, 1: INPUT "Enter decay time (in chnn.) ", T200
    IF T200 = 0 THEN GOTO 131844
131845 LOCATE 3, 1: INPUT "Enter reflection channel (>512) ", Tnc
    IF Tnc = 0 THEN GOTO 131845
    FOR i = 1 TO 512
    Iq01(i) = q01(i): Iq02(i) = q02(i)
    NEXT i
    FOR i = 1 TO 512
    'IF BIG = 1 THEN q01(i) = q01(i) - (dTB / 200 * i)
    'IF BIG = 2 THEN q02(i) = q02(i) - (dTB / 200 * i)
    IF BIG = 1 THEN q01(i) = q01(i) - (dTB * EXP((i - Tnc) / T200))
    IF BIG = 2 THEN q02(i) = q02(i) - (dTB * EXP((i - Tnc) / T200))

    NEXT i
    CLS
```

```
    GOSUB 1302
13185 SOUND 3000, 5: LOCATE 1, 1: INPUT "Need Retry   (y/n)   ", ReT$
    LOCATE 1, 1: PRINT "                                    "
    IF ReT$ = "y" THEN GOTO 13186
    IF ReT$ = "n" THEN GOTO 1310
    GOTO 13185
13186 FOR i = 1 TO 512
   q01(i) = Iq01(i): q02(i) = Iq02(i)
    NEXT i
    dTB = 0
    gndTB = 0
    sta5 = 0
     CLS
    GOSUB 1302
    GOTO 1310
1319 IF K$ = "s" THEN LOCATE 1, 1 ELSE GOTO 1320
    FOR i = 1 TO 512
   q01(i) = q100(i)
   q02(i) = q200(i)
    NEXT i
    GOTO 1003
1320 '═══════════ RESCALE X & Y ═══════════'
    IF K$ = "S" THEN LOCATE 1, 1 ELSE GOTO 13205
    INPUT "Enter Xmin  ", xminw
    INPUT "Enter Xmax  ", xmaxw
    INPUT "Enter Ymin  ", yminw
    INPUT "Enter Ymax  ", ymaxw
    CLS : GOSUB 1302
    GOTO 1310
13205 '═══════════ RESCALE Y ONLY ═══════════'
    IF K$ = "Z" THEN LOCATE 1, 1 ELSE GOTO 1321
    'xminw = 0
    'xmaxw = 512
    LOCATE 3, 1: INPUT "enter yminw =", yminw
    LOCATE 4, 1: INPUT "enter ymaxw =", ymaxw
    CLS : GOSUB 1302
    GOTO 1310
1321 '═══════════ PRESET SCALE ═══════════'
    IF K$ = "N" THEN LOCATE 1, 1 ELSE GOTO 1322
    xminw = 1
    xmaxw = 512
    yminw = -3000
    ymaxw = 100000
    CLS : GOSUB 1302
    GOTO 1310
REM ═══════ PRE-PULSE ALIGNMENT ═══════
1322 IF K$ = "X" THEN sta2 = 1 ELSE GOTO 1326
1323 LOCATE 1, 1: INPUT "Window (0,1,2)  ", Wind$
    LOCATE 1, 1: PRINT "                                    "
    IF Wind$ = "0" THEN GOTO 1310
   Wind = VAL(Wind$)
    LOCATE 1, 1: INPUT "Enter step ", dispX
    LOCATE 1, 1: PRINT "                                    "
    FOR i = 1 TO 512
   Iq01(i) = q01(i)
   Iq02(i) = q02(i)
    NEXT i
```

```
    'IF Wind = 1 THEN dispX1 = VAL(dispX$): GOSUB 1324: dispX01 = dispX01 + dispX1
    'IF Wind = 2 THEN dispX2 = VAL(dispX$): GOSUB 1325: dispX02 = dispX02 + dispX2
    IF Wind = 1 THEN dispX1 = dispX: GOSUB 1324: dispX01 = dispX01 + dispX1
    IF Wind = 2 THEN dispX2 = dispX: GOSUB 1325: dispX02 = dispX02 + dispX2

     CLS
     GOSUB 1302
     GOTO 1323
1324 'IF dispX1 > 0 THEN GOTO 13242
     'IF dispX1 < 0 THEN GOTO 13244
     GOTO 13242
13242 FOR i = 1 TO 512
     IF i + dispX1 > 512 THEN RETURN
     IF i + dispX1 < 1 THEN GOTO 13243
    q01(i) = Iq01(i + dispX1)
13243 NEXT i
     RETURN
13244 FOR i = 1 TO 512
     IF i - dispX1 > 512 THEN RETURN
     IF i - dispX1 < 1 THEN GOTO 13245
    q01(i) = Iq01(i - dispX1)
13245 NEXT i
     RETURN
1325 'IF dispX2 > 0 THEN GOTO 13252
     'IF dispX2 < 0 THEN GOTO 13254
     GOTO 13252
13252 FOR i = 1 TO 512
     IF i + dispX2 > 512 THEN RETURN
     IF i + dispX2 < 1 THEN GOTO 13253
    q02(i) = Iq02(i + dispX2)
13253 NEXT i
     RETURN
13254 FOR i = 1 TO 512
     IF i - dispX2 > 512 THEN RETURN
     IF i - dispX2 < 1 THEN GOTO 13255
    q02(i) = Iq02(i - dispX2)
13255 NEXT i
     RETURN
REM ═══════════ WINDOW BALANCE ═══════════
1326 IF K$ = "W" THEN sta3 = 1 ELSE GOTO 1328
1327 LOCATE 1, 1: INPUT "Window to balance (0,1,2) ", Wi$
    Wi = VAL(Wi$)
     LOCATE 1, 1: PRINT "                                    "
     IF Wi$ = "0" THEN GOTO 1310
     LOCATE 1, 1: INPUT "Enter window balance  (0-5) ", M$
     LOCATE 1, 1: PRINT "                                    "

     FOR i = 1 TO 512
     IF Wi$ = "1" THEN M1 = VAL(M$): q01(i) = q01(i) * M1
     IF Wi$ = "2" THEN M2 = VAL(M$): q02(i) = q02(i) * M2
     NEXT i
     IF Wi$ = "1" THEN M01 = M01 * M1
     IF Wi$ = "2" THEN M02 = M02 * M2
     CLS
     GOSUB 1302
     GOTO 1327
1328 IF K$ = "0" THEN CZO = i ELSE GOTO 1329
```

```
    sta4 = 1
    W = 330 + (i - xminw) * mt
    z = 330
    PSET (W, z)
    DRAW "c1;u250"
    LOCATE 22, 26: COLOR 7: PRINT "0-time CNL.="; CZO
    LOCATE 5, 57: PRINT sta4
    COLOR 15
    GOTO 1314
1329 IF K$ = "f" THEN GOTO 13295 ELSE GOTO 1335
13295 BK1 = BK10
   BK2 = BK20
   'dispX = dispX0
   'M = M0
   RETURN
REM ========== RESTART ==========
1335 IF K$ = "F" THEN GOTO 1470 ELSE GOTO 1338
1338 IF K$ = "A" THEN GOSUB 1344 ELSE GOTO 1339
1339 IF K$ = "Y" THEN GOSUB 13395 ELSE GOTO 13391
   GOTO 1313
13391 IF K$ = "D" THEN GOSUB 13397 ELSE GOTO 1314
   GOTO 1313
13395 Xi = i
    Yshift = ABS(q01(i) - q02(i))
    IF q01(Xi) >= q02(Xi) THEN Lg = 1
    IF q02(Xi) >= q01(Xi) THEN Lg = 2
     FOR i = 1 TO 512
    Iq01(i) = q01(i): Iq02(i) = q02(i)
     NEXT i
     FOR i = 1 TO nd
    IF Lg = 1 THEN q01(i) = q01(i) - Yshift
    IF Lg = 2 THEN q02(i) = q02(i) - Yshift
     NEXT i
     CLS
     GOSUB 1302
     GOTO 13185
     RETURN
13397 LOCATE 1, 1: INPUT "Enter Gapwidth  ", Gwth
    LOCATE 2, 1: INPUT "Enter decay time ( in chnn.) ", T200
    LOCATE 3, 1: INPUT "Enter reflection channel (>512) ", Tnc
    LOCATE 4, 1: INPUT "Enter which to correct   ", BIG
    'Xgw = i
    'IF q01(Xgw) >= q02(Xgw) THEN Lg = 1
    'IF q02(Xgw) >= q01(Xgw) THEN Lg = 2
     FOR i = 1 TO 512
    Iq01(i) = q01(i): Iq02(i) = q02(i)
     NEXT i
     FOR i = 1 TO nd
    'IF Lg = 1 THEN q01(i) = q01(i) - Gwth * i / 512
    'IF Lg = 2 THEN q02(i) = q02(i) - Gwth * i / 512
    IF BIG = 1 THEN q01(i) = q01(i) - (Gwth * EXP((i - Tnc) / T200))
    IF BIG = 2 THEN q02(i) = q02(i) - (Gwth * EXP((i - Tnc) / T200))
     NEXT i
     CLS
     GOSUB 1302
     GOTO 13185
     RETURN
```

```
REM ========== FUNCTION STATEMENT ==========
1100 LOCATE 8, 1: COLOR 15
    PRINT "Save 4D ..... 1     / Save 1D ..... 2"
    PRINT "Rescale Y .....3    / Data reading .... 4"
    PRINT "Calibration .. 5    / Smooth ..... 6"
    PRINT "Enlarge 123 .. 7    / See next ..... 8"
    PRINT "                                    "
    PRINT "                                    "
1200 LOCATE 13, 1
    INPUT "Selection    ", S
    IF S = 1 THEN GOSUB 1400  'Save 4D curve          '
    IF S = 2 THEN GOSUB 1340  'Save 1D curve          '
    IF S = 3 THEN GOSUB 1415  'Rescale Y              '
    IF S = 4 THEN GOSUB 1420  'Data reading           '
    IF S = 5 THEN GOTO 1010   'Calibration            '
    IF S = 6 THEN GOSUB 1345  'Smooth                 '
    IF S = 7 THEN GOSUB 1390  'Curve enlarement      '
    IF S = 8 THEN GOSUB 1470  "next step              '
    'LOCATE 16, 1: PRINT "                            "
    GOTO 1100
1330 FOR L = 8 TO 14
    LOCATE L, 1
    PRINT "                                  "
    NEXT L
1340 DIM Ix(260), Iy(260), Iz(260)
1341 INPUT "Which Curve to Save ? (1,2,3) ", SavC
    LOCATE 14, 1: PRINT "                                "
    IF SavC = CvNud THEN GOTO 1343
    LOCATE 14, 1: INPUT "Which Curve to Save ? (1,2,3) ", SavC
    SOUND 3000, 5: LOCATE 14, 1
1343 FOR i = 1 TO 512
    IF SavC = 1 THEN Ix(i) = x(i)
    IF SavC = 2 THEN Iy(i) = y(i)
    IF SavC = 3 THEN Iz(i) = z(i)
    NEXT i
    SMD = 1
    RETURN
1344 LOCATE 14, 1: PRINT "                                "
    FOR i = 1 TO 512
    IF SavC = 1 THEN x(i) = Ix(i)
    IF SavC = 2 THEN y(i) = Iy(i)
    IF SavC = 3 THEN z(i) = Iz(i)
    NEXT i
    CLS
    GOSUB 2000
    GOSUB 2500
    RETURN
1345 DIM i(260)
    LOCATE 14, 1: INPUT "Which Curve? (1,2,3) ", SmothCv
    LOCATE 15, 1: INPUT "3, 5, 7pt.  (3,5,7)  ", SmothPt
    FOR i = 1 TO 512
    IF SmothCv = 1 THEN i(i) = x(i)
    IF SmothCv = 2 THEN i(i) = y(i)
    IF SmothCv = 3 THEN i(i) = z(i)
    NEXT
    IF SmothPt = 3 THEN GOSUB 13457
    IF SmothPt = 5 THEN GOSUB 13458
```

```
    IF SmothPt = 7 THEN GOSUB 13459
    SMOTH = 1
    GOSUB 2000
    GOSUB 2500
    SOUND 3000, 2: LOCATE 14, 1: INPUT "Accept smoothed (pass=n) ", AcpSmoth$
    IF AcpSmoth$ = "y" THEN RETURN
    FOR i = 1 TO 512
    IF SmothCv = 1 THEN x(i) = i(i)
    IF SmothCv = 2 THEN y(i) = i(i)
    IF SmothCv = 3 THEN z(i) = i(i)
    NEXT
    GOSUB 2000
    GOSUB 2500
    RETURN
13457 FOR i = 2 TO 511
    IF SmothCv = 1 THEN x(i) = (i(i - 1) + i(i) + i(i + 1)) / 3
    IF SmothCv = 2 THEN y(i) = (i(i - 1) + i(i) + i(i + 1)) / 3
    IF SmothCv = 3 THEN z(i) = (i(i - 1) + i(i) + i(i + 1)) / 3
    NEXT
    RETURN
13458 FOR i = 3 TO 510
    IF SmothCv = 1 THEN x(i) = (i(i - 2) + i(i - 1) + i(i) + i(i + 1) + i(i + 2)) / 5
    IF SmothCv = 2 THEN y(i) = (i(i - 2) + i(i - 1) + i(i) + i(i + 1) + i(i + 2)) / 5
    IF SmothCv = 3 THEN z(i) = (i(i - 2) + i(i - 1) + i(i) + i(i + 1) + i(i + 2)) / 5
    NEXT
    RETURN
13459 FOR i = 4 TO 509
IF SmothCv = 1 THEN x(i) = (i(i - 3) + i(i - 2) + i(i - 1) + i(i) + i(i + 1) + i(i + 2) + i(i + 3)) / 7
IF SmothCv = 2 THEN y(i) = (i(i - 3) + i(i - 2) + i(i - 1) + i(i) + i(i + 1) + i(i + 2) + i(i + 3)) / 7 IF
SmothCv = 3 THEN z(i) = (i(i - 3) + i(i - 2) + i(i - 1) + i(i) + i(i + 1) + i(i + 2) + i(i + 3)) / 7
    NEXT
    RETURN
1350 INPUT "Which window ? (1-w1, 2-w2, 3-both)  ", windo
    INPUT "How many times (1-10)  ", EBWIN
    CLS
    GOSUB 1700
    GOSUB 2500
    RETURN
1360 FOR L = 1 TO 8
    LOCATE L, 1
    PRINT "                                        "
    NEXT L
    RETURN
1390 LOCATE 14, 1:
    INPUT "Enter Curve Number (1,2,3) ", CNB
    LOCATE 14, 1:
    INPUT "Enter Upper/ Lower Limit   ", ult, llt
    DRAW "bm380,330;"
    mz1 = 110 / (ult - llt)
1393 FOR i = 1 TO nd
    T = 380 + i * mt
    IF CNB = 1 THEN P(i) = x(i)
    IF CNB = 2 THEN P(i) = y(i)
    IF CNB = 3 THEN P(i) = z(i)
    IF P(i) > ult THEN GOTO 1395
    IF P(i) < llt THEN GOTO 1395
    P = 110 * CNB - (P(i) - llt) * mz1
```

```
    t0 = 380
    td = 380 + nd * mt
    p0 = 110 * CNB + llt * mz1
    PSET (T, P), 11
1395 NEXT i
    PSET (t0, p0): DRAW "c4;r220;"
    LOCATE 15, 1
    INPUT "Erase Enlarged P ? (default=n)  ", ee$
    LOCATE 15, 1
    PRINT "                                "
    IF ee$ = "y" THEN GOTO 1397 ELSE RETURN

1397 LOCATE 14, 1
    PRINT "                                "
    FOR i = 1 TO nd
    T = 380 + i * mt
    IF P(i) > ult THEN GOTO 1398
    IF P(i) < llt THEN GOTO 1398
    P = 110 * CNB - (P(i) - llt) * mz1
    t0 = 380
    td = 380 + nd * mt
    p0 = 110 * CNB + llt * mz1
    PSET (T, P), 0
1398 NEXT i
    PSET (t0, p0): DRAW "c0;r220;"
    GOSUB 2500
    RETURN

1400 LOCATE 16, 19: INPUT "Streak rate  (1,6 or 0)  ", rat
    IF rat = 1 THEN T = 1.147
    'IF Rat = 2 THEN T = 1.5
    'IF Rat = 3 THEN T = 2.35
    'IF Rat = 4 THEN T = 3.2
    IF rat = 6 THEN T = 1
    IF rat = 0 THEN LOCATE 18, 19: PRINT "Cancel Saving  !!": RETURN

1403 LOCATE 18, 19: PRINT "Filename? (ok=default,x) "
    LOCATE 20, 19: FILES$ = "c:" + FILE$ + ".TRA": PRINT FILES$
    LOCATE 19, 19: INPUT SF$
    IF SF$ = "x" THEN LOCATE 18, 19: PRINT "Exit !!": RETURN
    IF LEN(SF$) = 0 THEN GOTO 1405 ELSE FILE$ = SF$          'PC in 203   '
    LOCATE 18, 19: PRINT "STORING !!              "
REM ═══════════════════ DATA STORING ═══════════════════
1405 FILES$ = "c:" + FILE$ + ".TRA"
    FILEFIN$ = "c:" + FILE$ + ".FIN"
1406 OPEN FILES$ FOR OUTPUT AS #2
    OPEN FILEFIN$ FOR OUTPUT AS #1
    FOR i = 1 TO nd
    stk = (i - CZO) * T
    PRINT #1, stk; "       "; q1(i); "       "; q2(i); "       "; x(i); "       "; y(i); "       "; z(i); "       ";
z(i) * -1

'IF i = 1 THEN PRINT #2, stk; "       "; q1(i); "       "; q2(i); "       "; x(i); "       "; y(i); "       ";
z(i); "       "; z(i) * -1; "       "; M01; "       "; M02; "       "; BK1; "       "; BK2; "       ";
dispX01; "       "; dispX02
    'IF i > 1 THEN PRINT #2, stk; "       "; q1(i); "       "; q2(i); "       "; x(i); "       "; y(i); "
"; z(i); "       "; z(i) * -1
```

```
    IF i = 1 THEN PRINT #2, stk, q1(i), q2(i), x(i), y(i), z(i), -z(i), M01, M02, BK01, BK02,
dispX01, dispX02
    'IF i = 1 THEN PRINT #2, stk, q1(i), q2(i), x(i), y(i), z(i), -z(i), WB1, WB2, BK1, BK2, dispX1,
dispX2
    IF i > 1 THEN PRINT #2, stk, q1(i), q2(i), x(i), y(i), z(i), -z(i)
    NEXT i
    SOUND 2000, 20: LOCATE 18, 19: PRINT "Data saved in          ": STORE = 100
    LOCATE 19, 19: COLOR 12: PRINT FILES$; " & .FIN"
    IF ans0$ = "n" THEN GOTO 1413
    LPRINT "General results have saved in "; FILES$; " & "; FILEFIN$; "   "; DATE$; "   "; TIME$
    LPRINT BIG; "   Tail Difference="; dTB; "   Ground level="; gndTB
    LPRINT "Streak Rate="; rat; "   WB1="; M01; "   WB2="; M02; "   BK1="; BK01; "   BK2=";
BK02
    LPRINT "dispX1="; dispX01; "   dispX2="; dispX02; "   Zero-time="; CZO; "   Streak rate="; rat
    LPRINT "    "
1413 CLOSE
    RETURN
1415 LOCATE 13, 1:
    INPUT "Selection (1-top, 2-mid, 3-low, 4, 5, 0)  ", RsclCv
    LOCATE 13, 1: PRINT "                                          "
    IF RsclCv = 0 THEN RETURN
    Rscl = 1
    COLOR 11
    LOCATE 23, 39: PRINT RsclCv
    COLOR 15
    LOCATE 16, 19: INPUT "Ymin=", NuYmin
    LOCATE 17, 19: INPUT "Ymax=", NuYmax
    IF RsclCv = 1 THEN xmin = NuYmin: xmax = NuYmax
    IF RsclCv = 2 THEN ymin = NuYmin: ymax = NuYmax
    IF RsclCv = 3 THEN zmin = NuYmin: zmax = NuYmax
    GOSUB 2000
    GOSUB 2500
    RETURN

REM ======= CURSOR MOVEMENT FOR CALCULATED DATA =======
1420 LOCATE 8, 1
    PRINT "<l/L>.. left shift   /<r/R>.. right shift "
    PRINT "<a/b>... start/end   "
    PRINT "<p>..... print peak  /<z/Z>.. zoomed/zero "
    PRINT "<D>... Drawing Curve /<f>..... finish "
    PRINT "                                          "
    PRINT "                                          "
1422 LOCATE 13, 1:
    INPUT "Selection (1-top, 2-mid, 3-low, 4, 5, 0)  ", CC
    LOCATE 13, 1: PRINT "                                          "
    IF CC = 0 THEN RETURN
    COLOR 11
    LOCATE 23, 39: PRINT CC
    COLOR 15
1425 i = 50
    GOSUB 1450
    IF u1 > 0 THEN IF u1 < 110 THEN PSET (T, u1)
    IF u2 > 110 THEN IF u2 < 220 THEN PSET (T, u2)
    IF u3 > 220 THEN IF u3 < 330 THEN PSET (T, u3)
    IF y1 > 0 THEN IF y1 < 110 THEN PSET (T, y1), 14
    IF y2 > 0 THEN IF y2 < 110 THEN PSET (T, y2), 14
```

```
1430 K$ = INKEY$
   LOCATE 16, 1: PRINT "Channel ="; i
   PRINT "+ "; x(i); "   "
   PRINT "- "; y(i); "   "
   PRINT "/ "; z(i); "   "
   PRINT "1 "; q1(i); "   "
   PRINT "2 "; q2(i); "   "

1431 IF K$ = "r" THEN GOSUB 1450 ELSE GOTO 1432
   IF u1 > 0 THEN IF u1 < 110 THEN PSET (T, u1), 13
   IF u2 > 110 THEN IF u2 < 220 THEN PSET (T, u2), 13
   IF u3 > 220 THEN IF u3 < 330 THEN PSET (T, u3), 13
   IF y1 > 0 THEN IF y1 < 110 THEN PSET (T, y1), 3
   IF y2 > 0 THEN IF y2 < 110 THEN PSET (T, y2), 4
   i = i + 1: GOSUB 1450
   IF u1 > 0 THEN IF u1 < 110 THEN PSET (T, u1)
   IF u2 > 110 THEN IF u2 < 220 THEN PSET (T, u2)
   IF u3 > 220 THEN IF u3 < 330 THEN PSET (T, u3)
   IF y1 > 0 THEN IF y1 < 110 THEN PSET (T, y1), 14
   IF y2 > 0 THEN IF y2 < 110 THEN PSET (T, y2), 14
   GOTO 1430
1432 IF K$ = "l" THEN GOSUB 1450 ELSE GOTO 1433
   IF u1 > 0 THEN IF u1 < 110 THEN PSET (T, u1), 13
   IF u2 > 110 THEN IF u2 < 220 THEN PSET (T, u2), 13
   IF u3 > 220 THEN IF u3 < 330 THEN PSET (T, u3), 13
   IF y1 > 0 THEN IF y1 < 110 THEN PSET (T, y1), 3
   IF y2 > 0 THEN IF y2 < 110 THEN PSET (T, y2), 4
   i = i - 1: GOSUB 1450
   IF u1 > 0 THEN IF u1 < 110 THEN PSET (T, u1)
   IF u2 > 110 THEN IF u2 < 220 THEN PSET (T, u2)
   IF u3 > 220 THEN IF u3 < 330 THEN PSET (T, u3)
   IF y1 > 0 THEN IF y1 < 110 THEN PSET (T, y1), 14
   IF y2 > 0 THEN IF y2 < 110 THEN PSET (T, y2), 14
   GOTO 1430
1433 IF K$ = "a" THEN GOSUB 1450 ELSE GOTO 1434
   SC = i: MGL = 1
   PSET (T, 330): DRAW "c10;u330;"
   COLOR 11
   LOCATE 22, 1: PRINT "Left Margin ="; SC
   COLOR 15
   GOTO 1430
1434 IF K$ = "b" THEN GOSUB 1450 ELSE GOTO 1435
   EC = i: MGR = 1
   PSET (T, 330): DRAW "c10;u330;"
   COLOR 11
   LOCATE 23, 1: PRINT "Right Margin ="; EC
   COLOR 15
   GOTO 1430
1435 IF K$ = "z" THEN GOSUB 1460 ELSE GOTO 1436
   GOTO 1430
1436 IF K$ = "R" THEN GOSUB 1450 ELSE GOTO 1437
   IF u1 > 0 THEN IF u1 < 110 THEN PSET (T, u1), 13
   IF u2 > 110 THEN IF u2 < 220 THEN PSET (T, u2), 13
   IF u3 > 220 THEN IF u3 < 330 THEN PSET (T, u3), 13
   IF y1 > 0 THEN IF y1 < 110 THEN PSET (T, y1), 3
   IF y2 > 0 THEN IF y2 < 110 THEN PSET (T, y2), 4
   i = i + 10: GOSUB 1450
```

```
   IF u1 > 0 THEN IF u1 < 110 THEN PSET (T, u1)
   IF u2 > 110 THEN IF u2 < 220 THEN PSET (T, u2)
   IF u3 > 220 THEN IF u3 < 330 THEN PSET (T, u3)
   IF y1 > 0 THEN IF y1 < 110 THEN PSET (T, y1), 14
   IF y2 > 0 THEN IF y2 < 110 THEN PSET (T, y2), 14
   GOTO 1430
1437 IF K$ = "L" THEN GOSUB 1450 ELSE GOTO 1438
   IF u1 > 0 THEN IF u1 < 110 THEN PSET (T, u1), 13
   IF u2 > 110 THEN IF u2 < 220 THEN PSET (T, u2), 13
   IF u3 > 220 THEN IF u3 < 330 THEN PSET (T, u3), 13
   IF y1 > 0 THEN IF y1 < 110 THEN PSET (T, y1), 3
   IF y2 > 0 THEN IF y2 < 110 THEN PSET (T, y2), 4
   i = i - 10: GOSUB 1450
   IF u1 > 0 THEN IF u1 < 110 THEN PSET (T, u1)
   IF u2 > 110 THEN IF u2 < 220 THEN PSET (T, u2)
   IF u3 > 220 THEN IF u3 < 330 THEN PSET (T, u3)
   IF y1 > 0 THEN IF y1 < 110 THEN PSET (T, y1), 14
   IF y2 > 0 THEN IF y2 < 110 THEN PSET (T, y2), 14
   GOTO 1430

1438 IF K$ = "Z" THEN GOSUB 1500 ELSE GOTO 1439
   GOTO 1430
1439 IF K$ = "u" THEN SOUND 4000, 2 ELSE GOTO 1440
   IF CC = 1 THEN ConstA = x(i)
   IF CC = 2 THEN ConstB = y(i)
   IF CC = 3 THEN ConstC = z(i)
   CvNud = CC
14392 GOSUB 1450
14395 GOTO 1430

1440 IF K$ = "p" THEN GOTO 1442 ELSE GOTO 1443
1442 IF ans0$ = "n" THEN GOTO 14423
   LPRINT FILE$
   IF CC = 1 THEN LPRINT CC; "  Channel="; i; "  Peak Int.="; x(i)
   IF CC = 2 THEN LPRINT CC; "  Channel="; i; "  Peak Int.="; y(i)
   IF CC = 3 THEN LPRINT CC; "  Channel="; i; "  Peak Int.="; z(i)
14423 GOTO 1430
1443 IF K$ = "D" THEN GOTO 1444 ELSE GOTO 1448
1444 GOTO 1430
1445 CLOSE 1
   GOTO 1420
1448 IF K$ = "f" THEN RETURN
   GOTO 1430
1450 T = 380 + i * mt
   u1 = 110 - (x(i) - xmin) * mx
   u2 = 220 - (y(i) - ymin) * my
   u3 = 330 - (z(i) - zmin) * mz
   y1 = 110 - q1(i) * mwn1
   y2 = 110 - q2(i) * mwn2
   IF CC = 1 THEN u = u1: q(i) = x(i): RETURN
   IF CC = 2 THEN u = u2: q(i) = y(i): RETURN
   IF CC = 3 THEN u = u3: q(i) = z(i): RETURN
   IF CC = 4 THEN u = y1: q(i) = q1(i): RETURN
   IF CC = 5 THEN u = y2: q(i) = q2(i): RETURN

1460 'FOR l = 10 TO 20
   'LOCATE l, 1: PRINT "                                    "
```

```
    'next l
    IF MGL + MGR < 2 THEN PRINT "Incomplete region ": GOTO 1430
    FOR i = SC TO EC
    GOSUB 1450
    PSET (T, u), 14
    NEXT i
    GOSUB 1490
    LOCATE 15, 1: INPUT "Region O.K. ?    ", A$
    LOCATE 15, 1: PRINT "                  "
    IF A$ = "n" THEN GOSUB 1480 ELSE GOTO 1463
    DRAW "bm160,330;"
    FOR L = 1 TO 219
    DRAW "c0;nu110;bm+1,+0;"
    NEXT L
    DRAW "bm380,330;c15"
    DRAW "u110l220d110r220"
    GOTO 1425

1463 ROK = 1
    RETURN

1470 IF STORE = 0 THEN SOUND 4000, 2 ELSE GOTO 1475
    INPUT "Do you want to store data ? (y/n) ", ST$
    IF ST$ = "y" THEN GOSUB 1400: GOSUB 1403: GOTO 1475
    IF ST$ = "n" THEN GOTO 1475
1475 CLS
    PRINT "Last File was  "; FILE$
    CLEAR : GOTO 1000

1480 FOR i = SC TO EC
    GOSUB 1450
    PSET (T, u), 13
    NEXT i
    MGR = 0: MGL = 0
    RETURN
1490 wmin = 1000000: wmax = -1000000
    FOR i = SC TO EC
    IF q(i) > wmax THEN wmax = q(i)
    IF q(i) < wmin THEN wmin = q(i)
    NEXT i
    wmin1 = wmin: wmax1 = wmax
    LOCATE 7, 1: PRINT "WMIN = "; wmin1
    LOCATE 7, 25: PRINT " /WMAX = "; wmax1
    wmin = wmin1 - (wmax1 - wmin1) / 10
    wmax = wmax1 + (wmax1 - wmin1) / 10
    mw = 110 / (wmax - wmin)
    DRAW "bm380,330;c15"
    DRAW "u110l220d110r220"
    mt2 = 220 / (EC - SC)
    FOR i = SC TO EC
    T = 160 + (i - SC) * mt2
    d = 330 - (q(i) - wmin) * mw
    PSET (T, d), 14
    NEXT i
    t0 = 380: td = 380 + nd * mt
    w0 = 330 + wmin * mw
    PSET (t0, w0): DRAW "c2;l220;"
```

```
    RETURN

1500 CZO = i
    T = 380 + i * mt
    PSET (T, 330), 1
    DRAW "c1;u330;"
    LOCATE 4, 30: PRINT "/CZO="; CZO
    RETURN

1600 'xminw = 0
    'xmaxw = 512
    'yminw = -3000
    'ymaxw = 500000
    mt = 220 / 512
    IF windo = 3 THEN mwn1 = 110 / (ymaxw - yminw) * EBWIN: mwn2 = mwn1
    IF windo = 1 THEN mwn1 = 110 / (ymaxw - yminw) * EBWIN: mwn2 = 110 / (ymaxw - yminw)
    IF windo = 2 THEN mwn1 = 110 / (ymaxw - yminw): mwn2 = 110 / (ymaxw - yminw) * EBWIN
    LOCATE 1, 65: COLOR 3: PRINT "W1"
    LOCATE 1, 70: COLOR 4: PRINT "W2"
    COLOR 15
    FOR i = 1 TO 512
    T = 380 + i * mt
    'y1 = 110 - q1(i) * mwn1
    'y2 = 110 - q2(i) * mwn2
    y1 = 110 - q1(i) * mwn1
    y2 = 110 - q2(i) * mwn2
    PSET (T, y1), 3
    PSET (T, y2), 4
    NEXT i
    xT0 = 380 + CZO * mt
    yT0 = 330
    PSET (xT0, yT0)
    DRAW "c1;u330"
    RETURN

REM ========== SPIN POLARIZATION CALCULATION ==========
1700 LOCATE 5, 1
     PRINT ".....CALCULATING ....."
    xmin = 10000: xmax = -10000
    ymin = 10000: ymax = -10000
    zmin = 10000: zmax = -10000
    Xpan = 0
    Rscl = 0
    FOR i = 1 TO nd
    'LOCATE 9, 1: PRINT i
    x(i) = q1(i) + q2(i): IF x(i) = 0 THEN x(i) = .000001
    'LOCATE 10, 1: PRINT x(i)
    y(i) = q1(i) - q2(i): IF y(i) = 0 THEN y(i) = .000001
    'LOCATE 11, 1: PRINT y(i)
    z(i) = 100 * y(i) / x(i)
    IF z(i) = 0 THEN z(i) = .000001
    IF z(i) > 100 THEN z(i) = 100
    IF z(i) < -100 THEN z(i) = -100
    'LOCATE 12, 1: PRINT z(i)
    IF y(i) > ymax THEN ymax = y(i)
    IF y(i) < ymin THEN ymin = y(i)
    IF x(i) > xmax THEN xmax = x(i)
```

```
    IF x(i) < xmin THEN xmin = x(i)
    IF z(i) > zmax THEN zmax = z(i)
    IF z(i) < zmin THEN zmin = z(i)
    NEXT i
1750 GOTO 2000
2000 CLS
    GOSUB 1600
REM ========== PLOTTING PARAMETERS ==========
    LOCATE 1, 1: PRINT "File = "; FILE$
    LOCATE 1, 20: COLOR 11: PRINT Xpan
    LOCATE 1, 25: COLOR 11: PRINT Rscl
    LOCATE 1, 29: PRINT SMD; "("; SavC; ")"
    LOCATE 1, 38: PRINT SMOTH; "("; SmothC; ")"
    COLOR 15
    LOCATE 2, 1: PRINT "WB1="; M01; "  /WB2="; M02;
    LOCATE 3, 1: PRINT "BK1="; BK01; "  /BK2="; BK02;
    LOCATE 4, 1: PRINT "dispX01="; dispX01; "  /dispX02="; dispX02
    LOCATE 4, 30: PRINT "  /CZO="; CZO
    LOCATE 5, 1: PRINT "XMIN = "; xmin
    LOCATE 5, 25: PRINT " /XMAX = "; xmax
    LOCATE 6, 1: PRINT "YMIN = "; ymin
    LOCATE 6, 25: PRINT " /YMAX = "; ymax
    LOCATE 7, 1: PRINT "ZMIN = "; zmin
    LOCATE 7, 25: PRINT " /ZMAX = "; zmax
    CLOSE 2
    RETURN
2500 DRAW "bm380,330;"
    DRAW "c15;u330r220d330l220u110r220u110l220;"
    IF Xpan = 0 THEN GOSUB 2503: GOTO 2510
    IF Xpan = 1 THEN GOTO 2510
2503 xmin1 = xmin: xmax1 = xmax
    ymin1 = ymin: ymax1 = ymax
    zmin1 = zmin: zmax1 = zmax
    Xpan = 1
    RETURN
2510 xmin = xmin1 - (xmax1 - xmin1) / 10
    xmax = xmax1 + (xmax1 - xmin1) / 10
    ymin = ymin1 - (ymax1 - ymin1) / 10
    ymax = ymax1 + (ymax1 - ymin1) / 10
    zmin = zmin1 - (zmax1 - zmin1) / 10
    zmax = zmax1 + (zmax1 - zmin1) / 10
    IF Rscl = 1 THEN GOSUB 2512 ELSE GOTO 2513
    GOTO 2513
2512 IF RsclCv = 1 THEN xmin = NuYmin: xmax = NuYmax
    IF RsclCv = 2 THEN ymin = NuYmin: ymax = NuYmax
    IF RsclCv = 3 THEN zmin = NuYmin: zmax = NuYmax
    RETURN
2513 mt = 220 / 512
    mx = 110 / (xmax - xmin)
    my = 110 / (ymax - ymin)
    mz = 110 / (zmax - zmin)
    FOR i = 1 TO nd
    T = 380 + i * mt
    x = 110 - (x(i) - xmin) * mx
    IF x > 110 THEN GOTO 2520
    IF x < 0 THEN GOTO 2520
    PSET (T, x), 13
```

```
2520 y = 220 - (y(i) - ymin) * my
   IF y > 220 THEN GOTO 2540
   IF y < 110 THEN GOTO 2540
   PSET (T, y), 13
2540 z = 330 - (z(i) - zmin) * mz
   IF z > 330 THEN GOTO 2560
   IF z < 220 THEN GOTO 2560
   PSET (T, z), 13
2560 t0 = 380: td = 380 + nd * mt
   x00 = 110 + xmin * mx
   y0 = 220 + ymin * my
   z0 = 330 + zmin * mz
2600 NEXT i
   PSET (t0, x00): DRAW "c2;r220;"
   PSET (t0, y0): DRAW "c2;r220;"
   PSET (t0, z0): DRAW "c2;r220;"
   RETURN
5000 FOR L = 15 TO 21
   LOCATE L, 15
   PRINT "                              "
   NEXT L
   RETURN
   tmin = 10000000: tmax = -10000000
   IF FD = 5 THEN GOSUB 6080
6080 INPUT #2, A(C), B(C), C(C), q(C), M(C)
   IF B(C) > xmax THEN xmax = B(C)
   IF B(C) < xmin THEN xmin = B(C)
   IF C(C) > ymax THEN ymax = C(C)
   IF C(C) < ymin THEN ymin = C(C)
   IF q(C) > zmax THEN zmax = q(C)
   IF q(C) < zmin THEN zmin = q(C)
   IF M(C) > tmax THEN tmax = M(C)
   IF M(C) < tmin THEN tmin = M(C)
   RETURN
   PRINT "4.(@)  min = "; tmin; "    max = "; tmin
   IF FD = 5 THEN GOTO 6120 ELSE RETURN
6120 tmin = tmin - (tmax - tmin) / 10
   tmax = tmax + (tmax - tmin) / 10
   mt = 60 / (tmax - tmin)
   FOR i = 1 TO nd
   T = 380 + i * mt
   W = 60 - (M(i) - tmin) * mt
   t0 = 380: td = 380 + nd * mt
   w0 = 180 + tmin * mt
   PSET (T, W)
   NEXT i
   PSET (t0, y0): DRAW "l3r6l3u3d6;":PSET (td, y0): DRAW "l3r6l3u3d6;"
  RETURN
```

The following program <SPNEXFIT.BAS> fits the T.R. spin polarized data by using single exponential decaying model. ($\rho(t) = \rho(0)exp(-\frac{t}{\tau_s})$) where τ_s is the spin relaxation time constant.

```
   REM ========== THIS IS A FITTING ROUTINE ==========
    SCREEN 9
    LOCATE 2, 1
    PRINT "1. This Fitting routine recalls the stored <.tra> file from FLOPPY in B:   "; ""
    PRINT "3. The number of data points is fixed to 512                "
    PRINT "4. The fit result will be saved in C: with ext. <.FIT>    "
    PRINT "5. This is the final edition which is ready for MacPlot_Cricket"
    PRINT "6. Program will not run continuously  "
    PRINT "  "
    INPUT "Press enter to continue .....", G$
    CLS
    LOCATE 3, 1
    PRINT "************************************************************ "
    PRINT "**                                                        ** "
    PRINT "**                    SET DATE & TIME                     ** "
    PRINT "**    MAKE A SELECTION OF DRIVE FOR .fin  4000, 6404      ** "
    PRINT "**            DEFAULT = read-in <B:>  and  output <C:>    ** "
    PRINT "**                                                        ** "
    PRINT "************************************************************ "
    PRINT "  "
    INPUT "Press enter to continue .....", G$
900  CLS
    DIM q(520), q1(520), q2(520)
    DIM tm(520), x(520), y(520)
    DIM z(520), miz(520)
    DIM V(520)
    DIM stkstrin$(520)
    DIM FILE$(25)
    'DIM u(1040)
    DIM V2(520)
     PRINT "1 ..... FILES PRE-ENTERED"
    PRINT "2 ..... FILE ENTERED BY USER"
    PRINT "    "
    INPUT "Enter file arrangement selection   ", fa
    IF fa = 2 THEN GOTO 1000 ELSE GOTO 9000
    LOCATE 10, 1: INPUT "Enter initial file order =", ini
    f = ini
1000 GOSUB 4000        'input data          '
    GOSUB 5200        'curve selection     '
    GOSUB 5700        'draw curve          '
    GOSUB 5800        'function selection  '
    IF fa = 2 THEN GOTO 1000
    'LOCATE 1, 1: PRINT "Last file was "; FILE$(f)
    f = f + 1
    LOCATE 1, 1: PRINT "This file is "; FILE$(f)
    INPUT G$
1030 CLS
    GOTO 1000
REM ========== DATA INPUT ==========
4000 IF fa = 2 THEN INPUT "Enter file name ", FILE$(f)
    filefin$ = "b:" + FILE$(f) + ".tra"
```

```
    'filefin$ = "c:" + FILE$(f) + ".tra"
    CLS
    OPEN filefin$ FOR INPUT AS #1
    i = 0: LOCATE 1, 1: PRINT "Reading "; filefin$; " !!!!          file order:"; f
4100 IF EOF(1) THEN CLOSE 1: nd = i: GOTO 4300
    i = i + 1
    IF i = 1 THEN INPUT #1, tm(i), q1(i), q2(i), x(i), y(i), z(i), miz(i), WB1, WB2, BK1, BK2,
dispX1, dispX2
    IF i > 1 THEN INPUT #1, tm(i), q1(i), q2(i), x(i), y(i), z(i), miz(i)
    'LOCATE 4, 1: PRINT tm(i), q1(i), q2(i)
    'LOCATE 5, 1: PRINT x(i), y(i), z(i), miz(i)
    GOTO 4100
4300 IF nd <> 512 THEN STOP
4700 RETURN
REM ═══════════ CURVE SELECTION ═══════════
5200 LOCATE 2, 1: PRINT "Time ..... 1"
     LOCATE 3, 1: PRINT "Window 1 ..... 2"
     LOCATE 4, 1: PRINT "Window 2 ..... 3"
     LOCATE 5, 1: PRINT "Sum ..... 4"
     LOCATE 6, 1: PRINT "Difference ..... 5"
     LOCATE 7, 1: PRINT "Polarization ..... 6"

    LOCATE 10, 1: INPUT "Which variables for FITTING  (1-6)  ", V
    IF V = 1 THEN V$ = "Time"
    IF V = 2 THEN V$ = "Window 1"
    IF V = 3 THEN V$ = "Window 2"
    IF V = 4 THEN V$ = "Sum "
    IF V = 5 THEN V$ = "Difference "
    IF V = 6 THEN V$ = "Polarization"
    ymin = 100000000: ymax = -100000000
    FOR i = 1 TO 512
    IF V = 1 THEN V(i) = tm(i)
    IF V = 2 THEN V(i) = q1(i)
    IF V = 3 THEN V(i) = q2(i)
    IF V = 4 THEN V(i) = x(i)
    IF V = 5 THEN V(i) = y(i)
    IF V = 6 THEN V(i) = z(i)
    IF V = 7 THEN V(i) = miz(i)
    IF V(i) < ymin THEN ymin = V(i)
    IF V(i) > ymax THEN ymax = V(i)
    NEXT i
    xmin = tm(1): xmax = tm(512)
    RETURN
REM ═══════════ SCREEN GRAPHIC CONTROL ═══════════
5700 CLS
    LOCATE 1, 32: COLOR 12: PRINT filefin$;
    LOCATE 1, 50: COLOR 11: PRINT f
    LOCATE 1, 63: COLOR 12: PRINT V$
5720 COLOR 15
    LOCATE 23, 30: PRINT xmin
    LOCATE 23, 72: PRINT xmax
    LOCATE 22, 27: PRINT INT(ymin)
    LOCATE 8, 27: PRINT INT(ymax)
    mx = 350 / (xmax - xmin)
    my = 200 / (ymax - ymin)
    DRAW "bm250,300"
    DRAW "c15;u200r350d200l350"
```

```
    DRAW "c8;bm320,300;u200;br70;d200;br70;u200;br70;d200;"
    DRAW "c8;bm250,260;r350;bu40;l350;bu40;r350;bu40;l350;"
    x0 = 250: y0 = 300 + ymin * my
    PSET (x0, y0), 2: DRAW "r350"
    FOR i = 1 TO 4
    LOCATE 23, 32 + 8 * i: PRINT INT(xmin + i * (xmax - xmin) / 5)
    LOCATE 22 - 3 * i, 27: PRINT INT(ymin + i * (ymax - ymin) / 5)
    NEXT i
    FOR i = 1 TO 512
    x = 250 + (tm(i) - xmin) * mx
    y = 300 - (V(i) - ymin) * my
    IF x < 250 THEN GOTO 5750
    IF x > 600 THEN GOTO 5750
    IF y < 100 THEN GOTO 5750
    IF y > 300 THEN GOTO 5750
    PSET (x, y), 13: DRAW "l2r4l2u2d4;"
   'DRAW "u3d6u3l3r6;"
5750 NEXT i
    RETURN
REM ═══════════ FUNCTION SELECTION ═══════════
5800 GOSUB 6600
    LOCATE 8, 1: PRINT "Scaling.....1"
    LOCATE 9, 1: PRINT "Fitting.....2"
    LOCATE 10, 1: PRINT "Variable.....3"
    LOCATE 11, 1: PRINT "Exit.....4"
    'LOCATE 11, 1: PRINT "Fitting.....2"
    LOCATE 13, 1: INPUT "Enter Selection    ", S
    IF S = 1 THEN GOSUB 7000
    IF S = 2 THEN GOSUB 8000
    IF S = 3 THEN GOSUB 8400
    IF S = 4 THEN RETURN
    GOTO 5800
6600 FOR L = 8 TO 15
    LOCATE L, 1: PRINT "                    "
    NEXT L
    RETURN
REM ═══════════ SCALING GRAPH ═══════════
7000 GOSUB 6600
    LOCATE 7, 1: COLOR 13: PRINT "SCALING": COLOR 15
    LOCATE 8, 1: INPUT "xmin= ", xmin
    LOCATE 9, 1: INPUT "xmax= ", xmax
    LOCATE 10, 1: INPUT "ymin= ", ymin
    LOCATE 11, 1: INPUT "ymax= ", ymax
    'LOCATE 12, 1: INPUT "x-div.= ", xdiv
    'LOCATE 13, 1: INPUT "y-div.= ", ydiv
    GOSUB 5700
    LOCATE 13, 1: INPUT "Change scale ? (pass=n) ", CS$
    GOSUB 6600
    IF CS$ = "y" THEN GOTO 7000
    RETURN
REM ═══════════ FITTING ═══════════
8000 LOCATE 7, 1: COLOR 13: PRINT "FITTING": COLOR 15
    GOSUB 6600
    LOCATE 8, 1: PRINT "1 exponential....1"
    LOCATE 9, 1: PRINT "2 exponential....2"
    LOCATE 10, 1: PRINT "Other equation...3"
    LOCATE 11, 1: PRINT "Options.....4"
```

```
    LOCATE 12, 1: PRINT "Exit.....5"
    LOCATE 13, 1: INPUT "Select your fitting   ", FIT
    IF FIT = 1 THEN FIT$ = "single exponential fitting": LesErr = 100: GOSUB 8100
    IF FIT = 2 THEN FIT$ = "double exponential fitting": GOSUB 8200
    IF FIT = 4 THEN GOSUB 8500
    IF FIT = 5 THEN RETURN
    GOTO 8000
8100 GOSUB 6600
    LOCATE 2, 32: COLOR 11: PRINT FIT$: COLOR 15
    LOCATE 3, 32: PRINT "y=A*exp((x-d)/T)+B   "
    LOCATE 8, 1: INPUT "A= ", A$
    IF LEN(A$) = 0 THEN A = A1 ELSE A = VAL(A$)
    LOCATE 9, 1: INPUT "d= ", d$
    IF LEN(d$) = 0 THEN d = d1 ELSE d = VAL(d$)
    LOCATE 10, 1: INPUT "T= ", T$
    IF LEN(T$) = 0 THEN T = T1 ELSE T = VAL(T$)
    LOCATE 11, 1: INPUT "B= ", B$
    IF LEN(B$) = 0 THEN B = B1 ELSE B = VAL(B$)
8110 LOCATE 12, 1: INPUT "step= ", sp$
    IF LEN(sp$) = 0 THEN sp = sp1 ELSE sp = VAL(sp$)
    IF sp = 0 THEN GOSUB 8112 ELSE GOTO 8120
8112 LOCATE 12, 1: PRINT "                "
    LOCATE 12, 1: INPUT "step= ", sp$
    RETURN
8120 LOCATE 13, 1: PRINT "Press <enter> to fit "
    LOCATE 14, 1: INPUT "Press <0> to change ...", fitorc$
    IF fitorc$ = "0" THEN GOTO 8173
    IF LEN(fitorc$) <> 0 THEN GOTO 8120
    COLOR 10
    A1 = A
    d1 = d
    T1 = T
    B1 = B
    sp1 = sp
    LOCATE 2, 63: PRINT "A= "; A
    LOCATE 3, 63: PRINT "d= "; d
    LOCATE 4, 63: PRINT "T= "; T
    LOCATE 5, 63: PRINT "B= "; B
    LOCATE 6, 63: PRINT "step= "; sp
8140 COLOR 15
    FOR i = xmin TO xmax STEP sp
    u = A * EXP((i - d) / T) + B
    fx = 250 + (i - xmin) * mx
    fy = 300 - (u - ymin) * my
    IF fx < 250 THEN GOTO 8160
    IF fx > 600 THEN GOTO 8160
    IF fy < 100 THEN GOTO 8160
    IF fy > 300 THEN GOTO 8160
    PSET (fx, fy), 14
8160 NEXT i
    GOSUB 8200
8170 GOSUB 6600
8173 GOSUB 8900
    COLOR 15
    LOCATE 18, 1: PRINT "Retry----------1"
    LOCATE 19, 1: PRINT "Redraw---------2"
    LOCATE 20, 1: PRINT "Store & Exit---3"
```

```
    LOCATE 21, 1: PRINT "Exit----------4"
    LOCATE 22, 1: INPUT "Enter selection   ", SS
    GOSUB 8900
    IF SS = 1 THEN GOTO 8100
    IF SS = 2 THEN GOSUB 8700: GOSUB 5720: GOTO 8140
    IF SS = 3 THEN GOSUB 8180
    IF SS = 4 THEN RETURN
    GOTO 8173
8180 SOUND 4000, 2
    FILES$ = "c:" + FILE$(f) + ".FIT"
    LOCATE 18, 1: PRINT "Filename="; FILES$
    LOCATE 19, 1: INPUT "0 to exit ", NF$
    IF NF$ = "0" THEN RETURN
    IF LEN(NF$) > 0 THEN FILES$ = NF$: FILES$ = "c:" + FILES$ + ".FIT"
    LOCATE 20, 1: PRINT "STORING !!        "
REM ========================DATA STORAGE=====================
    OPEN FILES$ FOR OUTPUT AS #2
    PRINT #2, V
    FOR i = 1 TO nd
    IF tm(i) < xmin THEN GOTO 8185
    IF tm(i) > xmax THEN GOTO 8185
    u = A * EXP((tm(i) - d) / T) + B
    'IF Sd$ = "y" THEN PRINT #2, tm(i); "        "; V(i); "        "; u; "        "; V2(i)
    PRINT #2, tm(i); "        "; V(i); "        "; u; "        "; V2(i)
    'IF Sd$ = "n" THEN PRINT #2, tm(i); "        "; V(i); "        "; u; "        "; V2(i)
8185 NEXT i
    LPRINT FIT$; "  y=A*exp((x-d)/T)+B   "
    LPRINT "Standard Deviation ="; StndErr
    LPRINT "A="; A
    LPRINT "d="; d
    LPRINT "T="; T
    LPRINT "B="; B
    LPRINT " FIT ("; V; ") results saved in "; FILES$; "/ "; DATE$; "/ "; TIME$
    CLOSE
    LPRINT "    ": LPRINT "    "
    LOCATE 6, 32: COLOR 13: PRINT "Data saved: "; FILES$
      COLOR 15: RETURN
8200 ErrSqr = 0: nerr = 0
    FOR i = 1 TO nd
    IF tm(i) < d THEN GOTO 8280
    IF tm(i) > xmax THEN GOTO 8280
    IF V(i) < ymin THEN GOTO 8280
    IF V(i) > ymax THEN GOTO 8280
    u = A * EXP((tm(i) - d) / T) + B
    ErrSqr = ErrSqr + (V(i) - u) ^ 2: nerr = nerr + 1
8280 NEXT i
    StndErr = SQR(ErrSqr / nerr)
    IF StndErr < LesErr THEN LesErr = StndErr ELSE GOTO 8290
    FOR L = 3 TO 5
    PRINT "                          "
    NEXT L
    COLOR 6: LOCATE 3, 1: PRINT "A= "; A
    LOCATE 3, 15: PRINT "d= "; d
    LOCATE 4, 1: PRINT "T= "; T
    LOCATE 4, 15: PRINT "B= "; B
    LOCATE 5, 1: PRINT "Least Error= "; LesErr: COLOR 15
8290 SOUND 2000, 5
```

```
    LOCATE 4, 32: COLOR 13: PRINT "StndErr="; StndErr; "  "; nerr
    RETURN
8400 CLS
    GOSUB 5200
    GOSUB 5700
    RETURN
8500 GOSUB 6600
    LOCATE 8, 1: PRINT "Rescaling....1"
     LOCATE 11, 1: PRINT "Exit.....4"
    LOCATE 13, 1: INPUT "Your Selection   ", FIT2
    IF FIT2 = 1 THEN GOSUB 7000
    IF FIT2 = 4 THEN RETURN
    GOTO 8500
8700 FOR L = 8 TO 23
    LOCATE L, 27
    PRINT "                                    "
    NEXT L
    RETURN
8900 FOR L = 18 TO 23
    LOCATE L, 1
    PRINT "                          "
    NEXT L
    RETURN
```

BIBLIOGRAPHY

Chapter 1

E. B. Aleksandrov, ***Sov. Phys. Usp 15 436*** (1973)

G. L. Bir, A. G. Aronov, and G. E. Pikus, ***Sov. Phys. JETP 42, 705*** (1976)

H. Chao, K. S. Wong, R. E. Alfano, Unlu and Morkoc, ***J. SPIE 942 215*** (1988)

M. I. D'yakonov and V. I. Perel, ***Sov. Phys. JETP 38, 177*** (1974)

T. C. Damen, Karl Leo, Jagdeep Shah and J. E. Cunningham, ***Appl. Phys. Lett. 58(17) 1902*** (1991)

A. I. Ekimov and V. I. Safarov, ***Zh. Eksp. Teor. Fiz. Pis'ma 13 251*** (1971)

A. I. Ekimov and V. I. Safarov, ***Zh. Eksp. Teor. Fiz. Pis'ma 13 700*** (1971)

G. Fishman and G. Lampel, ***Phys. Rev. B 16 820*** (1977)

W. Happer, ***Rev. Mod. Phys. 44 169*** (1972)

Mark Johnson, ***Science 260 320*** (1993)

A. Kastler, ***Science 158 214*** (1967)

G. Lampel, ***Phys. Rev. Lett. 64, 491*** (1968)

R. J. Seymour, M. R. Junnarkar, and R. R. Alfano, ***Phys. Rev. B 24 3623*** (1981)

R. J. Seymour and R. R. Alfano, ***Appl. Phys. Lett. 37(2) 231*** (1980)

T. Uenoyama and L. J. Sham, Phys. ***Rev. Lett. 64(25) 3070*** (1989)

Y. Yafet, ***Solid State Phys. 15, 371*** (1963)

K. Zerrouati, F. Fabre, G. Bacquet, J. Bandet, J. Frandon and G. Lampel, D. Paget, ***Phys. Rev. B 37(3) 1334*** (1987)

Chapter 2

Sadao Adachi, ***J. Appl. Phys. 58(3) R1*** (1985)

J. Bardeen and W. Shockley, ***Phys. Rev. 80 72*** (1950)

G. L. Bir, A. G. Aronov, and G. E. Pikus, ***Sov. Phys. JETP 42, 705*** (1976)

G. L. Bir, G. E. Pikus, A. S. Skal, ***Sov. Phys. Semicond. 8 715*** (1974)

J. S. Blakemore, ***J. Appl. Phys. 53(10) R123*** (1982)

Esther M. Conwell, "***High Field Transport in Semiconductors***", Academic Press, New York, Chapter 3 (1967)

M. I. D'yakonov and V. I. Perel', ***Sov. Phys. JETP 33, 1053*** (1971)

M. I. D'yakonov and V. I. Perel, ***Sov. Phys. JETP 38, 177*** (1974)

G. Dresselhaus, ***Phys. Rev. 100 580*** (1955)

A. R. Edmond, "***Angular momentum in Quantum Mechanisms***" Princeton Univ. Press, New York, (1957)

H. Ehrenreich, ***J. Phys. Chem. Solids 2 131*** (1957)

R. Elliott, ***J. , Phys. Rev. 96, 2661*** (1954)

G. Fishman and G. Lampel, ***Phys. Rev. B 16 820*** (1977)

W. A. Harrison, ***Phys. Rev. 104 1281*** (1956)

A. R. Hutson, ***J. Appl. Phys. 32 2287*** (1961)

E. J. Johnson, R. J. Seymour and R. R. Alfano, "***Semiconductors Probed by Ultrafast Laser Spectroscopy***", Vol. II, Chapter 19, edited by R. R. Alfano, Academic Press, New York, (1984)

E. D. Kane, ***J. Phys. Chem. Solid 1 82*** (1956)

J. M. Luttinger, ***Phys. Rev. 102 1030*** (1956)

B. R. Nag, "***Semiconductors Probed by Ultrafast Laser Spectroscopy***", Vol. I, edited by R. R. Alfano, Academic Press, New York, Chapter 1, 3 (1984)

"***Optical Orientation***", Chapter 2, edited by F. Meier and B. P. Zakharchenya, Elsevier Science Publishers B. V. Leningrad (1984)

"*Optical Orientation*", Chapter 3, edited by F. Meier and B. P. Zakharchenya, Elsevier Science Publishers B. V. Leningrad (1984)

A. W. Overhauser, ***Phys. Rev. 89 689*** (1953)

A. L. Powell, C. C. Button, J, S. Roberts, and P. I. Rockett, ***Phys. Rev. Lett. 67(21) 3010*** (1991)Seymour R. J. , M. R. Junnarkar, and R. R. Alfano, Phys. Rev. B 24 3623 (1981)

J. F. Ryan, R. A. Taylor, A. J. Turberfield, and Angela Maciel, ***Phys. Rev. Lett. 53(19) 1841*** (1984)

R. J. Seymour and R. R. Alfano, ***Appl. Phys. Lett. 37(2) 231*** (1980)

Y. Yafet, ***Solid State Phys. 15, 371*** (1963)

K. Zerrouati, F. Fabre, G. Bacquet, J. Bandet, J. Frandon and G. Lampel, D. Paget, ***Phys. Rev. B 37(3) 1334*** (1987)

Chapter 3

H. Chao, K. S. Wong, R. E. Alfano, Unlu and Morkoc, ***J. SPIE 942 215*** (1988)

D. Z. Garbuzov, R. I. Dzhioev, L. M. Kanskaya, and V. G. Fleisher, ***Fiz. Tverd. Tela 14 1720*** (1972)

P. P. Ho, "***Semiconductors Probed by Ultrafast Laser Spectroscopy***", Vol. II, edited by R. R. Alfano, Academic Press, New York, Chapter 25, (1984)

A. Katz, "***Subpicosecond time resolved absorption and transient grating in GaAs***", Ph.D. thesis (1989)

A. Katz, H. Chao, M. Yang, Y. Budansky, A. Gorokhovsky, L. Kalpaxis, and R. R. Alfano, "***CPM femtosecond laser system user's guide***" IUSL internal documentary

N. Schiller, Y. Tsuchiya, E. Inuzuka, Y. Suzuki, K. Kinoshita, K. Kamiya, H. Iida, and R. R. Alfano, ***Optical Spectra*** June (1980)

Jagdeep Shah, B. Deveaud, T. C. Damen, W. T. Tsang, A. C. Gossard, and Lugli, ***Phys. Rev. Lett. 59 2222*** (1987)

Jagdeep Shah, T. C. Damen, B. Deveaud, and D. Block, ***Appl. Phys. Lett. 50 1307*** (1987)

C. V. Shank, *Science 219 (4588) 1027* (1983)

K. Shum, M. R. Junnarkar, H. Chao, R. R. Alfano, and H. Morkoc, *Phys. Rev. B 37 8923* (1988)

M. Yan, "*Ultrafast spectroscopy in conjugated organic and biological meterials*", Ph.D. thesis (1993)

K. Zerrouati, F. Fabre, G. Bacquet, J. Bandet, J. Frandon and G. Lampel, D. Paget, *Phys. Rev. B 37(3) 1334* (1987)

Chapter 4

Esther M. Conwell, "*High Field Transport in Semiconductors*", Academic Press, New York, Chapter 3 (1967)

E. J. Johnson, R. J. Seymour and R. R. Alfano, "*Semiconductors Probed by Ultrafast Laser Spectroscopy*", Vol. II, edited by R. R. Alfano, Academic Press, New York, Chapter 19, 199 (1984)

B. R. Nag, "*Semiconductors Probed by Ultrafast Laser Spectroscopy*", Vol. I, edited by R. R. Alfano, Academic Press, New York, Chapter 1, 3 (1984)

"*Optical Orientation*", edited by F. Meier and B. P. Zakharchenya, Elsevier Science Publishers B. V. Leningrad (1984)

T. Uenoyama and L. J. Sham, *Phys. Rev. Lett. 64(25) 3070* (1989)

K. Zerrouati, F. Fabre, G. Bacquet, J. Bandet, J. Frandon and G. Lampel, D. Paget, *Phys. Rev. B 37(3) 1334* (1987)

Chapter 5

A. Abragam, "*The Principles of Nuclear Magnetism*", Oxford University Press, London (1961)

D. D. Awschalom, J. M. Hong, L. L. Chang, and G. Grinstein, *Phys. Rev. Lett. 59 1733* (1987)

G. L. Bir, A. G. Aronov, and G. E. Pikus, *Sov. Phys. JETP 42, 705* (1976)

H. Chao and R. R. Alfano, (in preparation)

M. I. D'yakonov and V. I. Perel', ***Sov. Phys. JETP 33, 1053*** (1971)

R. J. Elliott, ***Phys. Rev. 96, 2661*** (1954)

E. J. Johnson, R. J. Seymour and R. R. Alfano, "***Semiconductors Probed by Ultrafast Laser Spectroscopy***", Vol. II, edited by R. R. Alfano, Academic Press, New York, Chapter 19, 199 (1984)

D. A. Kleinman and R. C. Miller, ***Phys. Rev. Lett. 46(1) 68*** (1981)

B. R. Nag, "***Semiconductors Probed by Ultrafast Laser Spectroscopy***", Vol. I, edited by R. R. Alfano, Academic Press, New York, Chapter 1, 3 (1984)

"***Optical Orientation***", edited by F. Meier and B. P. Zakharchenya, Elsevier Science Publishers B. V. Leningrad (1984)

K. Shum, Y. Takiguchi, J. M. Mohaidat, R. R. Alfano, K. Adomi and H. Morkoc, ***Phys. Rev. B 44(8) 4044*** (1991)

Y. Yafet, ***Solid State Phys. 15, 371*** (1963)

Chapter 6

H. Chao and R. R. Alfano, (unpublished, see Chapter 4 of this thesis)

H. Chao and R. R. Alfano, (unpublished, see Chapter 5 of this thesis)

B. R. Nag, "***Semiconductors Probed by Ultrafast Laser Spectroscopy***", Vol. I, edited by R. R. Alfano, Academic Press, New York, Chapter 1 (1984)

R. J. Seymour, M. R. Junnarkar, and R. R. Alfano, ***Phys. Rev. B 24 3623*** (1981)

Chapter 7

G. L. Bir, A. G. Aronov and G. E. Pikus, ***Sov. Phys. JETP 42, 705*** (1976)

M. I. D'yakonov and V. I. Perel, ***Sov. Phys. JETP 38, 177*** (1974)

E. J. Johnson, R. J. Seymour and R. R. Alfano, "***Semiconductors Probed by Ultrafast Laser Spectroscopy***", Vol. II, edited by R. R. Alfano, Academic Press, New York, Chapter 19, 199 (1984)

G. E. Pikus and A. N. Titkov, "*Optical Orientation*", Chapter 3, edited by F. Meier and B. P. Zakharchenya, Elsevier Science Publishers B. V. Leningrad (1984)

K. Zerrouati, F. Fabre, G. Bacquet, J. Bandet, J. Frandon and G. Lampel, D. Paget, *Phys. Rev. B 37(3) 1334* (1987)